

2010

Investigation and Optimization of a Solvent / Anti-Solvent Crystallization Process for the Production of Inhalation Particles

Swati Agrawal

Virginia Commonwealth University

Follow this and additional works at: <http://scholarscompass.vcu.edu/etd>

 Part of the [Pharmacy and Pharmaceutical Sciences Commons](#)

© The Author

Downloaded from

<http://scholarscompass.vcu.edu/etd/2244>

This Dissertation is brought to you for free and open access by the Graduate School at VCU Scholars Compass. It has been accepted for inclusion in Theses and Dissertations by an authorized administrator of VCU Scholars Compass. For more information, please contact libcompass@vcu.edu.

© Swati Agrawal 2010
All Rights Reserved

**INVESTIGATION AND OPTIMIZATION OF A SOLVENT / ANTI-SOLVENT
CRYSTALLIZATION PROCESS FOR THE PRODUCTION OF INHALATION
PARTICLES**

A dissertation submitted in partial fulfillment of the requirements for the degree of
Doctor of Philosophy at Virginia Commonwealth University

by

SWATI AGRAWAL

M.Pharm., India, Birla Institute of Technology and Science, 2006

B.Pharm., India, Uttar Pradesh Technical University, 2004

Director: MICHAEL HINDLE, Ph.D.
ASSOCIATE PROFESSOR, DEPARTMENT OF PHARMACEUTICS



Virginia Commonwealth University
Richmond, Virginia
July 2010

Acknowledgement

I would like to take this opportunity to express my gratitude to all the people who have helped me along the path to a successful completion of my Ph.D. endeavor.

First and foremost, I would like to thank my advisor, Dr. Hindle, for his constant guidance towards my research project. His constant encouragement and his untiring efforts have helped me grow professionally and made me a more confident person today.

I am grateful to my committee members, Drs. Byron, Peart, Kellogg, and Longest, for their valuable time and for providing me helpful suggestions and inputs towards my dissertation project.

I would like to acknowledge Dr. Everett Carpenter from the Department of Chemistry for providing me free access to the powder X-ray diffractometer in his laboratory as well as to his graduate students, Kyler, Dan, and Meghann who helped me with the instrument.

Thanks are due to Mike, Matt, and Marcela in the Bioanalytical lab for providing me various bits and pieces that I used during my project. I would like to acknowledge the help I received from Ashutosh, Aurijit, and Dr. Phil Mosier during my molecular modeling project. Thanks to the Pharmaceutics faculty for their help in the course of my graduate studies.

Thanks to Suparna for helping me get acquainted with the aerosol research group lab when I first joined the department and for lending me a patient ear many a times. I extend special thanks to Priya, Reshma and Reethi for helping me get settled when I first landed in the USA. Thanks to Prajakta, Bhawana, Megha, Renish, Poonam, and Suparna – my family away from home – for their friendship. Thanks to the Aerosol Research Group members and the graduate students in the Department of Pharmaceutics for making my time here at VCU School of Pharmacy a memorable one. Laura, Keyetta, Chris, and Romano deserve special thanks for being so efficient and making life in graduate school much easier.

I would like to thank the School of Pharmacy for providing me financial support and the VCU graduate school for the Dissertation assistantship.

Finally, I would like to thank Uday for his love, understanding, encouragement and support all these years. Last, but not the least, thanks to my mother for being there always. This dissertation is the result of her love, blessings and relentless efforts to keep me motivated at all times. Thanks Mom for always believing in me.

Table of Contents

	Page
Acknowledgement.....	ii
List of Tables.....	viii
List of Figures.....	xiii
List of Abbreviations.....	xxiii
Abstract.....	xxvi
Chapters	
I. INTRODUCTION.....	1
I.A Significance and background.....	1
I.A.1 Dry powder formulations for pulmonary drug delivery	2
I.A.1.1 Influence of drug particle characteristics on emitted dose.....	3
I.A.1.2 Influence of drug particle characteristics on fine particle fraction	6
I.A.1.3 Desirable attributes for a dry powder formulation.....	7
I.A.2 Rationale for using combination therapy for the treatment and maintenance of asthma	7
I.B Particle engineering for inhalation particles	9
I.B.1 Micronization.....	9
I.B.2 Alternate particle engineering techniques for producing inhalation particles	10
I.B.2.1 Sonocrystallization.....	10
I.B.2.2 Spray drying.....	12
I.B.2.3 Supercritical fluid technologies	13
I.B.2.4 Controlled precipitation techniques	15
I.C Solvent / anti-solvent crystallization.....	17
I.C.1 Theory of solvent / anti-solvent crystallization	17
I.C.1.1 Driving force for crystallization.....	18
I.C.1.2 Nucleation.....	19
I.C.1.3 Crystal growth.....	22
I.C.1.4 Crystal morphology	24
I.C.1.5 Role of different crystallization variables on particle characteristics	25

I.D.	Molecular modeling.....	27
I.D.1	Molecular modeling as a tool to study interactions.....	27
I.D.2	SYBYL software.....	28
I.D.3	GOLD program.....	30
I.D.4	HINT! program for interaction classification and quantitative scoring.....	30
I.E	Overview.....	31
II.	HYPOTHESES AND RESEARCH PLAN.....	33
II.A.	Hypothesis 1.....	33
II.B.	Hypothesis 2.....	33
II.C.	Hypothesis 3.....	34
II.D.	Hypothesis 4.....	34
III.	INVESTIGATION AND OPTIMIZATION OF A SOLVENT / ANTI-SOLVENT CRYSTALLIZATION PROCESS USING ALBUTEROL SULFATE AS A MODEL DRUG.....	36
III.A.	INTRODUCTION.....	36
III.B.	CHEMICALS.....	36
III.C.	METHODS.....	37
III.C.1	Crystallization of albuterol sulfate.....	37
III.C.1.1	Preparation of a supersaturated aqueous solution of albuterol sulfate.....	37
III.C.1.2	Crystallization by the anti-solvent method.....	37
III.C.1.3	Experimental design for screening the effects of crystallization conditions.....	38
III.C.1.4	Strategies investigated to reduce albuterol sulfate particle size.....	41
III.C.1.4.1	Effect of temperature difference between the solvent and anti-solvent... ..	41
III.C.1.4.2	Effect of isopropyl alcohol as the anti-solvent on albuterol sulfate particle size.....	42
III.C.1.5	Assessment of water / solvent loss.....	43
III.C.1.5.1	Karl Fischer titration.....	43
III.C.1.5.2	Thermogravimetric Analysis (TGA).....	44
III.C.1.6	Assessment of crystallinity.....	45
III.C.1.6.1	Differential Scanning Calorimetry (DSC).....	45
III.C.1.6.2	Optical microscopy.....	47
III.C.1.6.3	Powder X-ray diffraction.....	47
III.C.1.7	Scanning electron microscopy.....	47
III.C.1.8	Particle size determination by laser diffraction.....	48

III.C.1.9	High performance liquid chromatography (HPLC).....	48
III.D.	RESULTS AND DISCUSSION.....	50
III.D.1	Characterization of albuterol sulfate reference standard.....	50
III.D.2	Characterization of AS particles produced by solvent / anti-solvent crystallization.....	53
III.D.2.1	Characterization after a crystal maturation time = 0.....	53
III.D.2.1.1	Estimated % crystallinity.....	53
III.D.2.1.2	Particle size distribution.....	56
III.D.2.2	Characterization of AS particles after different crystal maturation times between 0 – 24 hours.....	71
III.D.2.2.1	Estimated % crystallinity.....	71
III.D.2.2.2	Mechanism of crystallization.....	83
III.D.2.2.3	Particle size distribution of AS particles after crystal maturation time = 24 hours.....	101
III.D.2.3	Comparison of AS particles engineered from solvent / anti-solvent crystallization with micronized AS.....	119
III.E	CONCLUSIONS.....	123
IV.	COMBINATION PARTICLES OF ALBUTEROL SULFATE AND IPRATROPIUM BROMIDE MONOHYDRATE.....	125
IV.A	INTRODUCTION.....	125
IV.B	CHEMICALS.....	125
IV.C	METHODS.....	126
IV.C.1	Solvent / Anti-solvent system used for combination particles.....	126
IV.C.2	Processing variables investigated for combination particles.....	126
IV.C.2.1	Solvent / Anti-solvent crystallization of combination particles using ethyl acetate as the anti-solvent.....	127
IV.C.2.2	Solvent / anti-solvent crystallization of combination particles using isopropyl alcohol as the anti-solvent.....	129
IV.C.2.3	Solvent / anti-solvent crystallization of combination particles using mixtures of isopropyl alcohol and ethyl acetate as anti-solvents.....	129
IV.C.2.4	Physical mixtures of AS and IB.....	130
IV.C.3	Solid-state characterization of combination particles.....	130
IV.C.3.1	Differential Scanning Calorimetry.....	130
IV.C.3.2	Hot stage microscopy.....	131
IV.C.3.3	Optical Microscopy.....	131

IV.C.3.4	Powder X-Ray Diffraction.....	132
IV.C.3.5	Scanning Electron Microscopy.....	132
IV.C.3.6	Particle Size Determination by Laser Diffraction.....	132
IV.C.3.7	High Performance Liquid Chromatography (HPLC).....	133
IV.C.4	Molecular Modeling.....	134
IV.D	RESULTS AND DISCUSSION.....	135
IV.D.1	Characterization of albuterol sulfate and ipratropium bromide monohydrate reference standards.....	135
IV.D.2	Effect of different processing variables on combination particle characteristics.....	140
IV.D.2.1	Crystallization of combination particles produced using ethyl acetate as the anti-solvent.....	141
IV.D.2.1.1	HPLC content uniformity analysis.....	141
IV.D.2.1.2	Thermal analysis.....	142
IV.D.2.1.3	Powder X-ray diffraction.....	153
IV.D.2.1.4	Particle size distribution of combination particles produced from ethyl acetate.....	159
IV.D.2.2	Crystallization of combination particles produced using isopropyl alcohol as the anti-solvent.....	162
IV.D.2.2.1	HPLC content uniformity analysis.....	162
IV.D.2.2.2	Thermal analysis of combination particles produced from isopropyl alcohol.....	166
IV.D.2.2.3	Powder X-ray diffraction.....	168
IV.D.2.2.4	Particle size distribution of the combination particles produced from isopropyl alcohol.....	176
IV.D.2.3	Crystallization of combination particles produced using mixtures of isopropyl alcohol and ethyl acetate as the anti-solvent.....	180
IV.D.2.3.1	Content uniformity analysis by HPLC.....	181
IV.D.2.3.2	Thermal analysis of combination particles produced from isopropyl alcohol:ethyl acetate = 1:10 (w/w).....	183
IV.D.2.3.3	Particle size distribution of combination particles produced from isopropyl alcohol:ethyl acetate = 1:10 (w/w).....	187
IV.D.3	A summary of the combination particles produced from different solvent / anti-solvent systems.....	190
IV.D.4	Molecular modeling of the combination particles.....	193
IV.E	CONCLUSIONS.....	202
V.	<i>IN VITRO</i> AEROSOL PERFORMANCE TESTING OF ALBUTEROL SULFATE PARTICLES AND COMBINATION PARTICLES OF ALBUTEROL SULFATE	

AND IPRATROPIUM BROMIDE MONOHYDRATE	203
V.A INTRODUCTION	203
V.B MATERIALS.....	203
V.C METHODS	204
V.C.1 Aerosol Performance Testing of Albuterol Sulfate Particles.....	204
V.C.1.1 Drug only studies	205
V.C.1.2 Drug / Lactose Blend Studies	206
V.C.2 Aerosol Performance Testing of Combination Particles	207
V.C.2.1 <i>In vitro</i> aerosol performance testing of combination particles	208
V.C.2.1.1 Drug only studies.....	208
V.C.2.1.2 Drug / lactose blend studies.....	209
V.D RESULTS AND DISCUSSIONS.....	210
V.D.1 Aerosol performance testing of albuterol sulfate particles	210
V.D.1.1 Drug only studies	210
V.D.1.2 Drug / lactose blend studies	226
V.D.2 Aerosol performance testing of combination particles	231
V.D.2.1 Drug only studies	232
V.D.2.2 Drug / lactose blend studies	238
V.E CONCLUSIONS.....	241
VI. OVERALL DISCUSSION AND SUMMARY	242
LIST OF REFERENCES.....	256
APPENDIX.....	266

List of Tables

	Page
Table I.1 Morphologies for pharmaceutical solids	24
Table III.1 Factorial experimental design for R _a ratio's of 1:200, 1:500, and 1:1000 (w/w)	41
Table III.2 System suitability parameters for the HPLC method	49
Table III.3 Characteristic AS peaks	51
Table III.4 Mean ± SD heats of fusion and estimated % crystallinity of AS particles precipitated using EA after crystal maturation time = 0	57
Table III.5 Mean ± SD heats of fusion and estimated % crystallinity values of AS particles precipitated using EA harvested after a crystal maturation time 0, filtered, and dried under ambient conditions for 24 hours	58
Table III.6 Mean ± SD volume median diameters and span indices of AS particles precipitated using EA produced after crystal maturation time = 0 under different crystallization conditions	63
Table III.7 Mean ± SD heats of fusion and estimated % crystallinity values for AS particles precipitated using EA produced from R _a ratio 1:200 (w/w) at different crystal maturation times	72
Table III.8 Mean ± SD heats of fusion and estimated % crystallinity values for AS particles precipitated using EA produced from R _a ratio 1:500 (w/w) at different crystal maturation times	73
Table III.9 Mean ± SD heats of fusion and estimated % crystallinity values for AS particles precipitated using EA obtained from R _a ratios 1:200 and 1:500 (w/w) after crystal maturation time 1440 minutes under different stirring speeds after filtration and drying	76
Table III.10 Mean ± SD heats of fusion and estimated % crystallinity values for AS particles precipitated using EA produced from R _a ratio 1:1000 (w/w) at different crystal maturation times	80
Table III.11 Statistical analysis of the effect of crystallization variables on particle crystallinity	82

Table III.12 Mean \pm SD % water contents (determined by Karl Fischer titration) and % weight loss (determined by TGA) for AS particles precipitated from EA produced after crystal maturation time 0 under different crystallization conditions	88
Table III.13 Mean \pm SD % water contents, % weight loss, and estimated % crystallinity for AS particles precipitated from EA produced from R _a ratio 1:200 (w/w) under different stirring speeds as a function of crystal maturation time	90
Table III.14 Mean \pm SD % water contents (determined by Karl Fischer titration) and % weight loss (determined by TGA) for AS particles precipitated from EA produced from R _a ratio 1:500 (w/w) under different stirring speeds as a function of crystal maturation time.....	93
Table III.15 Mean \pm SD % water contents (determined by Karl Fischer titration) and % weight loss (determined by TGA) for AS particles precipitated from EA produced from R _a ratio 1:1000 (w/w) under different stirring speeds as a function of crystal maturation time.....	96
Table III.16 Mean \pm SD volume median diameters and span indices of AS particles precipitated from EA produced from R _a ratio 1:200 (w/w) under different stirring speeds.....	104
Table III.17 Mean \pm SD volume median diameters and span indices of AS particles precipitated from EA produced from R _a ratio 1:500 (w/w) under different stirring speeds.....	107
Table III.18 Mean \pm SD volume median diameters and span indices of AS particles precipitated from EA produced from R _a ratio 1:1000 (w/w) under different stirring speeds.....	109
Table III.19 Statistical analysis of the effect of crystallization variables on Volume Median Diameter of AS particles	110
Table III.20 Effect of temperature difference between the drug solution and anti-solvent on the particle size of AS particles precipitated from EA	111
Table III.21 Particle size of AS particles produced from isopropyl alcohol and ethyl acetate under the optimized crystallization conditions	115
Table III.22 Particle size distribution parameters for micronized albuterol sulfate	121
Table IV.1 Initial drug solution concentrations of AS and IB and weights of ethyl acetate used as the anti-solvent for the solvent / anti-solvent crystallization process	128
Table IV.2 Crystallization conditions investigated with isopropyl alcohol as the anti-solvent..	129

Table IV.3 System suitability parameters for the HPLC method	134
Table IV.4 Characteristic X-ray peaks for reference standard ipratropium bromide	139
Table IV.5 Mean \pm SD measured % AS and IB and their ratios in the combination particles produced using ethyl acetate as the anti-solvent	141
Table IV.6 Thermal characteristics of AS / IB combination particles prepared using ethyl acetate as the anti-solvent	143
Table IV.7 Comparison of heats of fusion of combination particles with the corresponding physical mixtures	147
Table IV.8 Comparison of melting points of combination particles with the corresponding physical mixtures	148
Table IV.9 Comparison of dehydration temperatures of combination particles with the corresponding physical mixtures	149
Table IV.10 Characteristic diffraction peaks for the 6:1 (w/w) combination particles prepared using ethyl acetate as anti-solvent.....	156
Table IV.11 Mean \pm SD volume median diameters and cumulative % volumes < 5.0 μ m of combination particles produced using ethyl acetate as the anti-solvent.....	160
Table IV.12 AS IB ratios in the combination particles produced using isopropyl alcohol as the anti-solvent.....	162
Table IV.13 AS:IB ratio (w/w) in the impactor for the combination particles produced from IPA after 24 hours of crystallization.....	163
Table IV.14 Mean \pm SD thermal characteristics of AS / IB combination particles prepared using isopropyl alcohol as the anti-solvent.....	166
Table IV.15 Characteristic diffraction peaks for 2.8:1 (w/w) and 5.7:1 (w/w) combination particles produced from isopropyl alcohol	170
Table IV.16 Mean \pm SD volume median diameters and cumulative % volume < 5.0 μ m for the combination particles produced from isopropyl alcohol.....	176

Table IV.17 HPLC analysis results for combination particles produced from mixtures of isopropyl alcohol and ethyl acetate in different proportions	181
Table IV.18 HPLC analysis results for combination particles produced from isopropyl alcohol:ethyl acetate = 1:10 (w/w) at a temperature difference of 65°C between the solvent and anti-solvent	182
Table IV.19 Mean \pm SD thermal characteristics for the combination particles produced from isopropyl alcohol : ethyl acetate = 1:10 (w/w).....	183
Table IV.20 Mean \pm SD thermal characteristics of AS / IB combination particles prepared using isopropyl alcohol:ethyl acetate = 1:10 (w/w) as the anti-solvent at a temperature difference of 65°C between the solvent and anti-solvent	187
Table IV.21 Mean \pm SD volume median diameters of combination particles produced from different anti-solvents.....	189
Table IV.22 Mean \pm SD cumulative % volumes < 5.0 μ m for combination particles produced from different anti-solvents.....	189
Table IV.23 Favorable and unfavorable interactions between AS and IB	198
Table V.1 Description of optimized crystallization conditions used to produce albuterol sulfate particles	205
Table V.2 Description of crystallization conditions used to produce combination particles of AS/IB	208
Table V.3 Mean \pm SD in vitro aerosol performance characteristics of AS particles tested from different DPIs as drug only formulations (n=3).....	211
Table V.4 Volume / mass fraction of AS particles < 5.0 μ m obtained during laser diffraction and aerosolization (n=3)	219
Table V.5 In vitro aerosol performance of IPA-AS particles tested from the Novolizer® as drug / lactose formulations (n=3).....	226
Table V.6 Comparison between aerosol performance of IPA-AS drug only formulation and IPA-AS / lactose blend (n=3).....	230
Table V.7 Variation in the AS:IB ratio during aerosolization of the Combivent® pMDI	232

Table V.8 AS and IB ratio for combination particles 1 aerosolized through the Novolizer® as drug only formulations	234
Table V.9 AS and IB ratio for combination particles 2 aerosolized through the Novolizer® as drug only formulations	235
Table V.10 AS and IB ratio for combination particles 3 aerosolized through the Novolizer® as drug only formulations	236
Table V.11 In vitro aerosol performance characteristics of combination 1, 2, and 3 tested as drug only formulations (n=3).....	237
Table V.12 Blend homogeneity for combination 1, 2, and 3.....	238
Table V.13 AS:IB (w/w) ratios deposited on different stages of the impactor after aerosolization of combination 1, 2, and 3 as drug / lactose blends.....	239
Table V.14 In vitro aerosol performance characteristics of combination 1, 2, and 3 tested as drug/lactose blends (n=3)	239

List of Figures

	Page
Figure I.1 Schematic solubility diagram.....	18
Figure I.2 Schematic diagram showing metastable zone width with respect to nucleation type.....	20
Figure I.3 Schematic plot of Gibbs free energy change (Mullin, 2001) (Reproduced with permission from Elsevier).....	21
Figure I.4 A three dimensional crystal surface showing three types of growth sites (Mullin, 2001) (Reproduced with permission from Elsevier).....	23
Figure III.1 Experimental setup for albuterol sulfate crystallization (insets show the crystallization setup and paddle dimensions).....	40
Figure III.2 TGA temperature program	45
Figure III.3 DSC temperature program.....	46
Figure III.4 Representative DSC thermogram for reference standard albuterol sulfate measured at a heating rate of 10°C/min	50
Figure III.5 Representative X-ray powder diffractogram for reference standard albuterol sulfate.....	51
Figure III.6 X-ray powder diffractogram for albuterol sulfate reported by Ward et al (1995) (Reproduced with permission from Springer).....	52
Figure III.7 Cumulative % undersize volume distribution of reference albuterol sulfate	52
Figure III.8 Representative SEM image for reference albuterol sulfate.....	53
Figure III.9 X-ray powder diffractogram for AS particles precipitated using EA produced from R _a ratio 1:200 (w/w) at 500 r.p.m. after crystal maturation time 0, filtration and drying...	59
Figure III.10 X-ray powder diffractogram for AS particles precipitated using EA produced from R _a ratio 1:500 (w/w) at 500 r.p.m. after crystal maturation time 0, filtration and drying....	59

Figure III.11 X-ray powder diffractogram for AS particles precipitated using EA produced from R_a ratio 1:1000 (w/w) at 500 r.p.m. after crystal maturation time 0, filtration and drying..	59
Figure III.12 Particle size distribution of reference standard albuterol sulfate pre and post sonication	60
Figure III.13 Cumulative % undersize volume distribution for AS particles precipitated from EA produced from R_a ratio 1:200 (w/w) after crystal maturation time = 0 under four different stirring speeds.....	60
Figure III.14 Frequency volume distribution for AS particles precipitated from EA produced from R_a ratio 1:200 (w/w) after crystal maturation time = 0 under four different stirring speeds	61
Figure III.15 Cumulative % undersize volume distribution for AS particles precipitated from EA produced from R_a ratio 1:500 (w/w) after crystal maturation time = 0 under four different stirring speeds.....	61
Figure III.16 Frequency volume distribution for AS particles precipitated from EA produced from R_a ratio 1:500 (w/w) after crystal maturation time = 0 under four different stirring speeds	62
Figure III.17 Cumulative % undersize volume distribution for AS particles precipitated from EA produced from R_a ratio 1:1000 (w/w) after crystal maturation time = 0 under four different stirring speeds.....	62
Figure III.18 Frequency volume distribution for AS particles precipitated from EA produced from R_a ratio 1:1000 (w/w) after crystal maturation time = 0 under four different stirring speeds.....	63
Figure III.19 Scanning Electron Micrograph of AS particles precipitated using EA produced at 500 r.p.m. from a solvent / anti-solvent ratio of 1:200 (w/w) at crystal maturation time = 0 after filtration and drying.....	69
Figure III.20 Scanning Electron Micrograph of AS particles precipitated using EA produced at 500 r.p.m. from a solvent / anti-solvent ratio of 1:500 (w/w) at crystal maturation time = 0 after filtration and drying.....	69
Figure III.21 Scanning Electron Micrograph of AS particles precipitated using EA produced at 100 r.p.m. from a solvent / anti-solvent ratio of 1:1000 (w/w) at crystal maturation time = 0 after filtration and drying.....	70

Figure III.22 Scanning Electron Micrograph of AS particles precipitated using EA produced at 500 r.p.m from a solvent / anti-solvent ratio of 1:1000 (w/w) at crystal maturation time = 0 after filtration and drying.....	70
Figure III.23 Estimated % crystallinity of AS particles precipitated from EA as a function of crystal maturation time for R_a ratio 1:200 (w/w).....	73
Figure III.24 Estimated % crystallinity of AS particles precipitated from EA as a function of crystal maturation time for R_a ratio 1:500 (w/w).....	74
Figure III. 25 Representative DSC thermogram of AS particles precipitated from EA produced from R_a 1:200 at 200 r.p.m. after 1440 minutes.....	75
Figure III.26 Representative DSC thermogram for AS particles precipitated from EA produced from R_a 1:500 at 200 r.p.m. after 1440 minutes.....	75
Figure III.27 Representative DSC thermogram for AS particles precipitated from EA produced from R_a ratio 1:200 at 200 r.p.m. after 1440 minutes of crystallization, filtration, and drying.....	77
Figure III.28 Representative DSC thermogram for AS particles precipitated from EA produced from R_a ratio 1:500 at 200 r.p.m. after 1440 minutes of crystallization, filtration, and drying.....	77
Figure III.29 Powder X-ray diffractogram for AS particles precipitated from EA produced from R_a ratio 1:200 (w/w) after a crystal maturation time of 1440 minutes, filtration, and drying.....	78
Figure III.30 Powder X-ray diffractogram for AS particles precipitated from EA produced from R_a ratio 1:500 (w/w) after a crystal maturation time of 1440 minutes, filtration, and drying.....	78
Figure III.31 Estimated % crystallinity of AS particles precipitated from EA as a function of crystal maturation time for R_a ratio 1:1000 (w/w).....	81
Figure III.32 Powder X-ray diffractogram for AS particles precipitated from EA produced from R_a ratio 1:1000 (w/w) at 500 r.p.m. after crystal maturation time 1440 minutes, filtration, sonication, and drying.....	81
Figure III.33 Estimated % crystallinity and % water content for AS particles precipitated	

from EA produced from R_a ratio 1:200 (w/w) under different stirring speeds at different crystal maturation times	91
Figure III.34 Correlation analysis between estimated % crystallinity and % water content for AS particles precipitated from EA produced from R_a ratio 1:200 under all stirring speeds.....	92
Figure III.35 Estimated % crystallinity and % water content for AS particles precipitated from EA produced from R_a ratio 1:500 (w/w) under different stirring speeds at different crystal maturation times	94
Figure III.36 Correlation analysis between estimated % crystallinity and % water content for AS particles precipitated from EA produced from R_a ratio 1:500 under all stirring speeds.....	95
Figure III.37 % crystallinity and % water content for AS particles precipitated from EA produced from R_a ratio 1:1000 (w/w) under different stirring speeds at different crystal maturation times	97
Figure III.38 Correlation analysis between estimated % crystallinity and % water content for AS particles precipitated from EA produced from R_a ratio 1:1000 under stirring speeds 100 and 200 r.p.m	98
Figure III.39 Representative TGA profiles for AS particles precipitated from EA produced from R_a ratio 1:1000 at stirring speeds 100 and 800 r.p.m. after crystal maturation time = 0	99
Figure III.40 Cumulative % undersize volume distribution of AS particles precipitated from EA harvested after a crystal maturation time of 1440 minutes from R_a ratio 1:200 (w/w) under different stirring speeds	103
Figure III.41 Volume frequency distribution of AS particles precipitated from EA harvested after a crystal maturation time of 1440 minutes from R_a ratio 1:200 (w/w) under different stirring speeds	103
Figure III.42 Cumulative % undersize volume distribution of AS particles precipitated from EA produced from R_a ratio 1:200 (w/w) at 100 r.p.m. after crystal maturation time = 0 and crystal maturation time = 24 hours	104
Figure III.43 Cumulative % undersize volume distribution of AS particles precipitated from EA harvested after a crystal maturation time of 1440 minutes from R_a ratio 1:500 (w/w) under different stirring speeds	106
Figure III.44 Volume frequency distribution of AS particles precipitated from EA harvested	

after a crystal maturation time of 1440 minutes from R_a ratio 1:500 (w/w) under different stirring speeds	106
Figure III.45 Cumulative % undersize volume distribution of AS particles precipitated from EA harvested after a crystal maturation time of 1440 minutes from R_a ratio 1:1000 (w/w) under different stirring speeds	108
Figure III.46 Volume frequency distribution of AS particles precipitated from EA harvested after a crystal maturation time of 1440 minutes from R_a ratio 1:1000 (w/w) under different stirring speeds.....	108
Figure III.47 Cumulative % undersize volume distribution of AS particles precipitated from EA harvested under different conditions of temperature difference between the drug solution and anti-solvent.....	112
Figure III.48 Volume frequency distribution of AS particles precipitated from EA harvested under different conditions of temperature difference between the drug solution and anti-solvent.....	112
Figure III.49 Representative SEM image of AS particles produced from ethyl acetate at R_a ratio 1:200 (w/w), 200 r.p.m. and a temperature difference of 65°C.....	113
Figure III.50 Cumulative % undersize volume distribution of AS particles produced from isopropyl alcohol and ethyl acetate	114
Figure III.51 Volume frequency distribution of AS particles produced from isopropyl alcohol and ethyl acetate.....	115
Figure III.52 Powder X-ray diffractogram for AS particles precipitated from IPA produced from R_a ratio 1:200 (w/w) at 200 r.p.m. after crystal maturation time = 1440 minutes, filtration, sonication, and drying.....	117
Figure III.53 Scanning electron micrograph of AS particles produced from isopropyl alcohol.....	118
Figure III.54 Cumulative % undersize volume distribution of micronized albuterol sulfate	120
Figure III.55 Volume frequency distribution of micronized albuterol sulfate.....	120
Figure III.56 Cumulative % undersize volume distributions of micronized AS particles and AS particles produced from isopropyl alcohol and ethyl acetate	121

Figure III.57 Representative SEM image of micronized albuterol sulfate	122
Figure IV.1 DSC temperature program	131
Figure IV.2 Representative DSC thermogram for reference standard albuterol sulfate at 3°C/min	135
Figure IV.3 Representative DSC thermogram for reference standard ipratropium bromide	136
Figure IV.4 Representative TGA thermogram for reference standard ipratropium bromide	137
Figure IV.5 Representative powder X-ray diffractogram for reference standard ipratropium bromide	138
Figure IV.6 Powder X-ray diffraction of ipratropium bromide monohydrate reported by Corrigan et al. (2006) (Reproduced with permission from Elsevier)	138
Figure IV.7 Particle size distribution for reference standard ipratropium bromide	139
Figure IV.8 Representative SEM image for reference standard ipratropium bromide	140
Figure IV.9 Representative differential scanning thermogram for 1:1 (w/w) combination particles produced using ethyl acetate as anti-solvent	143
Figure IV.10 Representative differential scanning thermogram for 2:1 (w/w) combination particles produced using ethyl acetate as anti-solvent	144
Figure IV.11 Representative differential scanning thermogram for 6:1 (w/w) combination particles produced using ethyl acetate as anti-solvent	144
Figure IV.12 Representative differential scanning thermogram for 10:1 (w/w) combination particles produced using ethyl acetate as anti-solvent	145
Figure IV.13 DSC thermograms for a) AS:IB 10:1 co-spray dried, b) AS:IB 5:1 co-spray dried, c) AS:IB 2:1 co-spray dried, and d) AS:IB 2:1 physical mixture (Corrigan et al., 2006) (Reproduced with permission from Elsevier)	146
Figure IV.14 DSC thermograms of 1:1 (w/w) combination particles and the corresponding physical mixture	150

Figure IV.15 DSC thermograms of 2:1 (w/w) combination particles and the corresponding physical mixture.....	150
Figure IV.16 DSC thermograms of 6:1 (w/w) combination particles and the corresponding physical mixture.....	151
Figure IV.17 DSC thermograms of 10:1 (w/w) combination particles and the corresponding physical mixture.....	151
Figure IV.18 Powder X-ray diffractograms for 1:1 (w/w) AS/IB combination particles produced from ethyl acetate.....	154
Figure IV.19 Powder X-ray diffractogram for 1:1 (w/w) AS/IB physical mixture.....	154
Figure IV.20 Powder X-ray diffractogram for 2:1 (w/w) AS/IB combination particles produced from ethyl acetate.....	155
Figure IV.21 Powder X-ray diffractogram for 6:1 (w/w) AS/IB combination particles produced from ethyl acetate.....	155
Figure IV.22 XRPD of AS:IB 10:1 co-spray dried (continuous line) and crystalline AS (dashed line) (Corrigan et al., 2006) (Reproduced with permission from Elsevier.....	157
Figure IV.23 Representation of an interstitial crystalline solid solution (Adpated from Ghaste et al., 2009)	158
Figure IV.24 Cumulative % undersize volume distribution of different combination particles produced using ethyl acetate as the anti-solvent	159
Figure IV.25 Optical microscopic images for a) 1:1 (w/w) combination particles, b) 2:1 (w/w) combination particles, c) 6:1 (w/w) combination particles, and d) 10:1 (w/w) combination particles produced from ethyl acetate.....	161
Figure IV.26 Concentrations of AS and IB in the supernatant over a crystallization period of 24 hours.....	164
Figure IV.27 Representative DSC thermogram for 2.8:1 (w/w) combination particles produced from isopropyl alcohol.....	167

Figure IV.28 Representative DSC thermogram for 5.7:1 (w/w) combination particles produced from isopropyl alcohol.....	167
Figure IV.29 Powder X-ray diffractogram for 2.8:1 (w/w) combination particles	169
Figure IV.30 Powder X-ray diffractogram for 5.7:1 (w/w) combination particles	169
Figure IV.31 Powder X-ray diffraction spectra for a) Salicylic acid, b) Nicotinic acid, and c) 1:1 co-crystal of salicylic acid and nicotinic acid (Elbagerma et al., 2010) (Reproduced with permission from ACS).....	173
Figure IV.32 Chemical structures of albuterol sulfate and ipratropium bromide showing a possible site for H-bonding.....	175
Figure IV.33 Cumulative % volume undersize distribution of 2.8:1 (w/w) combination particles produced from the anti-solvent isopropyl alcohol.....	176
Figure IV.34 Volume frequency distribution of 2.8:1 (w/w) combination particles produced from the anti-solvent isopropyl alcohol	177
Figure IV.35 Cumulative % volume undersize distribution of 5.7:1 (w/w) combination particles produced from the anti-solvent isopropyl alcohol.....	177
Figure IV.36 Volume frequency distribution of 5.7:1 (w/w) combination particles produced from the anti-solvent isopropyl alcohol	178
Figure IV.37 SEM image of combination particles containing AS and IB in a nominal ratio of 2.8:1 (w/w) produced using isopropyl alcohol as the anti-solvent.....	178
Figure IV.38 SEM image of combination particles containing AS and IB in a nominal ratio of 5.7:1 (w/w) produced using isopropyl alcohol as the anti-solvent.....	179
Figure IV.39 Representative differential scanning thermogram for 1:1 (w/w) combination particles produced from isopropyl alcohol : ethyl acetate = 1:10 (w/w)	184
Figure IV.40 Representative differential scanning thermogram for 2:1 (w/w) combination particles produced from isopropyl alcohol : ethyl acetate = 1:10 (w/w)	184
Figure IV.41 Representative differential scanning thermogram for 6:1 (w/w) combination particles produced from isopropyl alcohol : ethyl acetate = 1:10 (w/w)	185

Figure IV.42 Representative differential scanning thermogram for 10:1 (w/w) combination particles produced from isopropyl alcohol : ethyl acetate = 1:10 (w/w)	185
Figure IV.43 Powder X-ray diffractogram for the 6.6:1 (w/w) combination particles produced from IPA:EA 1:10 (w/w).....	186
Figure IV.44 Cumulative % volume undersize distribution for 1:1 (w/w) combination particles produced from different anti-solvents	187
Figure IV.45 Cumulative % volume undersize distribution for 2:1 (w/w) combination particles produced from different anti-solvents	188
Figure IV.46 Cumulative % volume undersize distribution for 6:1 (w/w) combination particles produced from different anti-solvents	188
Figure IV.47 Cumulative % volume undersize distribution for 10:1 (w/w) combination particles produced from different anti-solvents	189
Figure IV.48 AS Crystal	194
Figure IV.49 IB Crystal	194
Figure IV.50 Water box for solvation of AS and IB molecules	195
Figure IV.51 Manual orientation between AS and IB with the highest HINT score.....	198
Figure IV.52 Albuterol Sulfate cube constructed of unit cells	199
Figure IV.53 A representative docking of IB in the AS crystal lattice.....	200
Figure IV.54 IB orientation with the highest HINT score	201
Figure V.1 Schematic diagram of a Novolizer® (Fenton et al., 2003) (Reproduced with permission from Wolters Kluwer)	213
Figure V.2 Schematic diagram for the Nektar PDS® dry powder inhaler (Davis et al., 2008) (Reproduced with permission from Elsevier).....	213
Figure V.3 Schematic diagram of a Rotahaler® (Chew et al., 2002) (Reproduced with permission from Elsevier).....	214

Figure V.4 Individual site deposition of different types of AS particles aerosolized from the Rotahaler® as drug only formulations (n=3).....	216
Figure V.5 Individual site deposition of different types of AS particles aerosolized from the Novolizer® as drug only formulations (n=3)	216
Figure V.6 Stage-wise deposition of different types of AS particles aerosolized from the Nektar PDS® as drug only formulations (n=3).....	217
Figure V.7 Air classifier technology in a Novolizer® dry powder inhaler (de Boer et al., 2003) (Reproduced with permission from Elsevier).....	220
Figure V.8 Cumulative % undersize mass distribution for the three types of AS particles tested from the Novolizer® as drug only formulations (n=3)	224
Figure V.9 Cumulative % undersize mass distribution for the three types of AS particles tested from the Rotahaler® as drug only formulations (n=3).....	224
Figure V.10 Cumulative % undersize mass distribution for the three types of AS particles (n=3).....	225
Figure V.11 Stage-wise deposition of commercial Novolizer® formulation and IPA-AS particles tested as drug / lactose formulations (n=3)	228
Figure V.12 Cumulative % undersize mass distribution for IPA-AS blend and the commercial Novolizer® formulation aerosolized from the Novolizer® (n=3).....	229
Figure V.13 % mass depositions of AS and IB from combination 1 aerosolized through the Novolizer® as drug only formulations (n=3)	234
Figure V.14 % mass depositions of AS and IB from combination 2 aerosolized through the Novolizer® as drug only formulations (n=3)	235
Figure V.15 % mass depositions of AS and IB from combination particles 3 aerosolized through the Novolizer® as drug only formulations (n=3).....	236

List of Abbreviations

®	Registered trademark
°	Degree
β	Beta
θ	Theta
°C	degree Celsius
ΔG	Free energy
ρ	Particle density
ρ ₀	Unit density of spherical calibration spheres
χ	Dynamic shape factor
μg	microgram
μm	micrometer
μL	microliter
AMP	Adenosine mono phosphate
ANOVA	Analysis of variance
API	Active pharmaceutical ingredient
ATR-FTIR	Attenuated total reflectance- fourier transform infra red
AS	Albuterol Sulfate
CFC	Chlorofluorocarbon
cm	centimeter
CSD	Cambridge structural database
% CV	Coefficient of variance
d _A	Aerodynamic diameter
dv	Volume equivalent diameter
DPI	Dry powder inhaler
DSC	Differential scanning calorimetry
EA	Ethyl acetate
ED	Emitted dose
e.g.	For example
<i>et al.</i>	and others
FBRM	Focused beam reflectance measurement
FPF	Fine particle fraction
FPD	Fine particle dose
g	gram
GA	Genetic Algorithm
GAS	Gas anti-solvent
GSD	Geometric standard deviation
HGCP	High gravity controlled precipitation
HINT	Hydropathic INTERactions

Hz	Hertz
HPLC	High Performance Liquid Chromatography
HPMC	Hydroxy propyl methyl cellulose
IB	Ipratropium Bromide Monohydrate
i.e.	that is
IPA	Isopropyl alcohol
J/g	Joules/gram
KF	Karl Fischer
KHz	Kilohertz
KV	Kilovolt
Log P	Octanol-water partition coefficient
L/min	Liters per minutes
mA	milliampere
mg	milligram
mL	milliliter
mM	millimolar
MMAD	Mass median aerodynamic diameter
MSZW	Metastable zone width
NGI	Next Generation Impactor
nm	nanometer
NIR	Near Infrared
PCA	Precipitation with compressed anti-solvent
PEG	Poly ethylene glycol
PFP	Penta fluoro phenyl
pMDI	Pressurized metered dose inhaler
PSD	Particle size distribution
PXRD	Powder X-ray Diffraction
R _a	Solvent / anti-solvent ratio
r _c	Critical radius
Re	Reynolds number
RH	Relative Humidity
r.p.m.	Revolutions per minute
RSD	Relative standard deviation
SAS	Supercritical anti-solvent
SEDS	Solution enhanced dispersion by supercritical fluids
SAXS	Solution atomization and crystallization by sonication
SCF	Supercritical fluid
SD	Standard deviation
sec	Second
SEM	Scanning Electron Microscopy
TGA	Thermo-gravimetric analysis

VMD
USP
UV
 X_A
w/v
w/w

Volume median diameter
United States Pharmacopoeia
Ultraviolet
Orbital electronegativity
Weight per volume
Weight per weight

Abstract

INVESTIGATION AND OPTIMIZATION OF A SOLVENT / ANTI-SOLVENT
CRYSTALLIZATION PROCESS FOR THE PRODUCTION OF INHALATION PARTICLES

By: Swati Agrawal, M.S.

A dissertation submitted in partial fulfillment of the requirements for the degree of Doctor of
Philosophy at Virginia Commonwealth University.

Virginia Commonwealth University, 2010

Major Director: MICHAEL HINDLE, Ph.D., Associate Professor, Department of Pharmaceutics

Dry powder inhalers (DPIs) are commonly used to deliver drugs to the lungs. The drug particles used in these DPIs should possess a number of key properties. These include an aerodynamic particle size $< 5\mu\text{m}$ and particle crystallinity for long term formulation stability. The conventionally used micronization technique to produce inhalation particles

offers limited opportunities to control and optimize the particle characteristics. It is also known to induce crystalline disorder in the particles leading to formulation instability. Hence, this research project investigates and optimizes a solvent/anti-solvent crystallization process capable of directly yielding inhalation particles using albuterol sulfate (AS) as a model drug. Further, the feasibility of the process to produce combination particles of AS and ipratropium bromide monohydrate (IB) in predictable proportions and in a size suitable for inhalation is also investigated.

The solvent / anti-solvent systems employed were water / ethyl acetate (EA) and water / isopropanol (IPA). Investigation and optimization of the crystallization variables with the water / EA system revealed that particle crystallinity was significantly influenced by an interaction between the drug solution / anti-solvent ratio (R_a ratio), stirring speed and crystal maturation time. Inducing a temperature difference between the drug solution and anti-solvent ($T_{\text{drug solution}} > T_{\text{anti-solvent}}$) resulted in smaller particles being formed at a positive temperature difference of 65°C. IPA was shown to be the optimum anti-solvent for producing AS particles (IPA-AS) in a size range suitable for inhalation. *In vitro* aerosol performance of these IPA-AS particles was found to be superior compared to the conventionally used micronized particles when aerosolized from the Novolizer®.

The solvent / anti-solvent systems investigated and optimized for combination particles were water / EA, water / IPA, and water / IPA:EA 1:10 (w/w). IPA was found to be the optimum anti-solvent for producing combination particles of AS and IB with the smallest size. These combination particles showed uniform co-deposition during *in vitro* aerosol performance testing from the Novolizer®. Pilot molecular modeling studies in conjunction with the analysis of particle interactions using HINT provided an improved understanding of the possible interactions between AS and IB within a combination particle matrix.

CHAPTER I

INTRODUCTION

I.A Significance and background

The purpose of this thesis was to investigate and optimize a solvent / anti-solvent crystallization process as a single-step particle engineering technique to produce drug particles with suitable characteristics for inhalation without the need for further size reduction. In order to do so, albuterol sulfate (AS) was chosen as a model drug. Furthermore, it was the purpose to extend this crystallization process to produce combination particles of albuterol sulfate and ipratropium bromide monohydrate (IB) in predictable fixed ratios with a size suitable for inhalation. In addition, *in silico* molecular modeling tools were used to study the interactions between albuterol sulfate and ipratropium bromide (IB) in these combination particles. In this chapter, a review of particle engineering for pulmonary drug delivery will discuss the desirable characteristics of inhalation particles for dry powder formulations, the disadvantages of micronization as a size reduction technique, alternative particle engineering techniques and the solvent / anti-solvent crystallization as a potential particle engineering process. In addition, the rationale for using combination therapy for the treatment and maintenance of asthma and the use of molecular modeling tools to investigate the interactions between two drugs in a combination particle matrix will also be discussed.

I.A.1 Dry powder formulations for pulmonary drug delivery

Dry powder formulations are becoming increasingly popular for pulmonary drug delivery. The drug particles constitute a principle component of these dry powder formulations. These drug particles are usually present in a micronized form either alone or more commonly as a binary mixture with large carrier particles. Lactose monohydrate is a typically used carrier in these dry powder formulations. The formulation is delivered by means of devices known as dry powder inhalers (DPIs). The efficiency of a dry powder formulation is usually characterized by some critical features. One of these features is the emitted dose (ED) which indicates the amount of drug that comes out from the device. This is important to characterize since it is only this mass of drug that is available for deposition. Another important feature is the fine particle fraction (FPF) which represents the fraction of drug $< 5.0 \mu\text{m}$ in aerodynamic diameter. The FPF denotes the dispersivity of the drug.

Pulmonary drug delivery from DPIs is a complex process and is influenced by the dry powder formulation, the device characteristics, and patient factors such as inhalation flow rate and breathing pattern. The dry powder formulation should possess certain desirable characteristics. These include a high ED, and a high FPF. Ideally, these factors should be independent of the inhalation flow rate. The drug particle characteristics such as the aerodynamic diameter, interparticulate interactions, particle morphology, and solid state form and structure significantly influence the efficiency of the dry powder inhalation system by influencing the emitted dose and the fine particle fraction.

I.A.1.1 Influence of drug particle characteristics on emitted dose

The emitted dose is significantly influenced by the size of the particles. For efficient lung delivery, the drug particles should possess an aerodynamic diameter ranging from 2.5-6.0 μm (Pritchard et al., 2001). Additionally, they should have a narrow particle size distribution (PSD) (Shekunov et al., 2003; Shekunov et al., 2004). The aerodynamic diameter, d_A , is defined as the diameter of a sphere of unit density, which reaches the same velocity in the air stream as a non-spherical particle of arbitrary density (Chow et al., 2007). This diameter defines the mechanism of particle deposition in the respiratory system. It has been shown that the aerodynamic diameter (d_A) generally depends on the airflow (particle Reynolds number, Re) as well as the particulate properties (geometric size, shape and density) and can, therefore, be calculated numerically using semi-empirical models. The well-known relationship depicted by Eq. I.1 below, though strictly applicable only at the Stokes flow regime of $Re < 0.1$, can be used to estimate the aerodynamic diameter (Chow et al., 2007):

$$d_A \text{ (Stokes)} \approx d_V \sqrt{\rho/\chi\rho_0} \quad \text{Equation I.1}$$

where d_V is the volume-equivalent diameter, ρ_0 is the unit density (of spherical calibration spheres), ρ is the particle density and χ is the dynamic shape factor, defined as the ratio of the drag force on a particle to the drag force on the particle volume-equivalent sphere at the same velocity. Thus d_A can be reduced by one or more of the following manipulations:

- (a) Decreasing the volume-equivalent particle diameter (d_V)
- (b) Reducing the particle density (ρ)
- (c) Increasing the particle dynamic shape factor (χ)

Traditionally, reduction of d_v has been carried out by micronization, usually by jet-milling. The small drug particles produced by micronization possess poor bulk flow properties and are cohesive particularly when present as a drug only formulation (Crowder et al., 2006; Rehman et al., 2004). The small size brings about particle cohesion by reducing the interparticulate distances. This results in an increase in Van der Waals forces of interaction thereby making the powders stick together as clumps and adversely affecting their flowability (Terzano and Colombo, 1999). The emitted dose of a powder is a function of its flow properties with better flowing powders exhibiting improved device emptying (Terzano and Colombo, 1999; Chow et al., 2007; Iida et al., 2001). Further, these small inhalation particles produced by micronization are also generally cohesive due to electrostatically charged surfaces produced during the milling process, filling and device manipulation (Terzano and Colombo, 1999; Chow et al., 2007; Louey et al., 2006; Danniher and Zhu, 2008; Iida et al., 2001). Electrostatically charged surfaces are subject to Coulombic forces of interaction and it has been suggested in the literature that such interactions are comparable in strength to the Van der Waals forces (Chan, 2006; Keil et al., 2006). The emitted dose is strongly and negatively influenced by the electrostatic deposition in the inhalers and on the mouthpieces (Chan, 2006).

Due to the poor flow properties of micronized inhalation particles when present as drug only formulations, a common practice is to blend the small drug particles with large carrier particles. Addition of large (50-100 μm) carrier particles in the form of lactose results in an increase in the interparticulate distances which therefore reduces the Van der Waal's forces making the particles less cohesive (Danniher and Zhu, 2008; Chow et al., 2007; Iida et al., 2001). The drug particles adhere to the surfaces of the carrier lactose particles. This adherence further reduces the cohesive forces between the drug-drug particles and promotes powder flow. The

improvement in powder flow for dry powder formulations of fluticasone propionate in the presence of lactose as a carrier has been studied by Louey et al. (2004). They employed measures of flowability such as the Carr's compressibility index calculated from tapped and bulk powder density and the vibrating spatula method to generate powder mass flow vs. time profiles. They showed an increase in powder flow with an increase in the lactose proportion in the dry powder formulation. Therefore, it is believed that the increase in emitted fraction in drug / lactose blend formulations is attributed to the role of lactose in promoting powder flow.

Apart from reducing the physical size of the particles by micronization, the aerodynamic diameter can also be reduced by reducing the particle density and increasing the dynamic shape factor. Decrease of both particle density and size is currently achieved by spray-drying (Platz et al., 2003, Edwards et al., 2003) or more recently, by spray-freeze drying (Shekunov et al., 2006, Shekunov et al., 2004, Truong-Lee et al., 2004, Shekunov et al., 2004). Theoretically, a smaller d_A can also be obtained with particles of non-spherical shapes, such as platelets, rods or fibers (Shekunov et al., 2003, Shekunov et al., 2006, Chan et al., 1995, Crowder et al., 2002), because the χ value for such particles can be as high as 10 (Shekunov et al., 2006). In terms of aerodynamic performance, changing the ruggedness of particle surfaces, as quantified by the surface fractal dimension (Shekunov et al., 2006, Chan et al., 2006), is analogous to a simultaneous reduction of the particle density and increase of the dynamic shape factor. The shape of the drug particles also influences their flow properties and hence the emitted dose. Spherical particles tend to pack more closely together compared to acicular particles. The closer packing leads to a decrease in the Van der Waals forces and makes these spherical particles more cohesive and therefore adversely affects their flow properties.

I.A.1.2 Influence of drug particle characteristics on fine particle fraction

FPF represents the mass fraction of the aerosol less than 5.0 μm and is considered to be respirable. This denotes the ability of the particle agglomerates to disperse into discrete individual particles during aerosolization. FPF is also influenced by the drug particle characteristics. The size of the particles has a significant influence on particle dispersivity in both drug only and drug / lactose formulations. Small micronized drug particles have a tendency to form agglomerates with each other in drug only formulations. These agglomerates need to be broken down into primary particles during aerosolization for a high FPF. Even though the primary size of these micronized particles is small, high cohesion leads to a reduction in their FPF. In drug / lactose blends, lactose particles possess active sites to which the small micronized drug particles adhere (Chow et al., 2007). These micronized particles have surfaces with high energy as a function of the micronization process and therefore adhere strongly to the lactose particles. The strong adherence will lead to reduced dispersion and hence reduce the FPF for these micronized drug particles. Particle morphology also influences the FPF. Acicular particles tend to adhere less strongly to the lactose surface due to the reduced surface area of contact available compared to spherical or plate-like particles (Louey et al., 2004).

Particle dispersibility is promoted by a large volume, low bulk density, and irregular particle morphology, all of which prevent close packing between the particles and hence hinder aggregation. Techniques such as spray drying utilize the concept of preparing porous particles with large volume and low bulk density and hence better dispersibility. The low powder bulk density has been observed for some non-spherical irregular particles produced by supercritical fluid (SCF) precipitation (Shekunov et al., 2003) and this may partially explain their enhanced performance.

I.A.1.3 Desirable attributes for a dry powder formulation

Based on the above attributes, a formulation intended for efficient pulmonary delivery should possess the following optimal characteristics: narrow aerodynamic particle size range, low surface energy and charge, non-spherical morphology, and low density or high porosity. The physical stability and solid-state structure of particles need to be considered in conjunction with their aerodynamic performance. It is preferred to use crystalline drug substances compared to their amorphous counterparts since crystalline substances are more stable and hence less prone to potential changes associated with solid-state transitions. Crystalline particles are typically non-spherical, have low-energy surfaces and are stable thermodynamically; however, they have a relatively high particle density and tend to pack more tightly with a high tapped bulk density. These properties, therefore, reduce the aerodynamic performance due to reduced dispersibility.

I.A.2 Rationale for using combination therapy for the treatment and maintenance of asthma

Apart from β_2 agonists, there are a number of other classes of compounds such as the corticosteroids and anticholinergics that are also used for the treatment and maintenance of asthma. All these compounds have different mechanisms of action. Both β_2 agonists and anticholinergics function as bronchodilators. However, they do so by different mechanisms. While β_2 agonists activate adenylyl cyclase and stimulate the production of cyclic adenosine 3',5'-monophosphate (AMP) thereby reducing intracellular calcium concentrations; anticholinergics competitively inhibit muscarinic cholinergic receptors and produce bronchodilation (Schreck et al., 2006). There have been numerous studies to investigate the impact of adding an anticholinergic such as ipratropium bromide to β_2 agonist therapy. These studies have proven

greater therapeutic benefit when the two classes of drugs are given together compared to treatment with a single class alone (Bryant et al., 1985, Ward et al., 1985).

In order to take advantage of the greater therapeutic benefit offered by synergistic therapy with β_2 agonists and anticholinergics, formulations containing the two of them together have been introduced. One such formulation is the Combivent[®] pMDI (Boehringer Ingelheim, Ridgefield, CT) - a microcrystalline suspension of albuterol sulfate (AS) and ipratropium bromide (IB) in a nominal ratio of 6:1 prepared in a blend of CFC propellants (Combivent Package Insert). This product has however, now been withdrawn from the market due to the inability of the manufacturers to manufacture it as a CFC-free formulation (Calderdale and Huddersfield). There are numerous processing difficulties associated with formulating these physical mixtures of micronized powders. Differences in the initial particle size distributions of the two powders and a tendency for segregation of the mixture into its individual components are well known (Nelson et al., 2003; Taki et al., 2006). These issues lead to variations in the intended drug ratio.

In this regard, combination particles containing fixed proportions of the two components may offer significant advantages. In order to investigate this potential, Jin et al. used a cooling crystallization process to produce combination particles of albuterol sulfate and ipratropium bromide in a nominal 6:1 (w/w) ratio (Jin et al., 2006). These particles, however, were too large for inhalation and required micronization to reduce their particle size to the inhalation size range. Formulation of these particles in a DPI (Dryhaler) and its *in vitro* aerosol performance testing revealed co-deposition of AS and IB compared to the commercial Combivent[®] pMDI.

I.B Particle engineering for inhalation particles

I.B.1 Micronization

Micronization or milling is the most commonly used technique to produce particles for use in marketed inhaler formulations. Such particles are initially produced by batch crystallization, followed by filtering, drying and are then micronized. The particle size reduction can be achieved by pressure, friction, attrition, impact, or shear. Vibration milling, ball milling and, in particular, jet-milling (fluid energy) are well-established and well-validated techniques used to manufacture dry powders for inhalation. In the jet-milling process, the starting material undergoes many impact events before a significant quantity of the required particle size fraction is achieved and separated from the larger particles by inertial impaction. This classification ensures that the particle size required for respiratory delivery is eventually obtained. The characteristic particle shape is either tabular or rounded leading to close packing between the milled particles (Shekunov et al., 2004). Micronization is also notorious for inducing electrostatic charge on the particle surface, which renders the milled material both cohesive and adhesive (Crowder et al., 2006; Rehman et al., 2004). Generation of amorphous domains renders the material unstable and prone to undergo recrystallization leading to crystal growth on the milled particle surface and formation of solid bridges between the particles. The material is then also prone to chemical decomposition and water sorption (Ward and Schultz, 1995; Pfeiffer et al., 2003). All these physical and chemical changes are highly undesirable, and can adversely affect the *in vitro* and *in vivo* performance of the respiratory formulations (Berard et al., 2002, Rasenack et al., 2004). Therefore, although micronization is a simple and convenient technique for size reduction, it is by nature a disruptive process and provides only limited opportunities to manipulate and control the particle characteristics. Therefore, it is desirable to develop alternate

particle engineering techniques capable of producing particles in a size range suitable for inhalation without the need for further size reduction.

I.B.2 Alternate particle engineering techniques for producing inhalation particles

I.B.2.1 Sonocrystallization

Sonocrystallization is the application of power ultrasound to the crystallization process and has shown potential for controlling the physical characteristics of the crystalline products. Sonocrystallization is predominantly utilized to bring about controlled nucleation in a crystallization process and to slow down crystal growth thereby resulting in small particles. Ultrasound induces nucleation by acoustic cavitation by creating areas of high and low pressure (Thompson et al., 1999). On implosion of the cavitations, areas of extremely high pressure and temperature are created over a short time interval. This process may induce an increase in the diffusion of the drug molecules and a concomitant decrease in the activation energy barrier for the formation of a stable nucleus or nuclei for crystal growth (Thompson et al., 1999). Variations in the amplitude and frequency of the ultrasonic energy may further control the rate of nucleation and crystal growth. Using ultrasound to generate nuclei in a reproducible way provides a well-defined start point for the crystallization process, and allows the developer to focus on controlling the crystal growth for the remainder of the residence time in the crystallizer. Using sonocrystallization, Dennehy et al. reported the formation of significantly smaller crystals of a drug substance relative to batch crystallization (Dennehy et al., 2003). Using an optimized sonocrystallization technique, Dhumal et al. reported the formation of AS particles with VMDs of $1.6 \pm 0.1 \mu\text{m}$ (Dhumal et al., 2009). They also incorporated a spray drying step in their process wherein the solvent / anti-solvent suspension containing the precipitated AS particles was spray

dried. Using these particles, the authors reported an emitted fraction of $74.6 \pm 1.4 \%$ and a % FPF of $44.2 \pm 1.3 \%$ expressed as a percentage of the nominal dose when tested from the Rotahaler at a flow rate of 28.3 L/min. These aerosol performance characteristics were significantly improved relative to micronized albuterol sulfate.

Kaerger et al. have utilized sonocrystallization in combination with solution atomization to develop a technique known as solution atomization and crystallization by sonication (SAXS) (Kaerger and Price, 2003). In this technique, the drug solution is atomized into solution droplets and added to an anti-solvent with an immersed ultrasonic probe. The authors claim that control of final particle size is achieved by modifying the initial atomized droplet size and sonication conditions to induce nucleation. Using this technique, they reported the formation of spherical particles in the inhalation size range. SAXS has also been used to produce combination particles of different anti-asthmatic compounds. Using this technique, Shur et al. have produced combination particles of fluticasone propionate and salmeterol with a VMD of $4.7 \pm 0.01 \mu\text{m}$ (Shur et al., 2006). The *in vitro* aerosol performance was tested by preparing a 1.6 % w/w blend with lactose which was aerosolized using the Monohaler. Results indicated significantly smaller emitted dose fractions for the combination particles compared to micronized powders. However, the % FPF for the two drugs was higher when tested as combination particles ($10.7 \pm 0.3\%$ for fluticasone propionate; $11.6 \pm 1.1\%$ for salmeterol) compared to a physical mixture of micronized drugs ($7.9 \pm 0.5\%$ for fluticasone propionate; $6.7 \pm 0.5\%$ for salmeterol). Pitchayajittipong et al. have also reported the formation of combination particles of budesonide and formoterol with a VMD of $4.17 \pm 0.04 \mu\text{m}$ using the SAXS technique (Pitchayajittipong et al., 2009). Using a 1.6% w/w drug / lactose blend in the Cyclohaler, a higher % FPF for the combination particles ($21.78 \pm 1.4 \%$ for Budesonide; $14.19 \pm 0.92 \%$ for formoterol) compared

to a physical mixture of micronized drugs (14.75 ± 0.63 % for Budesonide; 6.19 ± 1.87 % for Formoterol) was reported. However, these results showed a large difference in the % FPFs of the two drugs formulated in the combination particles indicating non-uniform deposition upon aerosolization. The authors attributed this difference to mechanical disruption of particles upon blending with lactose. They also report that upon formulating these particles in pMDIs, fine particle delivery of both drugs was similar. Although sonocrystallization appears to be a simple process for producing inhalation particles comprised of a single drug, its utility in producing fixed ratio combination particles that aerosolize to produce uniform co-deposition does not appear to be well established.

I.B.2.2 Spray drying

Spray drying (SD) is a popular particle engineering technique owing to its relative simplicity, availability of large scale equipment, and ease of operation. A typical SD process consists of four steps (Master et al., 1991):

- (a) Atomization of feed solution into a spray
- (b) Spray-air contact involving flow and mixing
- (c) Drying of sprayed droplets at elevated temperatures
- (d) Separation of dried product from the air.

For each of these operating steps, a wide variety of process designs are available, depending on specific applications. To modify or optimize the particulate product characteristics, advantages can be taken of the operating parameters of the SD process such as atomization pressure, feed properties, feed rate, airflow and drying temperature (inlet or outlet) (Master et al., 1991). For particle size control, the plain-jet air-blast atomizer offers the advantage of generating smaller

initial droplet size over ultrasonic atomizer, thus yielding particles within the respirable size range (Dunbar et al., 1998). Control of particle shape/morphology can be gained by varying the feed solvent (Gilani et al., 2005) or adjusting the outlet drying temperature (Maa et al., 1997). Both feed concentration and atomization rate can be concomitantly manipulated to generate particles with different degrees of surface corrugation (Chew et al., 2005). Common excipients such as lactose and polysorbate 20 (Tween 20) can also be added to the feed solution to yield particles with rougher surfaces (Maa et al., 1997).

Using the spray drying process, combination particles of albuterol sulfate and ipratropium bromide have been produced (Corrigan et al., 2006). These particles were spherical and ranged in size from 0.2-4.8 μm . However, these particles were amorphous in nature. Production of amorphous products is a common disadvantage associated with the spray drying process. Although there are advantages of increased dissolution and bioavailability associated with amorphous substances, they are relatively unstable compared to their crystalline counterparts. This instability might lead to recrystallization, crystal bridging and a subsequent increase in particle size thereby nullifying the earlier particle engineering efforts to generate small inhalation sized particles.

I.B.2.3 Supercritical fluid technologies

Supercritical fluid (SF) technology is considered to be an innovative and promising way to produce inhalation particles. A supercritical fluid is any substance at a temperature and pressure above its critical point. Of all the gases available for use as SFs, carbon dioxide is the most widely used because of its low critical temperature (31.1°C), which makes it particularly

suitable for heat sensitive materials. Broadly speaking, supercritical fluid crystallization technologies can be divided into two categories (Tong et al., 2006):

Firstly, precipitation from supercritical solutions, for example, the rapid expansion of supercritical solution (RESS). The drug is first dissolved in the SF to form a solution, which is then allowed to undergo expansion through an orifice to create extremely high supersaturation. This induces homogeneous nucleation and subsequent particle formation in the precipitation unit. This method relies on the fact that drug solubility can be reduced drastically by decreasing the SF density through the rapid expansion of the fluid. Primary factors influencing the particle properties include the drug solubility in SF, the dimensions of orifice, expansion time scale, and the operating pressure/temperature in the precipitator.

Secondly, precipitation using SFs as non-solvents or anti-solvents, for example, gas anti-solvent (GAS), supercritical anti-solvent (SAS), precipitation with compressed anti-solvents (PCA), aerosol spray extraction system (ASES), and solution enhanced dispersion by supercritical fluids (SEDS) (Tong and Chow, 2006). These methods utilize a similar concept to the use of anti-solvents in traditional solvent-based crystallization processes. The relatively low solubilities of drugs in carbon dioxide are used in this process. Initially, the drug is dissolved in a conventional organic solvent to form a solution. The drug is virtually insoluble in dense carbon dioxide while the solvent is completely miscible with dense carbon dioxide at the crystallization temperature and pressure (Subramaniyam et al., 1997). The solute is crystallized from solution in one of the three ways discussed below.

In the first method, the volume of the solution containing the drug is expanded several fold by mixing with dense carbon dioxide in a vessel. Since the expanded carbon dioxide solvent has a lower solvent strength than the pure solvent, the mixture becomes supersaturated, forcing

the solute to precipitate or crystallize as microparticles. This process is termed gas anti-solvent (GAS) recrystallization (Gallagher et al., 1989). Sodium cromoglycate has been synthesized using this technique (Jaarmo et al., 1997).

The second method involves spraying the drug solution through a nozzle as fine droplets into compressed carbon dioxide. This process is commonly known as the 'precipitation with compressed anti-solvent' (PCA) technique and employs a supercritical fluid as the anti-solvent (Dixon et al., 1993). Examples of PCA processed materials are indomethacin (Bodmeir et al., 1995), methylprednisolone acetate and hydrocortisone acetate (Schmitt et al., 1995). When a supercritical fluid is used as anti-solvent, the spray process is termed as 'supercritical anti-solvent' (SAS) process or 'aerosol spray extraction system' (ASES) (Subramaniam et al., 1997).

The third method, known as 'solution enhanced dispersion by supercritical fluids' (SEDS), utilizes a coaxial nozzle design with a mixing chamber. In this arrangement the drug in the organic solvent interacts and mixes with the SF anti-solvent in the mixing chamber of the nozzle prior to dispersion via a restricted orifice into a particle-formation vessel (York et al., 1999). High mass transfer rates are achieved with a high ratio of SF to solvent, and high velocity of the SF facilitates break up of solution feed (York et al., 1999). Using this technique, albuterol sulfate particles with a mass median diameter of 7.5 μm have been reported by Najafabadi et al. (Najafabadi et al., 2005).

I.B.2.4 Controlled precipitation techniques

Controlled precipitation utilizes the crystallization process to produce inhalation sized particles in a number of ways. One of the techniques is referred to as *in situ* micronization and employs crystal growth inhibitors in the crystallization medium. These crystal growth inhibitors

limit the growth of crystals by adsorbing onto the surface of the formed particles and blocking the passage of other drug molecules thereby limiting deposition of further drug molecules on the preformed particles and hence controlling size (Rasenack et al., 2002). Commonly used crystal growth inhibitors are polymeric in nature such as hydroxy propyl methyl cellulose (HPMC), and methyl cellulose. Beclomethasone dipropionate, budesonide, triamcinolone acetate and indomethacin crystals in the inhalation size range of 1-5 μm have been produced using this technique (Rasenack et al., 2002). However, this method is very specific for the drug and polymer for which it is developed and cannot be generalized for other drugs without carrying out a new development process. Furthermore, the crystal growth inhibitors are adsorbed to the surface of the formed particles. None of the polymers used thus far has proven lung safety records and hence such particles with appreciable levels of polymers on their surface cannot be used for lung delivery.

Another technique is the high gravity controlled anti-solvent precipitation. This technique utilizes solvent / anti-solvent precipitation in a high gravity controlled precipitator (HGCP). The HGCP is basically a rotating packed bed in which two liquid streams can be fed via distributors and mixed into the centre of a packed bed, which is subjected to high gravity due to centrifugal force. This causes the mixture to flow through the packing before leaving the reactor (Chiou et al., 2007). Due to high centrifugal force, the liquid stream is subjected to high stress and breaks into ribbons affording intense mixing between the drug solution and the anti-solvent which leads to very high levels of supersaturation and produces particles with a small particle size. Albuterol sulfate crystals with a VMD ranging from 2.2-4.8 μm were produced using this process (Chiou et al., 2006).

I.C. Solvent / anti-solvent crystallization

There are a number of particle engineering techniques for the formation of particles for respiratory drug delivery. However, most of these techniques are either complex with special equipment needs, and/or difficult to scale up. Solvent / anti-solvent crystallization as a particle engineering technique offers attractive benefits. The principle of solvent / anti-solvent crystallization is rapid precipitation by generation of high supersaturation levels leading to the formation of small crystals. However, because of its rapid nature, it is difficult to control the particle characteristics of products formed from this technique. This has led to the use of additional growth control methods such as the use of growth inhibitors or ultrasound. It would be advantageous to develop a simple solvent / anti-solvent crystallization process that controls particle size through hydrodynamic factor optimization alone. In order to do so, it is important to understand the mechanism of solvent / anti-solvent crystallization and the influence of critical processing variables on particle characteristics for controlling the final product.

I.C.1 Theory of solvent / anti-solvent crystallization

Crystallization is defined as a phase change that results in the formation of a crystalline solid (Myerson, 1999). The most common type of crystallization is crystallization from solution, in which a drug is dissolved in a solvent and crystallization is induced by changing the state of the system in some way that reduces the solubility of the drug. In solvent / anti-solvent crystallization, this reduction in solubility is achieved by an anti-solvent. The kinetic process of crystallization involves two main steps: nucleation and crystal growth and the properties of the formed particles are determined by them.

I.C.1.1 Driving force for crystallization

Figure I.1 shows the schematic solubility/super solubility diagram.

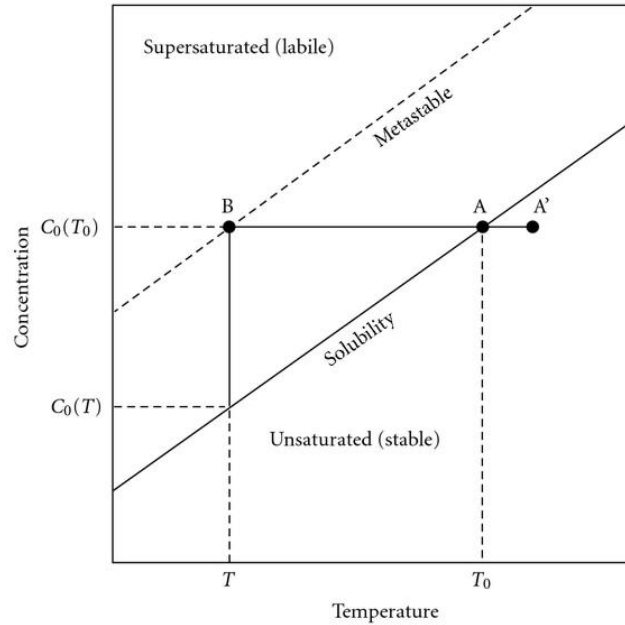


Figure I.1 Schematic solubility diagram

Crystallization can take place over the concentration range limited by the equilibrium composition of the system at specified conditions. Thermodynamic equilibrium refers to the solutions saturated with respect to the solute (i.e., the concentration of the solution represents the solubility value for that solid phase); the rates of dissolution and crystallization are equal under these conditions. A solution with solute concentration below the saturation limit (shown by solid line) is termed under-saturated and existing crystals will dissolve. In order for crystallization to occur, the system must be brought into a non-equilibrium state where the concentration of the solute exceeds its equilibrium concentration (i.e., the solution is supersaturated). The driving force for crystallization is therefore the degree of supersaturation, expressed as the difference in concentration between the supersaturated and saturated solutions. The most common methods to

create supersaturation in a solution include temperature change, solvent evaporation, chemical reaction, pH change, and alteration in solvent composition. The metastable limit (dashed line) defines the compositions at which spontaneous crystallization occurs and the region bounded by the solubility curve and the metastable limit is termed metastable zone. The metastable zone width (MSZW) depends on purity of the system, thermal history of solution and density of foreign particles present in the solution and is of practical importance since it defines the working area for designed crystallizations (Beckmann, 2000).

I.C.1.2 Nucleation

Nucleation involves the aggregation of dissolved molecules in the supersaturated solution into organized clusters (embryos) thus developing a surface that separates them from the environment. This nucleation process can be split into two main categories (Zettlemoyer, 1969; Mullin, 2001): (1) primary nucleation, when no crystals are initially present in the solution, and (2) secondary nucleation, when crystals of the solute are already present or are deliberately added to the solution as seeds. Primary nucleation is further classified into homogeneous nucleation, which occurs spontaneously in bulk solutions, and heterogeneous nucleation, which is induced by foreign particles. Homogeneous nucleation rarely occurs in large volumes (greater than 100 μ l), as most solutions contain random impurities which may induce nucleation (Perepezko, 1994; Gunton, 1999). Although heterogeneous and/or secondary nucleations are commonly encountered in practice, homogeneous nucleation forms the basis for classical nucleation theory. Metastable zone widths (MSZW) with respect to nucleation type are schematically shown in Figure I.2.

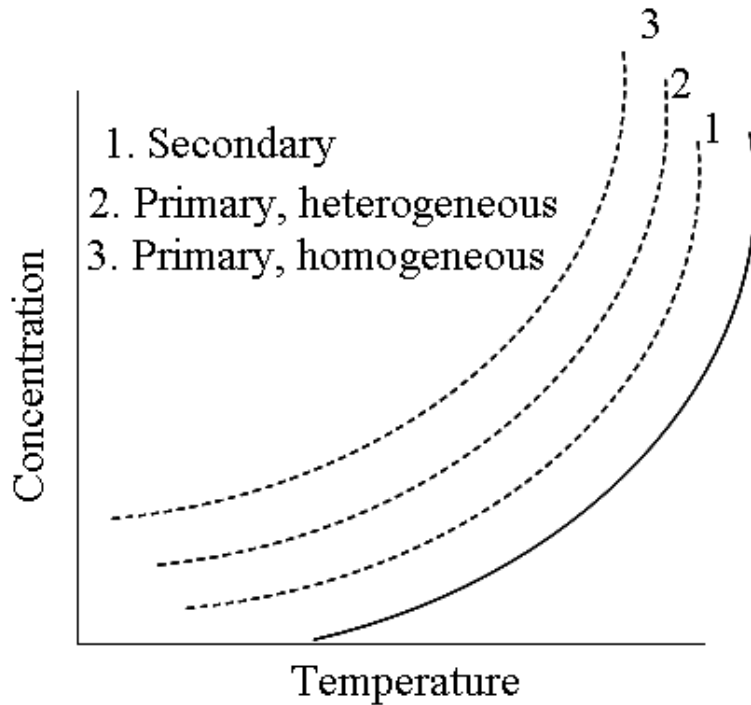


Figure I.2 Schematic diagram showing metastable zone width with respect to nucleation type

It is observed that the MSZW is narrowest for secondary nucleation and increases successively for primary heterogeneous and primary homogeneous nucleation. This is because the energy barrier to induce nucleation is smallest for secondary nucleation since seeds are already present to act as embryos. For primary homogeneous nucleation, this energy barrier is highest since nucleation has to occur by spontaneous fluctuations in solvent density and composition (Mullin, 2001; Mersmann, 2001).

I.C.1.2a Classical nucleation theory

Classical nucleation theory (Volmer, 1939; Gibbs, 1948; Nielsen, 1964) was originally derived for the condensation of vapor into liquid and has been extended to crystallization from solutions. According to this theory, the free energy change (ΔG_{total}) for a cluster undergoing a phase transition is given by

$$\Delta G_{\text{total}} = \Delta G_{\text{surface}} + \Delta G_{\text{volume}}$$

where ΔG_{volume} is a volume free energy term that is proportional to the cube of the radius and favors aggregation of molecules. $\Delta G_{\text{surface}}$ is a surface free energy term that is proportional to the square of the radius of the cluster and favors the dissolution of molecular clusters. Thus for a small radius, r , where the positive surface energy predominates, the nucleus is unstable and tends to dissolve. Eventually, the cluster attains the critical size ($r = r_c$) at which the surface term and volume term exactly balance. At this point the total free energy of the cluster attains a maximum, which corresponds to the activation free energy of nucleation (ΔG^*) as shown in Figure I.3.

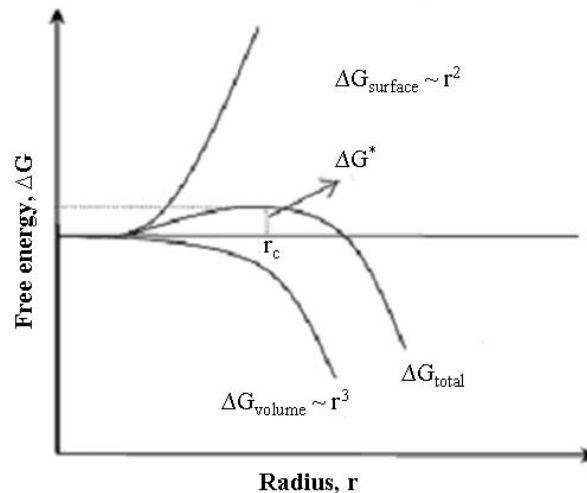


Figure I.3 Schematic plot of Gibbs free energy change (Mullin, 2001) (Reproduced with permission from Elsevier)

Supersaturation is required to overcome the free energy barrier to nucleation. After this stage, the cluster becomes viable and is termed a nucleus, which eventually grows into a crystal. For a polymorphic system, the polymorph that nucleates first is thought to come from the cluster that exhibits the fastest growth rate as a result of its lowest free energy barrier to nucleation. However, the nature of the polymorph that eventually crystallizes is determined by the combination of the relative nucleation rates and the relative crystal growth rates of the

polymorphs (Bernstein et al., 1999). Recent theoretical and experimental evidence however suggests that the classical nucleation theory may not be qualitatively correct (Oxtoby, 1998; Davey et al., 2002; Vekilov, 2004; Parveen et al., 2005). The latest studies suggest that nucleation of solutes from solution is a two-step process (Wolde and Frenkel, 1997; Galkin and Vekilov, 2000; Vekilov, 2004; Chattopadhyay et al., 2005): the creation of a droplet of a dense liquid, metastable with respect to the crystalline state, followed by ordering within this droplet to form a three-dimensional lattice structure.

I.C.1.3 Crystal growth

Once formed, nuclei begin to grow larger through the addition of solute molecules to the crystal lattice, and this stage of the crystallization process is known as crystal growth. Crystal growth is a multi-step process (Rodríguez-Hornedo and Murphy, 1999, Davey and Garside, 2000), which includes (1) transport of a growth unit (a single molecule, atom, ion, or cluster) from or through the bulk solution to an impingement site, which is not necessarily the final growth site (i.e. site of incorporation into the crystal); (2) adsorption of the growth unit at the impingement site, (3) diffusion of the growth units from the impingement site to a growth site, and (4) incorporation into the crystal lattice. Desolvation of the growth unit may take place anywhere in steps 2–4 or the solvent may be adsorbed with the growth unit. The relative importance of each step depends on the surface structure of the crystals and the properties of the solution (Meenan et al., 2002). Based on their ability to capture arriving growth units, three types of crystal surfaces (and thus growth sites created by these surfaces) can be differentiated (Hartman and Perdock, 1955): kink, step and flat faces, which provide three, two and one surface bond(s), respectively (Figure I.4)

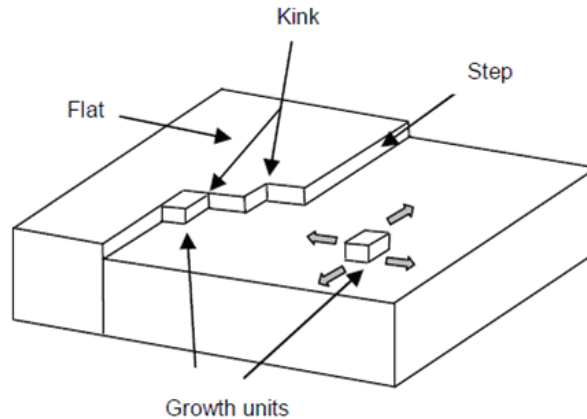


Figure I.4 A three dimensional crystal surface showing three types of growth sites (Mullin, 2001) (Reproduced with permission from Elsevier)

Assuming the linear relationship between a face growth rate and the total binding energy of a growth unit to the surface, the final shape of a crystal is defined by the slowest growing flat faces. Crystal growth theories are therefore concerned with the mechanisms by which these faces grow.

I.C.1.3a Crystal growth theories

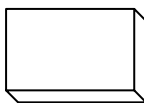
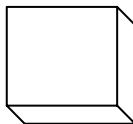
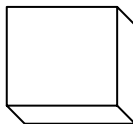
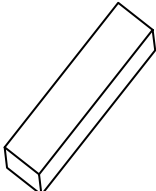
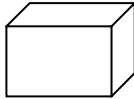
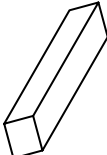
The possible pathways by which a growth unit passes from solution to become integrated into the crystal lattice are known as growth mechanisms. Two mechanisms are considered to be important for the actual process of growth on crystal faces – two-dimensional (2-D) nucleation and screw dislocation (Davey and Garside, 2000). Two-dimensional nucleation, also called the Birth and Spread (B+S) model, occurs when nuclei at the crystal surfaces act as sources of steps that allow for the further incorporation of growth units (Volmer, 1922). This mechanism has gained popularity, since it is simple yet based on firm thermodynamic and kinetic principles. However, it mainly accounts for the crystal growth observed at high supersaturations (Rodríguez-Hornedo et al., 2006). An alternative mechanism suggested by Burton, Cabera and Frank (BCF) underlines the assumption that growth occurs by flow of steps across the surface (Burton et al., 1951). Screw dislocation, a common

crystal defect formed when one region of the crystal is pushed up through one (or more) unit cells relative to another region, can be an infinitive source of these steps, onto which oncoming growth units can be incorporated. Since screw dislocations exist on crystal faces at low supersaturation levels, the model suggest that the growth can take place under realistic conditions.

I.C.1.4 Crystal morphology

At equilibrium, the external shape of a crystal, also termed habit, form or morphology, is determined by its internal structural symmetry. In practice, crystal morphology is usually described in terms of length, width and thickness. Within the pharmaceutical industry the classifications of crystal shapes adopted by either British Standard (BS 2955:1993) or the US Pharmacopoeia (monograph 776) (Table I.1) are commonly used for routine microscopical examination of solid materials.

Table I.1 Crystal Morphologies for pharmaceutical solids

Equant	Crystals with similar length, width, and thickness		
Flakes	Thin, flat crystals of similar width and length		
Plates	Flat, tabular crystals with similar width and length but thicker than flakes		
Laths	Elongated, thin, and blade-like crystals		
Needles	Acicular, thin, and highly elongated crystals having similar width and breadth		
Columnar	Elongated, prismatic crystals with greater width and thickness than needles		
			

Experimentally obtained crystals however exhibit a growth habit since the crystal growth is a non-equilibrium process. The equilibrium form can be achieved through an aging process, which

involves solvent mediated dissolution and regrowth of the crystal faces equilibrated in a saturated solution over time (Stranski and Honigmann, 1950; Saska and Myerson, 1987).

I.C.1.5 Role of different crystallization variables on particle characteristics

In order to efficiently use the solvent / anti-solvent crystallization process to yield particles with desirable and reproducible characteristics, it is important to understand the effect of different crystallization variables. Literature has predominantly focused on the effect of crystallization variables on particle size. There are reports by O'Grady et al about the effect of anti-solvent addition location, addition rate and stirring speed on particle size of benzoic acid crystals wherein the authors have reported a parabolic relationship of particle size with stirring speed in conjunction with the addition location (O'Grady et al., 2001). When the anti-solvent is added close to the impeller, an increase in agitation intensity results in a narrower MSZW, possibly due to the increased probability of contact between solute molecules. When the anti-solvent is added close to the wall, an increase in agitation results in a wider MSZW and a significant improvement in the batch-to-batch repeatability (O'Grady et al., 2001). These results can be explained in terms of mixing conditions at each of the addition locations. Close to the impeller, mixing conditions allow for the rapid incorporation of the anti-solvent and a homogenous mixture of solution and anti-solvent. However, close to the wall, mixing conditions are less suitable and areas of supersaturation build up leading to narrower MSZWs and a reduction in the batch-to-batch repeatability. In this situation, when the agitation is increased, the local areas of supersaturation can be dissipated, to some degree, and the MSZW is wider and the batch-to-batch repeatability improves. Abdel-Al et al. (2004) have studied the effect of different supersaturation ratios on crystallization of calcium sulfate dehydrate. They have reported the

formation of large crystals at lower supersaturation ratios. Genoveva et al. (2007) have reported the effect of agitation speed on the particle size of $\text{Zr}(\text{HPO}_4)_2 \cdot \text{H}_2\text{O}$. They have described an increase in crystal size as a function of increasing agitation.

Monitoring of the crystallization process is necessary to understand the effects of different crystallization variables. The techniques employed have ranged from the traditional methods such as particle harvesting and characterization by powder X-ray diffraction, particle sizing methods, differential scanning calorimetry, isothermal microcalorimetry, and dynamic vapor sorption gravimetry. Newer real time in-situ monitoring techniques are now being used as part of the QbD initiative including focused beam reflectance measurement (FBRM) (Markande et al., 2007), attenuated total reflectance-fourier transform infra red (ATR-FTIR) (Yu et al., 2006; Barrett et al., 2005), Raman spectroscopy (Falcon et al., 2004), and ultrasound spectroscopy (Hipp et al., 2000). These online or *in situ* monitoring techniques have enabled high-throughput screening of the effects of crystallization variables and hence faster optimization of the crystallization process. Yu et al have used ATR-FTIR for the monitoring and control of solvent / anti-solvent crystallization of paracetamol from a water-acetone mixture (Yu et al., 2006). Using this technique, they have monitored the nucleation kinetics and have utilized feedback control for the addition of anti-solvent and have hence maintained constant supersaturation throughout the crystallization process thereby leading to a narrow particle size distribution. Penttila and co-workers have used fluorescence spectroscopy to monitor the solvent / anti-solvent crystallization of L-lysine monohydrochloride (Penttila and Berglund, 1996). Emission spectra have been recorded and intensity changes in the emission spectrum have been used to monitor the effect of anti-solvent addition rate on particle size distribution. The most commonly used *in situ* monitoring tool is the FBRM. This technique uses laser light to measure

the particle size distribution *in situ*. The particle size distribution is obtained as a chord length distribution which is obtained as a product of the time of backscattering of the laser beam from one edge of an individual particle to another and the scan speed. This *in situ* analysis of the particle size is very useful because it provides information on when to terminate the crystallization process. This technique can also detect the appearance of nuclei in the crystallization medium and can hence be used to determine the metastable zone width; and important crystallization parameter (Sheikhzadeh et al., 2008).

I.D. Molecular modeling

I.D.1 Molecular modeling as a tool to study interactions

The molecular modeling methods function on the principle of molecular mechanics, often referred to as the Force Field method. Molecular mechanics is the application of classical mechanics to molecules. Classical mechanics is used to describe the motion of macroscopic objects. In molecular mechanics, atoms are treated as spheres whose mass depends on the element. Chemical bonds are treated as springs whose stiffness depends on which elements are bound together and whether the bond is single, double or triple. Other types of springs are used to model changes in bond angles, and dihedral angles. Each of these springs will have spring constants associated with them. Experimental and theoretical methods are used to determine these parameters. Additional equations from classical physics, such as Coulomb's law are used to handle any electrostatic interactions present within a molecule. The sum of all energy terms that apply to a particular molecule are added together to give the "steric" or potential energy of the molecule. All the equations and associated parameters used to calculate each energy term are collectively called the force field.

In real molecules, there are forces present other than those between bonded atoms. There may be charges present that can repel or attract. Repulsions between non-bonded atoms that are close together in space might also occur. These forces may act to change bond angles or cause twisting around single bonds. To describe the energy of the system, all of the different types of applicable interactions need to be taken into account. The sum of the energy of all of these various components is the basis of a force field. A force field allows for calculation of all the forces on the system which in turn gives the energy of the system. There is an intimate connection between structure and energy and hence, molecular mechanics calculations always involve both. In order to find the structure or predict geometry, it is necessary to examine the energy to find where energy minima and hence the stable geometries exist.

I.D.2 SYBYL software

Sybyl is a software that employs the molecular mechanics principles to perform molecular modeling studies. It is a general molecular modeling program written by Tripos. SYBYL is a comprehensive computational tool kit for molecular design and analysis, with a special focus on the creation of new chemical entities. Sybyl provides essential construction and analysis tools for both organic and inorganic molecular structures. It employs molecular mechanics or the force field method to calculate the molecular geometry, energies and various other properties of the compound of interest (Tripos Bookshelf Force Field Manual 2006). A force field is used to calculate the interaction forces for both bonding (covalent) and non-bonding (Van der Waals and electrostatic) interactions for all the atoms in the molecule. The molecule can rotate, vibrate and translate in response to the inter- and intra-molecular forces acting upon it to attain its most favored conformation in space (Schlick 2000). Electrostatic point charges on

the atoms in a molecule drawn in Sybyl can be calculated using various empirical methods, one of them being the Gasteiger-Huckel method. In this method, the calculation of charges on the molecule is based on the relationship between the orbital electronegativity and the atomic charge given by equation I.1 (Tripos Bookshelf Force Field Manual 2006):

$$X_A = a_A + b_A \cdot Q + c_A \cdot Q^2 \quad \text{Equation I.1}$$

Where X_A = orbital electronegativity and is represented as a function of the total charge (Q) on an atom (A), and a_A , b_A and c_A are the coefficients of the quadratic equation based on the ionization potential and electron affinity of the atom.

The energy associated with a molecular model of a compound is a function of its atomic coordinates. Energy minimization needs to be carried out in Sybyl after a molecular model is constructed. In the process of energy minimization, the atomic coordinates of the constructed molecular model are iteratively changed until a minimum energy value relative to the energy associated with the initial set of atomic coordinates is obtained. The resulting atomic coordinates corresponding to the local energy minimum correspond to the favored structural conformation of the molecule in space (Tripos Bookshelf Force Field Manual 2006).

The properties of the molecules can be studied in vacuum. However, since in real practice, most of the interactions happen in a solvent system, the software offers three options to take into account the solvent effects in the study of molecular interactions. These include:

1. A distance dependent dielectric screening term in the force field to simulate the solvent screening effects on electrostatic charge

2. Implicit solvation of the molecule by adding a new term/terms to the force field to account for solvent effects
3. Explicit inclusion of solvent molecules in the calculation of the intermolecular forces (Tripos Bookshelf Force Field Manual 2006).

Sybyl has several inbuilt programs that allow the study of interactions between compounds. Two of these programs are discussed in the subsequent sections.

I.D.3 GOLD program

GOLD is a program for calculating the docking modes of small molecules in protein binding sites. It applies a genetic algorithm for generating ligand-docked poses and the results are scored by an empirical function based on interaction possibilities derived from atom-atom contact probabilities in the Cambridge Structural Database (CSD).

I.D.4 HINT! program for interaction classification and quantitative scoring

HINT! or the Hydrophobic Interaction is a program that uses the experimental data from solvent partitioning experiments between water and 1-octanol ($\text{LogP}_{o/w}$) for interaction classification and quantitative scoring. HINT was created to specifically include all non-covalent interactions. Hydrophobic and polar interactions, which are collectively referred to as hydrophobicity, between molecules in biologically important systems are empirically quantified. In this scheme, hydrophobic attractions between species include hydrogen-bonding, acid-base interactions, Coulombic attractions as well as hydrophobic interactions. All of these are related to solvent partitioning phenomena because the dissolution of a ligand in a mixed solvent system (such as water/1-octanol) involves the same fundamental processes and atom-atom interactions

as biomolecular interactions within or between proteins and ligands. HINT scores each atom-atom interaction, within or between the molecules with the following equation (Kellogg et al., 2000):

$$b_{ij} = a_i S_i a_j S_j T_{ij} R_{ij} + r_{ij} \quad \text{Equation I.2}$$

where b_{ij} is the interaction score between atoms i and j , a is the hydrophobic atom constant, S is the solvent accessible area, T_{ij} is a logic function which returns a value of 1 or -1 depending on the character of the interacting polar atoms ($a < 0$ for polar atoms), there are three possibilities: acid-acid, base-base and acid-base of which only the acid-base interactions are scored positively/favorably. R_{ij} is the exponential e^{-r} (r is the distance between the atoms i and j) and r_{ij} is an implementation of the Lennard-Jones potential function. The total HINT interaction score is given by the sum of the individual interaction scores ($\sum \sum b_{ij}$). The HINT convention is that favorable interactions are scored with $b_{ij} > 0$ and unfavorable interactions are scored with $b_{ij} < 0$. The logic function T_{ij} returns a value of 1 or -1 depending on the character of the interacting polar atoms (i.e. $a < 0$): there are three possibilities: acid-acid, acid-base, or base-base; only acid-base is scored favorably. T_{ij} also flags hydrogen bonds which are in the HINT model a special case of acid-base interactions.

I.E Overview

This dissertation is organized to address the investigation and optimization of a solvent / anti-solvent crystallization process to produce particles for inhalation. Chapter II states the individual hypotheses and the specific aims that will be addressed in the succeeding chapters.

Each of the chapters consists of a brief introduction, a materials and methods section, followed by a results and discussion section. Chapter III describes the investigation and optimization of the solvent / anti-solvent crystallization process to produce particles suitable for inhalation using albuterol sulfate as the model drug. Chapter IV discusses the further optimization of this crystallization method to produce combination particles of albuterol sulfate and ipratropium bromide monohydrate. Characterization of these combination particles by different analytical techniques to understand the nature of interactions between albuterol sulfate and ipratropium bromide is also described. *In silico* molecular modeling tools to carry out a computational analysis of the possible interactions between albuterol sulfate and ipratropium bromide within a combination particle matrix constitutes the final section of this chapter. The *in vitro* aerosol performance of the engineered albuterol sulfate particles and combination particles of albuterol sulfate and ipratropium bromide produced from the optimized solvent / anti-solvent crystallization process is investigated as dry powder formulations in Chapter V. Comparison with conventionally used micronized powders in commercial formulations is also discussed. Finally, Chapter VI summarizes the results from each chapter as they relate to the original hypotheses.

CHAPTER II

HYPOTHESES AND RESEARCH PLAN

II.A. Hypothesis 1

An understanding of the degree of influence of crystallization variables such as the solvent/anti-solvent ratio, agitation speed, temperature, and crystal maturation time upon particle characteristics allows optimization and control of the final product and its aerosol performance. More specifically, it was hypothesized that micro-crystals of AS with suitable characteristics for dry powder inhalation could be produced by proper selection and optimization of the crystallization variables.

In order to test this hypothesis, a solvent / anti-solvent crystallization process was investigated with respect to the effect of crystallization variables on two particle characteristics; particle crystallinity and particle size. Solid-state characterization techniques were used to characterize the final products.

II.B. Hypothesis 2

The solvent / anti-solvent crystallization process can be further optimized to produce combination particles of albuterol sulfate (AS) and ipratropium bromide monohydrate (IB) in predictable ratios with suitable characteristics for inhalation.

In order to test this hypothesis, the crystallization conditions were studied and eventually and optimized to produce combination particles of AS and IB in predictable ratios of 1:1, 2:1,

6:1, and 10:1 (w/w). The performance of different anti-solvents in the form of ethyl acetate, isopropanol and mixtures of the two were reviewed at selected initial drug concentrations, drug solution / anti-solvent ratio, stirring speed, and crystallization conditions. Particles characterization was carried out to understand the nature of the interactions between AS and IB to distinguish them from physical mixtures of AS and IB.

II.C. Hypothesis 3

Molecular modeling tools can be used to identify and understand the likely interactions between AS and IB within a combination particle matrix.

Molecular modeling software Sybyl 8.0 was used to study interactions between randomly orientated AS and IB molecules and the HINT program was employed to classify and score favorable and unfavorable interactions between the molecules. Furthermore, a unit cell of AS was constructed and GOLD program was used to perform docking experiments wherein the effects of introducing a single molecule of IB were studied within the AS unit cell. HINT was again employed to classify and score the favorable and unfavorable interactions between AS and IB in this cell arrangement.

II.D. Hypothesis 4

It is hypothesized that the albuterol sulfate particles and combination particles of albuterol sulfate and ipratropium bromide monohydrate can be engineered with superior aerosol performance properties as compared to the conventionally used micronized albuterol sulfate and physical mixtures of separately micronized AS and IB.

In order to test this hypothesis, the engineered particles of albuterol sulfate and combination particles of AS and IB were formulated as dry powder inhaler formulations. Their *in vitro* aerosol performance testing was assessed using different dry powder inhalers. The *in vitro* aerosol performance of the engineered AS particles was compared to a reference commercial dry powder formulation of albuterol sulfate (Novolizer®) containing micronized albuterol sulfate mixed with carrier lactose while the *in vitro* aerosol performance of the combination particles was compared to the commercial formulation containing individually micronized AS and IB as a physical mixture (Combivent® pMDI).

CHAPTER III
INVESTIGATION AND OPTIMIZATION OF A SOLVENT / ANTI-SOLVENT
CRYSTALLIZATION PROCESS USING ALBUTEROL SULFATE AS A MODEL
DRUG

III.A. INTRODUCTION

In this chapter the effects of solvent / anti-solvent crystallization conditions on particle characteristics; predominantly particle size and crystallinity were investigated using albuterol sulfate (AS) as a model drug. Since an understanding and control of the critical processing variables is integral to producing particles with desirable characteristics, the influence of crystallization variables upon precipitated particle characteristics was determined to allow optimization and control of the final product. Specifically, it was hypothesized that micro-crystals of AS with suitable characteristics for inhalation (i.e.; complete crystallinity and size range between 1-5 μm) can be produced by proper selection and optimization of the crystallization variables.

III.B. CHEMICALS

Albuterol Sulfate ((RS)-1- (4-hydroxy-3-hydroxymethylphenyl)-2-(tert-butylamino) ethanol sulfate): Spectrum Chemical Mfg. Corp., New Brunswick, NJ

HPLC grade ethyl acetate: Fischer Scientific, Pittsburgh, PA

HPLC grade isopropyl alcohol: Fischer Scientific, Pittsburgh, PA

HPLC grade methanol: Fischer Scientific, Pittsburgh, PA

Ammonium Formate: Fischer Scientific, Pittsburgh, PA

Lactose Monohydrate: DMV Fonterra Excipients, Princeton, NJ

III.C. METHODS

III.C.1 Crystallization of albuterol sulfate

III.C.1.1 Preparation of a saturated aqueous solution of albuterol sulfate

An aqueous solution of AS (concentration: 0.22g/g) was prepared by weighing 0.14g of albuterol sulfate into a glass beaker and adding 0.5g water to achieve the required concentration. The beaker was covered with parafilm and heated to 40°C. Following dissolution of albuterol sulfate, the saturated solution was allowed to cool to room temperature (25-27°C) (Nocent et al., 2001).

III.C.1.2 Crystallization by the anti-solvent method

The experimental setup is shown in Figure III.1. In each experiment, an appropriate amount of ethyl acetate (based on the drug solution / anti-solvent ratio (R_a ratio) being tested) was added to a 1000mL cylindrical flat-bottomed vessel (Height = 15.2 cm, ID = 10.1 cm). The aqueous solution of albuterol sulfate was added to ethyl acetate over a 30 second period at a fixed infusion rate of 1 mL/min by means of a syringe pump (Harvard Apparatus, Holliston, MA) using a 500 μ L Hamilton gastight syringe. The drug solution was transferred to the crystallization vessel via a 12 cm PEEK tubing (ID = 0.007 inches, Upchurch Scientific, Oak Harbor, WA) which was held in a fixed position 5 cm above the anti-solvent. Mixing between the drug solution and anti-solvent was achieved by a stirrer (Caframo stirrer type RZR 50,

Wiarnton, ON, Canada) with a single bladed paddle with dimensions of $5.1 \times 2.5 \times 1.5$ cm. Stirring was initiated with the addition of the drug solution and was carried out for a fixed 30 minute period at a range of stirring speeds. Experiments were carried out at room temperature (25-27°C) resulting in no temperature difference between the AS solution and ethyl acetate unless otherwise stated. Following the 30 minute stirring period, the AS particles were either harvested immediately (crystal maturation time = 0) or allowed to remain in the solvent/anti-solvent mixture for upto 1440 minutes (24 hours) resulting in different crystal maturation times ranging from 0-24 hours. Particles were recovered from the anti-solvent by vacuum filtration using a 0.45µm nylon membrane filter (45mm diameter; Fischer Scientific, Pittsburgh, PA) housed in a glass filter unit. The filter paper containing the wet cake was washed with and the particles resuspended in 4mL of the saturated filtrate solution. This concentrated suspension was sonicated at 40KHz for 45minutes in a Branson ultrasonic bath to allow complete evaporation of the filtrate solution and to maintain particle separation during solvent removal. The particles were then dried for 24 hours at room temperature. Samples were then stored in sealed containers in a dessicator containing dried silica as the dessicant at room temperature.

III.C.1.3 Experimental design for screening the effects of crystallization conditions

A multi-factorial experiment was designed using JMP software (JMP, version 7.0, SAS Institute Inc., Cary, NC). Albuterol sulfate was crystallized from its aqueous solution using the general crystallization method described in section III.C.1.2. The factors investigated are shown in Table III.1 for the three R_a ratios of 1:200, 1:500, and 1:1000 (w/w). For each of the three R_a ratios, the effects of stirring speed at four levels of 100, 200, 500, and 800 r.p.m. and crystal maturation times ranging from 0-1440 minutes were examined. Two response variables were

investigated. These were the geometric median diameter ($D_{0.5}$) of the particles as measured by laser diffraction and crystallinity as assessed by differential scanning calorimetry. Preliminary studies revealed little effect of crystal maturation time on the final particle size. Therefore, the particle size measurements were carried out only at two extremes of the crystallization period i.e.; after 0 and 24 hours. AS samples for particle size measurement were prepared by vacuum filtration, sonication and subsequent drying at room temperature described in section III.C.1.8. To examine the effect of crystal maturation time, the particle crystallinity was measured at different time points during the 24 hour period. These time points were 0, 60, 120, 180, and 1440 minutes. Particles were characterized for their % crystallinity by DSC immediately after sampling from the crystallization vessel described in section III.C.1.6.1. Particle crystallinity was also examined by observation under plane-polarized light using an optical microscope. An additional assessment was performed using X-ray powder diffraction on particles collected after a 24 hour crystal maturation time as described in section III.C.1.6.3. The water content of the particles was measured by coulometric Karl Fischer titration and complementary weight loss analysis was carried out by thermogravimetric analysis on samples collected at the different crystal maturation time points. These measurements were carried out on particles sampled directly from the crystallization vessel. Drug yields were quantified using gravimetric analysis using Equation III.1. AS content in each sample was estimated using HPLC following dissolution of a known weight of particles, as described in section III.C.1.9.

$$\text{Drug Yield in Particles} = \left(\frac{\text{Mass of AS particles after filtration, sonication, and drying}}{\text{Mass of AS in the starting drug solution}} \right) \times 100 \quad \text{Equation III.1}$$

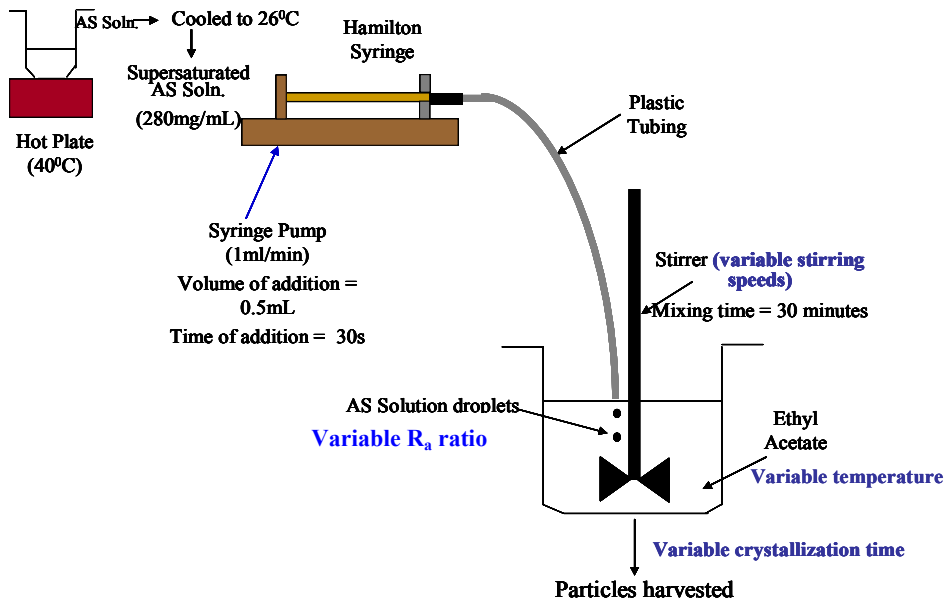


Figure III.1 Experimental setup for albuterol sulfate crystallization (insets show the crystallization setup and the paddle dimensions)

III.C.1.4 Strategies investigated to reduce albuterol sulfate particle size

III.C.1.4.1 Effect of temperature difference between the drug solution and anti-solvent

Using the crystallization conditions that yielded the smallest particles under isothermal conditions, the effect of a temperature difference between the drug solution and anti-solvent on particle size was investigated ($T_{\text{solution}} > T_{\text{anti-solvent}}$). In order to create this difference, the temperature of the anti-solvent was reduced by cooling the crystallization vessel in either ice (5°C) or dry ice (-40°C) for the 30 minute duration of mixing. The temperature of the drug solution was maintained at 25-27°C. This resulted in temperature differences of 20°C and 65°C for ice and dry ice respectively. The crystallization conditions employed were a drug solution concentration of 0.22g/g, R_a ratio of 1:200 (w/w), an infusion rate of 1mL/min, a stirring speed of 200 r.p.m., a stirring time of 30 minutes, and a total crystal maturation time of 1440 minutes.

Table III.1 Factorial experimental design for R_a ratio's of 1:200, 1:500, and 1:1000 (w/w)

Stirring speed (r.p.m.)	Crystal maturation time (minutes)
100	0
	60
	120
	180
	1440
200	0
	60
	120
	180
	1440
500	0
	60
	120
	180
	1440
800	0
	60
	120
	180
	1440

A 30 minute stirring period and cooling duration was chosen since particle formation was observed to take place throughout this time period. Since crystallization temperature theoretically influences particle size predominantly by affecting the nucleation and growth phases of the crystallization process, this 30 minute period was deemed to be most critical. At the end of mixing, the crystallization vessel was kept at room temperature for 1440 minutes before harvesting the particles by vacuum filtration. These particles were then re-suspended in 4mL of the saturated filtrate and sonicated to dryness at 40 KHz for 45 minutes. The particles were then dried at room temperature for 24 hours before storing them in sealed containers in a dessicator containing dried silica as the dessicant at room temperature until further analysis.

III.C.1.4.2 Effect of isopropyl alcohol as the anti-solvent on albuterol sulfate particle size

Using the crystallization conditions that yielded the smallest particles with ethyl acetate, the effect on AS particle size of an alternate anti-solvent, isopropyl alcohol, was investigated (Dhumal et al., 2009). The conditions employed used identical equipment with a drug solution concentration of 0.22g/g, R_a ratio of 1:200 (w/w), an infusion rate of 1mL/min, a stirring speed of 200 r.p.m., a stirring time of 30 minutes, and a total crystal maturation time of 1440 minutes. The temperature of both the drug solution and anti-solvent was 25-27°C, thereby resulting in no temperature difference. Once again, the particles were harvested by vacuum filtration, followed by re-suspension in 4mL of the saturated filtrate solution, sonication to dryness at 40 KHz for 45 minutes and subsequent drying at room temperature for 24 hours.

III.C.1.5 Assessment of water / solvent loss

III.C.1.5.1 Karl Fischer titration

The % water content in the AS particles at different crystal maturation times of 0, 60, 120, 180, and 1440 minutes was measured using a Moisture Meter, Model VA-05 (Mitsubishi, White Plaine, NY). In order to measure the in-process water content during crystal maturation, AS particles in concentrated suspension were sampled directly from the base of the crystallization vessel and subjected to water content determination without filtration. A background water content titration was performed to account for any residual water held in the titration vessel. Determinations were performed as follows: Albuterol sulfate particles were sampled from the crystallization vessel and quickly transferred to an aluminum pan. Due to the rapid initial solvent loss, an initial weight of the sample was not determined. The aluminum pan was placed in the thermal solid-state accessory of the Moisture Meter with the oven preheated to 140°C. Dry compressed air (100mL/min) was passed over the sample pan and the released water vapor transferred into the titration vessel for quantification. Following titration, the sample was weighed and this final dry weight together with the Karl Fischer determined mass of water was used to calculate the % water content in the AS particle samples as shown in Equation III.2.

$$\% \text{ Water Content} = \left(\frac{\text{KF determined mass of water}}{\text{(Final dry weight of sample + KF determined mass of water)}} \right) \times 100 \quad \text{Equation III.2}$$

The Karl Fischer method was validated using lactose monohydrate powder with known water content. The % water content of lactose monohydrate was determined using the method described in section III.C.1.5.1. The measured % water content was found to be $4.8 \pm 0.4\%$ after

three replicate measurements. This value was consistent with the reported certificate of analysis value of 4.0-6.0% and a calculated % of 4.8% representing the water of crystallization present as a monohydrate. In the solid-state, this water was known to be released at temperatures around 140°C and therefore, was suitable for validating the Karl Fischer method (Listiohadi et al., 2008).

III.C.1.5.2 Thermogravimetric Analysis (TGA)

The AS samples were also analyzed at different crystal maturation times of 0, 60, 120, 180, and 1440 minutes by TGA (Pyris1 TGA equipped with a data station Pyris Software for Windows, version 3.81, Perkin Elmer, Covina, CA). The method involved sampling the AS particles and quickly transferring them into an aluminum pan. The samples were heated under a stream of flowing dry nitrogen (Fischer Scientific, Pittsburgh, PA) at 30-35mL/min. The heating temperature program employed was: a 10 minute hold at 25°C followed by heating to 140°C at 10°C/min, holding at 140°C for 5 minutes followed by heating to 250°C at 10°C/min as shown in Figure III.2. It should be noted that unlike KF titration which is a specific method for the determination of water, the TGA method determines non specific weight loss that could include both water and anti-solvent. The weight loss was measured as the reduction in mass from the start of the temperature program until 140°C beyond which no weight loss was observed until the onset of melting. The final dry weight of the sample before melting together with the TGA determined weight change was used to calculate the % solvent content in the samples as shown in Equation III.3. The TGA determined non-specific solvent content was compared with the KF determined water content.

$$\% \text{ Solvent Content} = \left(\frac{\text{Total weight loss between 25-140}^\circ\text{C}}{\text{Final dry weight of sample} + \text{TGA determined mass of water}} \right) \times 100 \quad \text{Equation III.3}$$

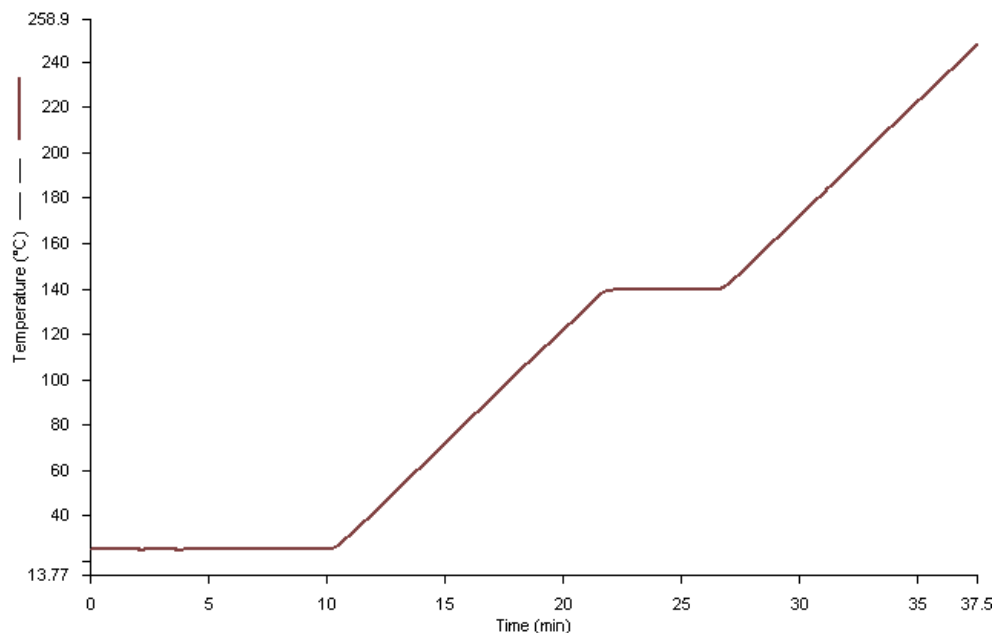


Figure III.2 TGA temperature program

III.C.1.6 Assessment of crystallinity

III.C.1.6.1 Differential Scanning Calorimetry (DSC)

DSC analysis was carried out using a DSC 7 (Perkin Elmer, Covina, CA) equipped with a data station Thermal Analysis Controller 7/DX, Pyris Software for Windows, version 3.81. AS particles were sampled from the crystallization vessel at different time points of 0, 60, 120, 180, and 1440 minutes. These samples were transferred into aluminum pans. The pans were immediately sealed non-hermetically and the weight of the sample was recorded. The samples were then heated under a flowing stream of dry nitrogen (Fischer Scientific, Pittsburgh, PA) as

the purge gas at a flow rate of 30-35mL/min. The temperature program used was: a 10 minute hold at 25°C followed by heating to 250°C at 10°C/min. Figure III.3 shows the temperature program.

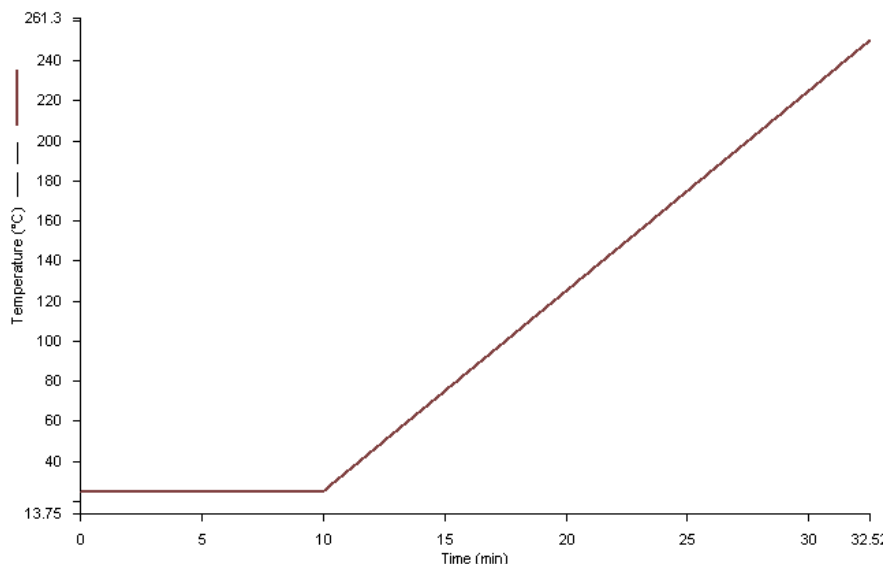


Figure III.3 DSC temperature program

The enthalpy of fusion was measured by integrating the endothermic peak associated with melting and normalizing for solvent-corrected dry sample weight. The % crystallinity of the particles was then calculated by equation III.4 (Huang et al, 2000; Bassett et al, 1988; Toda et al, 1995):

$$\% \text{ Crystallinity} = \left(\frac{\text{Enthalpy of fusion for the sample}}{\text{(Enthalpy of fusion for the reference standard)}} \right) \times 100 \quad \text{Equation III.4}$$

The enthalpy of fusion for reference crystalline AS (Spectrum Chem. Mfg. Corp., New Brunswick, NJ) was taken as a mean value from three replicate measurements. When using DSC to measure crystallinity in literature, some allowances have also been made for the sample recrystallizing upon heating by separately integrating the recrystallization exotherm and subtracting this value from the enthalpy of fusion (Huang et al., 2000). However, in our case, no recrystallization exotherm was observed. Therefore, the above mentioned formula was used for all DSC estimations of % crystallinity.

III.C.1.6.2 Optical microscopy

AS particles were sampled from the crystallization vessel at different crystal maturation times of 0, 60, 120, 180, and 1440 minutes and directly observed under a polarizing optical microscope (Optiphot, Nikon, Tokyo, Japan). Presence of birefringence under crossed polars was noted as an indicator of crystallinity.

III.C.1.6.3 Powder X-ray diffraction

AS samples were subjected to analysis by powder X-Ray diffraction (Panalytical XRPD, Panalytical Inc, Westborough, MA) by scanning from $5^{\circ}2\theta$ - $35^{\circ}2\theta$ over a period of 2 hours at 45 KV and 40mA. The presence of sharp, characteristic diffraction peaks and no halo was taken as an indicator of crystallinity. The diffractograms were compared to reference crystalline AS (Spectrum Chem. Mfg. Corp., New Brunswick, NJ) scanned under the same program.

III.C.1.7 Scanning electron microscopy

Particle morphology was observed using a scanning electron microscope (EVO 50 XVP scanning electron microscope (SEM) equipped with digital image acquisition). The samples were prepared for analysis by sputter coating for 2 minutes using a EMS 550x sputter coater. Imaging was performed at 15kV.

III.C.1.8 Particle size determination by laser diffraction

The particle size distribution of the AS samples was measured by laser diffraction using the Mastersizer 2000 equipped with the Scirocco dry dispersion accessory (Malvern, Westborough, MA). The air flow and feed rate were adjusted to control the powder dispersion. The optimized particle size measurement conditions sufficient to achieve deagglomeration of primary particles without attrition were an air pressure of 2 bar and a feed rate of 50%. Obscuration was deemed acceptable when readings occurred in the range of 2-6% over a measurement cycle time of 10 seconds. Triplicate measurements were made for each sample. Crystallization batch-to-batch reproducibility was assessed using three replicate crystallization experiments in each case.

III.C.1.9 High performance liquid chromatography (HPLC)

Samples were assayed for %AS content by HPLC by a validated method. The method employed a Waters 2690 separations module, a 2996 PDA detector, a Restek Allure PFP column (15×3.2mm), a mobile phase of 75% methanol and 25% ammonium formate buffer (20mM, pH 3.4) at a flow rate of 0.75mL/min and an injection volume of 100 µL. Precision of the method was estimated by assaying the 0.1 µg/mL standard 9 times and calculating the % RSD. The accuracy was determined by using the HPLC method to analyze the 0.1 µg/mL standard 9 times

and then calculated as a percentage of the analyte recovered by the assay. The limit of detection and quantitation were calculated from equation III.5 and III.6.

$$\text{Limit of Detection} = \frac{3.3 \times \text{SD of calibration curve intercept}}{\text{Mean slope of the calibration curve}} \quad \text{Equation III.5}$$

$$\text{Limit of Quantitation} = \frac{10 \times \text{SD of calibration curve intercept}}{\text{Mean slope of the calibration curve}} \quad \text{Equation III.6}$$

Table III.2 shows the system suitability parameters for this method.

Table III.2 System suitability parameters for the HPLC method

System Suitability Parameter	Value
Linearity range	0.1-100 µg/mL
Precision	1.02%
Accuracy	99.6%
Limit of detection	0.03 µg/mL
Limit of quantitation	0.1 µg/mL

To measure the % AS content, accurately weighed particles were dissolved in water to prepare a solution of adequate concentration in a target range of 20-25 µg/mL. UV detection was performed at 276nm. The stoichiometric AS content was calculated using equation III.7.

$$\% \text{ AS content} = \left(\frac{\text{AS mass determined by HPLC}}{\text{Sample weight}} \right) \times 100 \quad \text{Equation III.7}$$

III.D. RESULTS AND DISCUSSION

III.D.1 Characterization of albuterol sulfate reference standard

Figure III.4 shows a representative thermogram for albuterol sulfate reference standard (Spectrum Chem. Mfg. Crp., New Brunswick, NJ) which was the starting material for all crystallization experiments. A single thermal event was observed which corresponded to the melting of AS. Melting is an endothermic process and is shown as the sharp peak in the thermogram. The mean enthalpy of fusion for AS was 200 ± 1.8 J/g with a mean melting point of $204 \pm 0.6^\circ\text{C}$ calculated from three replicate measurements. These values agreed with the heat of fusion of approximately 198.0 J/g and a melting point of approximately 200°C reported in literature (Begat et al, 2002, Ticehurst et al, 1994) under similar heating profiles.

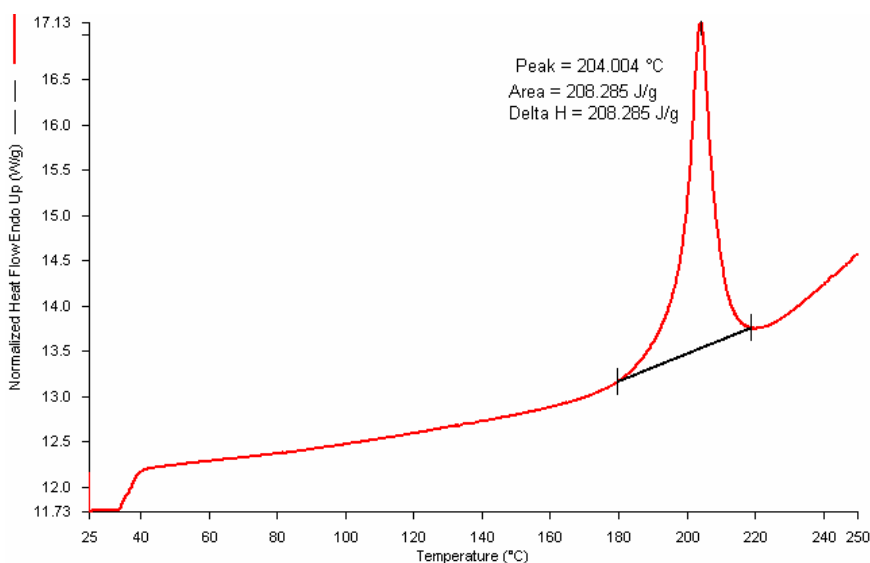


Figure III.4 Representative DSC thermogram for reference standard albuterol sulfate measured at a heating rate of $10^\circ\text{C}/\text{min}$

The % water content as measured by KF titration was 0.4 ± 0.2 %. This agreed with the Certificate of Analysis for AS (% water content = 0.4-0.6%). Thermogravimetric analysis yielded a similar value of 0.5 ± 0.3 % for weight loss. Figure III.5 shows the X-Ray powder

diffraction pattern for reference albuterol sulfate. The characteristic peak positions are tabulated in Table III.3. This diffraction pattern agreed with the reported diffraction pattern for albuterol sulfate in literature (Ward et al, 1995) as shown in Figure III.6.

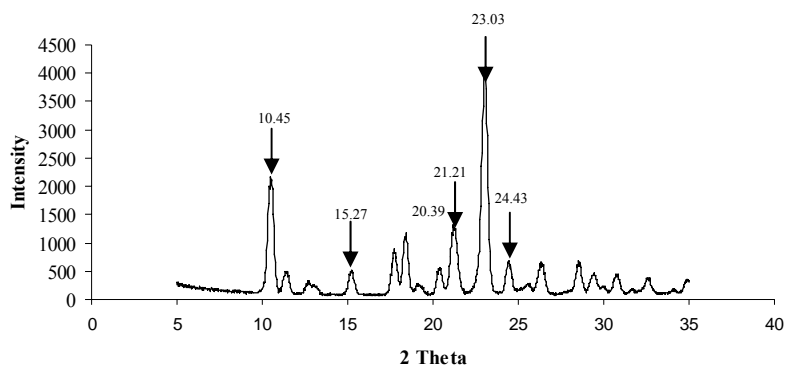


Figure III.5 Representative X-ray powder diffractogram for reference standard albuterol sulfate

Table III.3 Characteristic AS peaks

2θ	Intensity
10.45	2097
11.47	494
12.93	248
15.27	508
17.75	885
18.43	1177
19.35	228
20.39	576
21.21	1325
23.03	4058
24.43	694
25.67	280
26.39	642
28.63	652
29.51	434

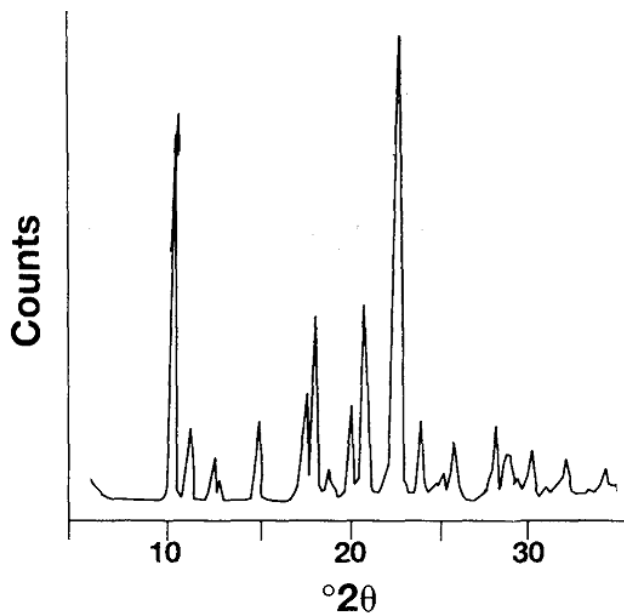


Figure III.6 X-ray powder diffractogram for albuterol sulfate reported by Ward et al. (1995) (Reproduced with permission from Springer)

The particle size distribution of reference albuterol sulfate is shown in Figure III.7. The average VMD measured from three replicate measurements was $9.8 \pm 0.2 \mu\text{m}$. Figure III.8 shows a representative microscopic image of reference AS. The particles appeared to be a mixture of plate-like and columnar in shape.

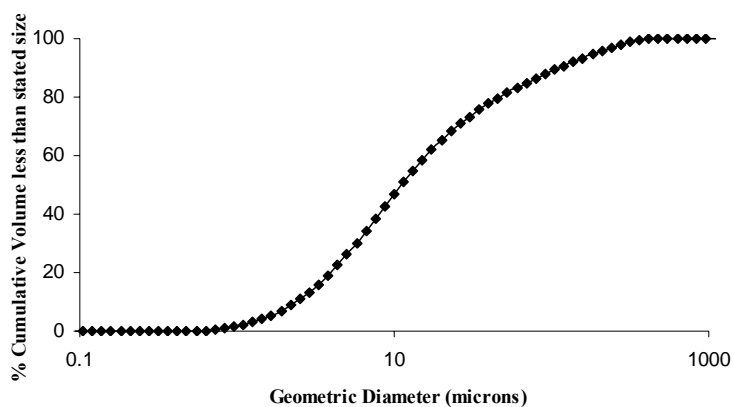


Figure III.7 Cumulative % undersize volume distribution of reference albuterol sulfate

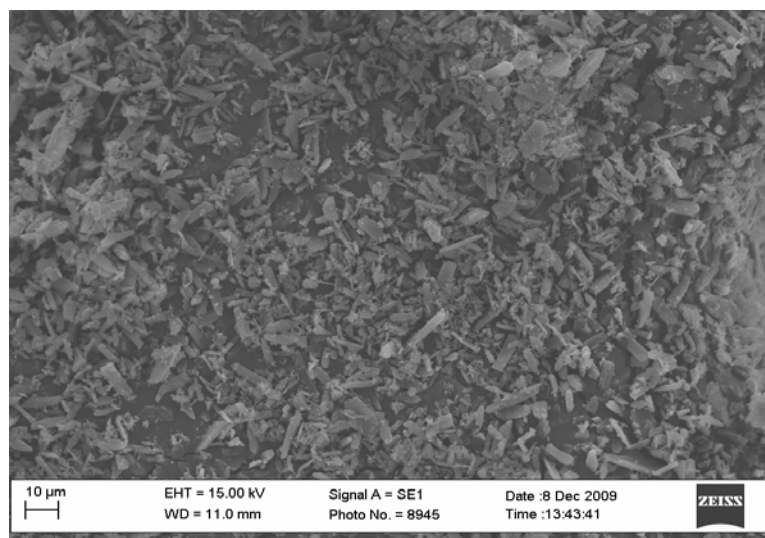


Figure III.8 Representative SEM image for reference albuterol sulfate

III.D.2 Characterization of AS particles produced by solvent / anti-solvent crystallization

III.D.2.1 Characterization after a crystal maturation time = 0

III.D.2.1.1 Estimated % crystallinity

In the solvent / anti-solvent crystallization process, particle formation was observed to occur immediately after addition of the drug solution to the anti-solvent. These results were not surprising given the nature of solvent / anti-solvent crystallization which is a rapid precipitation process. This particle formation appeared to be complete at the end of the mixing period of 30 minutes which was designated as crystal maturation time = 0. Completion of particle formation was confirmed by calculation of drug yields which were between 97-99 % for all crystallization conditions. At this time, these particles were sampled from the crystallization vessel and the % crystallinity was estimated using DSC by the method described in section III.C.1.6.1. As a technique, DSC is usually believed to be sufficiently sensitive to detect amorphous contents above 5% (Ward et al., 1995; Pfeiffer et al., 2003; Gorny et al., 2007). Table III.4 shows the

heats of fusion and estimated % crystallinity (expressed as mean \pm SD from three replicate crystallization experiments) for AS samples obtained after a crystal maturation time = 0 from the three R_a ratios at the four different stirring speeds employed. The heats of fusion for all particles were significantly smaller compared to reference albuterol sulfate ($\Delta H_f = 200 \pm 1.8$ J/g) indicating incomplete crystallinity. For R_a ratio 1:200 (w/w), similar values for estimated % crystallinity were obtained at all stirring speeds (p-value > 0.05 , Tukey's HSD), indicating no significant influence of stirring speed on estimated % crystallinity. Similarly, for R_a ratios 1:500 and 1:1000 (w/w), there was no influence of stirring speed on % crystallinity at crystal maturation time = 0 with similar values being obtained under all stirring speeds investigated (p-value > 0.05 , Tukey's HSD). Moreover, the estimated % crystallinity values were comparable for all R_a ratios as well. For example, R_a ratios 1:200, 1:500, and 1:1000 (w/w) yielded similar estimated % crystallinity values of $66.3 \pm 1.5\%$, $55.4 \pm 2.9\%$, and $49.4 \pm 20.2\%$ for particles produced at 100 r.p.m. at crystal maturation time = 0. In a similar manner, comparable values for estimated % crystallinity were obtained at the other 3 stirring speeds for all R_a ratios. Therefore, these results indicated a significant finding that after stirring for 30 minutes (crystal maturation time = 0), complete crystallization had not taken place regardless of the crystallization conditions.

These results showing incomplete crystallization after 30 minutes stirring were contrary to those reported by Nocent et al. (2001). In their study, the formation of crystalline AS particles was reported after 30 minutes mixing. However, it was unclear whether their particles were crystalline at the time of sampling or whether crystallization took place during the harvesting and drying steps. The authors failed to describe the handling of their particles following harvesting or the method for crystallinity assessment. Our studies have demonstrated that subsequent drying of

particles can induce solid-state crystallization. Partially crystalline AS particles obtained at each of the R_a ratios and stirring speeds after crystal maturation time = 0 were harvested by the method described in section III.C.1.2 and subjected to drying under ambient relative humidity (40% R.H.) and temperature (25°C) conditions for 24 hours. Table III.5 shows the heats of fusion and estimated % crystallinity values for these particles. These particles were found to be completely crystalline. The crystalline nature of these particles was confirmed by powder X-ray diffraction. Representative X-ray powder diffractograms for AS particles produced from R_a ratio 1:200, 1:500, and 1:1000 (w/w) after crystal maturation time = 0 at 500 r.p.m. after filtration and drying are shown in Figures III.9, III.10, and III.11. For all of these diffractograms, characteristic peaks were observed at 2θ values of 10.45, 15.27, 20.39, 21.21, 23.03, and 24.43 which were similar to those of reference AS. These results along with the absence of any halo indicated the virtually complete crystalline nature of these particles. This change in crystallinity of these samples confirms that complete crystallization had not taken place in solution after stirring for 30 minutes. In addition, it suggests that the particles characterized by Nocent et al. (2001) required that they were harvested and dried in order to obtain 100% crystallinity under conditions that were not specified by the authors.

It was mentioned in section III.A that particle crystallinity and size were the two major response variables of interest. Therefore, the AS particles produced after a crystal maturation time = 0 were characterized for their particle size distribution using laser diffraction as described in section III.C.1.8. Since the measurement of particle size necessitated drying, all of these particles were harvested by the method described in section III.C.1.2 and dried. Hence, these particles were completely crystalline.

III.D.2.1.2 Particle size distribution

Particle size was measured by laser diffraction using harvested AS particles that were subjected to filtration, sonication and drying as described in section III.C.1.8. The sonication step was included to bring about particle deagglomeration and dispersion of particle aggregates into primary particles. However, it was also possible that the sonication step itself may bring about a change in particle size. There are predominantly two main mechanisms by which this may be happening. The particles are being sonicated after re-suspending them in the concentrated filtrate solution. This filtrate solution evaporates during sonication which would lead to some degree of secondary precipitation of AS on the pre-formed particles. The amount of albuterol sulfate present in the saturated filtrate solution was therefore calculated based on its equilibrium solubility in the final crystallizing medium according to equation III.8:

$$\text{Amount of AS in the filtrate solution} = \frac{\text{Equilibrium solubility of AS in the crystallization medium}}{\text{Volume of the filtrate used for sonication}} \times \text{Volume of the filtrate used for sonication} \quad \text{Equation III.8}$$

Based on the above equation, the amount of albuterol sulfate present in the saturated filtrate solution was calculated as 0.4 mg, 0.6 mg, and 1.0 mg for R_a ratios 1:200, 1:500, and 1:1000 respectively. These small amounts comprised of less than 1% of the total amount of AS. Therefore, it is highly improbable that they had a significant impact on the particle size distribution due to drug addition to the primary particles. Another mechanism by which sonication may bring about a change in particle size is by breaking down the primary particles. In order to rule this out, reference standard albuterol sulfate was suspended in 4.0mL of the saturated filtrate solution and sonicated to dryness at 40 KHz for 45 minutes. As shown in Figure III.12, the particle size distribution did not change after sonication. The VMD was statistically comparable pre and post sonication ($9.8 \pm 0.2 \mu\text{m}$ vs. $9.6 \pm 0.3 \mu\text{m}$). Statistical analysis by one-

way ANOVA yielded a non-significant p-value (>0.05) thereby suggesting that sonication does not bring about an actual breakdown of primary particles. Figures III.13 and III.14 show the cumulative % undersize volume distributions and frequency distributions for the AS particles obtained after crystal maturation time = 0 from R_a ratio 1:200 (w/w) under the four different stirring speeds investigated. Similar particle size distributions for R_a ratios 1:500 and 1:1000 are shown in Figures III.15, III.16, III.17, and III.18. Table III.6 shows the average VMDs and span indices for these AS particles produced after a crystal maturation time = 0 from three R_a ratios under the four different stirring speeds. Span index is a measure of the spread of the distribution and is measured as the ratio of the difference of the 90th and 10th percentile diameter and the VMD. The particle size distributions for AS particles obtained from all R_a ratios under the four stirring speeds were bimodal (Figure III.14, III.16, III.17).

Table III.4 Mean \pm SD heats of fusion and estimated % crystallinity of AS particles precipitated using EA after crystal maturation time = 0

R_a ratio (w/w)	Stirring speed (r.p.m.)	Heat of fusion (Mean \pm SD) J/g	Estimated % crystallinity (Mean \pm SD)
1:200	100	132.6 \pm 2.9	66.3 \pm 1.5
	200	128.0 \pm 7.3	64.0 \pm 3.6
	500	123.9 \pm 11.9	62.0 \pm 5.9
	800	145.8 \pm 20.2	72.9 \pm 10.1
1:500	100	110.7 \pm 5.9	55.4 \pm 2.9
	200	137.9 \pm 19.0	69.0 \pm 9.5
	500	128.1 \pm 21.7	64.0 \pm 10.8
	800	130.6 \pm 47.3	65.3 \pm 23.7
1:1000	100	98.8 \pm 40.3	49.4 \pm 20.2
	200	109.2 \pm 8.9	54.6 \pm 4.4
	500	103.3 \pm 5.8	51.7 \pm 2.9
	800	99.3 \pm 11.4	49.7 \pm 5.7

Table III.5 Mean \pm SD heats of fusion and estimated % crystallinity values of AS particles precipitated using EA harvested after a crystal maturation time 0, filtered, and dried under ambient conditions for 24 hours

R_a ratio (w/w)	Stirring speed (r.p.m.)	Heat of fusion (Mean \pm SD) J/g	Estimated % crystallinity (Mean \pm SD)
1:200	100	199.1 \pm 1.2	99.0 \pm 0.6
	200	197.8 \pm 3.9	98.2 \pm 1.9
	500	197.6 \pm 1.6	98.2 \pm 0.8
	800	201.6 \pm 1.9	100.8 \pm 0.9
1:500	100	200.3 \pm 1.0	100.1 \pm 0.5
	200	200.0 \pm 2.8	100.0 \pm 1.5
	500	199.8 \pm 0.5	99.8 \pm 0.2
	800	196.7 \pm 1.4	97.8 \pm 0.7
1:1000	100	199.5 \pm 2.1	99.2 \pm 1.2
	200	196.3 \pm 1.7	97.7 \pm 0.8
	500	198.3 \pm 2.5	99.2 \pm 1.2
	800	199.3 \pm 2.0	99.2 \pm 0.9

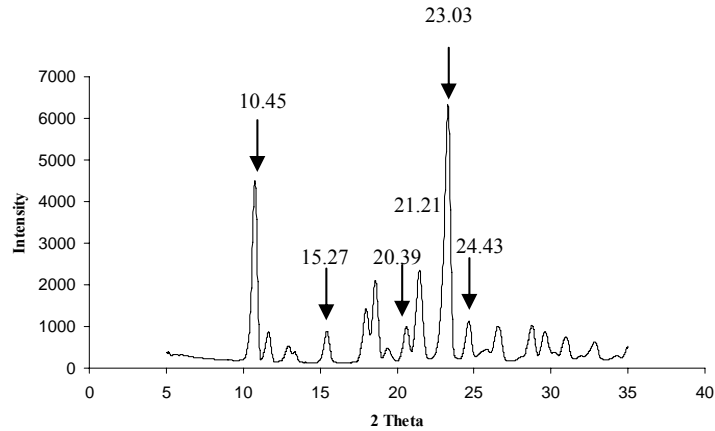


Figure III.9 X-ray powder diffractogram for AS particles precipitated using EA produced from R_a ratio 1:200 (w/w) at 500 r.p.m. after crystal maturation time 0, filtration and drying

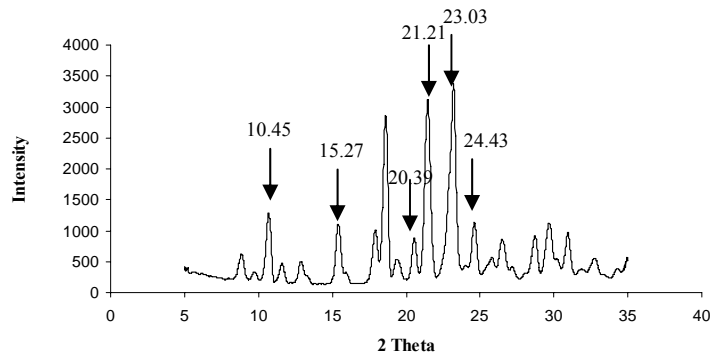


Figure III.10 X-ray powder diffractogram for AS particles precipitated using EA produced from R_a ratio 1:500 (w/w) at 500 r.p.m. after crystal maturation time 0, filtration and drying

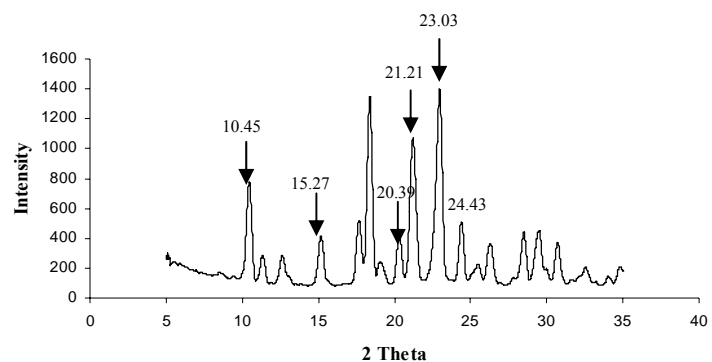


Figure III.11 X-ray powder diffractogram for AS particles precipitated using EA produced from R_a ratio 1:1000 (w/w) at 500 r.p.m. after crystal maturation time 0, filtration and drying

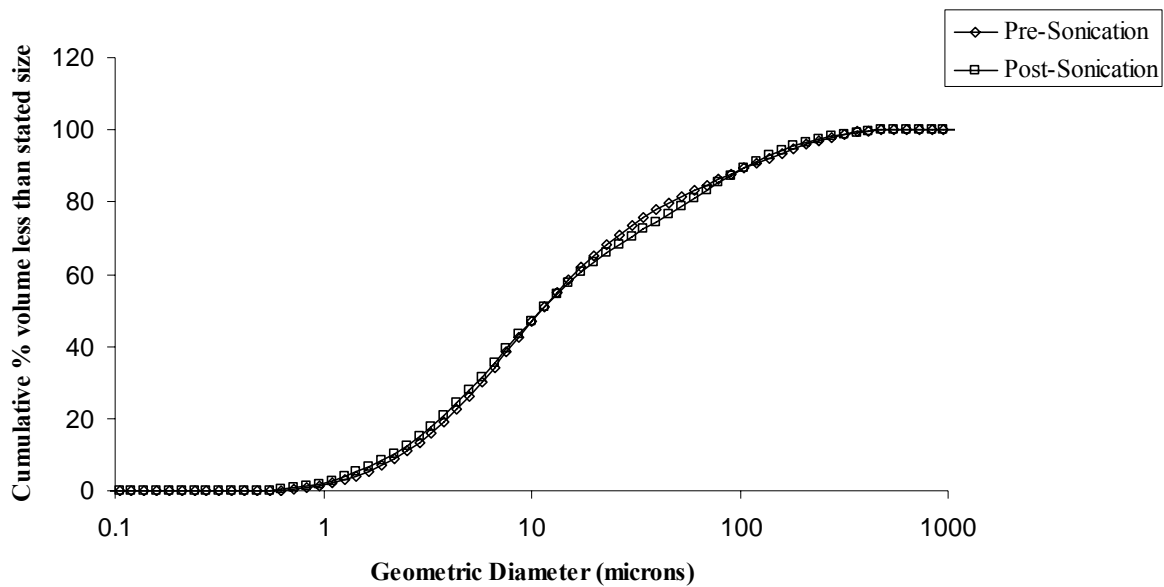


Figure III.12 Particle size distribution of reference standard albuterol sulfate pre and post sonication

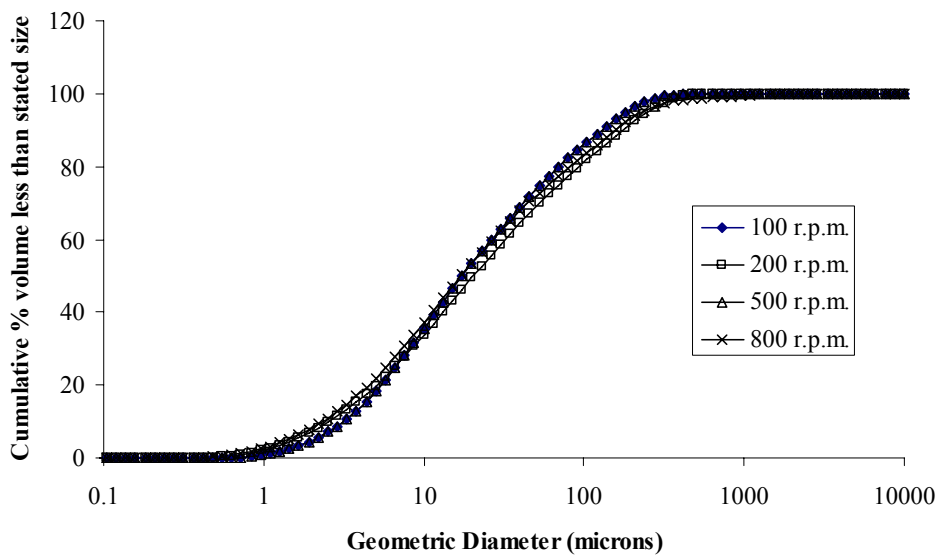


Figure III.13 Cumulative % undersize volume distribution for AS particles precipitated using EA produced from R_a ratio 1:200 (w/w) after crystal maturation time = 0 under four different stirring speeds

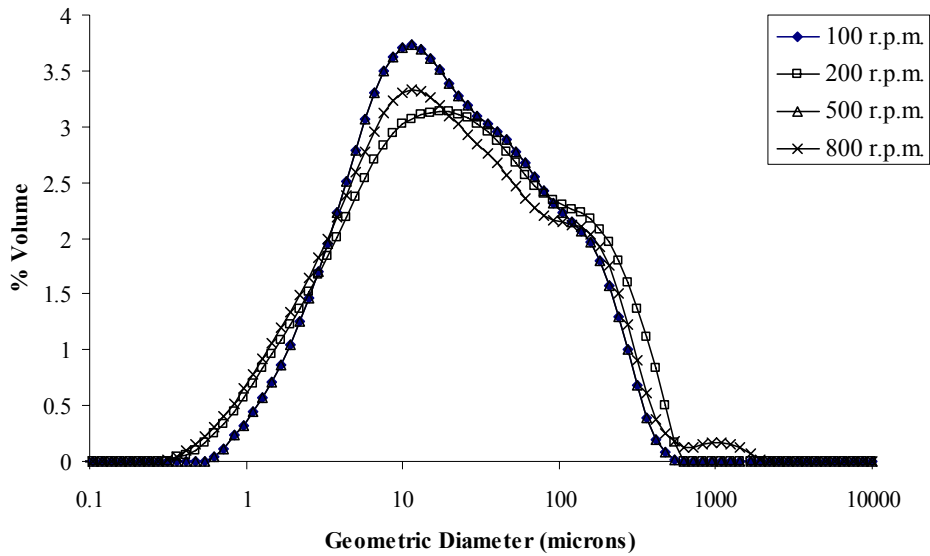


Figure III.14 Frequency volume distribution for AS particles precipitated using EA produced from R_a ratio 1:200 (w/w) after crystal maturation time = 0 under four different stirring speeds

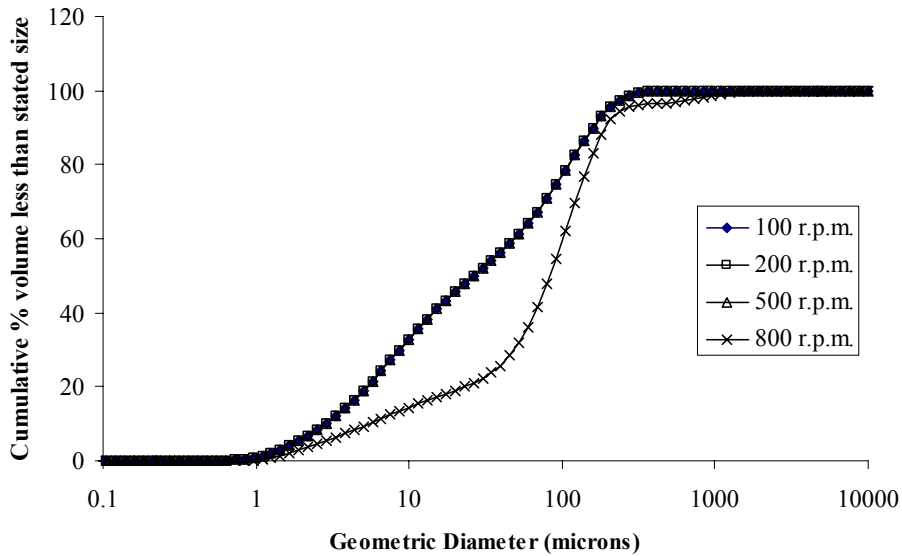


Figure III.15 Cumulative % undersize volume distribution for AS particles precipitated using EA produced from R_a ratio 1:500 (w/w) after crystal maturation time = 0 under four different stirring speeds

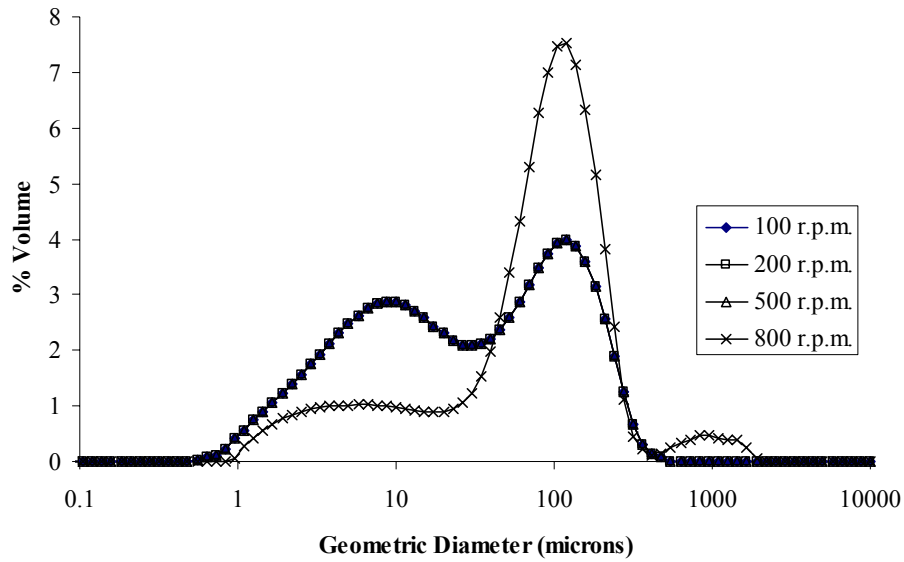


Figure III.16 Frequency volume distribution for AS particles precipitated using EA produced from R_a ratio 1:500 (w/w) after crystal maturation time = 0 under four different stirring speeds

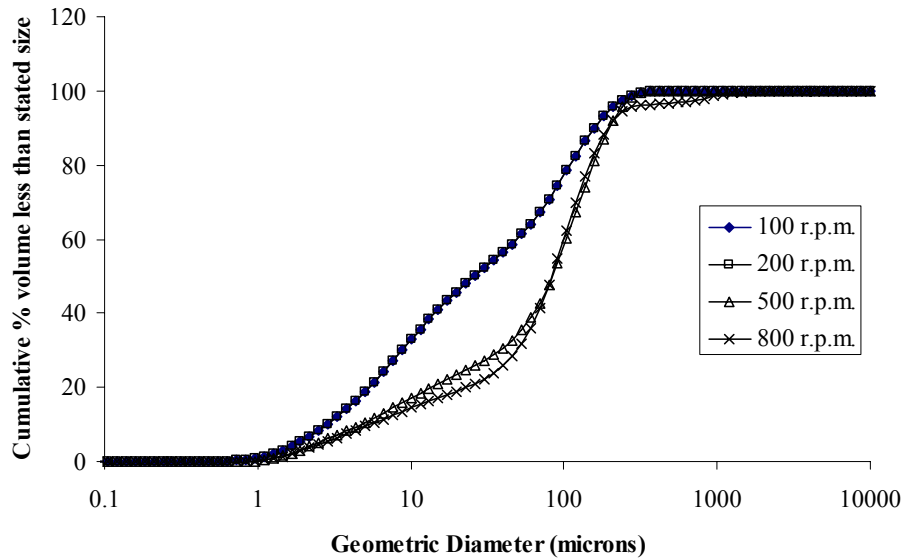


Figure III.17 Cumulative % undersize volume distribution for AS particles precipitated using EA produced from R_a ratio 1:1000 (w/w) after crystal maturation time = 0 under four different stirring speeds

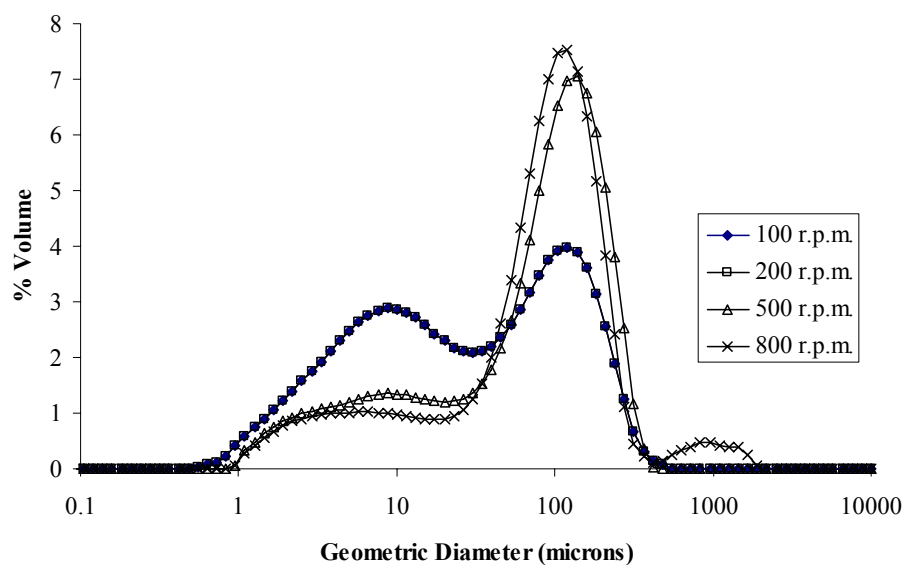


Figure III.18 Frequency volume distribution for AS particles precipitated using EA produced from R_a ratio 1:1000 (w/w) after crystal maturation time = 0 under four different stirring speeds

Table III.6 Mean \pm SD volume median diameters and span indices of AS particles precipitated using EA produced after crystal maturation time = 0 under different crystallization conditions

R_a ratio (w/w)	Stirring speed (r.p.m.)	VMD \pm SD (μm)	Span index
1:200	100	18.9 ± 7.9	7.7
	200	17.9 ± 7.4	8.9
	500	19.9 ± 8.0	7.8
	800	18.7 ± 6.7	8.5
1:500	100	25.6 ± 5.4	5.9
	200	28.6 ± 3.3	6.2
	500	26.6 ± 10.9	6.1
	800	95.6 ± 28.9	2.2
1:1000	100	26.7 ± 6.0	6.3
	200	32.9 ± 12.6	5.9
	500	90.7 ± 8.2	2.5
	800	93.4 ± 4.2	2.2

If VMD is assumed to be a representative median sign that indicates the feasibility of using a powdered drug for inhalation purposes, R_a ratio 1:200 (w/w) resulted in the formation of AS particles with comparable average VMDs of 18.9 ± 7.9 , 17.9 ± 7.4 , 19.9 ± 8.0 , and 18.7 ± 6.7 μm under the four stirring speeds of 100, 200, 500, and 800 r.p.m. respectively indicating that stirring speed had no influence on particle size (Table III.6). Overall particle size distributions were very broad as indicated by the large span values of 7.7, 8.9, 7.8, and 8.5 for particles produced at 100, 200, 500, and 800 r.p.m. respectively. For R_a ratio 1:500, particles with statistically indistinguishable VMDs of 25.6 ± 5.4 , 28.6 ± 3.3 , and 26.6 ± 10.9 μm were produced at 100, 200, and 500 r.p.m. respectively (p-value > 0.05, Tukey's HSD). However, significantly larger particles with a VMD of 95.6 ± 28.9 μm were produced at 800 r.p.m (p-value < 0.05, Tukey's HSD). Therefore, for R_a ratio 1:500 (w/w), there was a counter-intuitive influence of stirring speed where the highest stirring speed of 800 r.p.m. producing significantly larger particles compared to the lower stirring speeds of 100, 200, and 500 r.p.m. For R_a ratio 1:1000, particles produced at 100, and 200 r.p.m. had similar VMDs of 26.7 ± 6.0 , and 32.9 ± 12.6 μm which were significantly smaller than the particles produced at 500 (VMD = 90.7 ± 8.2 μm) and 800 (93.4 ± 4.2 μm) r.p.m. Hence, for R_a ratio 1:1000 (w/w) also, stirring speed had a significant influence with larger particles being produced at higher stirring speeds of 500 and 800 r.p.m. Furthermore, R_a ratio 1:200 (w/w) resulted in the formation of smallest particles compared to the other R_a ratios at all stirring speeds investigated. For example, at a stirring speed of 100 r.p.m., particles produced from R_a ratio 1:200 (w/w) had a VMD of 18.9 ± 7.9 μm which was significantly smaller than the VMDs of 25.6 ± 5.4 μm and 26.7 ± 6.0 μm produced from R_a ratios 1:500 (w/w) and 1:1000 (w/w) respectively.

Some of these results can be at least partly explained on the basis of the supersaturation ratios that prevailed at the different R_a ratios. The supersaturation values for a solvent / anti-solvent crystallization in terms of an index described as the supersaturation ratio in equation III.9 by Murnane et al., (2008) have been expressed (Murnane et al., 2008).

$$\text{Supersaturation Ratio} = \text{Ln} \left(\frac{(C_s \times W_s)}{(E_{cs} \times W_{cs})} \right) \quad \text{Equation III.9}$$

In the above equation, C_s is the concentration of the drug solution, W_s is the weight of the drug solution, E_{cs} is the equilibrium solubility of the drug in the final solvent / anti-solvent mixture, and W_{cs} is the weight of the final crystallizing medium. Applying this equation, the “supersaturation ratios” were calculated for the three solvent / anti-solvent ratios as 5.2, 4.5, and 3.4 for R_a ratios 1:200, 1:500, and 1:1000 respectively. Thus, R_a ratios 1:200 had higher supersaturation levels compared to R_a ratios of 1:500 (w/w) and 1:1000 (w/w).

The largest supersaturation ratio (5.2) for the 1:200 R_a ratio should result in an increased driving force for crystallization and a theoretical decrease in the metastable zone width (MSZW) which is the allowable supersaturation level for a crystallization process. Spontaneous nucleation cannot take place in this metastable zone and narrower the MSZW, the faster should be the nucleation process, with nucleation predominating over crystal growth, resulting in the formation of smaller particles. Hence, for R_a ratio 1:200 (w/w), the largest supersaturation ratio was expected to lead to a narrower MSZW and increased formation of fines with nucleation predominating over crystal growth. For this ratio, however, increasing the agitation speed failed

to produce a significant change in the VMD with comparable average VMDs of 18.9 ± 7.9 , 17.9 ± 7.4 , 19.9 ± 8.0 , and 18.7 ± 6.7 μm under the four stirring speeds of 100, 200, 500, and 800 r.p.m. respectively ($p\text{-value} > 0.05$; Tukey's HSD). This appeared to indicate that the supersaturation effect predominated over the mixing and turbulence effects on crystal growth.

Notably, addition of a highly saturated drug solution to the anti-solvent leads to very high supersaturation at the point of addition and this is not taken into account in these calculations of supersaturation ratios. However, stirring the mixture is believed to lead to fairly rapid and uniform mixing resulting in the dissipation of this localized supersaturation and a more uniform, albeit lower supersaturation ratio being attained in the final crystallization mixture. However, if the supersaturation is very high as is the case with R_a ratio 1:200, even the higher stirring speeds appeared to be insufficient to bring about uniform mixing faster than the local zones of high supersaturation and high nucleation rates could result in overall small particle sizes. Generation of such high supersaturation levels also leads to crash precipitation, and hence a broader particle size distribution which is indicated by the large span values for the 1:200 (w/w) particles. This explanation was strengthened by the results obtained with the other two R_a ratios. R_a ratio 1:500 failed to show any significant effect of stirring speed on particle size at stirring speeds of 100, 200, and 500 r.p.m. until at 800 r.p.m., there was a significant increase in particle size. The same effect was seen at a lower stirring speed for R_a ratio 1:1000 (w/w) (Table III.6). The trend was clear therefore; high nucleation rates at high supersaturation values appeared to dominate at R_a ratio 1:200 (w/w). As supersaturation was progressively reduced however, mixing (producing lower supersaturation values rapidly at high rates of stirring) allowed crystal growth to dominate in cases where VMD was observed to increase significantly (R_a ratio 1:500, 1:1000).

In practice, the application of crystal theory in all technologic situations that are aimed at controlling the interplay of hydrodynamics (mixing) as well as solvent-solute and solute-solute interactions with molecular-structure dependent kinetics is bound to require experimental review. In differently designed systems, an increase of particle size with increased agitation has been explained by Mullin (2001) with particle size showing a parabolic dependence on stirring speed. Particle size passed through a minimum as the stirring speed was increased due apparently to particle collisions that resulted in attrition. However, beyond a certain stirring speed, the particle size increased once again due to the particle collisions that led to aggregate formation. Such a parabolic relationship of particle size with stirring speed was also been reported by O'Grady et al. (2001), Abdel-Al et al. (2004), and Genoveva et al. (2007). In studies carried out by O'Grady et al., the effect of stirring speed was investigated in conjunction with anti-solvent addition location, and addition rate (O'Grady et al., 2001). When the anti-solvent was added closer to the impeller, an increase in agitation intensity was claimed to result in a narrower MSZW, possibly due to the increased probability of contact between solute molecules. When the anti-solvent was added closer to the vessel wall, there was a significant improvement in their batch-to-batch repeatability. Those results showed the importance of mixing conditions at each of the addition locations in solvent / anti-solvent crystallizers. The overall effects however, must be influenced by the relative and drug-dependent rates at which nuclei are formed, disintegrate and crystals grow in different solvent environments.

The interplay between the supersaturation levels and stirring speeds was also reflected in particle morphology. R_a ratios 1:200 and 1:500 (w/w) under all stirring speeds yielded particles that were irregular in morphology as shown in Figures III.19 and III.20. Particle morphology is known to be influenced by the supersaturation levels prevailing in the crystallization vessel at

different sites (Mersmann, 2001). Ideally, under efficient mixing conditions, similar supersaturation is expected throughout the crystallization vessel at a given time. However, inefficient mixing, particularly in the presence of high supersaturation levels can lead to zones of locally high and low supersaturation that may cause one plane of the crystal to grow faster than another. Non-homogeneous solute concentrations can thus result in the observable irregular morphology.

For the R_a ratio 1:1000 (w/w) stirring speed had a significant influence on particle size where larger particles with VMDs of 90.7 ± 8.2 , and 93.4 ± 4.2 μm were produced at 500 and 800 r.p.m. compared to the 26.7 ± 6.0 , and 32.9 ± 12.6 μm particles produced at 100, and 200 r.p.m. This effect may once again be explained by increased agitation bringing about greater mixing, reduced zones of locally high supersaturation, and hence, an increased metastable zone width. The effect of stirring speed is most predominant in this R_a ratio due to its smallest supersaturation ratio (3.2). These factors would lead to an increased formation of larger particles. The interplay between mixing and supersaturation was reflected in particle morphology. Particles produced at the lower stirring speeds of 100 and 200 r.p.m. were irregular in shape (Figure III.21) and appeared similar to the particles produced from R_a ratio 1:200 and 1:500 (w/w) under the same stirring speeds. This was due to inefficient mixing at lower stirring speeds. Conversely, at higher stirring speeds of 500 and 800 r.p.m., spherical particles were produced (Figure III.22) due to efficient mixing, homogeneous supersaturation and hence equivalent growth on all crystal faces.

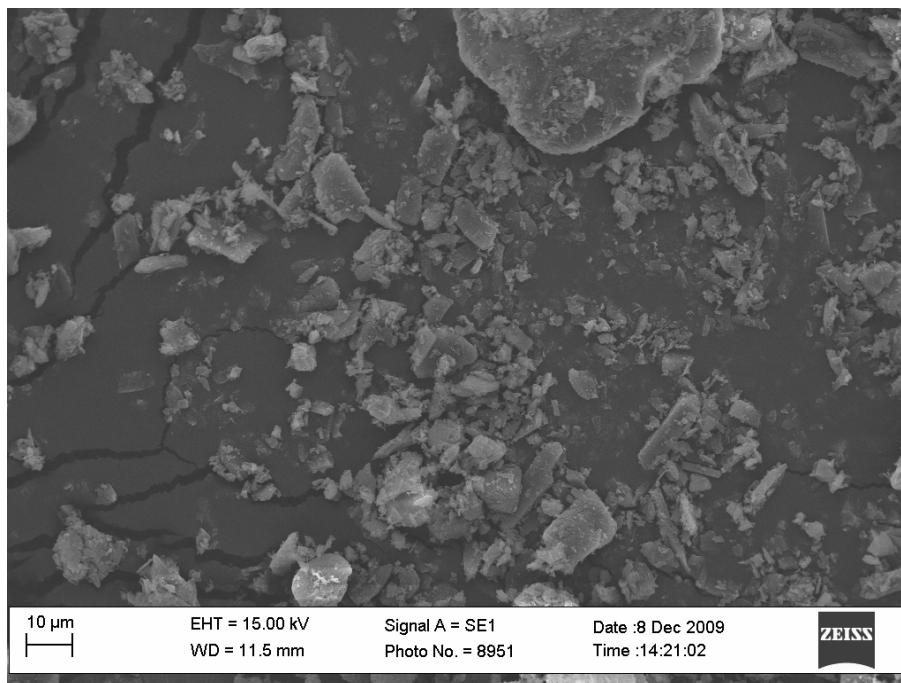


Figure III.19 Scanning Electron Micrograph of AS particles precipitated using EA produced at 500 r.p.m. from a solvent / anti-solvent ratio of 1:200 (w/w) at crystal maturation time = 0 after filtration and drying

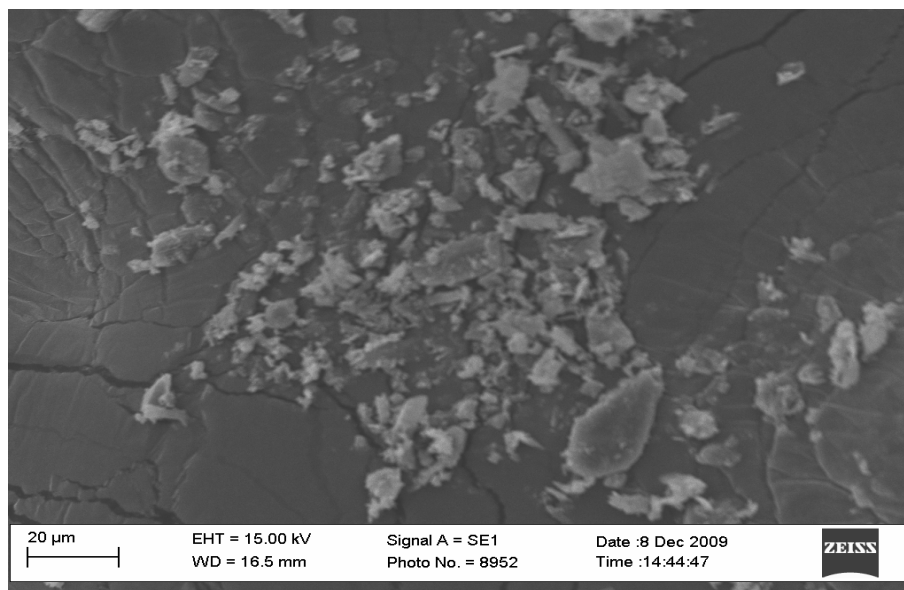


Figure III.20 Scanning Electron Micrograph of AS particles precipitated using EA produced at 500 r.p.m. from a solvent / anti-solvent ratio of 1:500 (w/w) at crystal maturation time = 0 after filtration and drying

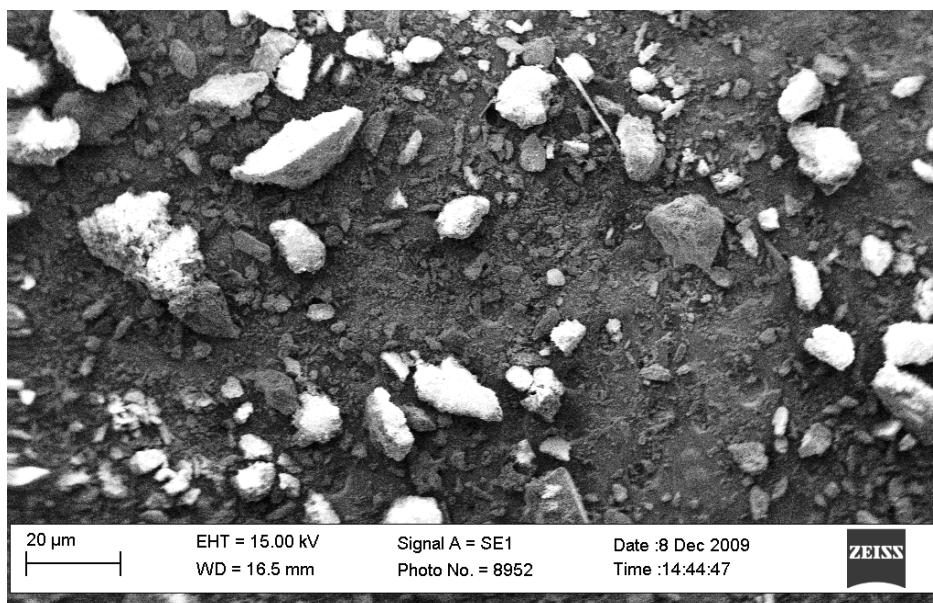


Figure III.21 Scanning Electron Micrograph of AS particles precipitated using EA produced at 100 r.p.m. from a solvent / anti-solvent ratio of 1:1000 (w/w) at crystal maturation time = 0 after filtration and drying

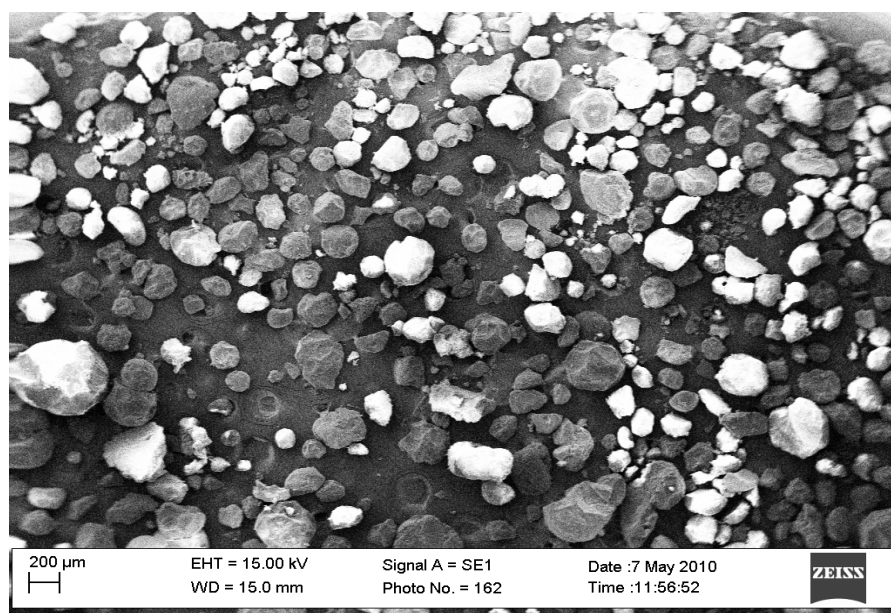


Figure III.22 Scanning Electron Micrograph of AS particles precipitated using EA produced at 500 r.p.m. from a solvent / anti-solvent ratio of 1:1000 (w/w) at crystal maturation time = 0 after filtration and drying

In summary, in the experimental crystallizer described in this thesis, after a crystal maturation time = 0, partially crystalline particles of AS were produced under all crystallization conditions. These particles completed their crystallization during filtration and drying. Particle size distributions of the particles revealed an effect of different crystallization conditions such as R_a ratio and stirring speed on particle size. These effects were explained on the basis of the interplay between the effects of the supersaturation ratio and the speed at which mixing was accomplished. R_a ratio 1:200 (w/w), where supersaturation was highest resulted in the smallest particles under all four stirring speeds relative to R_a ratios of 1:500 and 1:1000 (w/w). However, these particles were approximately 20 μm in diameter with broad PSDs and remained unsuitable for inhalation. It must be remembered that these particles produced after a crystal maturation time = 0 were only partially crystalline and underwent complete crystallization upon harvesting and drying. Because it has been demonstrated in literature that harvesting partially crystalline particles can induce solid-state crystallization (Ward et al., 1995; Pfeiffer et al., 2003) leading to the formation of crystalline bridges between adjacent particles such an event is considered undesirable particularly for aerosol formulations where size and the ability to disperse the individual particles is a primary concern.

In an attempt to bring about complete solution crystallization, the particles produced after a crystal maturation time = 0 were allowed to remain in the solvent / anti-solvent mixture for longer crystallization periods upto 24 hours since crystallization is a time dependent process. The subsequent sections address the characteristics of those particles.

III.D.2.2 Characterization of AS particles after different crystal maturation times between 0 – 24 hours

III.D.2.2.1 Estimated % crystallinity

Tables III.7, and III.8, show the heats of fusion and calculated % crystallinity values for AS particles produced from R_a ratios 1:200, and 1:500 (w/w) at different time points under the four different stirring speeds investigated. For R_a ratio 1:200 (w/w), increased heats of fusion and hence increased estimated % crystallinity values were observed for all stirring speeds as a function of increasing crystal maturation time. Figure III.23 reveals a similar trend of increasing crystallinity as a function of increasing crystal maturation time for each of the stirring speeds for the 1:200 (w/w) R_a ratio.

Table III.7 Mean ± SD heats of fusion and estimated % crystallinity values for AS particles precipitated from EA produced from R_a ratio 1:200 (w/w) at different crystal maturation times

Stirring speed (r.p.m.)	Crystal maturation time (minutes)	Heat of fusion (Mean ± SD) J/g	Estimated % crystallinity (Mean ± SD)
100	0	132.6 ± 2.9	66.3 ± 1.5
	60	157.2 ± 10.1	78.6 ± 5.0
	120	160.1 ± 2.4	80.1 ± 1.2
	1440	202.1 ± 2.1	101.0 ± 1.1
200	0	128.0 ± 7.3	64.0 ± 3.6
	60	135.3 ± 3.8	67.7 ± 1.9
	120	160.5 ± 3.6	80.3 ± 0.8
	1440	194.3 ± 6.9	97.2 ± 3.5
500	0	123.9 ± 11.9	62.0 ± 5.9
	60	152.2 ± 5.7	76.3 ± 2.9
	1440	198.4 ± 1.5	99.2 ± 0.8
800	0	147.8 ± 20.2	72.9 ± 10.1
	60	162.7 ± 2.6	81.4 ± 1.4
	120	173.5 ± 4.4	86.8 ± 2.2
	180	184.0 ± 13.6	92.0 ± 6.8
	1440	201.6 ± 2.6	100.8 ± 1.3

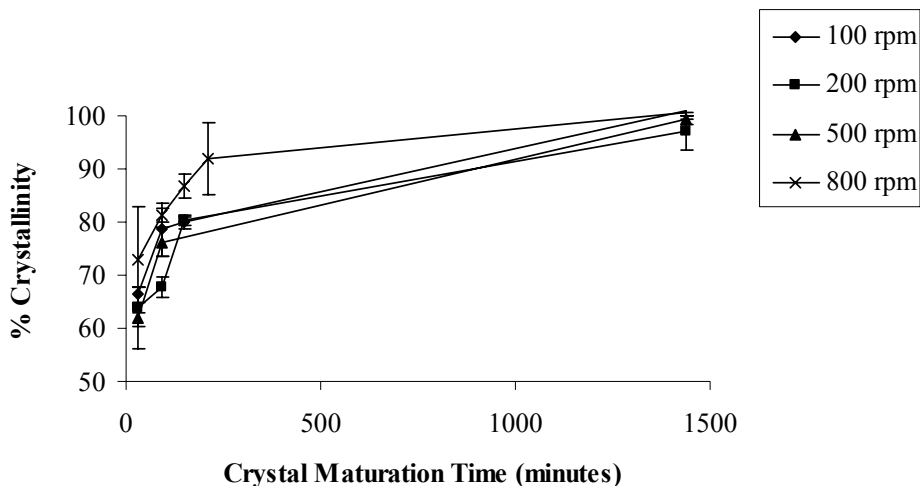


Figure III.23 Estimated % crystallinity of AS particles precipitated from EA as a function of crystal maturation time for R_a ratio 1:200 (w/w)

Table III.8 Mean \pm SD heats of fusion and estimated % crystallinity values for AS particles precipitated from EA produced from R_a ratio 1:500 (w/w) at different crystal maturation times

Stirring speed (r.p.m.)	Crystal maturation time (minutes)	Heat of fusion (Mean \pm SD) J/g	Estimated % crystallinity (Mean \pm SD)
100	0	110.7 \pm 5.9	55.4 \pm 2.9
	60	114.1 \pm 8.1	57.0 \pm 4.1
	180	168.8 \pm 6.1	84.4 \pm 3.1
	1440	199.5 \pm 0.7	99.7 \pm 0.4
200	0	137.9 \pm 19.0	69.0 \pm 9.5
	60	145.1 \pm 11.8	72.6 \pm 5.9
	120	154.1 \pm 3.0	77.0 \pm 1.5
	180	174.1 \pm 3.3	87.0 \pm 1.7
500	1440	199.5 \pm 12.5	99.8 \pm 6.5
	0	128.1 \pm 21.7	64.0 \pm 10.8
	60	141.6 \pm 7.1	70.8 \pm 3.5
	120	149.7 \pm 4.5	74.8 \pm 2.3
800	180	182.4 \pm 2.0	91.2 \pm 1.0
	1440	199.6 \pm 0.6	99.8 \pm 0.3
	0	130.6 \pm 47.3	65.3 \pm 23.7
	60	145.9 \pm 10.7	73.0 \pm 5.4
800	120	173.1 \pm 6.2	86.6 \pm 3.1
	180	190.3 \pm 1.6	95.2 \pm 0.8
	1440	196.0 \pm 6.7	98.0 \pm 3.4

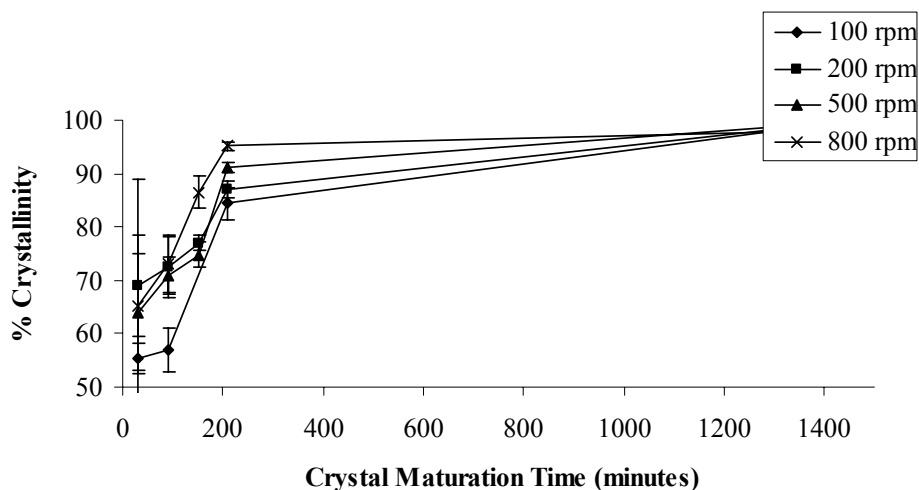


Figure III.24 Estimated % crystallinity of AS particles precipitated from EA as a function of crystal maturation time for R_a ratio 1:500 (w/w)

For all four stirring speeds, complete crystallinity was observed at the end of 1440 minutes of crystallization for the R_a ratio 1:200 (w/w) particles. Similar results were obtained for the R_a ratio 1:500 (w/w) where AS particles produced under all four stirring speeds underwent an increase in % crystallinity as a function of crystal maturation time (Table III.8, Figure III.24). These particles were also completely crystalline at the end of 1440 minutes of crystallization.

In both cases however, particles produced at the higher stirring speed of 800 r.p.m. showed a faster rate of crystal maturation than the others. There was no obvious explanation for this observation. Representative DSC thermograms for AS particles produced from R_a ratio 1:200 and 1:500 (w/w) at 200 r.p.m. after 1440 minutes are shown in Figures III.25 and III.26. Similar heats of fusion compared to reference AS and sharp melting peaks were indicative of approximately 100% crystallinity. These particles were also assessed for their % crystallinity after filtration and drying under ambient conditions for 24 hours. The values for these particles are shown in Table III.9.

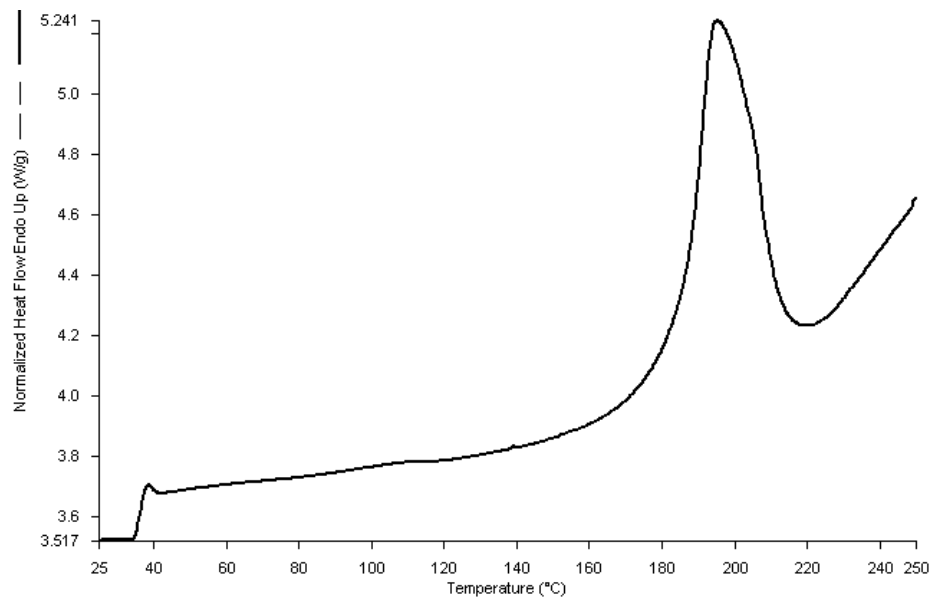


Figure III.25 Representative DSC thermogram of AS particles precipitated from EA produced from R_a 1:200 at 200 r.p.m. after 1440 minutes

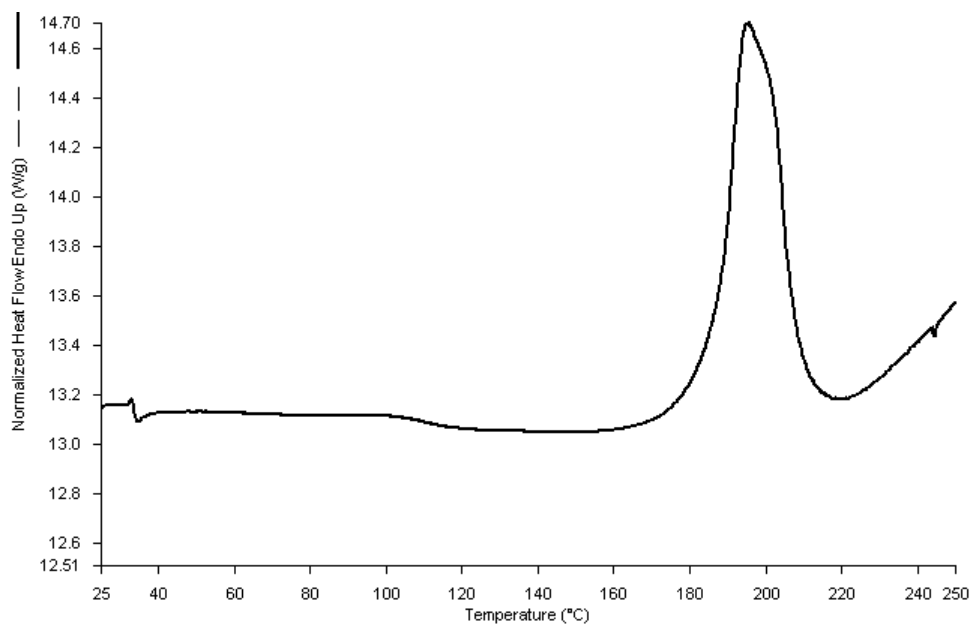


Figure III.26 Representative DSC thermogram for AS particles precipitated from EA produced from R_a 1:500 at 200 r.p.m. after 1440 minutes

Table III.9 Mean \pm SD heats of fusion and estimated % crystallinity values for AS particles precipitated from EA obtained from R_a ratios 1:200 and 1:500 (w/w) after crystal maturation time 1440 minutes under different stirring speeds after filtration and drying (Shown in parentheses are the measured estimated % crystallinities prior to filtration and drying)

R_a Ratio (w/w)	Stirring speed (r.p.m.)	Heat of fusion (Mean \pm SD) J/g	Estimated % crystallinity (Mean \pm SD)
1:200	100	200.1 \pm 1.1	100.0 \pm 0.9 (101.0 \pm 1.1)
	200	195.8 \pm 3.2	98.2 \pm 2.5 (97.2 \pm 3.5)
	500	199.4 \pm 1.4	99.6 \pm 1.0 (99.2 \pm 0.8)
	800	200.6 \pm 1.3	100.2 \pm 0.7 (100.8 \pm 1.3)
1:500	100	199.5 \pm 1.3	99.7 \pm 0.6 (99.7 \pm 0.4)
	200	200.5 \pm 2.5	100.1 \pm 1.2 (99.8 \pm 6.5)
	500	198.4 \pm 1.2	99.8 \pm 0.6 (99.8 \pm 0.3)
	800	196.0 \pm 3.7	98.0 \pm 1.8 (98.0 \pm 3.4)

No difference in the heats of fusion was observed compared to the values measured at the end of 1440 minutes of crystallization indicating that crystallization was complete at 1440 minutes. Figures III.27 and III.28 show the representative thermograms for AS particles produced from R_a ratios 1:200 and 1:500 (w/w) at 200 r.p.m. after 1440 minutes of crystallization, filtration and drying. These thermograms are similar to those for reference AS and to particles produced under similar conditions before filtration and drying (Figures III.25, III.26) indicating that after 1440 minutes 100% crystalline AS particles were produced in the solution state. The filtered and dried particles were also subjected to powder X-ray diffraction. The diffractograms are shown in Figures III.29 and III.30 for AS particles produced at 200 r.p.m. from R_a ratios 1:200 and 1:500 (w/w) respectively. For both of these particles characteristic peaks were observed at 2 θ values of 10.45, 15.27, 17.75, 21.21, 23.03, and 24.43 which were comparable to the characteristic peaks for reference AS once again indicating that these particles were crystalline and of the same polymorphic form as the standard and other AS crystals. Since,

the powder X-ray diffraction analysis sample preparation necessitated particle drying; this analysis could not be carried out on particles immediately sampled from the crystallization vessel.

The heats of fusion and estimated % crystallinity values for AS particles produced from R_a ratio 1:1000 (w/w) at different crystal maturation time points are shown in Table III.10. This R_a ratio revealed a difference in the crystallization behavior as a function of crystal maturation time depending upon the stirring speed employed as shown in Table III.10 and Figure III.31.

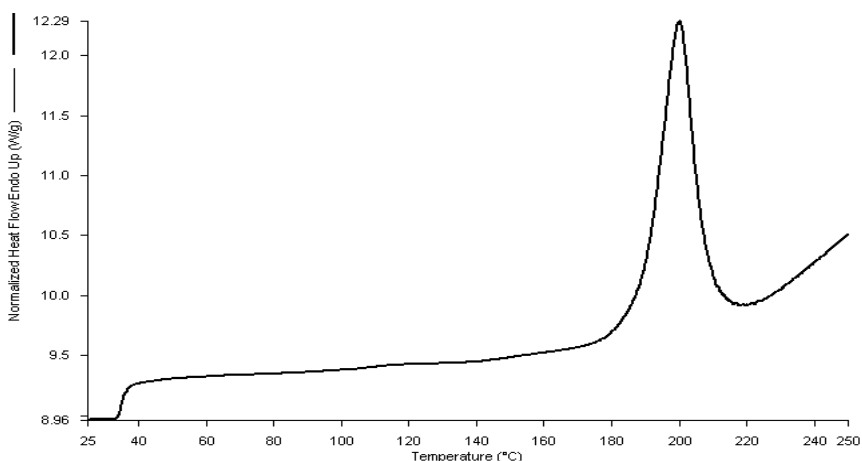


Figure III.27 Representative DSC thermogram for AS particles precipitated from EA produced from R_a ratio 1:200 at 200 r.p.m. after 1440 minutes of crystallization, filtration, and drying

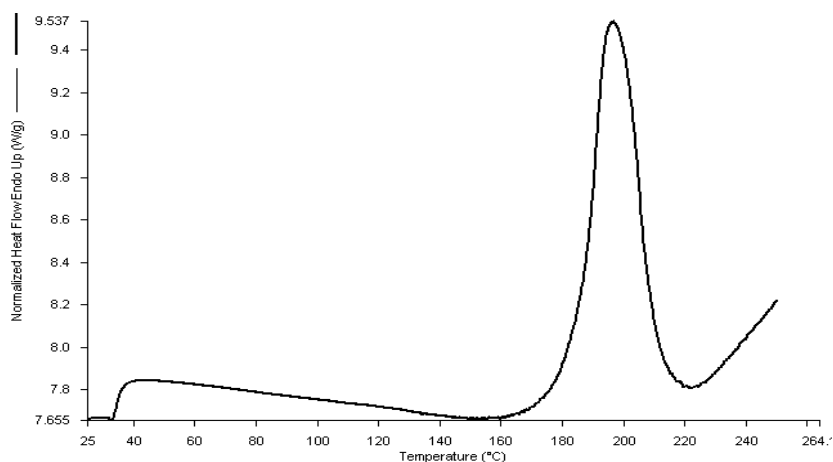


Figure III.28 Representative DSC thermogram for AS particles precipitated from EA produced from R_a ratio 1:500 at 200 r.p.m. after 1440 minutes of crystallization, filtration, and drying

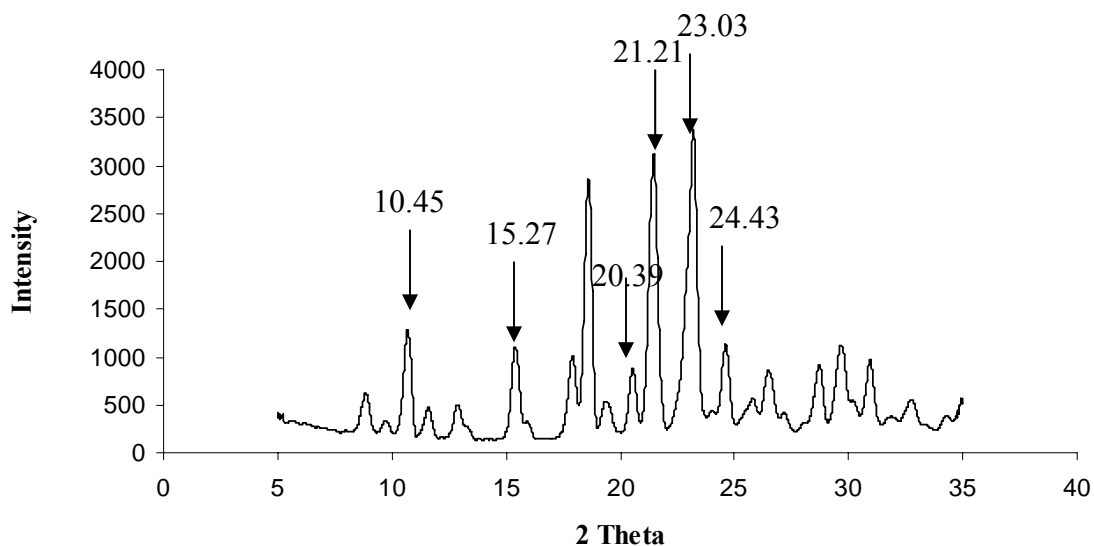


Figure III.29 Powder X-ray diffractogram for AS particles precipitated from EA produced from R_a ratio 1:200 (w/w) after a crystal maturation time of 1440 minutes, filtration, and drying

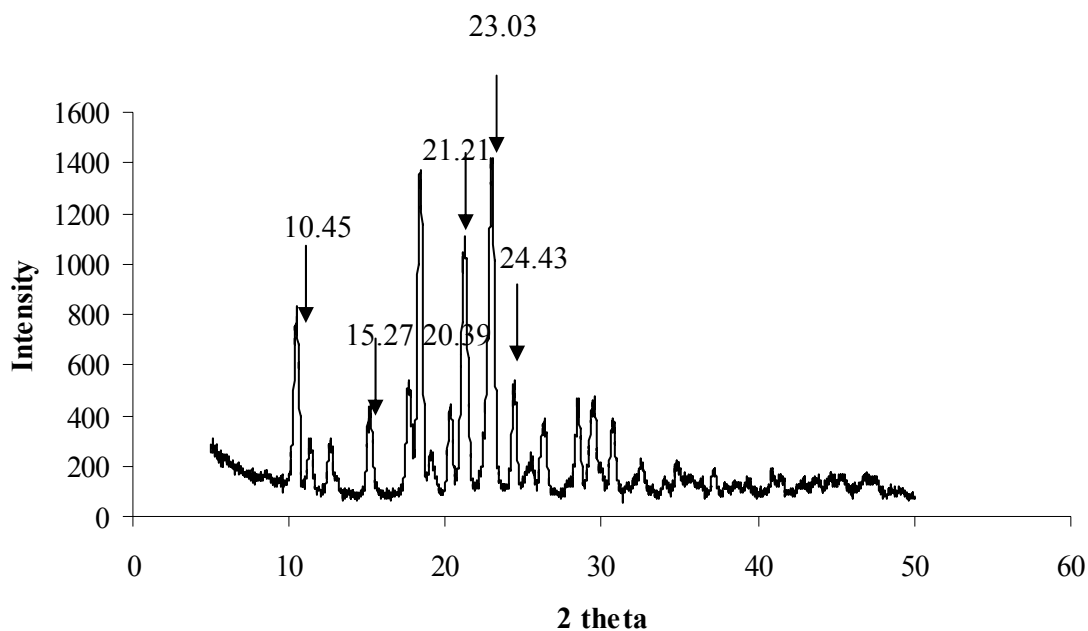


Figure III.30 Powder X-ray diffractogram for AS particles precipitated from EA produced from R_a ratio 1:500 (w/w) after a crystal maturation time of 1440 minutes, filtration, and drying

Particles produced from R_a ratio 1:1000 (w/w) using the lower stirring speeds (i.e.; 100 and 200 r.p.m.) underwent an increase in % crystallinity as a function of crystal maturation time and attained 100% crystallinity at the end of 1440 minutes. Thermal analysis of these particles after filtration, and drying revealed no difference in the heats of fusion and estimated % crystallinity values relative to those obtained before filtration (100 r.p.m.: $\Delta H_f = 198.6 \pm 2.4$ J/g, estimated % crystallinity = $98.8 \pm 0.7\%$; 200 r.p.m.: $\Delta H_f = 199.2 \pm 2.8$ J/g, estimated % crystallinity = $99.3 \pm 0.8\%$) thereby indicating that the particles produced after a crystal maturation time of 1440 minutes at 100 and 200 r.p.m. were 100% crystalline and did not undergo any changes in their solid form and structure upon harvesting and drying. These 100 and 200 r.p.m. particles were therefore observed to behave similarly to particles produced at each of the stirring speeds with the R_a ratios 1:200 and 1:500 (w/w) illustrating the fact that crystal maturation could occur within and without the bulk of the mother liquor. In contrast, despite having similar initial % crystallinity at crystal maturation time = 0, compared to the 100 and 200 r.p.m. particles (49.4 ± 20.2 and $54.6 \pm 4.4\%$ respectively), the particles produced at 500 and 800 r.p.m. (51.7 ± 2.9 and 49.7 ± 5.7 % respectively) showed markedly different crystallization behavior as a function of crystal maturation time. Table III.10 shows that at both stirring speeds (i.e.; 500 and 800 r.p.m.), estimated % crystallinity decreased over prolonged crystal maturation times where the final % crystallinity at 1440 minutes for 500 and 800 r.p.m. particles was 38.0 ± 3.9 and $36.4 \pm 6.5\%$ respectively. Given that the only change in these experiments was stirring speed, it is tempting to speculate that the nature of these crystals initially seeded at 500 and 800 r.p.m. had a crystal structure that was polymorphically different to that seen in the other particles. This was something that could not be confirmed by crystallography because of the need to dry the product before study. However, when these particles were harvested by filtration

and dried under ambient conditions for 24 hours, complete crystallization was then found to occur. This was indicated by their heats of fusion (199.8 ± 2.7 J/g for particles produced at 500 r.p.m., 200.2 ± 1.8 J/g for particles produced at 800 r.p.m.) which resulted in estimated % crystallinity values of $99.9 \pm 1.3\%$ for particles produced at 500 r.p.m., $100.0 \pm 0.8\%$ for particles produced at 800 r.p.m. respectively.

Table III.10 Mean \pm SD heats of fusion and estimated % crystallinity values for AS particles precipitated from EA produced from R_a ratio 1:1000 (w/w) at different crystal maturation times

Stirring speed (r.p.m.)	Crystal maturation time (minutes)	Heat of fusion (Mean \pm SD) J/g	Estimated % crystallinity (Mean \pm SD)
100	0	98.8 ± 40.3	49.4 ± 20.2
	60	118.9 ± 8.6	59.4 ± 4.3
	180	158.4 ± 3.4	79.2 ± 1.8
	1440	198.3 ± 11.1	99.2 ± 5.6
200	0	109.2 ± 8.9	54.6 ± 4.4
	60	114.5 ± 11.3	57.3 ± 5.7
	1440	189.3 ± 15.4	94.7 ± 7.7
500	0	103.3 ± 5.8	51.7 ± 2.9
	60	79.3 ± 27.1	39.6 ± 13.5
	180	66.9 ± 26.0	33.5 ± 13.0
	1440	76.0 ± 7.9	38.0 ± 3.9
800	0	99.3 ± 11.4	49.7 ± 5.7
	60	76.5 ± 34.0	38.2 ± 17.0
	120	61.7 ± 18.5	30.9 ± 9.2
	1440	72.7 ± 13.0	36.4 ± 6.5

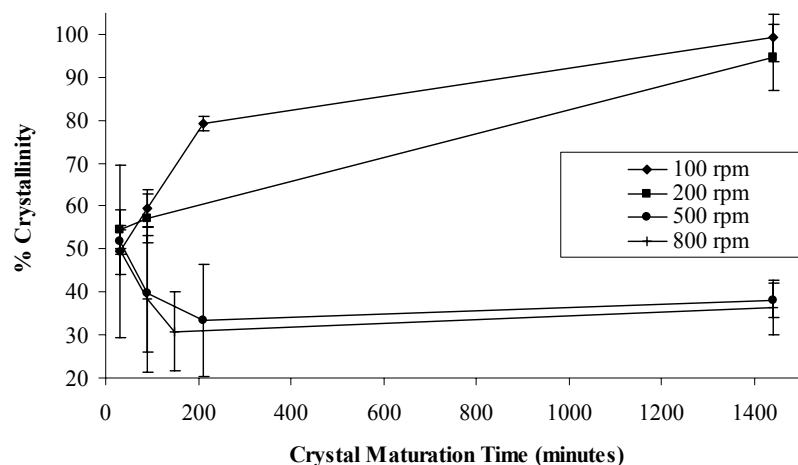


Figure III.31 Estimated % crystallinity of AS particles precipitated from EA as a function of crystal maturation time for R_a ratio 1:1000 (w/w)

A representative powder X-ray diffractogram for the particles produced at 500 r.p.m. from R_a ratio 1:1000 (w/w) after 1440 minutes of crystallization, filtration, sonication and drying under ambient conditions is shown in Figure III.32. This diffractogram showed characteristic peaks at the same positions as reference AS and no halo indicating the crystalline nature of these particles.

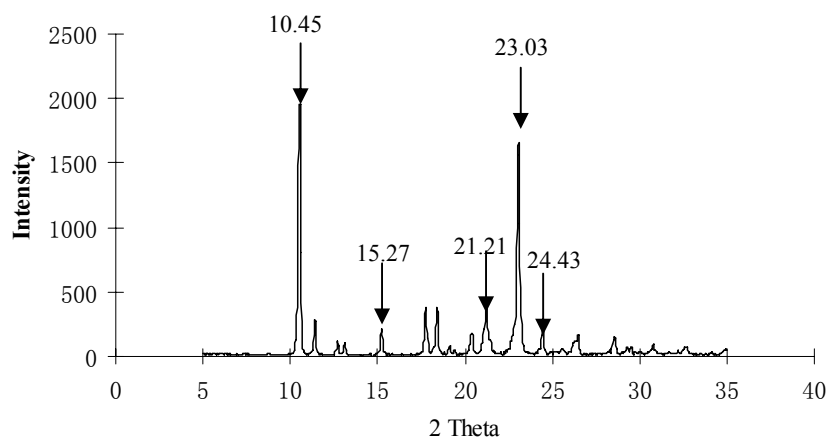


Figure III.32 Powder X-ray diffractogram for AS particles precipitated from EA produced from R_a ratio 1:1000 (w/w) at 500 r.p.m. after crystal maturation time 1440 minutes, filtration, sonication, and drying

The results for estimated % crystallinity therefore showed an influence of the crystallization conditions, notably the speed of mixing, on the crystallization kinetics of AS particles. In order to understand the effects that different crystallization variables had on the estimated % crystallinity of AS particles, the data for estimated % crystallinity was statistically analyzed without any transformation using JMP 7.0 as the statistical software. The model fitting platform was used to analyze the data for each response variable wherein the variables were split into:

- 1) Main Factors: R_a ratio, stirring speed, crystal maturation time
- 2) Interactions: R_a ratio \times stirring speed \times crystal maturation time
- 3) Response variable: Estimated % crystallinity

The results for statistical analysis of the estimated % crystallinity are shown in Table III.11.

Table III.11 Statistical analysis of the effect of crystallization variables on AS particle crystallinity

Source	Degrees of freedom	F-value	p-value
Model	52	20.4	<0.0001
R_a Ratio	2	60.9	<0.0001
Stirring Speed	6	41.5	<0.0001
Crystal maturation time	4	58.9	<0.0001
R_a Ratio \times Stirring Speed \times Crystal maturation time	40	4.8	<0.0001
R^2	0.89		
Adj R^2	0.85		

The model was found to be significant and capable of accounting for 85% of the variability in the estimated % crystallinity. The three main factors showed a significant interaction. Therefore, it is not possible to comment on the influence of any one crystallization

variable on the estimated % crystallinity although it can be said that the estimated % crystallinity of the AS particles was influenced by R_a ratio, stirring speed, and crystal maturation time where all these parameters significantly interacted with each other.

In summary, it was demonstrated that a crystal maturation time = 0 was insufficient to bring about complete solution crystallization regardless of the crystallization conditions employed. These particles were found to undergo complete crystallization in the solid-state. Prolonging the crystallization for longer time periods was an effective means of bringing about complete solution crystallization for particles produced under all crystallization conditions except those produced from R_a ratio 1:1000 (w/w) at 500 and 800 r.p.m. These particles also underwent complete crystallization in the solid state. A complex interplay between the different crystallization variables was also revealed wherein R_a ratio, stirring speed and crystal maturation time revealed a significant interaction in their influence on estimated % crystallinity. In order to understand these effects, the mechanism of crystallization was investigated.

III.D.2.2.2 Mechanism of crystallization

Crystallization is a dynamic process. The basic driving force for a crystallization process is supersaturation as discussed in section I.A.3.1.1. Supersaturation levels are influenced by the crystallization conditions. Therefore, the role of supersaturation was investigated as a means of explaining the observed effects of different crystallization variables on estimated % crystallinity.

III.D.2.2.2a Role of supersaturation

The two most significant observations for the solvent / anti-solvent crystallization of AS were:

- 1) Incomplete crystallization after a crystal maturation time = 0
- 2) Increase in estimated % crystallinity with increasing crystal maturation time for all crystallization conditions except R_a ratio 1:1000 (w/w) at 500 and 800 r.p.m.

This partial crystallinity of AS particles after a crystal maturation time 0 was not surprising because of the nature of crystallization which is a kinetic process described in terms of two distinct steps, nucleation and crystal growth driven by the supersaturation levels. The properties of the crystals obtained are the result of the kinetic relationship between these two processes. The role of supersaturation in influencing particle size was discussed in section III.D.2.1.2. In solvent / anti-solvent crystallization, this supersaturation is attained very rapidly owing to the drowning out effect of the anti-solvent which reduces the solubility of the solute and causes it to precipitate out (Beckmann, 2000). This precipitation process is a combination of two steps; nucleation and crystal growth. Nucleation is the first decisive step in crystallization. Nucleation of solutes from solution is a two-step process (Wolde and Frenkel, 1997; Galkin and Vekilov, 2000; Vekilov, 2004; Chattopadhyay et al., 2005): the creation of a droplet of a dense liquid, metastable with respect to the crystalline state, followed by ordering within this droplet to form a three-dimensional lattice structure. The second step involved in crystallization is crystal growth. Crystal growth is a multi-step process (Rodríguez-Hornedo and Murphy, 1999, Davey and Garside, 2000), which includes (1) transport of a growth unit (a single molecule, atom, ion, or cluster) from or through the bulk solution to an impingement site, which is not necessarily the final growth site (i.e. site of incorporation into the crystal); (2) adsorption of the growth unit at the impingement site, (3) diffusion of the growth units from the impingement site to a growth site, and (4) incorporation into the crystal lattice. This final step of incorporation of molecules into the crystal lattice is a determinant of crystallinity. The crystallinity is determined by the

formation of a perfect crystalline lattice which is a time dependent process (Mullin, 2001). Therefore, even though particle formation may occur rapidly in solvent / anti-solvent crystallization, the re-organization of the molecular units into the crystal lattice takes time and is drug-dependent. This time dependent nature of the crystallization process may be responsible for the incomplete crystallinity after a crystal maturation time = 0 observed for all conditions.

The differences in the crystallization behavior as a function of time that were observed for particles produced under different crystallization conditions may be explained by the supersaturation levels. Supersaturation drives the nucleation process which is the first decisive step in crystallization and involves clustering of solute molecules to form embryos that grow into nuclei. According to the classical nucleation theory (Volmer, 1939; Gibbs, 1948; Nielsen, 1964), an activation energy barrier needs to be overcome for nucleation to proceed. A certain degree of supersaturation is required to overcome the free energy barrier to nucleation. Higher the supersaturation, lower is the free energy barrier to nucleation and hence, faster is the nucleation process. After this stage, the cluster becomes viable and is termed a nucleus, which eventually grows into a crystal. Hence, it is easier to form nuclei at higher supersaturation levels leading to an increased driving force for crystallization. This leads to faster nucleation and therefore, faster subsequent crystallization.

The supersaturation levels for the three R_a ratios were calculated in section III.D.2.1.2 as:

R_a ratio 1:200 (w/w): 5.2

R_a ratio 1:500 (w/w): 4.5

R_a ratio 1:1000 (w/w): 3.4

The higher levels of supersaturation for R_a ratios 1:200 and 1:500 (w/w) would lead to a higher driving force for crystallization, faster nucleation, and hence faster subsequent

crystallization. This mechanism might account for the observation that particles produced from R_a ratio 1:200 and 1:500 (w/w) underwent complete solution crystallization over a 24 hour period. For R_a ratio 1:1000, a difference in crystallization behavior was observed as a function of the crystallization conditions wherein particles produced at 100 and 200 r.p.m. underwent complete solution crystallization over a 24 hour period while particles produced under 500 and 800 r.p.m. did not do so. These differences cannot be explained solely by the role of supersaturation since the supersaturation ratio would be the same for R_a ratio 1:1000 (w/w) irrespective of stirring speed. Therefore, in order to explain these differences in crystallization behavior, the role of water in solution crystallization was investigated.

III.D.2.2.2b Role of water

It is known that in the solid state, the amount of water present in a crystallizing particle plays an important role in determining the rate of crystallization. Crowley and Zografi (2002) have discussed the role of absorbed water in bringing about crystallization of amorphous drug/poly(vinylpyrrolidone) dispersions and have stated that water uptake by the amorphous dispersion can bring about recrystallization. Similar work by Marsac et al. (2008) on Nifedipine and Felodipine solid dispersions has also revealed a significant role of water in recrystallization of the amorphous solid dispersions. Wu and Yu (2006) have explored the role of sorbed moisture in bringing about surface crystallization of indomethacin. The work carried out by Schmitt et al. (1998) on the nucleation and crystallization kinetics of amorphous lactose has shown that moisture uptake by amorphous lactose is capable of bringing about an amorphous to crystalline transition. The moisture induced surface crystallization of spray dried amorphous lactose has also been studied by Mahlin et al. (2003) with similar results as Schmitt et al. (1998). Ballesteros

et al. (2002) have utilized microcalorimetric measurements to investigate the interactions of water vapor with amorphous pharmaceutical solids. This interaction has also been explored using Fourier transform Raman spectroscopy by Taylor et al. (2000). Ward et al. (1995) have investigated the role of moisture in bringing about solid-state recrystallization of partially amorphous albuterol sulfate. They reported that exposure to relative humidities greater than 50% was required for complete recrystallization. However, these studies investigated the solid-state crystallization of AS. In this section, the role of water in the solution crystallization i.e.; crystallization in particles suspended in solution is described. The % water content in the AS particles was measured by coulometric KF titration at different time points during the 0-1440 minutes crystallization period. In addition, solvent weight loss was similarly investigated using TGA.

III.D.2.2.2b.1 % water content after crystal maturation time = 0

Table III.12 shows the results of % water content determined using Karl Fischer titration and % weight loss determined using TGA in AS particles produced under different crystallization conditions at crystal maturation time = 0. The estimated % crystallinity values at crystal maturation time = 0 for each of these conditions are also shown in the table. The values for solvent loss obtained by the TGA agreed with the specific % water content determined by Karl Fischer titration (significant positive correlation with $R = 0.96$, $p\text{-value} < 0.0001$) indicating that the TGA method could also be used to assess % water content of the initially formed 'semi-crystalline' particles. For R_a ratio 1:200 (w/w), at crystal maturation time = 0, there was no difference in % water content for particles produced at 100, and 200 r.p.m. An increase in %water content was observed at stirring speeds of 500 and 800 r.p.m. that may explain the more

rapid arrival of complete crystallization at longer maturation times (Figure III.23, and III.24). However, despite a change in the % water content for the R_a ratio 1:200 (w/w) particles as a function of stirring speed, there was no significant change in estimated % crystallinity as shown in Table III.12 at a maturation time = 0. Particles produced from R_a ratio 1:500 (w/w) showed similar % water contents under all four stirring speeds (p-value > 0.05, Tukey's HSD). This similarity in initial water contents at crystal maturation time = 0 was also reflected in similarity in estimated % crystallinity values for these particles (Table III.12). Therefore, for R_a ratios 1:200 and 1:500 (w/w), there did not appear to be a significant influence of stirring speed on % water content implying that the the stirring speeds employed were not been sufficiently high to bring about efficient mixing between the drug solution and anti-solvent leading to zones of locally high supersaturation causing solute-solute interactions to dominate during particle precipitation.

Table III.12 Mean \pm SD % water contents (determined by Karl Fischer titration) and % weight loss (determined by TGA) for AS particles precipitated from EA produced after crystal maturation time 0 under different crystallization conditions

R_a ratio (w/w)	Stirring speed (r.p.m.)	% Weight loss (Mean \pm SD)	% Water (Mean \pm SD)	Estimated % crystallinity (Mean \pm SD)
1:200	100	24.6 \pm 7.5	23.4 \pm 6.5	66.3 \pm 1.5
	200	23.5 \pm 4.8	24.4 \pm 8.3	64.0 \pm 3.6
	500	33.9 \pm 1.4	33.5 \pm 1.7	62.0 \pm 5.9
	800	43.2 \pm 1.4	44.2 \pm 1.4	72.9 \pm 10.1
1:500	100	37.7 \pm 8.4	30.0 \pm 1.8	55.4 \pm 2.9
	200	33.1 \pm 4.4	32.0 \pm 6.8	69.0 \pm 9.5
	500	27.9 \pm 6.4	29.9 \pm 7.5	64.0 \pm 10.8
	800	32.1 \pm 6.6	29.8 \pm 6.0	65.3 \pm 23.7
1:1000	100	25.3 \pm 4.8	26.9 \pm 7.5	49.4 \pm 20.2
	200	27.2 \pm 4.3	25.9 \pm 8.1	54.6 \pm 4.4
	500	10.5 \pm 1.2	9.1 \pm 1.9	51.7 \pm 2.9
	800	12.2 \pm 3.5	11.7 \pm 3.3	49.7 \pm 5.7

In contrast to the results for 1:200 and 1:500 (w/w) R_a ratios, the % water content in particles produced from R_a ratio 1:1000 (w/w) was observed to decrease at higher stirring speeds. The particles produced under lower stirring speeds of 100, and 200 r.p.m. had significantly higher % water contents at crystal maturation time = 0 than the particles produced at the higher stirring speeds of 500, and 800 r.p.m.

While differences in % water content were not related to estimated % crystallinity values because similar values for % crystallinity were obtained for particles produced under all crystallization conditions as shown in Table III.12 the fact that the only significant deviation in water content was only observed for particles produced at crystal maturation time = 0 for the R_a ratio 1:1000 (w/w) when mixed at 500 and 800 r.p.m. was impossible to ignore. It appeared therefore, that these particles with % water contents around 10% began at a crystal maturation time = 0, with a comparable % crystallinity to all the others (Table III.12). Unlike all the other AS particles, however, these particles showed evidence of reduced water content. This change in content appeared to coincide with either a lack of subsequent recrystallization or a net fall in crystallinity over time when left in contact with the mother liquor (Figure III.31).

III.D.2.2.b.2 % water content at crystal maturation times between 0 – 24 hours

Table III.13 shows the % water contents for AS particles produced from R_a ratio 1:200 (w/w) under different stirring speeds at different crystal maturation times. The TGA estimated % weight loss and estimated % crystallinity values from DSC measurements are also shown. Once again, the % weight loss estimated from the TGA agreed with the % water content measured by Karl Fischer titration indicating the suitability of the TGA method to estimate % water content also.

Table III.13 Mean \pm SD % water contents, % weight loss, and estimated % crystallinity for AS particles precipitated from EA produced from R_a ratio 1:200 (w/w) under different stirring speeds as a function of crystal maturation time

Stirring speed (r.p.m.)	Crystal maturation time (minutes)	% Weight loss (Mean \pm SD)	% Water (Mean \pm SD)	Estimated % crystallinity (Mean \pm SD)
100	0	24.6 \pm 7.5	23.4 \pm 6.5	66.3 \pm 1.5
	60	15.7 \pm 2.4	16.5 \pm 1.1	78.6 \pm 5.0
	120	6.8 \pm 0.9	6.8 \pm 0.4	80.1 \pm 1.2
	1440	0.9 \pm 1.2	0.9 \pm 1.1	101.0 \pm 1.1
200	0	23.5 \pm 4.8	24.4 \pm 8.3	64.0 \pm 3.6
	60	17.2 \pm 4.3	16.1 \pm 0.3	67.7 \pm 1.9
	120	9.8 \pm 2.4	12.6 \pm 0.8	80.3 \pm 0.8
	1440	5.2 \pm 0.9	5.4 \pm 0.4	97.2 \pm 3.5
500	0	33.9 \pm 1.4	33.5 \pm 1.7	62.0 \pm 5.9
	60	25.6 \pm 4.3	27.6 \pm 2.6	76.3 \pm 2.9
	1440	2.0 \pm 1.0	2.0 \pm 0.9	99.2 \pm 0.8
800	0	43.2 \pm 1.4	44.2 \pm 1.4	72.9 \pm 10.1
	60	35.4 \pm 2.8	38.6 \pm 1.2	81.4 \pm 1.4
	120	11.7 \pm 1.9	12.9 \pm 1.7	86.8 \pm 2.2
	180	9.9 \pm 2.6	10.7 \pm 1.3	92.0 \pm 6.8
	1440	3.9 \pm 1.8	4.4 \pm 1.4	100.8 \pm 1.3

Figure III.33 shows the estimated % crystallinity values and % water contents for R_a ratio 1:200 (w/w) particles at different stirring speeds as a function of crystal maturation time. It was observed that the % water content in the particles decreased as the crystal maturation time increased and this decrease in % water content was accompanied by an increase in the estimated % crystallinity of the AS particles produced from R_a ratio 1:200 (w/w) under all four stirring speeds. At the end of 1440 minutes, the % water content in these particles was approximately 1-5% and crystallization appeared to be complete with estimated % crystallinity values of 97-101%. A correlation analysis between % water content and estimated % crystallinity for R_a ratio 1:200 (w/w) for all four stirring speeds resulted in a strong, negative correlation ($R = -0.71$, p -value < 0.0001) as shown in Figure III.34. Table III.14 shows the % water contents for AS particles produced from R_a ratio 1:500 (w/w) under different stirring speeds at different crystal

maturation times. The TGA estimated % weight loss and estimated % crystallinity values from DSC measurements are also shown. Figure III.35 shows the estimated % crystallinity values and % water contents for R_a ratio 1:500 (w/w) particles at different stirring speeds as a function of crystal maturation time.

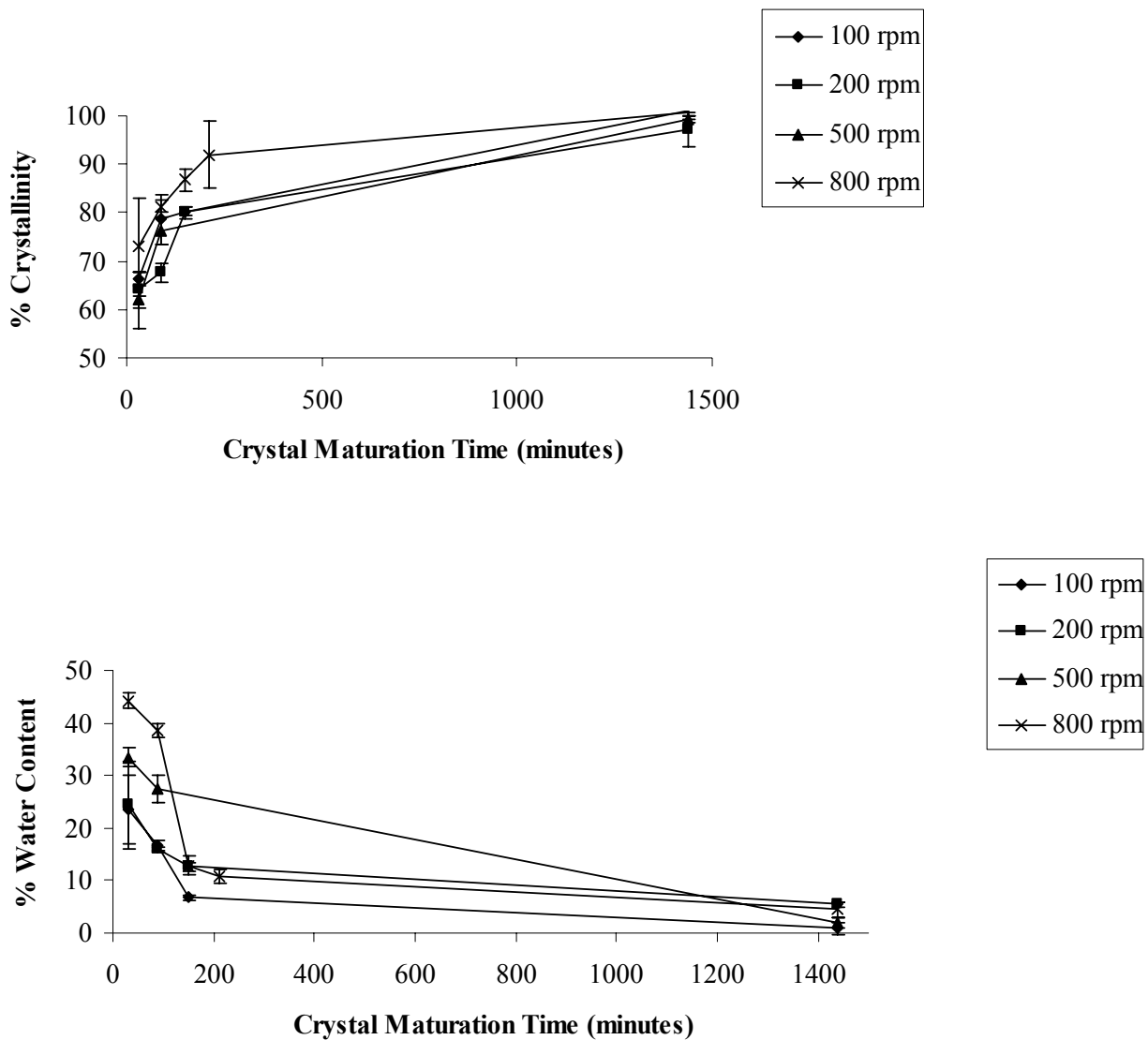


Figure III.33 Estimated % crystallinity and % water content for AS particles precipitated from EA produced from R_a ratio 1:200 (w/w) under different stirring speeds at different crystal maturation times

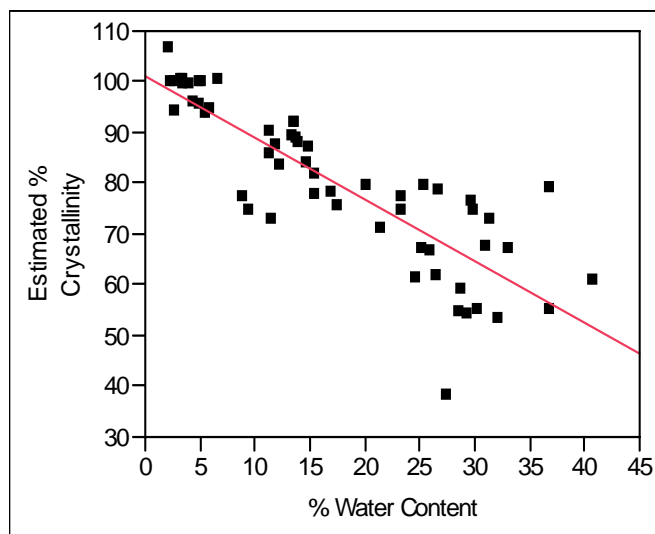


Figure III.34 Correlation analysis between estimated % crystallinity and % water content for AS particles precipitated from EA produced from R_a ratio 1:200 under all stirring speeds

Table III.14 Mean \pm SD % water contents (determined by Karl Fischer titration) and % weight loss (determined by TGA) for AS particles precipitated from EA produced from R_a ratio 1:500 (w/w) under different stirring speeds as a function of crystal maturation time

Stirring speed (r.p.m.)	Crystal maturation time (minutes)	% Weight loss (Mean \pm SD)	% Water (Mean \pm SD)	Estimated % crystallinity (Mean \pm SD)
100	0	37.7 \pm 8.4	30.0 \pm 1.8	55.4 \pm 2.9
	60	29.2 \pm 2.6	28.4 \pm 1.9	57.0 \pm 4.1
	180	15.4 \pm 3.5	14.6 \pm 0.8	84.4 \pm 3.1
	1440	3.8 \pm 0.9	3.2 \pm 0.6	99.7 \pm 0.4
200	0	33.1 \pm 4.4	32.0 \pm 6.8	69.0 \pm 9.5
	60	28.7 \pm 3.2	28.0 \pm 2.9	72.6 \pm 5.9
	120	15.7 \pm 2.4	16.5 \pm 1.0	77.0 \pm 1.5
	180	13.4 \pm 1.8	13.2 \pm 1.8	87.0 \pm 1.7
	1440	3.4 \pm 1.2	3.6 \pm 1.7	99.8 \pm 6.5
500	0	27.9 \pm 6.4	29.9 \pm 7.5	64.0 \pm 10.8
	60	25.6 \pm 2.6	26.9 \pm 5.4	70.8 \pm 3.5
	120	11.4 \pm 1.9	10.7 \pm 1.9	74.8 \pm 2.3
	180	10.3 \pm 2.8	12.5 \pm 1.2	91.2 \pm 1.0
	1440	5.7 \pm 1.0	5.5 \pm 0.9	99.8 \pm 0.3
800	0	32.1 \pm 6.6	29.8 \pm 6.0	65.3 \pm 23.7
	60	25.4 \pm 3.6	26.0 \pm 3.4	73.0 \pm 5.4
	120	12.8 \pm 1.5	12.5 \pm 0.7	86.6 \pm 3.1
	180	5.4 \pm 1.2	5.0 \pm 0.8	95.2 \pm 0.8
	1440	3.0 \pm 0.5	2.7 \pm 0.6	98.0 \pm 3.4

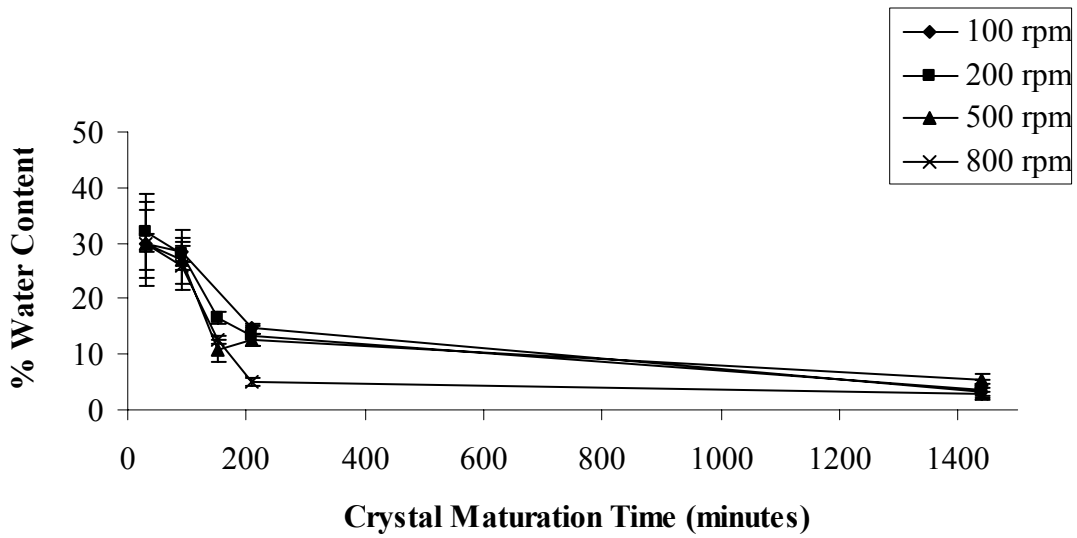
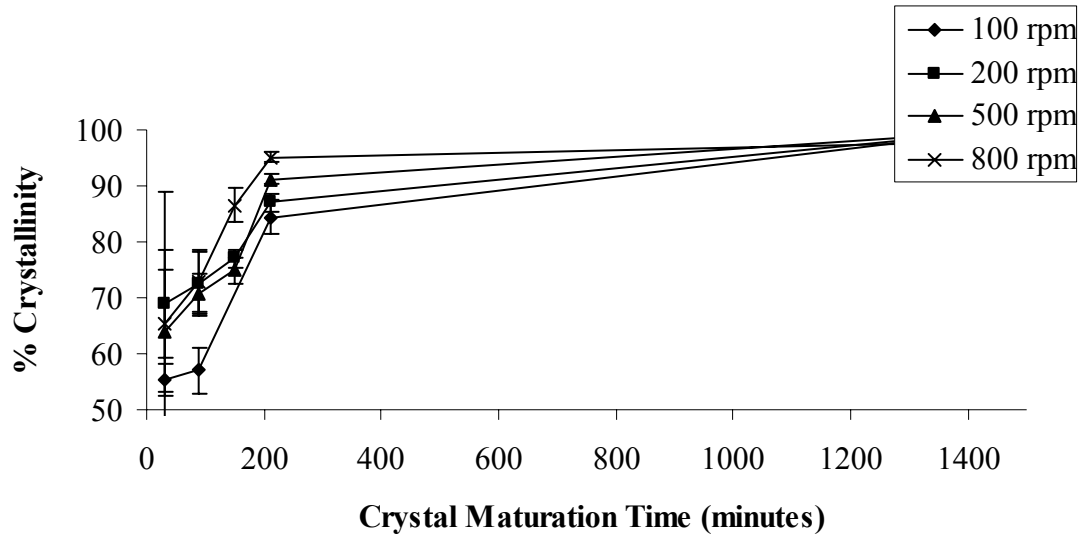


Figure III.35 Estimated % crystallinity and % water content for AS particles precipitated from EA produced from R_a ratio 1:500 (w/w) under different stirring speeds at different crystal maturation times

It was observed that the % water content in the particles decreased as the crystal maturation time increased and this decrease in % water content was accompanied by an increase in the estimated % crystallinity of the AS particles produced from R_a ratio 1:500 (w/w) under all four stirring speeds. At the end of 1440 minutes of crystallization, the % water content in these particles was approximately 3-5% and crystallization appeared to be complete with estimated % crystallinity values of 98-100%. A correlation analysis between % water content and estimated % crystallinity for R_a ratio 1:500 (w/w) for all four stirring speeds resulted in a strong and negative correlation ($R = -0.85$, $p\text{-value} < 0.0001$) as shown in Figure III.36.

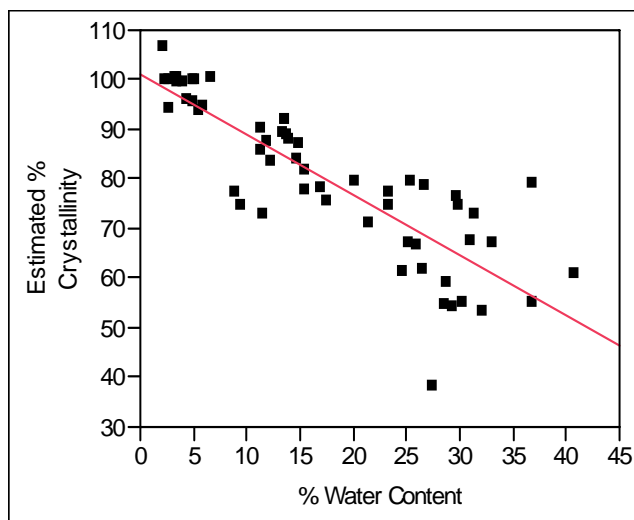


Figure III.36 Correlation analysis between estimated % crystallinity and % water content for AS particles precipitated from EA produced from R_a ratio 1:500 under all stirring speeds

These results for R_a ratio 1:500 (w/w) were therefore similar to R_a ratio 1:200 (w/w) where a similar correlation between estimated % crystallinity and % water content was observed as a function of crystal maturation time for all four stirring speeds. In contrast, particles produced from R_a ratio 1:1000 (w/w) behaved differently in terms of crystallization behavior and

accompanying water loss. These differences were observed to be related to the stirring speeds. Table III.15 shows the % water contents for AS particles produced from R_a ratio 1:1000 (w/w) under different stirring speeds at different crystal maturation times. The TGA estimated % weight loss and estimated % crystallinity values from DSC measurements are also shown.

Table III.15 Mean ± SD % water contents (determined by Karl Fischer titration) and % weight loss (determined by TGA) for AS particles precipitated from EA produced from R_a ratio 1:1000 (w/w) under different stirring speeds as a function of crystal maturation time

Stirring speed (r.p.m.)	Crystal maturation time (minutes)	% Weight loss (Mean ± SD)	% Water (Mean ± SD)	Estimated % crystallinity (Mean ± SD)
100	0	25.3 ± 4.8	26.9 ± 7.5	49.4 ± 20.2
	60	21.2 ± 1.3	20.9 ± 0.4	59.4 ± 4.3
	180	15.4 ± 2.4	16.9 ± 0.9	79.2 ± 1.8
	1440	3.6 ± 2.5	3.4 ± 2.3	99.2 ± 5.6
200	0	27.2 ± 4.3	25.9 ± 8.1	54.6 ± 4.4
	60	16.5 ± 1.8	15.5 ± 1.2	57.3 ± 5.7
	1440	3.3 ± 3.4	1.9 ± 2.4	94.7 ± 7.7
500	0	10.5 ± 1.2	9.1 ± 1.9	51.7 ± 2.9
	60	7.2 ± 1.8	6.7 ± 3.1	39.6 ± 13.5
	180	5.1 ± 1.6	5.0 ± 3.3	33.5 ± 13.0
	1440	4.4 ± 0.8	3.7 ± 1.7	38.0 ± 3.9
800	0	12.2 ± 3.5	11.7 ± 3.3	49.7 ± 5.7
	60	10.2 ± 2.4	9.6 ± 3.6	38.2 ± 17.0
	120	8.2 ± 1.9	7.8 ± 3.5	30.9 ± 9.2
	1440	4.0 ± 1.0	3.7 ± 0.7	36.4 ± 6.5

Figure III.37 shows the estimated % crystallinity values and % water contents for R_a ratio 1:1000 (w/w) particles at different stirring speeds as a function of crystal maturation time.

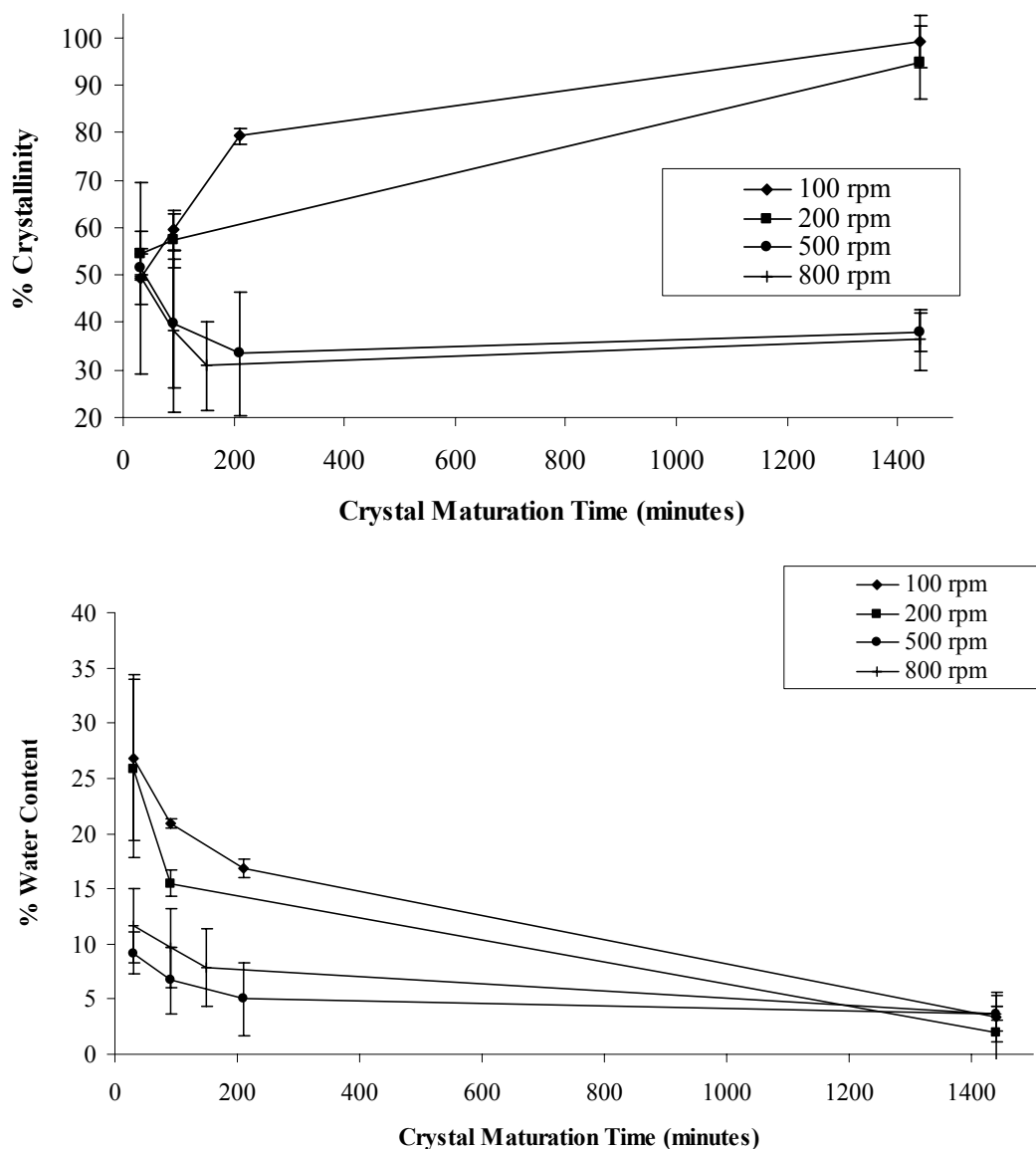


Figure III.37 Estimated % crystallinity and % water content for AS particles precipitated from EA produced from R_a ratio 1:1000 (w/w) under different stirring speeds at different crystal maturation times

For R_a ratio 1:1000 (w/w), the % water content decreased in particles produced at all four stirring speeds. At the end of 1440 minutes of crystallization, the final % water content was between 2-4%. This decrease in % water content was accompanied by a corresponding increase in estimated % crystallinity for particles produced at 100 and 200 r.p.m. as shown in Table III.15

and Figure III.37. For these particles, a significant negative correlation was observed between % water content and estimated % crystallinity ($R = -0.76$, $p\text{-value} < 0.0001$) as shown in Figure III.38. These results were therefore similar to the results obtained for R_a ratios 1:200 and 1:500 (w/w) where particles produced at all four stirring speeds underwent a decrease in % water content with an accompanying increase in estimated % crystallinity as a function of crystal maturation time.

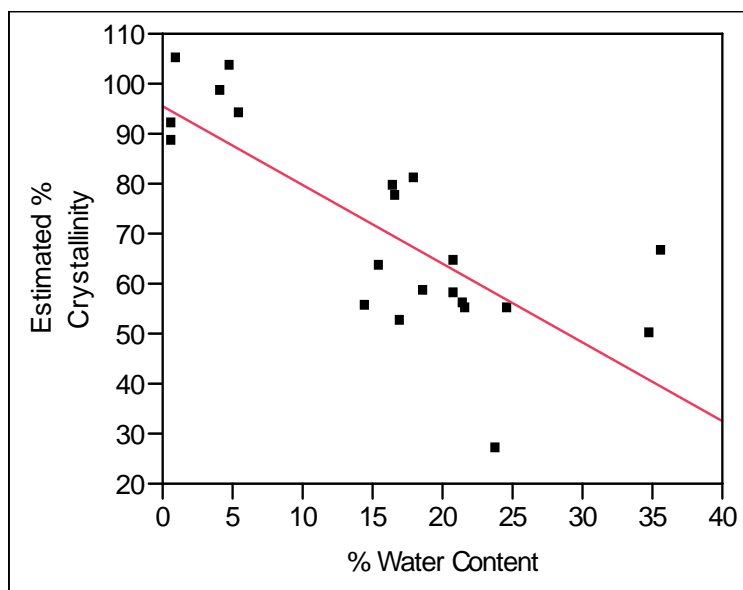


Figure III.38 Correlation analysis between estimated % crystallinity and % water content for AS particles precipitated from EA produced from R_a ratio 1:1000 under stirring speeds 100 and 200 r.p.m.

However, particles produced from R_a ratio 1:1000 (w/w) at 500 and 800 r.p.m. behaved differently in terms of crystallization behavior and accompanying water loss. A decrease in % water content was observed as a function of crystal maturation time reaching $\approx 4.0\%$ at the end of 1440 minutes which was similar to the final water content for AS particles produced under other crystallization conditions. However, this decrease was not accompanied by a corresponding

increase in estimated % crystallinity as shown in Table III.15 and Figure III.37. Therefore, this difference in crystallization behavior could not be explained by the change in % water content as a function of crystal maturation time. However, these particles contained significantly lower levels of water (i.e.; $\approx 10\%$) at crystal maturation time = 0 compared to particles produced under other crystallization conditions that contained higher % water contents (i.e.; $> 20\%$). Even though this initial % water content did not show a relationship with estimated % crystallinity at crystal maturation time = 0, it nevertheless influenced the subsequent crystallization behavior as a function of crystal maturation time.

TGA analysis revealed differences in the binding state of water which were related to its initial level at crystal maturation time = 0. Figure III.39 shows the representative water loss profiles for the AS particles produced from R_a ratio 1:1000 at 100 and 800 r.p.m. after mixing for 30 minutes (crystal maturation time = 0). The particles produced at 100 r.p.m. containing higher levels of water started to lose this water at ambient temperatures of 25°C . In contrast, water loss from the AS particles produced at 800 r.p.m. did not begin until a much higher temperature of 60°C had been attained. These results indicated that the water was bound much more tightly in the case of these latter particles produced from R_a ratio 1:1000 at higher stirring speeds.

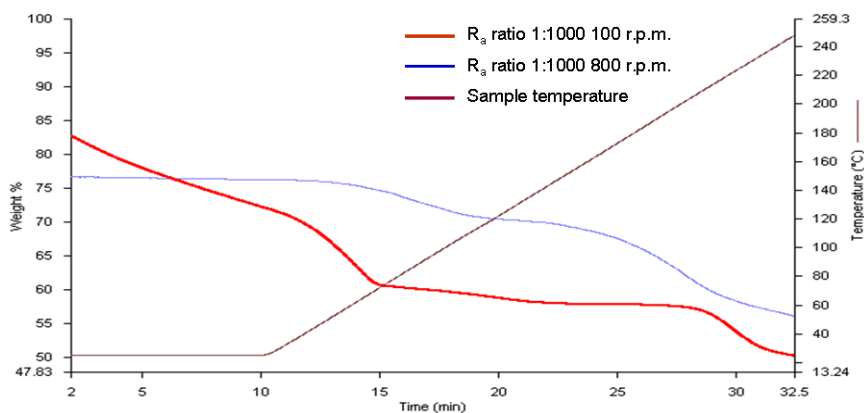


Figure III.39 Representative TGA profiles for AS particles precipitated from EA produced from R_a ratio 1:1000 at stirring speeds 100 and 800 r.p.m. after crystal maturation time = 0

These results therefore brought into focus the significant role of water in solution crystallization of AS. Water can not only induce an amorphous to crystalline transition by its ability to act as a plasticizer. When incorporated into the amorphous regions of particles, water brings about an increase in molecular mobility and hence leads to molecular rearrangement required for crystallization. This is referred to as its plasticizing effect. The plasticizing effect of water has been described in literature for solid-state crystallization. Hancock and Shamblin (2001) have investigated the role of water in bringing about molecular mobility of amorphous pharmaceuticals resulting in solid-state crystallization. Zografi and co-workers (1988) stated that this plasticizing effect of water is related to both its quantity and existence state in the particles. Water can exist in either a “solvent-like” or “bound” state in the solids. At higher moisture contents, water molecules are believed to be able to cluster and to begin the process of forming “solvent-like” water. In the “solvent-like” state, water molecules have greater mobility. This existence state of water exerts a much more efficient plasticizing effect compared to the “bound” water. Therefore, the crystallization behavior in the experimental system described in this thesis is likely explained by considering the quantity and existence state of water in the albuterol sulfate particles that are first formed by precipitation. AS particles produced from R_a ratios 1:200 and 1:500 (w/w) under all stirring speeds and those produced from R_a ratio 1:1000 (w/w) at 100 and 200 r.p.m. were shown to contain high water levels approximately 30% by weight. Moreover, water loss from these molecular associations was observed to start at low temperatures $\sim 25^\circ\text{C}$. This high level of water appeared to exist in the “solvent-like” state and behave as efficient plasticizer leading to complete crystallization. In contrast, AS particles produced from R_a ratio 1:1000 (w/w) at 500 and 800 r.p.m. contained low levels of water which appeared to be present in a “highly bound” state that could not be as easily removed using TGA.

It remains possible that these ‘precrystalline forms’ or molecular associations of AS+H₂O have completely different structures where only one converted readily to AS as a function of crystal maturation time.

In summary, it was demonstrated that at crystal maturation time = 0, the crystallization conditions did not have a significant influence on final collected particle crystallinity. Regardless of the crystallization conditions used, incompletely crystalline particles were produced. Longer crystal maturation times influenced particle crystallinity. This influence was related to the crystallization conditions wherein particles produced from R_a ratios 1:200 and 1:500 (w/w) under all four stirring speeds and particles produced from R_a ratio 1:1000 (w/w) under 100 and 200 r.p.m. underwent complete solution crystallization as a function of crystal maturation time. However, particles produced from R_a ratio 1:1000 (w/w) under 500 and 800 r.p.m. failed to convert to crystals completely when held for 24 hours in the mother liquor. The role of supersaturation and water was investigated to explain these differences. It was observed that the % water content in the particles was influenced by the crystallization conditions and that loosely bound water was able to promote crystallization while tightly bound water blocked the phenomenon. These differences in the plasticizing effect of water may have been responsible for the differences in the solution crystallization behavior of the AS particles. This was an important finding as it demonstrates the significant role that water plays in the crystallization process. Harvesting and drying all the products however, resulted in complete crystallization and formation of a single polymorphic form of AS.

III.D.2.2.3 Particle size distribution of AS particles after crystal maturation time = 24 hours

The particle size was the second response variable of interest since it was an objective to produce completely crystalline particles directly in a size range suitable for inhalation (1-5 μm) without the need for further size reduction by micronization. Investigation of the crystallization process yielded completely crystalline particles from all crystallization conditions except R_a ratio 1:1000 (w/w) at 500 and 800 r.p.m. Therefore, it was of interest to measure the particle size of these particles.

Figure III.40 shows the cumulative % undersize volume distribution of AS particles produced from R_a ratio 1:200 (w/w) at the four different stirring speeds after a crystal maturation time = 24 hours. The volume frequency distribution of these particles is shown in Figure III.41. The VMDs and span indices of these particles are shown in Table III.16. As was the case with the particles harvested at crystal maturation time = 0, particles harvested after crystal maturation time = 24 hours from R_a ratio 1:200 (w/w) did not reveal any influence of stirring speed on particle size. This can be seen from Figures IV.40 and IV.41 which show overlying PSDs for the particles produced under the different stirring speeds. A statistical analysis of the VMDs revealed no significant difference between the particles produced at 100, 200, 500, and 800 r.p.m. (p -value > 0.05, Tukey's HSD). However, compared to the particles harvested at crystal maturation time = 0, particles produced after crystal maturation time = 24 hours were significantly smaller in size. Figure IV.42 shows the cumulative % undersize volume distributions of AS particles produced from R_a ratio 1:200 (w/w) under a stirring speed of 100 r.p.m. at crystal maturation time = 0 and crystal maturation time = 24 hours. Table III.16 shows the VMDs and span indices of the particles produced from R_a ratio 1:200 (w/w) under different stirring speeds at a crystal maturation time = 0 and 24 hours. A statistical analysis of the VMDs revealed that significantly smaller particles (VMD = 10-12 μm) were produced at crystal maturation time = 24 hours

compared to crystal maturation time = 0 (VMD = 19-20 μm) (p-value < 0.05, one-way ANOVA).

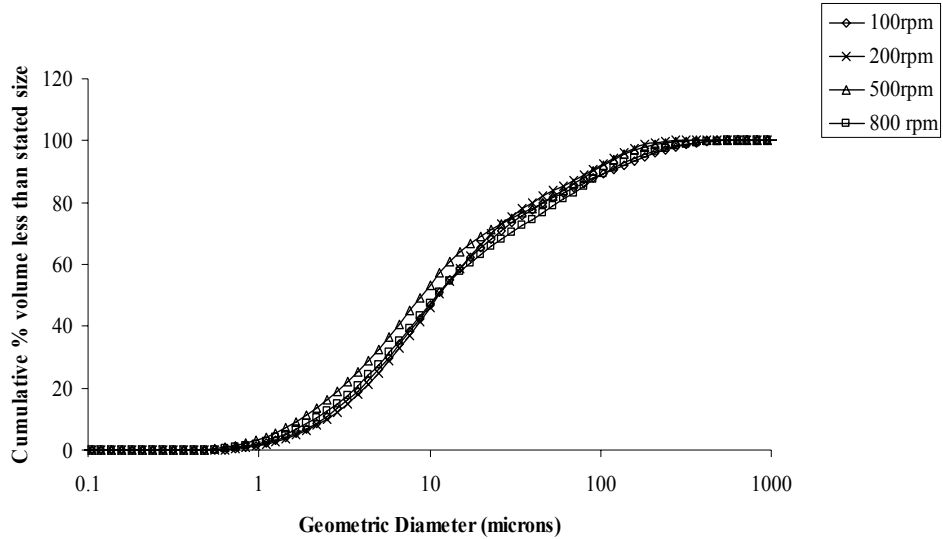


Figure III.40 Cumulative % undersize volume distribution of AS particles precipitated from EA harvested after a crystal maturation time of 1440 minutes from R_a ratio 1:200 (w/w) under different stirring speeds

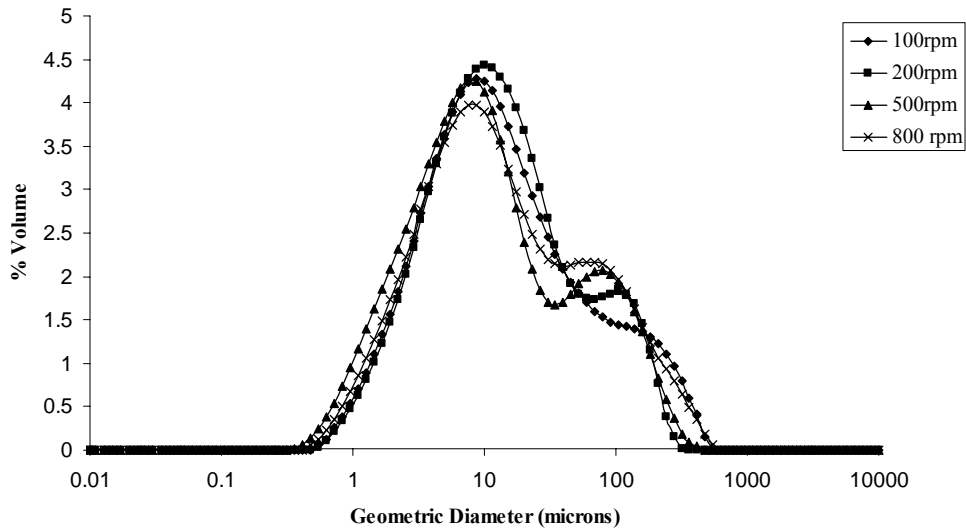


Figure III.41 Volume frequency distribution of AS particles precipitated from EA harvested after a crystal maturation time of 1440 minutes from R_a ratio 1:200 (w/w) under different stirring speeds

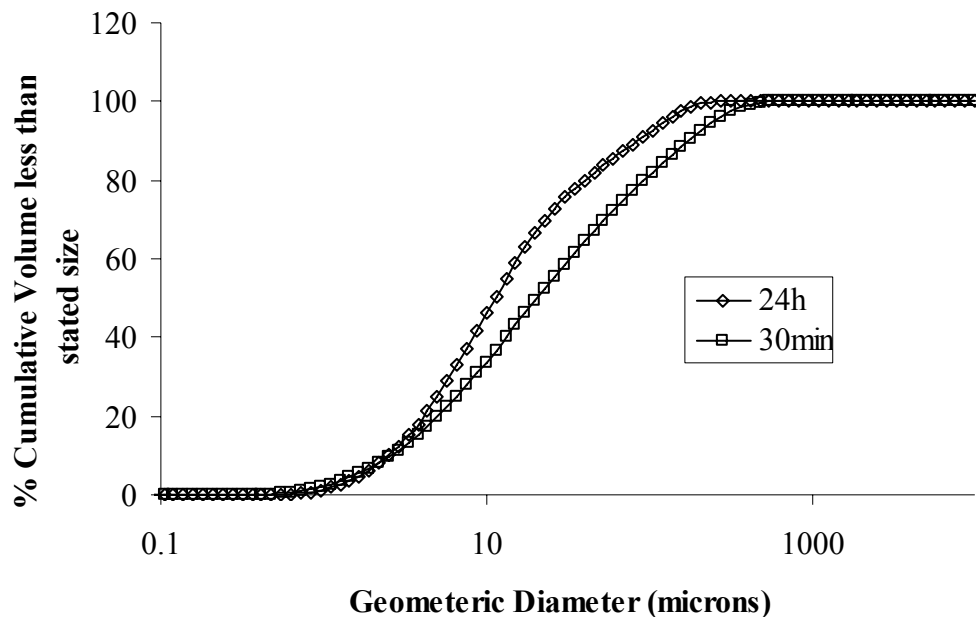


Figure IV.42 Cumulative % undersize volume distribution of AS particles precipitated from EA produced from R_a ratio 1:200 (w/w) at 100 r.p.m. after crystal maturation time = 0 and crystal maturation time = 24 hours

Table III.16 Mean \pm SD volume median diameters and span indices of AS particles precipitated from EA produced from R_a ratio 1:200 (w/w) under different stirring speeds

Stirring speed (r.p.m.)	Crystal maturation time =0		Crystal maturation time =24 hours	
	VMD \pm SD (μm)	Span index	VMD \pm SD (μm)	Span index
100	18.9 \pm 7.9	7.7	10.5 \pm 1.4	10.2
200	17.9 \pm 7.4	8.9	9.7 \pm 0.7	7.7
500	19.9 \pm 8.0	7.8	11.5 \pm 1.0	10.3
800	18.7 \pm 6.7	8.5	11.5 \pm 1.7	8.9

This influence of crystal maturation time on particle size may appear paradoxical to crystallization theory that implies only crystal growth occurs with increasing time. However, in this case the nature of the particles comes into picture. The AS particles at crystal maturation

time = 0 and crystal maturation time = 24 hours differ in their % crystallinity. At crystal maturation time = 0, partially crystalline particles were produced which underwent complete crystallization upon filtration and drying in the solid-state prior to sizing. On the other hand, particles produced at crystal maturation time = 24 hours were completely crystalline and no changes in crystallinity were observed in the solid-state prior to sizing. Therefore, it is hypothesized that the larger size of the particles produced at crystal maturation time = 0 compared to crystal maturation time = 24 hours may be an outcome of solid-state crystallization which is known for the formation of crystal bridges between adjacent particles, particle fusion and an increase in particle size. This is particularly detrimental for aerosol formulations where size is a primary concern. Therefore, these results demonstrate the importance of harvesting completely crystalline particles that are not prone towards further crystallization in the solid state. However, even though the particles produced after crystal maturation time = 24 hours were smaller in size compared to particles produced at crystal maturation time = 0, they were in a size range of 10-11 μm and hence were not small enough for inhalation (i.e.; between 1-10 μm , preferably between 1-5 μm).

The cumulative % undersize volume distributions and volume frequency distributions of particles produced from R_a ratio 1:500 (w/w) under different stirring speeds after crystal maturation time = 24 hours are shown in Figures III.43 and III.44 respectively. Bimodal distributions were observed. The VMDs and span indices of these particles are shown in Table III.17 along with the VMDs and span indices of particles produced from R_a ratio 1:500 (w/w) under different stirring speeds after crystal maturation time = 0. As was the case with R_a ratio 1:200 (w/w), particles produced from R_a ratio 1:500 (w/w) under all stirring speeds after crystal maturation time = 24 hours were significantly smaller (p-value < 0.05, one-way ANOVA) than

particles produced from R_a ratio 1:500 (w/w) under corresponding stirring speeds at crystal maturation time = 0. Therefore, these results once again illustrated the importance of harvesting completely crystalline particles. Another important point was that the particles produced from R_a ratio 1:500 (w/w) under stirring speeds 100, 200, and 500 r.p.m. after crystal maturation time = 24 hours were significantly smaller in size (VMD = 20-22 μm) than the particles produced at 800 r.p.m. after crystal maturation time = 0 (VMD = $90.3 \pm 13.6 \mu\text{m}$).

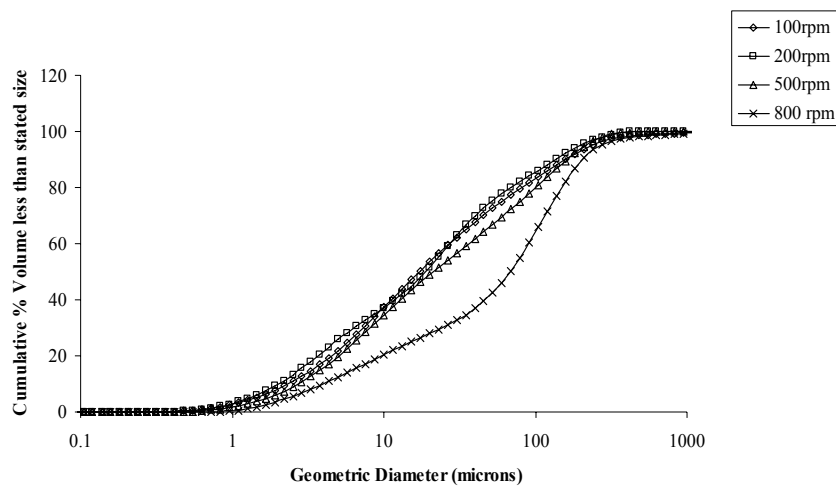


Figure III.43 Cumulative % undersize volume distribution of AS particles precipitated from EA harvested after a crystal maturation time of 1440 minutes from R_a ratio 1:500 (w/w) under different stirring speeds

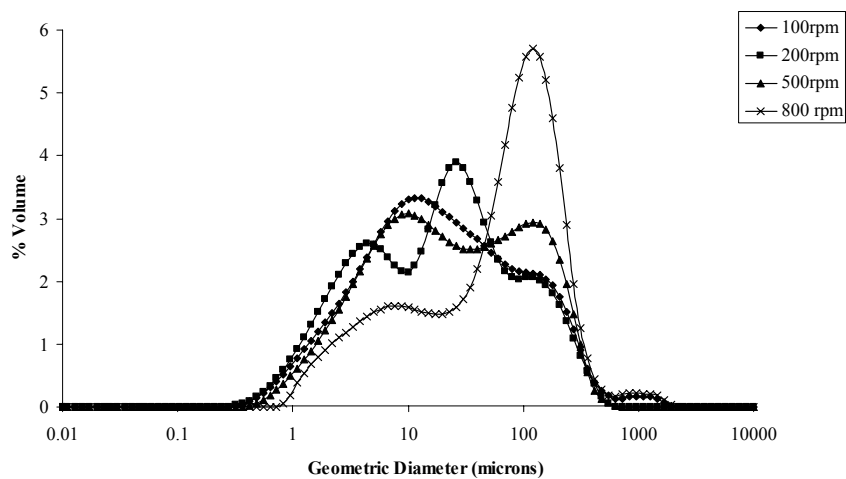


Figure III.44 Volume frequency distribution of AS particles precipitated from EA harvested after a crystal maturation time of 1440 minutes from R_a ratio 1:500 (w/w) under different stirring speeds

Table III.17 Mean \pm SD volume median diameters and span indices of AS particles precipitated from EA produced from R_a ratio 1:500 (w/w) under different stirring speeds

Stirring speed (r.p.m.)	Crystal maturation time =0		Crystal maturation time =24 hours	
	VMD \pm SD (μm)	Span index	VMD \pm SD (μm)	Span index
100	25.6 \pm 5.4	5.9	19.9 \pm 5.7	9.1
200	28.6 \pm 3.3	6.2	22.0 \pm 3.2	6.8
500	26.6 \pm 10.9	6.1	22.4 \pm 2.4	7.8
800	95.6 \pm 28.9	2.2	90.3 \pm 13.6	3.1

However, all of the particles produced from R_a ratio 1:500 (w/w) were significantly larger in size than the particles produced from R_a ratio 1:200 (w/w) under corresponding stirring speeds after crystal maturation time = 24 hours and were hence too large for inhalation. For R_a ratio 1:1000 (w/w), bimodal PSDs were obtained as shown in Figures III.45 and III.46. The VMDs of the particles (shown in Table III.18) produced at 100 and 200 r.p.m. were comparable to each other and to those produced from R_a ratio 1:500 (w/w) under corresponding stirring speeds (p-value > 0.05, one-way ANOVA). However, significantly larger particles were produced at 500 and 800 r.p.m. for R_a ratio 1:1000 (w/w) compared to 100 and 200 r.p.m. for the same R_a ratio (p-value < 0.05, Tukey's HSD). Particles produced from R_a ratio 1:1000 (w/w) at 100 and 200 r.p.m. after crystal maturation time = 0 were also significantly smaller than the particles produced at crystal maturation time = 0 from the same R_a ratio at corresponding stirring speeds as shown in Table III.18. However, there was no difference in the VMDs of particles produced at 500 and 800 r.p.m. after crystal maturation time = 0 and crystal maturation time = 24 hours (p-value > 0.05, one-way ANOVA). It must be remembered that these particles remained partially crystalline even after crystal maturation time = 24 hours and underwent complete crystallization in the solid-state in a manner similar to the particles harvested at crystal

maturation time = 0. These results therefore, supported the hypothesis that the larger size of the particles that were harvested following a crystal maturation time = 0 was due to solid-state crystallization that occurred during the particle isolation process.

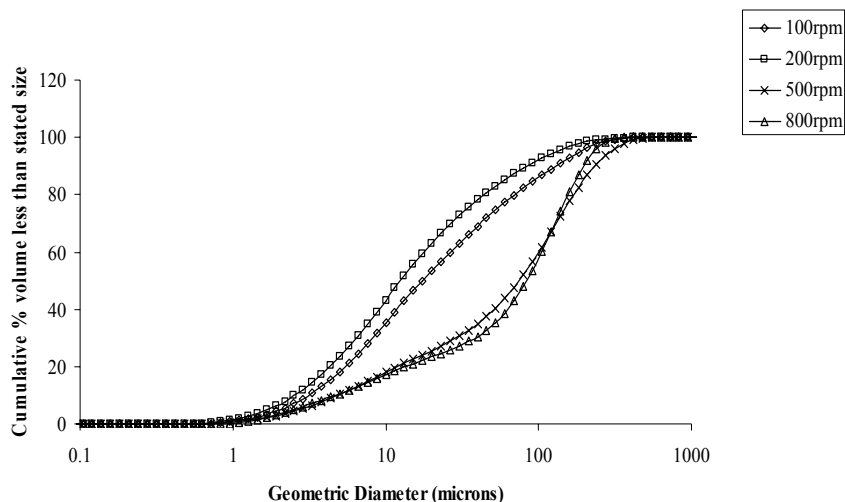


Figure III.45 Cumulative % undersize volume distribution of AS particles precipitated from EA harvested after a crystal maturation time of 1440 minutes from R_a ratio 1:1000 (w/w) under different stirring speeds

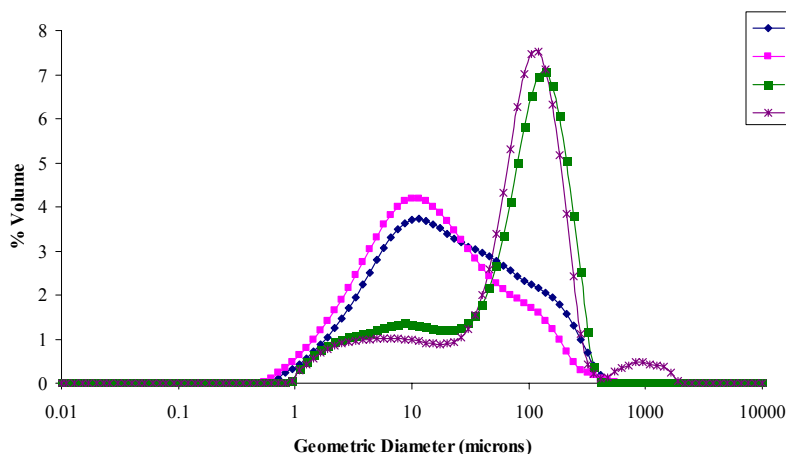


Figure III.46 Volume frequency distribution of AS particles precipitated from EA harvested after a crystal maturation time of 1440 minutes from R_a ratio 1:1000 (w/w) under different stirring speeds

Table III.18 Mean \pm SD volume median diameters and span indices of AS particles precipitated from EA produced from R_a ratio 1:1000 (w/w) under different stirring speeds

Stirring speed (r.p.m.)	Crystal maturation time =0		Crystal maturation time =24 hours	
	VMD \pm SD (μm)	Span index	VMD \pm SD (μm)	Span index
100	26.7 \pm 6.0	6.3	20.5 \pm 3.8	7.7
200	32.9 \pm 12.6	5.9	21.3 \pm 1.3	6.7
500	90.7 \pm 8.2	2.5	99.5 \pm 11.6	2.1
800	93.4 \pm 4.2	2.2	95.7 \pm 3.0	2.2

Therefore, in a manner similar to the particle size of particles at crystal maturation time = 0, particle size after a crystal maturation time = 24 hours was also found to be a function of the crystallization conditions wherein variables such as R_a ratio, and stirring speed significantly influenced the particle size of the AS particles. The smallest particle size was produced from R_a ratio 1:200 (w/w) under all stirring speeds employed. The stirring speed of 200 r.p.m. yielding particles with a VMD of 9.7 \pm 0.7 μm after crystal maturation time = 24 hours was therefore found to be the optimized condition among all the crystallization conditions studied.

The possible explanation for the effect of the crystallization variables on particle size was discussed in section III.D.2.1.2 dealing with particle size distribution at crystal maturation time = 0. However, in a crystallization process, the effect of a single crystallization condition cannot be treated in isolation since there are interactions between the different variables. Therefore, a statistical analysis of the particle size distribution data was carried out in the JMP 7.0 software without any transformation. The model fitting platform was used to analyze the data for each response variable wherein the variables were split into:

- 4) Main Factors: R_a ratio, stirring speed, crystal maturation time
- 5) Interactions: R_a ratio \times stirring speed \times crystal maturation time

6) Response variable: Volume Median Diameter

The results for statistical analysis of the volume median diameter are shown in Table III.19.

Table III.19 Statistical analysis of the effect of crystallization variables on Volume Median Diameter of AS particles

Source	Degrees of freedom	F-value	p-value
Model	20	16.5	<0.0001
R _a Ratio	2	50.4	<0.0001
Stirring Speed	8	28.7	<0.0001
Crystal maturation time	1	0.009	< 0.0001
R _a Ratio × Stirring Speed × Crystal maturation time	11	1.3	< 0.0001
R ²	0.95		
Adj R ²	0.92		

The model was found to be significant and accounted for 95% of the variability in the volume median diameter. The three factors showed a significant interaction as is shown by a p-value < 0.0001. The volume median diameter of the particles was significantly influenced by R_a ratio, stirring speed, and crystal maturation time interacting with each other and it was not possible to comment on the influence of any one variable by treating it separately from the others.

In summary, it was demonstrated that harvesting the completely crystalline particles after a crystal maturation time = 24 hours resulted in the formation of significantly smaller particles compared to the partially crystalline particles harvested at crystal maturation time = 0. This effect was attributed to solid-state crystallization in the partially crystalline particles. Furthermore, different crystallization variables showed a significant impact on the particle size wherein the smallest VMD ($\approx 10 \mu\text{m}$) was obtained from R_a ratio 1:200 (w/w) at 200 r.p.m. after

a crystal maturation time = 24 hours. However, the PSD of these particles was very broad (span index = 7.7) and they were not in a size small enough for inhalation. Therefore, further optimization of the solvent / anti-solvent crystallization process was needed to produce AS particles small enough for inhalation.

In an attempt to reduce the size of the AS particles the influence of the temperature difference between the solvent and anti-solvent was investigated. The temperature differences studied were 20°C and 65°C produced by cooling the anti-solvent in ice and dry ice respectively for the 30 minute duration of stirring. The temperature of the drug solution was 25°C. The crystallization conditions chosen for these experiments were a R_a ratio of 1:200 (w/w), a stirring speed of 200 r.p.m. and a crystal maturation time = 24 hours since it was shown that these crystallization conditions resulted in the smallest AS particles among all the conditions investigated. Table III.20 shows the results for particle sizes obtained under a temperature difference of 20 and 65°C. The particle size results for the temperature difference = 0°C are also shown for comparison. The cumulative % undersize volume distributions of the particles produced at the three temperature differences investigated are shown in Figure III.47 with the volume frequency distributions shown in Figure III.48.

Table III.20 Effect of temperature difference between the drug solution and anti-solvent on the particle size of AS particles precipitated from EA

	$\Delta T = 0^{\circ}\text{C}$	$\Delta T = 20^{\circ}\text{C}$	$\Delta T = 65^{\circ}\text{C}$
Average VMD \pm SD (μm)	9.7 \pm 0.7	10.4 \pm 0.6	8.8 \pm 0.6
Volume < 5 μm	24.9	29.2	34.4
Volume < 10 μm	46.0	52.5	58.3
Span index	7.7	7.5	7.8

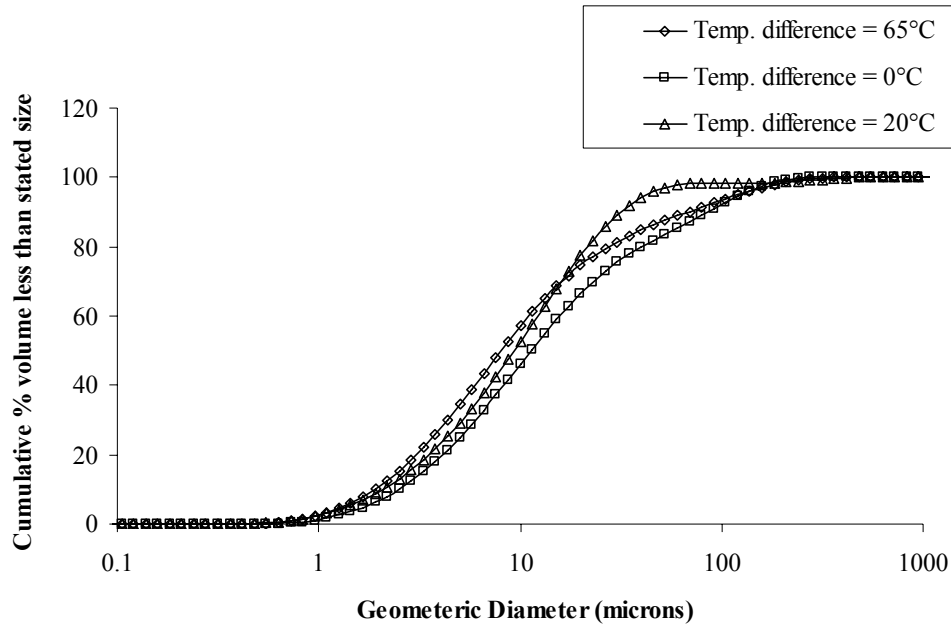


Figure III.47 Cumulative % undersize volume distribution of AS particles precipitated from EA harvested under different conditions of temperature difference between the drug solution and anti-solvent

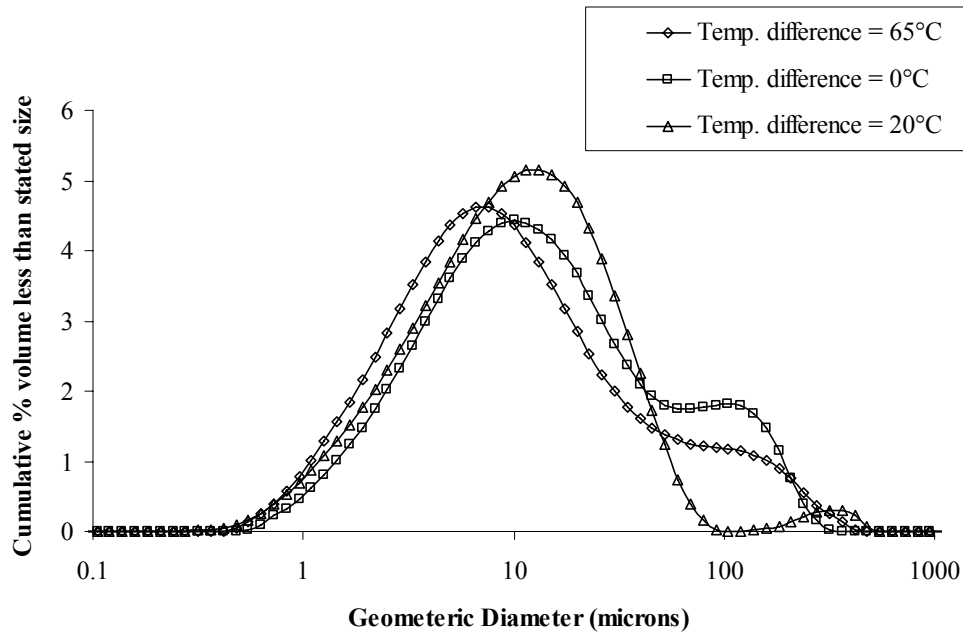


Figure III.48 Volume frequency distribution of AS particles precipitated from EA harvested under different conditions of temperature difference between the drug solution and anti-solvent

The PSDs obtained were bimodal for all temperature differences studied. A temperature difference of 20°C did not result in a significant reduction in the particle size compared to a temperature difference = 0°C (VMD of $10.4 \pm 0.6 \mu\text{m}$ vs. $9.7 \pm 0.7 \mu\text{m}$). However, a larger temperature difference of 65°C between the solvent and anti-solvent resulted in a small but significant reduction ($p\text{-value} < 0.05$, Tukey's HSD) in particle size (Table III.20). Moreover, there was also a significant increase in the volume of particles below $5\mu\text{m}$ (34.4 vs. 24.9%) which is commonly believed to represent the fraction that is respirable. This effect of temperature difference may be attributed to the low anti-solvent temperature used to produce it. A reduced temperature of the anti-solvent would result in reduced AS solubility, higher supersaturation and hence a greater dominance of nucleation leading to the production of a large number of smaller particles. The particles produced at a temperature difference of 65°C were also analyzed for their estimated % crystallinity by DSC. Their heat of fusion was $199.1 \pm 1.3 \text{ J/g}$ resulting in an estimated % crystallinity of $99.0 \pm 0.5\%$. Particle morphology was observed to be tabular as shown in Figure III.49.

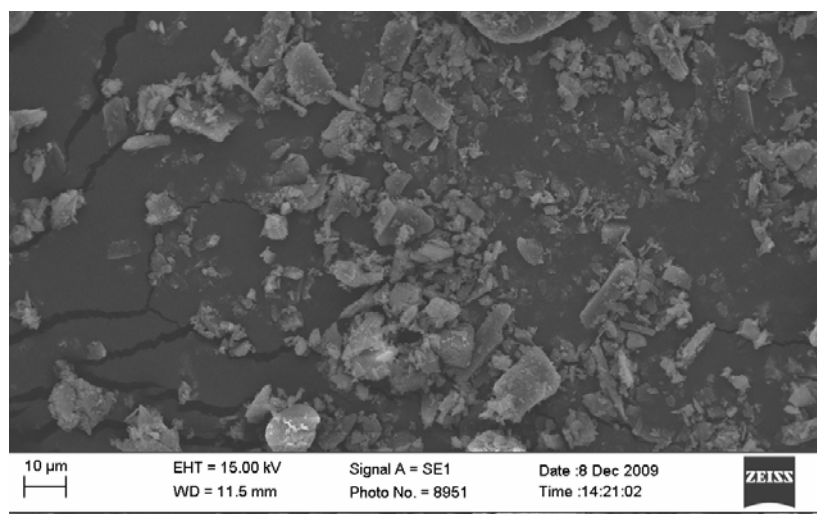


Figure III.49 Representative SEM image of AS particles produced from ethyl acetate at R_a ratio 1:200 (w/w), 200 r.p.m. and a drug solution-anti-solvent temperature difference of 65°C

Therefore, based on these results, the optimized crystallization conditions in a solvent / anti-solvent system of water / ethyl acetate that produced completely crystalline and smallest AS particles were a R_a ratio of 1:200 (w/w), an infusion rate of 1mL/min, a stirring speed of 200 r.p.m. for 30 minutes, a temperature difference of 65°C between the solvent / and anti-solvent and a total crystal maturation time of 24 hours. However, even though it was possible to reduce the size of AS particles by optimization of the crystallization conditions, the particles produced were still not in a size optimum for inhalation (1-5 μm).

In order to produce smaller AS particles, isopropyl alcohol was tested as the anti-solvent since studies in literature have specifically reported its efficiency as an anti-solvent for albuterol sulfate (Dhumal et al., 2009). The crystallization conditions used were a R_a ratio 1:200 (w/w), an infusion rate of 1mL/min, a stirring speed of 200 r.p.m. for 30 minutes and a total crystal maturation time of 24 hours with no temperature difference between the solvent and anti-solvent. Figure III.50 and III.51 show the cumulative % undersize volume distributions and volume frequency distributions for the particles produced from isopropyl alcohol. The PSDs for the particles produced from ethyl acetate under the optimized conditions discussed above are also shown for comparison.

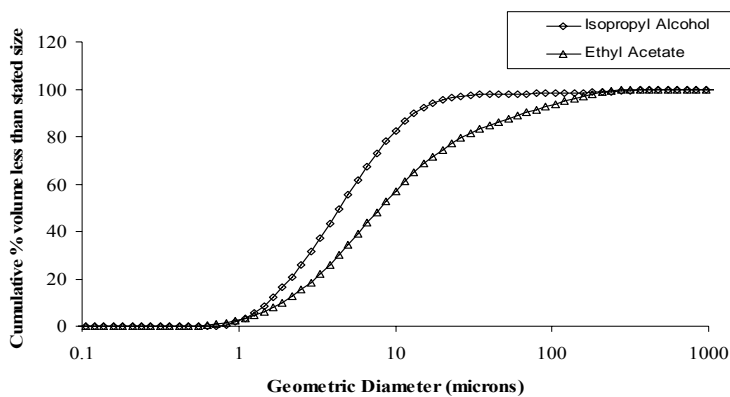


Figure III.50 Cumulative % undersize volume distribution of AS particles produced from isopropyl alcohol and ethyl acetate

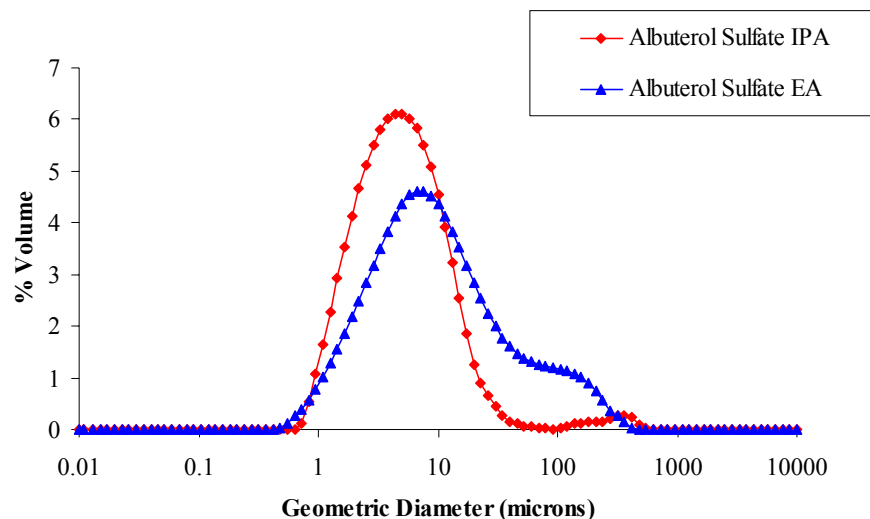


Figure III.51 Volume frequency distribution of AS particles produced from isopropyl alcohol and ethyl acetate

The particle size distribution of particles produced from IPA was observed to be apparently unimodal when compared to the particles produced from ethyl acetate. Furthermore, the VMD of IPA particles was $4.9 \pm 0.3 \mu\text{m}$ which was significantly smaller relative to the VMD of $8.8 \pm 0.6 \mu\text{m}$ produced by ethyl acetate ($p\text{-value} < 0.05$, one-way ANOVA). The span values shown in Table III.21 revealed that isopropyl alcohol resulted in a significantly narrower PSD compared to ethyl acetate.

Table III.21 Particle size of AS particles produced from isopropyl alcohol and ethyl acetate under the optimized crystallization conditions

	Isopropyl alcohol	Ethyl acetate
Average VMD \pm SD (μm)	4.9 ± 0.3	8.8 ± 0.6
Volume $< 5 \mu\text{m}$ (%)	55.6 ± 0.8	34.4 ± 1.2
Volume $< 10 \mu\text{m}$ (%)	82.6 ± 0.6	57.1 ± 0.8
Span index	2.4	7.6

Dhumal et al. have previously carried out the formation of AS particles using a similar solvent / anti-solvent system of water and isopropyl alcohol (Dhumal et al., 2009). They reported

that using mechanical stirring alone, particles with a volume median (SD) diameter (VMD) of 22.3 (2.55) μm were produced. In that study, AS particles were produced using water as the solvent, a saturated drug solution concentration of 250mg/mL, IPA as the anti-solvent and a R_a ratio of 1:16 $^w/w$, however, no information about the stirring speed was provided. Possible reasons for the smaller particle size distribution of the AS particles produced in our study include the optimized stirring conditions taken together with different crystallization vessel geometry.

It was possible that the formation of smaller particles by using IPA as the anti-solvent may be explained by the relative kinematic viscosities of IPA and ethyl acetate. Kinematic viscosity is sometimes referred to in terms of diffusivity of momentum. Indeed, dimensionally, it is given by the ratio of fluid viscosity to fluid density resulting in dimensions identical to diffusivity or diffusion coefficient (M^2T^{-1}). It describes the ratio of viscous force to inertial force. Therefore, a fluid having a higher kinematic viscosity will offer more resistance to movement compared to a fluid with a lower kinematic viscosity. Since drug molecules need to diffuse through the fluid to deposit on pre-formed nuclei and the solvents also need to mix, an increased resistance to solute movement should result in reduced diffusion of drug molecules and hence a lowered growth rate. The kinematic viscosities were calculated for IPA and ethyl acetate as 2.49×10^{-2} Stokes and 4.75×10^{-3} Stokes respectively. This 10 fold difference in kinematic viscosities may be a possible explanation for the formation of smaller particles in IPA compared to ethyl acetate.

Thermal analysis of the particles produced from isopropyl alcohol revealed a heat of fusion of 200.2 ± 1.8 J/g which resulted in an estimated % crystallinity of $100.0 \pm 1.2\%$ after 24 hours of crystallization indicating complete crystallization. The powder X-ray diffraction pattern for these particles is shown in Figure III.52 with characteristics peaks comparable to reference

AS indicating the formation of the same polymorphic form as the reference and the AS particles produced from EA. Therefore, the issues of solid-state crystallization and crystal bridging associated with harvesting partially crystalline particles did not arise.

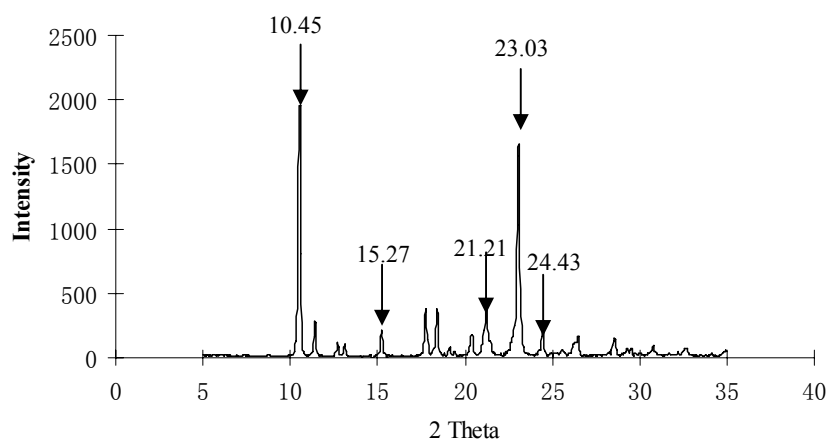


Figure III.52 Powder X-ray diffractogram for AS particles precipitated from IPA produced from R_a ratio 1:200 (w/w) at 200 r.p.m. after crystal maturation time 1440 minutes, filtration, sonication, and drying

Isopropyl alcohol also produced particles with a different morphology compared to ethyl acetate. Figure III.53 shows the representative scanning electron micrograph of AS particles produced from IPA. Compared to ethyl acetate that generated tabular particles, use of IPA as the anti-solvent resulted in the formation of elongated, rod-like particles. This effect may be explained by the relative polarity of IPA vs. ethyl acetate where IPA is a more polar solvent relative to ethyl acetate. Solvent polarity influences crystal habit and growth of different faces by the interaction between the solvent molecules and the different crystal faces, which is believed to change crystal morphology (Mullin, 2001). Albuterol sulfate is a polar molecule with higher solubility in relatively polar solvents. Therefore, in a non-polar solvent, such as ethyl acetate, the small particles that are immediately formed tend to agglomerate to reduce the particle surface

area in contact with the non-polar liquid, and thus to diminish the surface tension established between the albuterol sulfate polar molecule and the non-polar liquid. In fact, generally, with a higher amount of polar solvent, crystals are acicular, while the increase of non-polar liquid favors isodimensional growth and a slight tendency to crystal agglomeration. According to Leger et al, AS has a monoclinic structure (Leger et al., 1978). The monoclinic unit cell contains 4 AS molecules. Along the “b” axis, phenol rings are coplanar, in facing positions, interacting with each other hydrophobically. In presence of hydrophilic solvents, the polar groups can establish hydrogen bonds with water molecules, so AS molecules tend preferentially to grow along the “b” axis, which is the more hydrophobic, by the overlap of several phenol rings. By diminishing the hydrophilic nature of the solvent, the possibility that the polar groups can establish hydrogen bonds with the solvent diminishes, and thus crystal tends to grow in all directions isodimensionally.

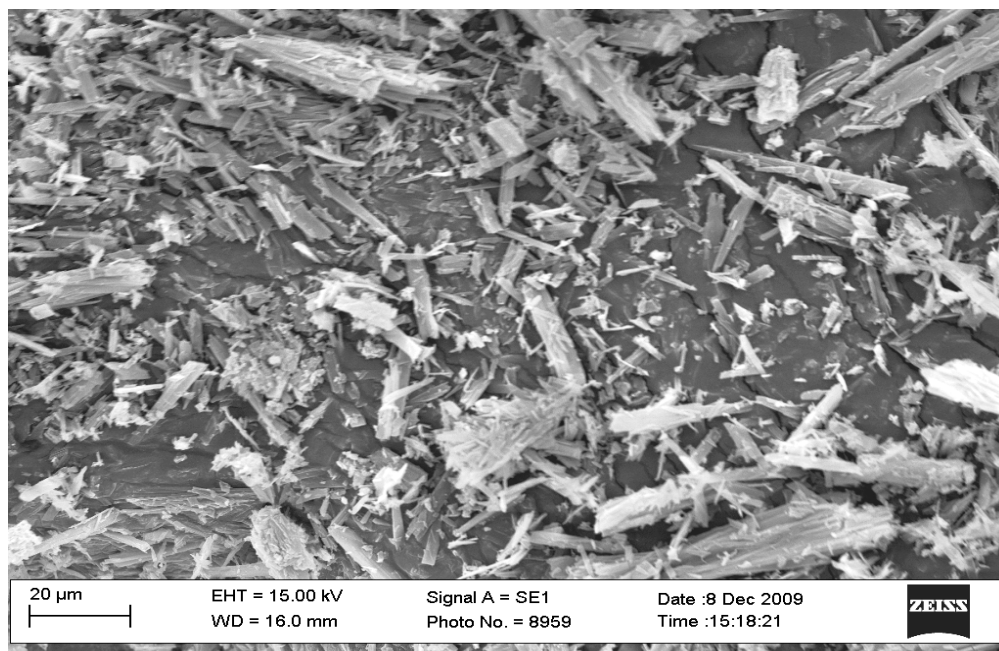


Figure III.53 Scanning electron micrograph of AS particles produced from isopropyl alcohol

Utilizing isopropyl alcohol as the anti-solvent while using the crystallization conditions previously optimized for ethyl acetate resulted in AS particles that were completely crystalline, in a size suitable for inhalation (1-5 μm) with a narrower PSD compared to particles formed with ethyl acetate as the anti-solvent. These results therefore demonstrated the importance of optimizing the crystallization conditions in particle engineering and revealed that by investigation and optimization of these conditions, it was possible to utilize a simple solvent / anti-solvent system to produce particles with the desired characteristics.

III.D.2.3 Comparison of AS particles engineered from solvent / anti-solvent crystallization with micronized AS

At this point, it is interesting to compare the properties of the engineered particles from the optimized solvent / anti-solvent processes using water / ethyl acetate and water / isopropyl alcohol as the solvent / anti-solvent systems with the conventionally used micronized AS particles for aerosol formulations. Micronized AS particles revealed a heat of fusion of 190.3 ± 1.8 J/g resulting in an estimated % crystallinity value of $95.2 \pm 1.3\%$. Figure III.54 shows the cumulative % undersize volume distribution of the micronized AS particles. The volume frequency distribution is shown in Figure III.55. Figure III.56 shows a comparative cumulative % undersize volume distribution of micronized AS particles with AS particles produced from IPA and EA under the optimized crystallization conditions discussed in the previous sections. The PSD parameters for these three types of AS particles are shown in Table III.22. Micronized AS had a smaller VMD relative to the smallest AS particles produced from IPA (4.9 ± 0.3 μm) and ethyl acetate (8.8 ± 0.6 μm). The span indices were comparable for micronized AS and AS particles produced from IPA (i.e.; 2.2). However, ethyl acetate produced a broader PSD evident from its large span index of 7.7.

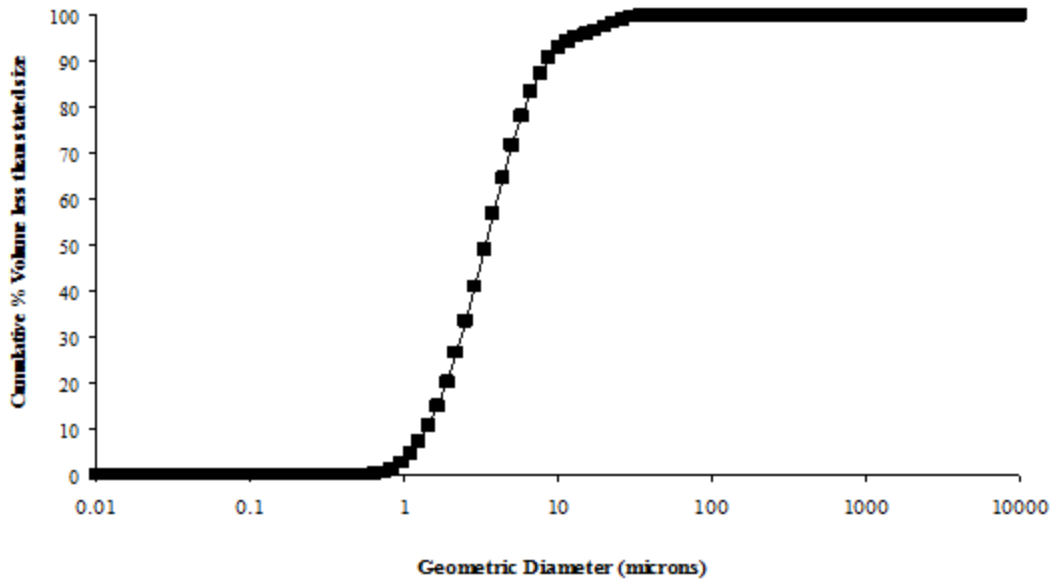


Figure III.54 Cumulative % undersize volume distribution of micronized albuterol sulfate

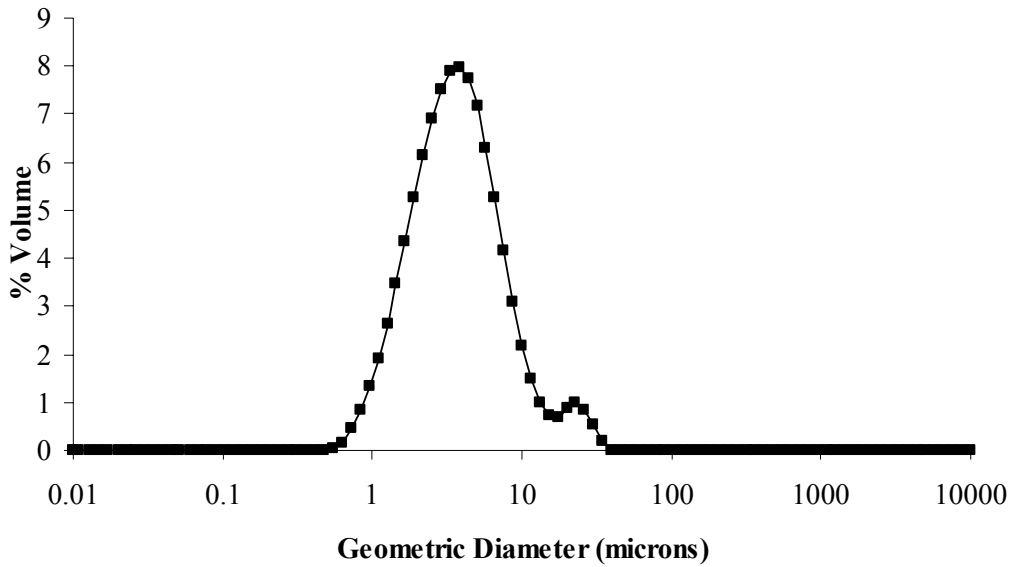


Figure III.55 Volume frequency distribution of micronized albuterol sulfate

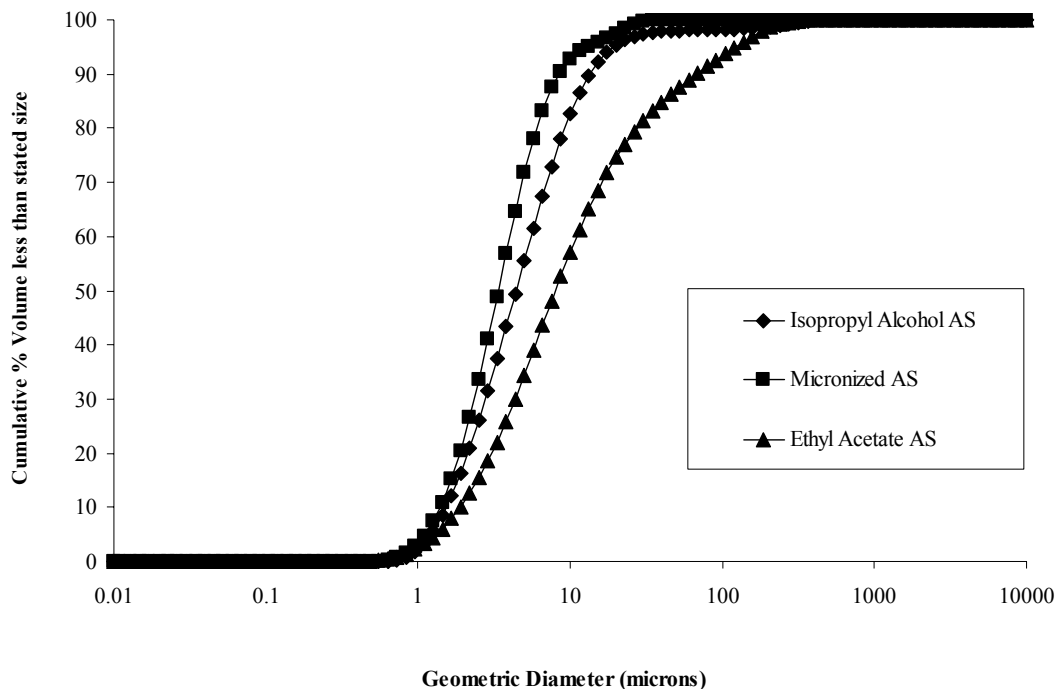


Figure III.56 Cumulative % undersize volume distributions of micronized AS particles and AS particles produced from isopropyl alcohol and ethyl acetate

Table III.22 Particle size distribution parameters for micronized albuterol sulfate

Particles	Average VMD ± SD (µm)	Span index	% Volume < 5 µm	% Volume < 10 µm
Micronized AS	3.9 ± 0.3	2.2	71.8 ± 3.4	92.7 ± 1.2
Ethyl Acetate AS	8.8 ± 0.6	7.7	34.4 ± 1.2	57.1 ± 0.8
Isopropyl Alcohol AS	4.9 ± 0.3	2.2	55.6 ± 0.8	82.6 ± 0.6

Figure III.57 shows a representative SEM image of micronized AS particles. Compared to the AS particles that exhibited elongated, rod-like morphology (Figure III.52), micronized AS had a tabular platelet-like morphology which resembled that of AS particles produced from ethyl acetate (Figure III.49).

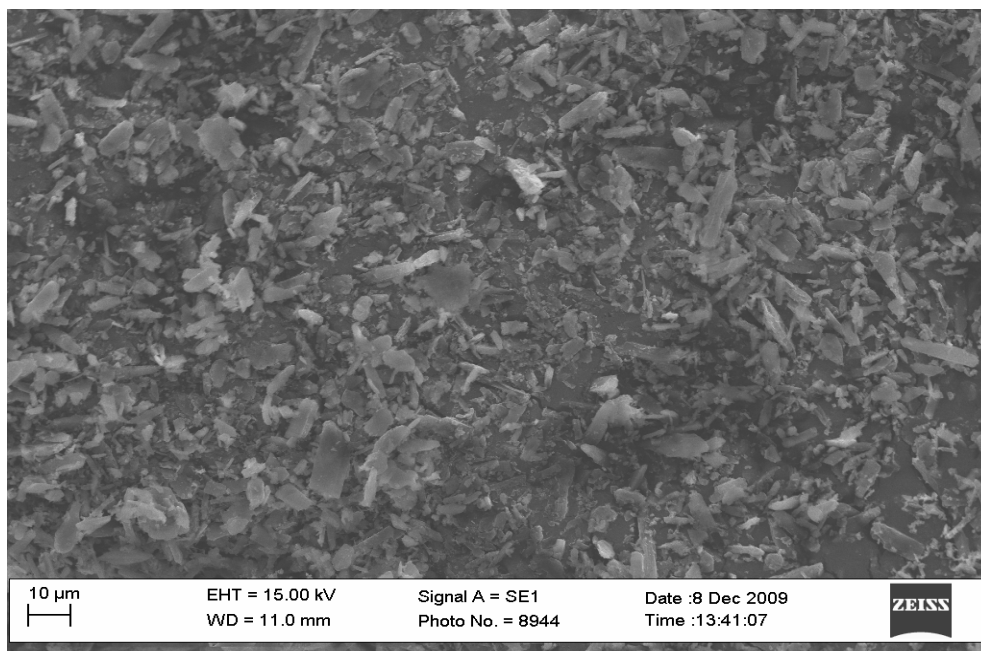


Figure III.57 Representative SEM image of micronized albuterol sulfate

Therefore, AS particles produced from the solvent / anti-solvent crystallization process possessed different particle characteristics compared to the conventionally used micronized particles. However, these particle size distributions were obtained from the Malvern which is calibrated for spherical particles. The AS particles produced from ethyl acetate and micronization were tabular and plate-like as shown in Figures III.49 and III.56 respectively. The particles produced from IPA were elongated and rod-like as shown in Figure III.52. Therefore, PSD obtained from the Malvern may not be an accurate measure. Further, Malvern measures the geometric diameter of the particles. The aerosol performance of particles is a strong function of their aerodynamic diameter which cannot be determined using the Malvern. *In vitro* aerosol performance studies using impactors are necessary to determine the inhalation efficiency of these particles. Hence, although ethyl acetate produced large particles ($VMD = 8.8 \pm 0.6 \mu\text{m}$) compared to micronized particles ($VMD = 3.9 \pm 0.3 \mu\text{m}$) and AS particles produced from IPA

(VMD = $4.9 \pm 0.3 \mu\text{m}$), the *in vitro* aerosol performance of these three types of AS particles was tested. These results will be discussed in Chapter V.

III.E CONCLUSIONS

One of the hypotheses of this project was that an understanding of the degree of influence of critical crystallization variables upon particle characteristics will allow optimization and control of the final product. In this chapter, the investigation of the solvent/anti-crystallization process for albuterol sulfate using water as the solvent and ethyl acetate as the anti-solvent was carried out using a DoE experimental approach to study the impact of crystallization variables on particle characteristics; predominantly particle crystallinity and particle size. These studies yielded insight into the fundamentals influencing the particle characteristics. Hydrodynamic conditions alone without any external energy source or crystal growth modifiers were shown to control the particle size distribution of albuterol sulfate with supersaturation levels exercising significant influence. Significant interactions between the different crystallization variables were discovered and particle size distribution was found to be influenced by them. This is an important finding since interpretation of the influence of a single crystallization variable without taking other interacting variables into consideration is likely to lead to erroneous analysis. Particle crystallinity was also found to be influenced by the complex interplay between the crystallization variables and % water content was shown to be a simple surrogate marker for monitoring solution crystallization. The importance of harvesting completely crystalline particles was also demonstrated and this required maturation times spent in the mother liquor that depended upon the way in which crystallization was induced. Temperature difference between the drug solution and anti-solvent was found to have a small but significant impact on the

particle size of AS particles produced from ethyl acetate. Optimization of the solvent / anti-solvent system of water / ethyl acetate led to the formation of completely crystalline AS particles with a particle size between 1-10 μm and a VMD of 8.8 μm while those particles were not in the optimum size range for aerosol formulations (i.e.; 1-5 μm). Further optimization of the solvent / anti-solvent crystallization process using isopropyl alcohol as the anti-solvent led to the formation of significantly smaller AS particles with a VMD of 4.9 μm and a narrower PSD compared to those isolated from ethyl acetate. Complete crystallinity for these particles was also observed. These particles were therefore deemed to be suitable for inhalation. The aerosol performance of those particles is discussed in Chapter V. These studies showed that it was possible to use simple hydrodynamic control and known supersaturation conditions to produce microcrystals of AS with desirable characteristics for inhalation.

CHAPTER IV
COMBINATION PARTICLES OF ALBUTEROL SULFATE AND IPRATROPIUM
BROMIDE MONOHYDRATE

IV.A INTRODUCTION

In this chapter a solvent / anti-solvent crystallization process to produce combination particles of albuterol sulfate (AS) and ipratropium bromide monohydrate (IB) in varying proportions is investigated. The commercial combination product containing these two active pharmaceutical ingredients (APIs) is Combivent® pMDI which is formulated as a physical mixture of individually micronized AS and IB in a nominal ratio of 6:1 (w/w) suspended in a CFC propellant with soy lecithin as the surfactant. Since such physical mixtures suffer from powder segregation and hence, loss of fixed drug ratio during aerosolization, it may be desirable to produce combination particles with fixed proportions of AS and IB and with suitable characteristics for inhalation. If these particles can be directly produced in a size suitable for inhalation, the disadvantages associated with micronization can be overcome. It is hypothesized that these combination particles can be produced in predictable ratios with suitable characteristics for inhalation by a single-step crystallization process.

IV.B CHEMICALS

Albuterol Sulfate ((RS)-1- (4-hydroxy-3-hydroxymethylphenyl)-2-(tert-butylamino) ethanol sulfate): Spectrum Chemical Mfg. Corp., New Brunswick, NJ

Ipratropium Bromide monohydrate ([8-methyl-8-(1-methylethyl)- 8-azoniabicyclo[3.2.1] oct-3-yl] 3-hydroxy-2-phenyl-propanoate): Spectrum Chemical Mfg. Corp., New Brunswick, NJ

HPLC grade ethyl acetate: Fischer Scientific, Pittsburgh, PA

HPLC grade isopropyl alcohol: Fischer Scientific, Pittsburgh, PA

HPLC grade methanol: Fischer Scientific, Pittsburgh, PA

Ammonium Formate: Fischer Scientific, Pittsburgh, PA

IV.C METHODS

IV.C.1 Solvent / Anti-solvent system used for combination particles

Combination particles of AS and IB were produced in different ratios of 1:1, 2:1, 6:1 and 10:1 (w/w) using a solvent / anti-solvent crystallization setup essentially similar to that employed for AS described in section III.C.1. The details of the crystallization variables further investigated and optimized for producing combination particles in a size suitable for inhalation will be discussed in the following sections.

IV.C.2 Processing variables investigated for combination particles

The processing variables investigated for the combination particles included the anti-solvent used, the temperature difference between the solvent and anti-solvent, initial concentration of AS and IB in the aqueous drug solution, and total crystal maturation time. Investigation of the effect of anti-solvent on particle characteristics was the first step. Ethyl acetate and mixtures of ethyl acetate and isopropyl alcohol were investigated at fixed conditions of R_a ratio, initial drug concentrations, and crystal maturation time. The effect of temperature difference between solvent and anti-solvent was also studied for an optimized mixture of ethyl

acetate and isopropyl alcohol. Further, isopropyl alcohol was investigated as the anti-solvent at variable R_a ratios, initial drug concentrations, and crystal maturation time.

IV.C.2.1 Solvent / Anti-solvent crystallization of combination particles using ethyl acetate as the anti-solvent

In all experiments, water was used as the solvent. The crystallization conditions when using ethyl acetate as the anti-solvent were same as the optimized crystallization conditions for AS alone as discussed in chapter III. These conditions are outlined below:

R_a ratio = 1:200 (w/w)

Infusion rate = 1 mL/min

Stirring speed = 200 r.p.m.

Stirring time = 30 minutes

Crystal maturation time = 24 hours

Solvent temperature = 25°C

Anti-solvent temperature = 25°C

An aqueous solution of AS and IB was prepared by weighing the appropriate amounts of AS and IB into a glass beaker and adding water to achieve the required concentration (% w/w). The beaker was covered with parafilm and heated to 40°C. Following dissolution of AS and IB, the saturated solution was allowed to cool to room temperature (25-27°C). Table IV.1 describes the concentration of the two APIs in the starting aqueous solution, the weight of the drug solution, and the weight of the anti-solvent to achieve a solvent / anti-solvent ratio of 1:200 (w/w) for the 1:1, 2:1, 6:1, and 10:1 (w/w) combination particles.

Table IV.1 Initial drug solution concentrations of AS and IB and weights of ethyl acetate used as the anti-solvent for the solvent / anti-solvent crystallization process

Nominal AS:IB Ratio (w/w)	AS conc. (g/g)	IB conc. (g/g)	Wt. of AS+IB (g)	Wt. of drug solution (g)	Wt. of anti-solvent (g)
1:1	0.22	0.22	0.24	0.66	131.0
2:1	0.22	0.11	0.19	0.65	130.6
6:1	0.22	0.04	0.16	0.65	130.0
10:1	0.22	0.02	0.15	0.65	130.8

The concentration of AS was kept constant and despite of small change in the mass of IB, the total weight of the drug solution and the weight of the anti-solvent was kept constant. This was required in order to avoid hydrodynamic changes due to differences in energy transfer and dissipation during mechanical agitation of the crystallization medium. The aqueous drug solution of AS and IB was added to ethyl acetate over a 30 second period at a fixed infusion rate of 1 mL/min by means of a syringe pump (Harvard Apparatus, Holliston, MA) using a 500 μ L Hamilton gastight syringe. The solution was transferred to the crystallization vessel via a 12 cm PEEK tubing (ID = 0.007 inches, Upchurch Scientific, Oak Harbor, WA) which was held in a fixed position 5 cm above the anti-solvent. Mixing between the drug solution and anti-solvent was achieved by a stirrer (Caframo stirrer type RZR 50, Warton, ON, Canada) with paddle dimensions of 2 \times 1 \times 0.6 inches. Stirring was initiated with the addition of the drug solution and was carried out for a fixed 30 minute period. Experiments were carried out at room temperature (25-27 $^{\circ}$ C) with no temperature difference between the drug solution and anti-solvent unless otherwise stated. Following the 30 minute stirring, the particles were allowed to remain in the solvent/anti-solvent mixture for 24 hours. Particles were recovered from the anti-solvent by vacuum filtration using a 0.45 μ m membrane filter (45mm diameter; Fischer Scientific, Pittsburgh, PA) housed in a glass filter unit. The filter paper containing the wet cake was washed with and the particles were re-suspended in 4mL of the saturated filtrate solution. This

concentrated suspension was sonicated at 40KHz for 45minutes to allow complete evaporation of the filtrate solution. The particles were then dried overnight at room temperature. Samples were then stored in sealed containers in a dessicator at room temperature.

IV.C.2.2 Solvent / anti-solvent crystallization of combination particles using isopropyl alcohol as the anti-solvent

Isopropyl alcohol (IPA) was investigated as the anti-solvent. These studies were carried out to produce combination AS/IB particles in a nominal 6:1 (w/w) ratio in size suitable for inhalation. The different crystallization conditions studied are listed in Table IV.2. The infusion rate of the drug solution was 1mL/min. The stirring speed was 200 r.p.m. for R_a ratio 1:200 (w/w). However, magnetic stirring was used with R_a ratio 1:20 (w/w) due to the small volume of anti-solvent. Both solvent and anti-solvent temperature was 25°C with no temperature difference between the two. Particles were harvested using the procedure described in section IV.C.2.1.

Table IV.2 Crystallization conditions investigated with isopropyl alcohol as the anti-solvent

R_a ratio (w/w)	AS conc. (g/g)	IB conc. (g/g)	Crystal maturation time
1:200	0.22	0.04	24 hours
1:20	0.38	0.22	24 hours
1:20	0.38	0.22	5 minutes
1:20	0.38	0.06	30 seconds

IV.C.2.3 Solvent / anti-solvent crystallization of combination particles using mixtures of isopropyl alcohol and ethyl acetate as anti-solvents

Combination particles with AS:IB ratios of 1:1, 2:1, 6:1, and 10:1 (w/w) were produced from anti-solvents containing IPA and EA mixed in different proportions of 1:1, 1:2, 1:5, and 1:10 (w/w). The initial AS and IB concentrations used for the combination particles were same

as listed in Table IV.1. The crystallization conditions used were also same as those used with ethyl acetate. The anti-solvent composed of IPA:EA = 1:10 (w/w) was also used for investigating the effect of temperature difference between the solvent and anti-solvent on particle size. This anti-solvent was cooled in dry ice for the 30 minute duration of stirring resulting in a temperature difference of 65°C between the solvent and anti-solvent.

IV.C.2.4 Physical mixtures of AS and IB

In order to confirm the formation of combination particles of AS and IB and differentiate them from physically mixed AS and IB, physical mixtures of the two APIs were prepared for comparison. These physical mixtures were prepared by blending of AS and IB in proportions of 1:1, 2:1, 6:1, and 10:1 (w/w) by geometric mixing using a mortar and pestle. The blend homogeneity of these physical mixtures was determined by weighing and analyzing 10 samples by the HPLC analysis method described in section IV.C.3.6. A % RSD of less than 5.0% for AS and IB was taken as evidence of acceptable blend homogeneity.

IV.C.3 Solid-state characterization of combination particles

The combination particles subjected to filtration, sonication and subsequent drying at room temperature for 24 hours were characterized by different solid-state analytical techniques.

IV.C.3.1 Differential Scanning Calorimetry

DSC analysis was carried out using a DSC 7 (Perkin Elmer, Covina, CA) equipped with a data station Thermal Analysis Controller 7/DX, Pyris Software for Windows, version 3.81. The combination particles were transferred into aluminum pans. The pans were immediately sealed

non-hermetically and the weight of the sample was recorded. The samples were then heated under a flowing stream of nitrogen as the purge gas at a flow rate of 30-35mL/min. The temperature program used was: a 10 minute hold at 25°C followed by heating to 150°C at 10°C/min, followed by heating to 250°C at 3°C/min. Figure IV.1 shows a representative temperature program.

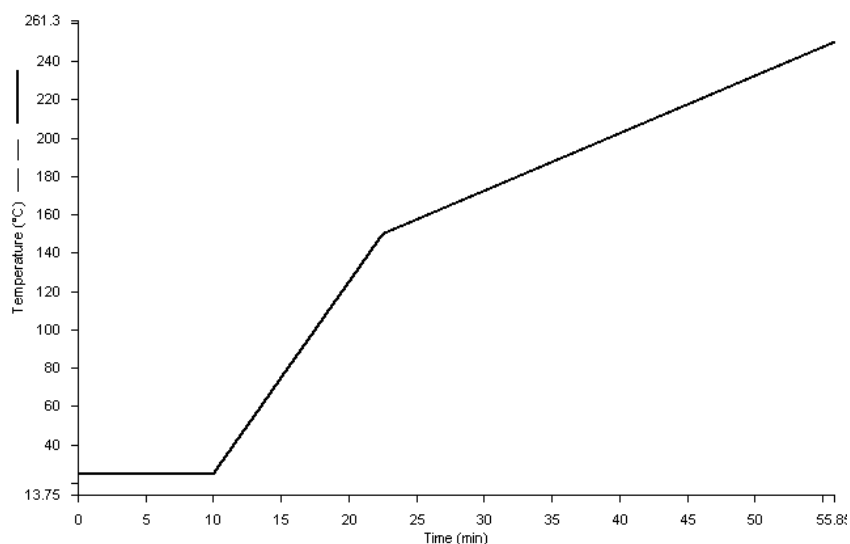


Figure IV.1 DSC temperature program

IV.C.3.2 Hot stage microscopy

Combination particles were observed under a hot stage microscope in order to visually observe the thermal events taking place. The temperature program employed was similar to that used for DSC i.e.; holding at 25°C for 10 minutes, heating from 25-150°C at 10°C/min followed by heating from 150-250°C at 3°C/min.

IV.C.3.3 Optical Microscopy

The particles were observed and photographed under a polarizing optical microscope (Optiphot, Nikon, Tokyo, Japan) using different magnifications (50X, 100X, 400X, 600X). Presence of birefringence was noted as an indicator of crystallinity. Uniform particle morphology with absence of two distinct particle shapes was also taken as evidence supporting the formation of combination particles.

IV.C.3.4 Powder X-Ray Diffraction

The particles were subjected to analysis by powder X-Ray diffraction (Panalytical XRPD, Panalytical Inc, Westborough, MA) by scanning from $5^{\circ}2\theta$ - $35^{\circ}2\theta$ over a period of 2 hours at 45 KV and 40mA. The presence of sharp, characteristic diffraction peaks and no halo was taken as an indicator of crystallinity. Moreover, shifts in peak positions, appearance of new peaks unrelated to those of pure AS or pure IB, or disappearance of peaks was taken as an indication of interactions between AS and IB as opposed to physical mixtures.

IV.C.3.5 Scanning Electron Microscopy

Particle morphology was observed using a scanning electron microscope (EVO 50 XVP scanning electron microscope (SEM) equipped with digital image acquisition). The samples were prepared for analysis by putting them on double-sided sticky tapes mounted onto aluminum stubs and sputter coating them for 2 minutes using a EMS 550x sputter coater. Imaging was performed at 15kV.

IV.C.3.6 Particle Size Determination by Laser Diffraction

The particle size distribution of the combination particles was measured by laser diffraction using the Mastersizer 2000 equipped with the Scirocco dry dispersion accessory (Malvern, Westborough, MA). The air flow and feed rate were adjusted to control the powder dispersion. The optimized particle size measurement conditions sufficient to achieve deagglomeration of primary particles without attrition were an air pressure of 2 bar and a feed rate of 50%. Obscuration limits between 2-6% and a measurement cycle time of 10 seconds were employed. Triplicate measurements were made for each sample. Crystallization batch to batch reproducibility was assessed using three replicate crystallization experiments in each case.

IV.C.3.7 High Performance Liquid Chromatography (HPLC)

Samples were assayed for %AS and % IB content by a validated HPLC method. The method employed a Waters 2690 separations module, a 2996 PDA detector, a Restek Allure PFP column (15×3.2mm), a mobile phase of 75% methanol and 25% ammonium formate buffer (20mM, pH 3.4) at a flow rate of 0.75mL/min and an injection volume of 100 µL. Standard solutions containing both AS and IB were prepared in water. Precision of the method was estimated by assaying the standard with 0.1 µg/mL of AS and 0.1 µg/mL of IB 9 times and calculating the % RSD for both AS and IB. The accuracy was determined by using the HPLC method to analyze the standard containing 0.1 µg/mL of AS and 0.1 µg/mL of IB and then calculated as a percentage of AS and IB recovered by the assay. LOD and LOQ were estimated using the method described in section III.C.1.9. Table IV.3 shows the system suitability parameters for this method. To measure the % AS and % IB content, accurately weighed particles were dissolved in water to prepare a solution of adequate concentration. UV detection was performed at 276nm for AS and at 210 nm for IB.

Table IV.3 System suitability parameters for the HPLC method

System suitability parameter	Value for AS	Value for IB
Linearity range	0.1-100 µg/mL	0.5-100 µg/mL
Precision	1.02%	0.99%
Accuracy	99.6%	99.8%
Limit of detection	0.03 µg/mL	0.2 µg/mL
Limit of quantitation	0.1 µg/mL	0.5 µg/mL

% AS content was measured as described in equation III.7. % IB content was calculated according to equation IV.1.

$$\% \text{ IB content} = \left(\frac{\text{IB mass determined by HPLC}}{\text{Sample weight}} \right) \times 100 \quad \text{Equation IV.1}$$

IV.C.4 Molecular Modeling

Molecular modeling tools were used to study the interactions between AS and IB within a combination particle matrix. The molecular modeling software Sybyl (version 8.0, Tripos, Inc., St. Louis, MO) that employs molecular mechanics or the force field method to calculate the molecular geometry, energies and various other properties of the compound of interest was used (Tripos force field manual, 2006; Kellogg et al., 2000). AS and ipratropium (IP) crystal structures were downloaded from the Cambridge crystallographic database using the Conquest interface. The two crystal structures were manually oriented relative to each other in a random manner in the Sybyl 8.0 platform. Explicit solvation with water was carried out. Energy minimization was carried out with 100000 iterations. The constraints employed were Gasteiger-

Huckel charges, a dielectric constant of 1, and a gradient of 0.05. Post energy minimization molecules were partitioned to calculate their Log P values which perform the basis of all further calculations. Hydrophobic Interaction (HINT) scores were then calculated between the two molecules. In order to remove the possibility of bias associated with manual orientation of the two molecules, another program called GOLD was used. GOLD is a program used to dock ligands into proteins and works by identifying a cavity in the protein. In order to use this program, a unit cell for AS was constructed in Sybyl 8.0. Using this unit cell a 2×2×2 cube was made where 8 unit cells were stacked together. At a time, one albuterol molecule from each corner of the cube was removed and one IB molecule was docked into this cavity using GOLD. The GOLD program was set up to perform 10 GA runs. Each of these runs was then scored using HINT and the positive and negative interactions were identified.

IV.D RESULTS AND DISCUSSION

IV.D.1 Characterization of albuterol sulfate and ipratropium bromide monohydrate reference standards

Figure IV.2 shows a reference thermogram for albuterol sulfate reference standard which was the starting material for all crystallization experiments.

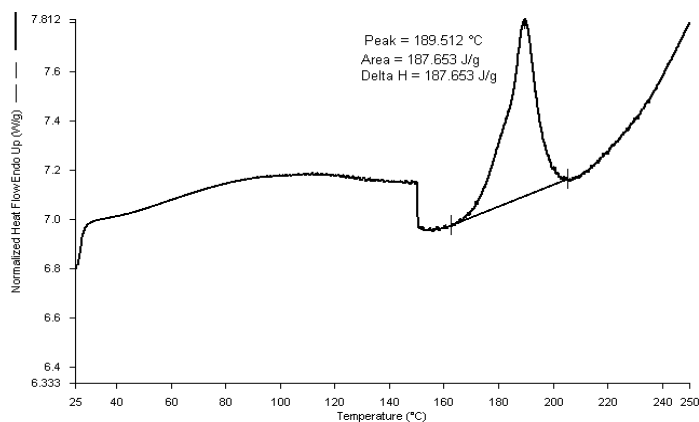


Figure IV.2 Representative DSC thermogram for reference standard albuterol sulfate heated at 3°C/min

A single thermal event was observed which was due to the melting of AS. This was confirmed by hot stage microscopy. Melting is an endothermic process and is shown as the sharp peak in the thermogram. The mean enthalpy of fusion for AS was 188.6 ± 2.6 J/g with a mean melting point of $189.5 \pm 0.5^\circ\text{C}$ calculated from three replicate measurements employing the DSC measurement process described in section IV.C.3.1. Figure III.5 showed the X-ray powder diffraction pattern for reference albuterol sulfate. The characteristic peak positions were tabulated in Table III.3. However, to compare the peak intensities with those of IB, the characteristic AS peaks and their intensities are listed again in Table IV.4. The particle size distribution of reference albuterol sulfate was shown in Figure III.6. The average VMD measured from three replicate measurements was 9.8 ± 0.2 μm . Figure III.7 showed a representative microscopic image of reference AS. The particles appeared to be plate-like in shape.

Figure IV.3 shows a representative thermogram for ipratropium bromide reference standard.

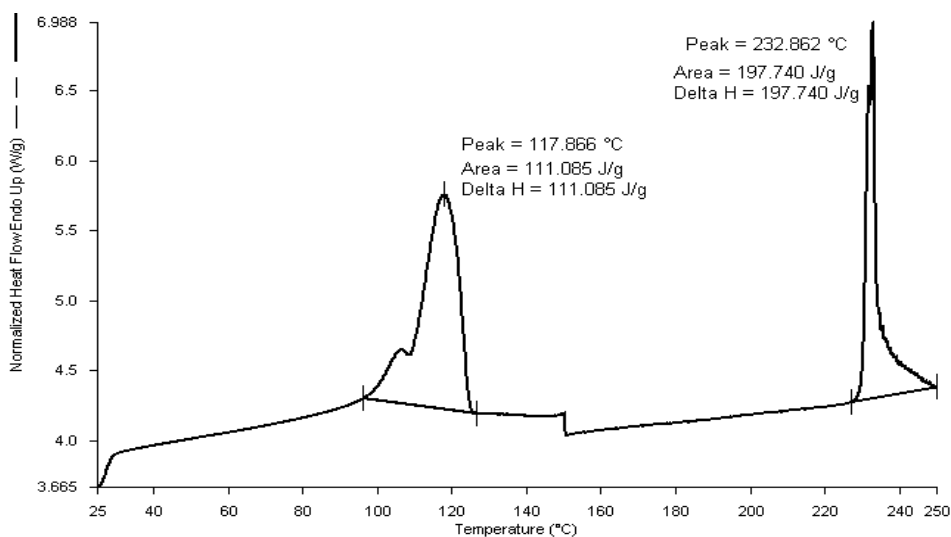


Figure IV.3 Representative DSC thermogram for reference standard ipratropium bromide

Two thermal events were observed. The first endothermic thermal event was due to the loss of the single molecule of water of crystallization. This endothermic thermal event revealed two peaks, one at 108°C and the second at 117°C. The loss of water is shown in the thermogravimetric analysis profile (Figure IV.4). The mean heat of dehydration calculated as integrating the two endothermic peaks together was 110.2 ± 3.5 J/g as calculated from three replicate measurements. The second thermal event was also endothermic and was due to the melting of IB. The mean melting point was $232.6 \pm 0.7^\circ\text{C}$ with a mean heat of fusion of 196.5 ± 2.9 J/g as calculated from three replicate measurements. These thermal events were confirmed by hot stage microscopy and agreed with the reported melting point of 237°C for IB by Corrigan et al. (2006).

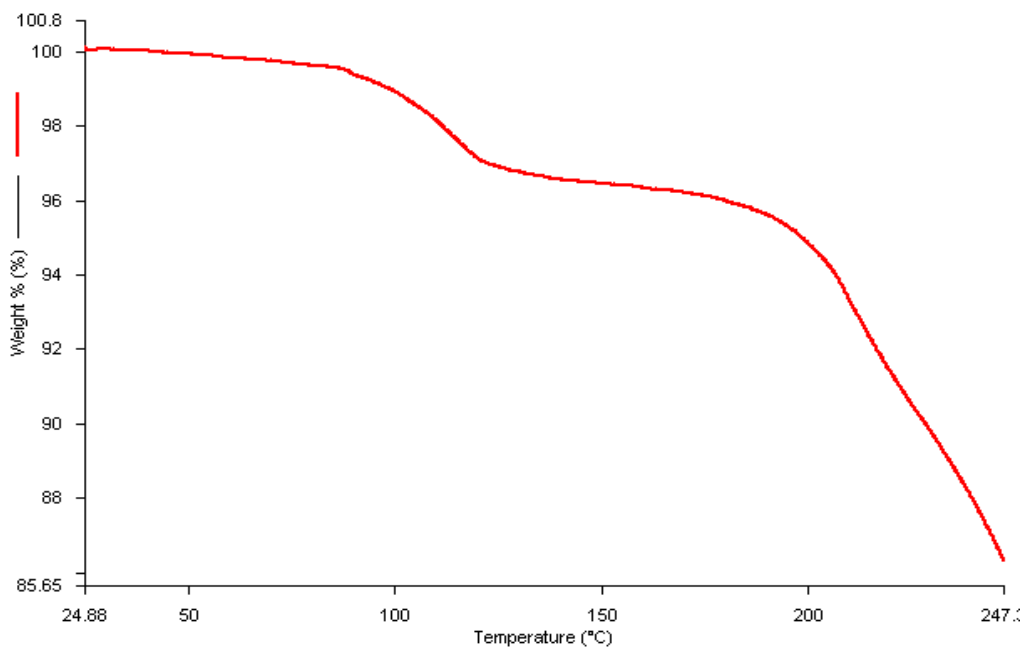


Figure IV.4 Representative TGA thermogram for reference standard ipratropium bromide

The representative X-ray diffraction pattern for IB reference standard is shown in Figure IV.5 with the characteristic peak positions shown in Table IV.4. The diffraction pattern agreed with that reported in literature by Corrigan et al, 2006 as shown in Figure IV.6. The peak intensities for IB were smaller by orders of magnitude compared to those for AS indicating an absence of long range order in the IB crystal lattice.

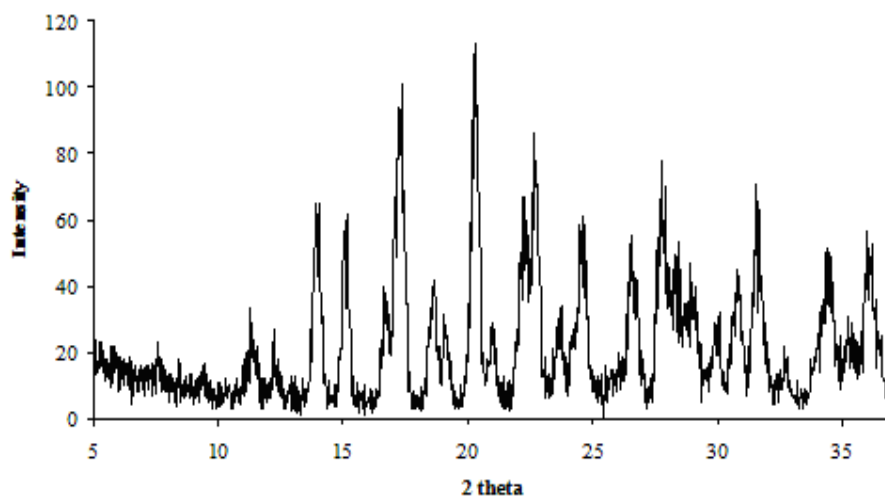


Figure IV.5 Representative powder X-ray diffractogram for reference standard ipratropium bromide

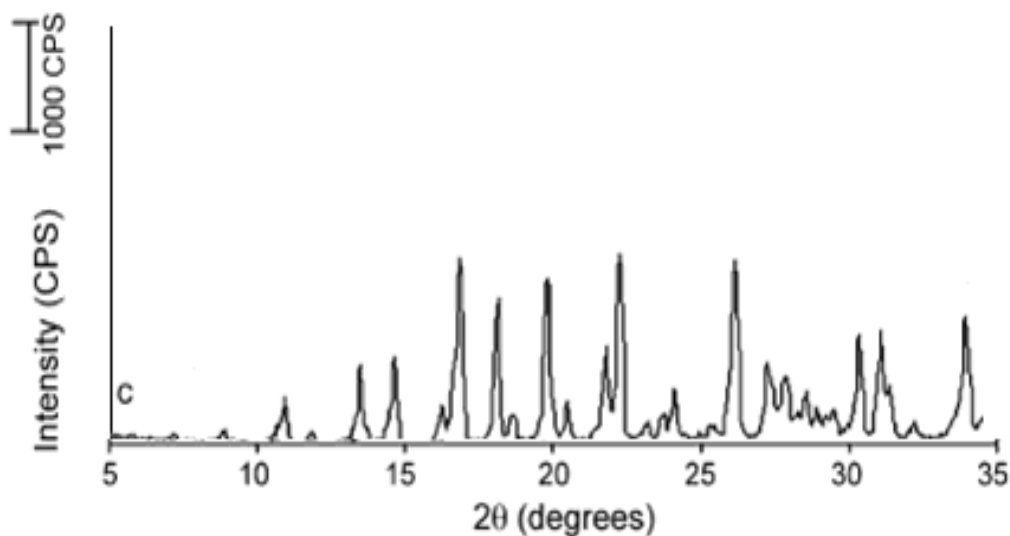


Figure IV.6 Powder X-ray diffraction of ipratropium bromide monohydrate reported by Corrigan et al. (2006) (Reproduced with permission from Elsevier)

Table IV.4 Characteristic X-ray peaks for reference standard ipratropium bromide

Albuterol Sulfate		Ipratropium Bromide	
2θ	Peak intensity	2θ	Peak intensity
10.45	2097	13.93	65
11.47	494	15.15	62
12.93	248	17.33	101
15.27	508	20.29	113
17.75	885	22.35	60
18.43	1177	22.75	71
19.35	228	24.67	61
20.39	576	27.93	70
21.21	1325	31.59	71
23.03	4058		
24.43	694		
25.67	280		
26.39	642		
28.63	652		
29.51	434		
30.85	448		
32.69	388		

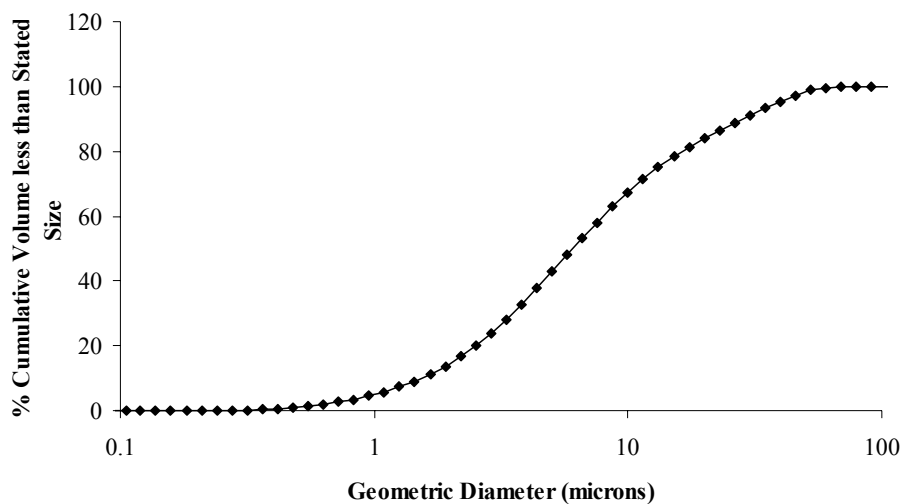


Figure IV.7 Particle size distribution for reference standard ipratropium bromide

The particle size distribution of reference ipratropium bromide is shown in Figure IV.7. The average VMD measured from three replicate measurements was $6.5 \pm 0.4 \mu\text{m}$. Figure IV.8 shows a representative microscopic image of reference IB. The particles appeared to be elongated and rod-like in shape.

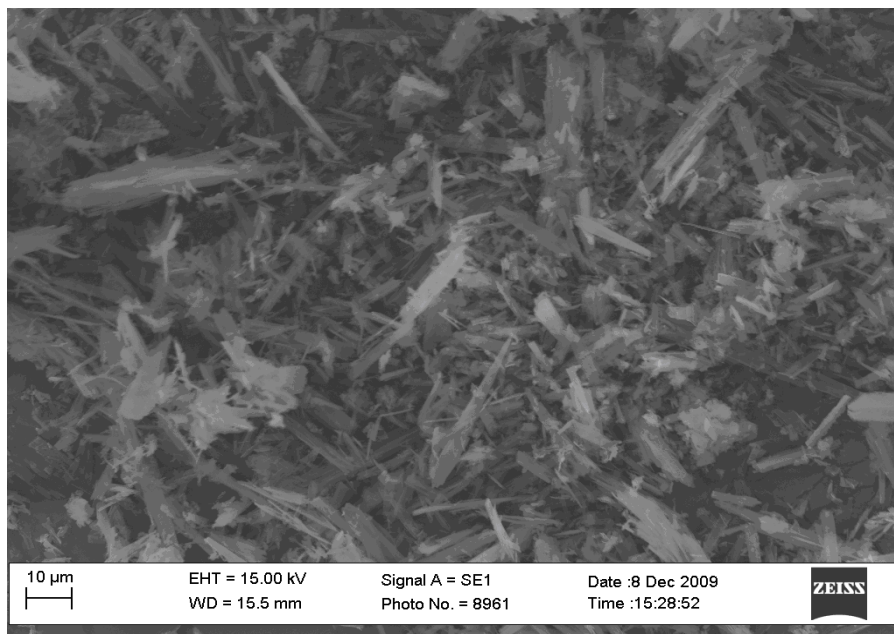


Figure IV.8 Representative SEM image for reference standard ipratropium bromide

IV.D.2 Effect of different processing variables on combination particle characteristics

Particles produced under different crystallization conditions were characterized using a number of analytical tools. It was desirable for these particles to possess certain characteristics in order for them to be suitable for inhalation. Of primary importance was the formation of individual particles that contained both AS and IB in a fixed ratio and not as separately precipitated physical mixtures. This was necessary in order to overcome the problem of segregation of physical mixtures into their individual components during inhalation leading to a loss of the fixed drug ratio. Another desirable characteristic was particle crystallinity since

crystalline particles are considered to be more stable compared to their amorphous counterparts. The final characteristic of interest was particle size since one of the aims of this project was to produce particles directly in a size suitable for inhalation in order to overcome the detrimental effects of micronization.

IV.D.2.1 Crystallization of combination particles produced using ethyl acetate as the anti-solvent

IV.D.2.1.1 HPLC content uniformity analysis

The results for the HPLC analysis of the combination particles are presented in Table IV.5. The measured proportion of AS and IB in the precipitated particles was similar to the starting proportions in the aqueous drug solution i.e.; particles with AS:IB ratios of 1:1, 2.1:1, 6.2:1, and 10.7:1 (w/w) were produced from starting drug solutions with AS:IB ratios of 1:1, 2:1, 6:1, and 10:1 (w/w) respectively.

Table IV.5 Mean \pm SD measured % AS and IB and their ratios in the combination particles produced using ethyl acetate as the anti-solvent

Starting AS:IB ratio (w/w)	Measured AS:IB ratio (w/w)	% AS	% IB
1:1	1:1	48.7 \pm 0.2	51.3 \pm 0.3
2:1	2.1:1	67.4 \pm 0.8	32.6 \pm 0.2
6:1	6.2:1	86.2 \pm 0.3	13.8 \pm 0.5
10:1	10.7:1	91.4 \pm 0.7	8.6 \pm 0.9

These results indicated that both drugs precipitated out completely in this solvent / anti-solvent system. This was expected since AS and IB have similar solubilities of 5.0 \pm 0.2 and 2.6 \pm 0.2 μ g/mL in ethyl acetate. These results are supported by the literature which states that the composition of the co-precipitated particles is dictated by the relative solubilities of the two

components with success more likely in a solvent in which the solubilities of the two components are similar (Chiarella et al., 2007). The % AS and % IB in the combination particles were reproducible as shown by the associated small standard deviation values thereby suggesting the formation of combination particles with reproducible proportions of AS and IB.

HPLC revealed the bulk characteristics of the particles produced from ethyl acetate. However, it is equally important to consider the particle properties at the molecular level. In this study, DSC and powder X-ray diffraction have been used to investigate these properties. At this point it is useful to define a number of terms that will be discussed. “Co-crystal” is a term used to describe the binding of two or more components within one periodic line lattice without making or breaking covalent bonds (Aakeroy and Salmon, 2005). A new crystal lattice is generated which is different from either of the individual components. “Combination particle” is a term used to describe the existence of two or more components in single particles. These components may exist as a single phase with one of the components included in the crystal lattice of the other or as separate phases. In combination particles a new crystal lattice is not generated as is the case with co-crystals. “Physical mixture” is a term used to describe the existence of two or more components in the form of a blend with each component present as a separate phase. Thermal analysis and PXRD of the particles produced from ethyl acetate was carried out in order to elucidate the nature of these particles.

IV.D.2.1.2 Thermal analysis

Table IV.6 shows the results from the thermal characterization of the particles prepared using ethyl acetate as the anti-solvent. Representative thermograms for the different combination particles are shown in Figures IV.9, IV.10, IV.11 and IV.12. For the 1:1, 2.1:1, and 6.2:1 (w/w)

combination particles, two thermal events were observed. The first thermal event was endothermic and was attributed to the loss of one mole of water of crystallization from IB. The heats of dehydration are shown in Table IV.6. The numbers in parentheses indicated the calculated heat of dehydration associated with the loss of one mole of water of crystallization from IB when present in that particular proportion. No dehydration peak was observed for the 10.7:1 (w/w) particles due to the sensitivity limit of the DSC which was unable to detect the water loss from the small proportion of IB as shown in Figure IV.12.

Table IV.6 Thermal characteristics of AS / IB combination particles prepared using ethyl acetate as the anti-solvent

AS:IB (w/w)	Measured heat of dehydration (J/g) (Calculated)	Dehydration temperature (°C)	Heat of fusion (J/g)	Melting point (°C)
1:1	51.3 ± 4.8 (54.9)	114.4 ± 0.6	60.3 ± 2.7	177.9 ± 0.1
2.1:1	31.6 ± 3.3 (34.8)	110.4 ± 0.3	94.2 ± 3.3	184.3 ± 0.1
6.2:1	14.5 ± 3.6 (14.8)	107.5 ± 0.1	153.4 ± 1.3	183.1 ± 0.1
10.7:1	163.5 ± 2.4	182.3 ± 0.1

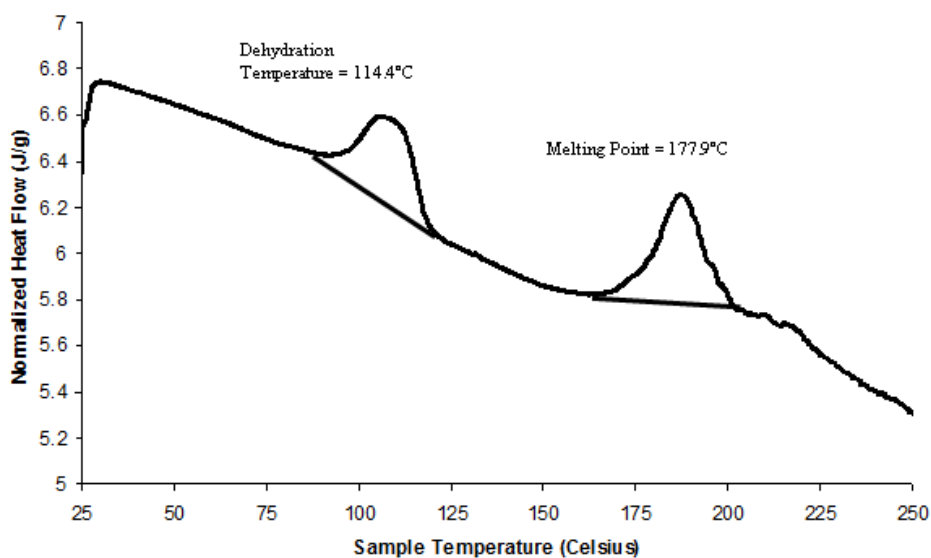


Figure IV.9 Representative differential scanning thermogram for 1:1 (w/w) combination particles produced using ethyl acetate as anti-solvent

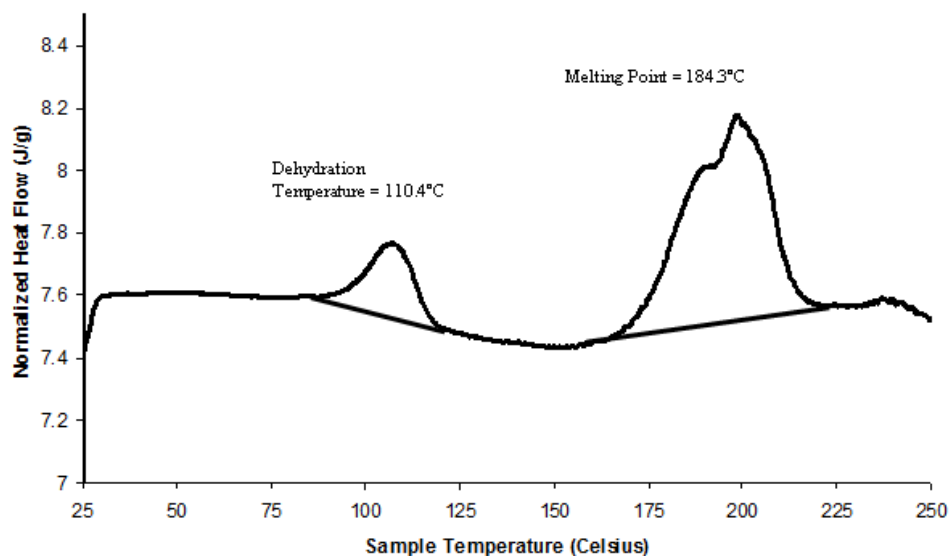


Figure IV.10 Representative differential scanning thermogram for 2:1 (w/w) combination particles produced using ethyl acetate as anti-solvent

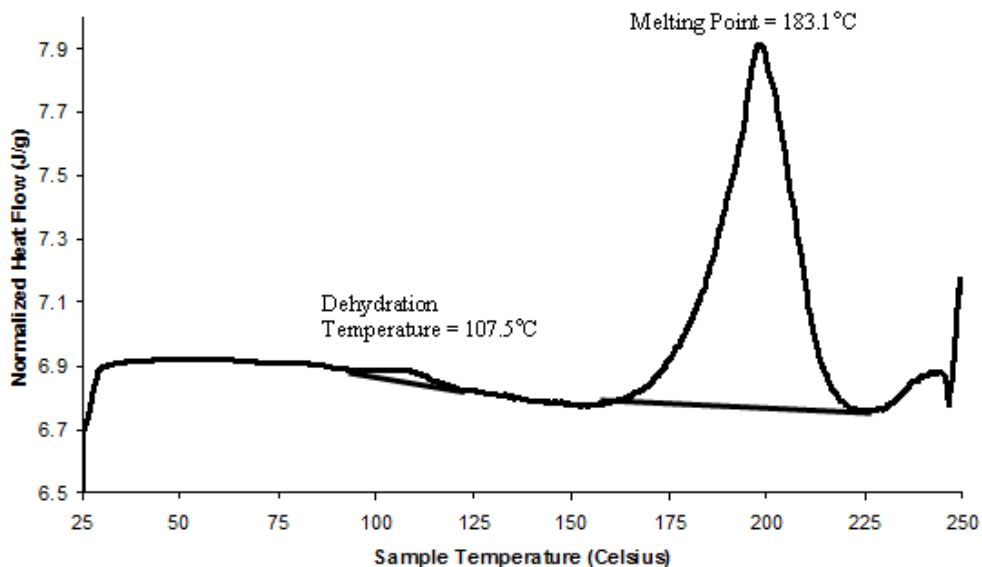


Figure IV.11 Representative differential scanning thermogram for 6:1 (w/w) combination particles produced using ethyl acetate as anti-solvent

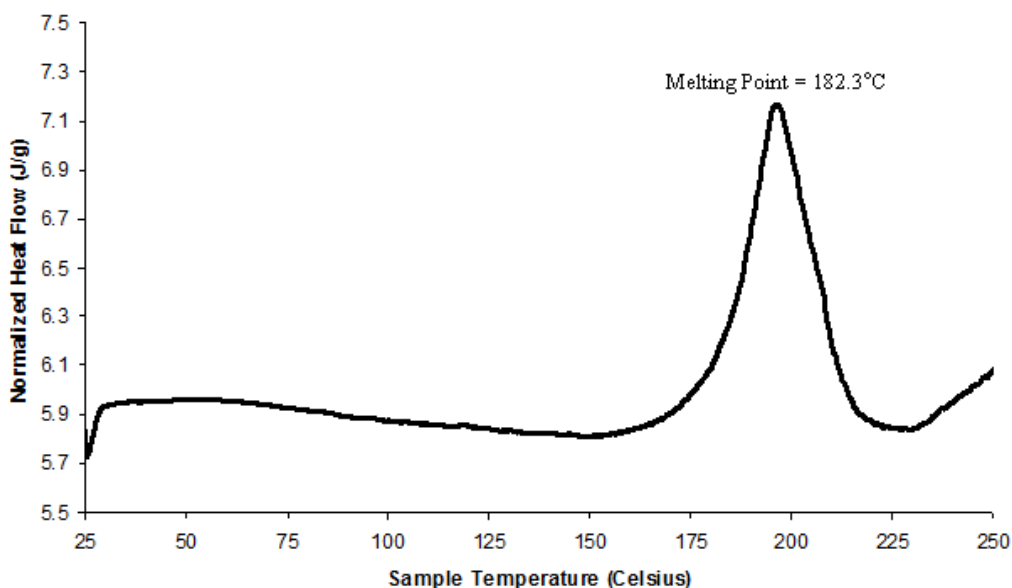


Figure IV.12 Representative differential scanning thermogram for 10:1 (w/w) combination particles produced using ethyl acetate as anti-solvent

The measured heats of dehydration for the different combination particles did not reveal any statistical difference compared to the calculated heat of dehydration from the loss of one mole of water of crystallization from IB in the particular ratios (p -values > 0.05 , one-way ANOVA). This suggested that the formed combination particles contained IB in a completely hydrated form. Moreover, the presence of a dehydration endotherm attributable to the loss of water of crystallization also pointed strongly towards IB being present in a crystalline form since this water is incorporated into the crystal lattice. However, the dehydration endotherm had a single peak as opposed to the double peak present in IB (Figure IV.3).

The second thermal event was attributed to the melting of the combination particles. This was also confirmed by observing the particles under the hot stage microscope. A single melt was observed for the combination particles. The 1:1, 2:1, 6:1 and 10:1 combination particles melted at significantly lower temperatures of $177.9 \pm 0.1^\circ\text{C}$, $184.3 \pm 0.1^\circ\text{C}$, $183.1 \pm 0.1^\circ\text{C}$, and $182.3 \pm$

0.1°C respectively compared to AS ($189.5 \pm 0.5^\circ\text{C}$) and IB ($232.6 \pm 0.7^\circ\text{C}$) (p-values < 0.05, one-way ANOVA) as shown in Table IV.6 and Figures IV.9, 10, 11, and 12. The melting points for the 1:1 (w/w) combination particles were significantly lower (p-value < 0.05, Tukey's HSD) compared to the melting points for the 2:1, 6:1 and 10:1 (w/w) combination particles which were statistically comparable (p-value > 0.05, Tukey's HSD). These 1:1 (w/w) combination particles also had the lowest heat of fusion at a mean value of 60.3 ± 2.7 /g. The heat of fusion increased with the proportion of AS in the combination particles. A correlation analysis between the heat of fusion and the AS:IB ratio revealed a significant positive correlation ($R = 0.9045$, p-value < 0.0001). However, these heats of fusion remained significantly lower than for pure AS (188.6 ± 2.6 J/g) and pure IB (196.5 ± 2.9 J/g).

Corrigan et al. (2006) had prepared combination particles of AS and IB by co-spray drying. The thermal analysis of their particles is shown in Figure IV.13. The absence of a sharp melting peak was indicative of the amorphous nature of these particles. In contrast, the combination particles prepared using the experimental procedure described for ethyl acetate resulted in thermograms showing sharp melting peaks as shown in Figures IV.9, IV.10, IV.11, and IV.12 indicating that they were not amorphous.

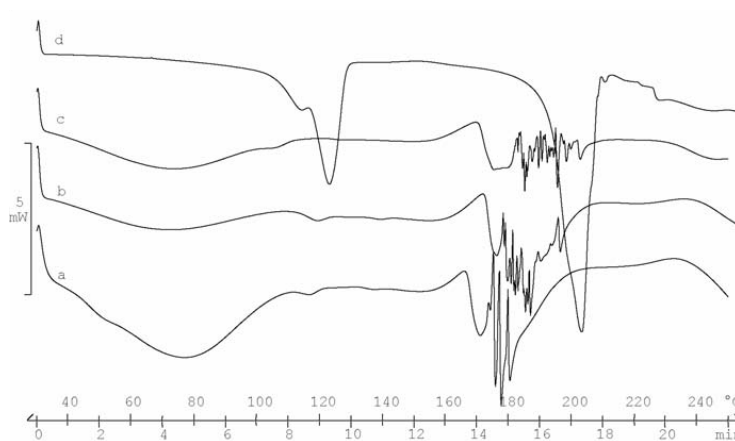


Figure IV.13 DSC thermograms for a) AS:IB 10:1 co-spray dried, b) AS:IB 5:1 co-spray dried, c) AS:IB 2:1 co-spray dried, and d) AS:IB 2:1 physical mixture (Corrigan et al., 2006) (Reproduced with permission from Elsevier)

In order to understand whether AS and IB were interacting in these particles or were present as a physical mixture, the thermal characteristics of the precipitated particles were compared to those of corresponding physical mixtures of AS and IB. The thermal analysis of the physical mixtures was performed using the same temperature program employed for the combination particles. The results for heat of fusion of the combination particles vs. physical mixtures are shown in Table IV.7 which also shows the calculated heat of fusion for AS in the absence of any interaction based upon the nominal AS ratio.

Table IV.7 Comparison of heats of fusion of combination particles with the corresponding physical mixtures

AS:IB (w/w)	Measured heat of fusion for combination particles	Measured heat of fusion for physical mixtures	Calculated heat of fusion for AS (J/g)
1:1	60.3 ± 2.7	108.4 ± 3.4	95.0
2.1:1	94.2 ± 3.3	134.2 ± 2.2	126.7
6.2:1	153.4 ± 1.3	166.0 ± 2.8	162.9
10.7:1	163.5 ± 2.4	179.7 ± 3.6	172.7

A statistical comparison did not reveal any significant difference (p-value > 0.05, one-way ANOVA) between the measured heat of fusion for the physical mixtures and the calculated heat of fusion for AS in the same proportion provided there is no interaction between AS and IB. The 1:1, 2:1, 6:1, and 10:1 (w/w) physical mixtures showed heats of fusion of 108.4 ± 3.4 J/g, 134.2 ± 2.2 J/g, 166.0 ± 2.8 J/g, and 179.7 ± 3.6 J/g which were comparable to the calculated heats of fusion of 95.0 J/g, 126.7 J/g, 162.9 J/g, and 172.7 J/g for AS when present in the respective stoichiometric proportions. These results indicated that in the physical mixtures prepared by blending of AS and IB, there was no interaction between the two drugs.

However, the heat of fusion for the 1:1, 2:1, 6:1, and 10:1 (w/w) combination particles were significantly lower (p-value < 0.05, one-way ANOVA) compared to the calculated heat of fusion for AS in these proportions in the absence of any interactions. These results may indicate interactions between AS and IB in the combination particles resulting in an alteration of their heats of fusion. Table IV.8 shows the comparison of the melting points for the combination particles with the corresponding physical mixtures. The melting point for reference standard AS was $189.5 \pm 0.5^\circ\text{C}$. The melting point for the 1:1 (w/w) physical mixture was $183.5 \pm 0.2^\circ\text{C}$ which was significantly lower than the melting point for pure AS (p-value < 0.05, one-way ANOVA). For the 2:1, 6:1, and 10:1 (w/w) physical mixtures, there was no significant difference in melting points compared to AS (p-value > 0.05, one-way ANOVA). However, the combination particles in all stoichiometric ratios exhibited significantly lower melting points compared to AS (p-value < 0.05, one-way ANOVA). These differences once again indicated interactions between AS and IB when present in the combination particles which led to the alteration of the melting point. Furthermore, these results were in contrast to the melting points for the physical mixtures which were comparable to the AS melting point (except for the 1:1 (w/w) physical mixture) and indicated that there was no interaction between the two drugs when blended together.

Table IV.8 Comparison of melting points of combination particles with the corresponding physical mixtures

AS:IB (w/w)	Combination particles ($^\circ\text{C}$)	Physical mixture ($^\circ\text{C}$)
1:1	177.9 ± 0.1	183.5 ± 0.2
2.1:1	184.3 ± 0.1	185.9 ± 0.2
6.2:1	183.1 ± 0.1	188.8 ± 0.1
10.7:1	182.3 ± 0.1	188.8 ± 0.1

The dehydration temperatures of the combination particles and the corresponding physical mixtures are shown in Table IV.9. All four physical mixtures revealed no significant difference in the dehydration temperature relative to dehydration at $116.5 \pm 2.8^\circ\text{C}$ exhibited by pure IB (p-value > 0.05, one-way ANOVA).

Table IV.9 Comparison of dehydration temperatures of combination particles with the corresponding physical mixtures

AS:IB (w/w)	Combination particles ($^\circ\text{C}$)	Physical mixtures ($^\circ\text{C}$)	
1:1	114.4 ± 0.6	108.2 ± 0.3	115.2 ± 0.4
2.1:1	110.4 ± 0.3	107.8 ± 0.2	113.7 ± 0.6
6.2:1	107.5 ± 0.1	106.9 ± 0.4	111.7 ± 0.2
10.7:1

Furthermore, as shown in Figure IV.3, the loss of one mole of water of crystallization from IB was in two phases with a small shoulder being observed at $\approx 108^\circ\text{C}$ and a bigger peak at 116.5°C . This water loss was similar to that observed from the dehydration endotherms for the physical mixtures as shown in Figures IV.14, IV.15, IV.16, and IV.17. In contrast, the combination particles showed a dehydration endotherm that appeared as a single peak without any shoulder as shown in Figures IV.14, 15, 16, and 17. Since this mole of water is incorporated in the IB crystal lattice, any interaction of IB with AS would influence the nature of its release. Therefore, these results showing differences in the behavior of water of crystallization between co-precipitated particles and physical mixtures indicated a difference in the interaction between AS and IB when present in a combination particle matrix relative to a simple physical mixture.

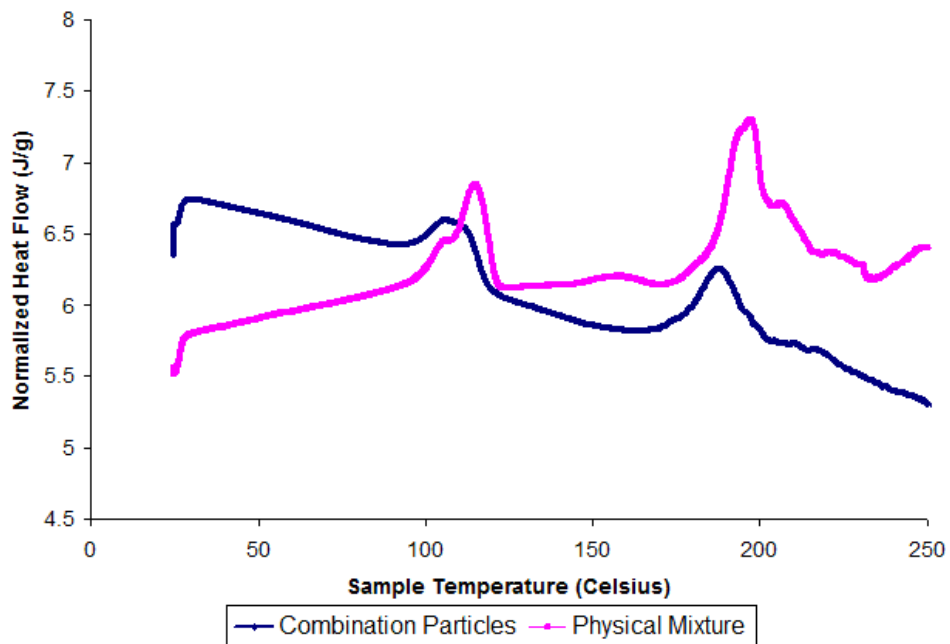


Figure IV.14 DSC thermograms of 1:1 (w/w) combination particles and the corresponding physical mixture

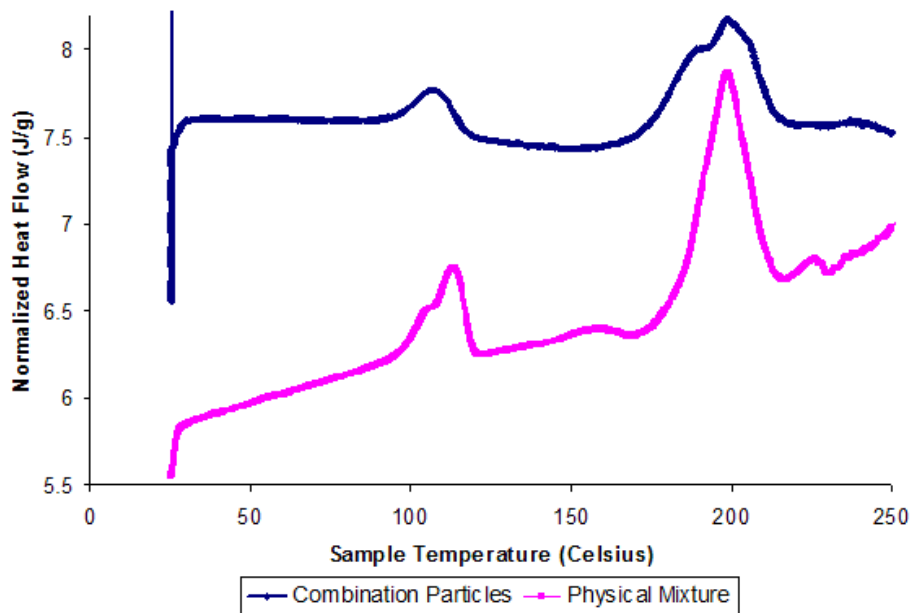


Figure IV.15 DSC thermograms of 2:1 (w/w) combination particles and the corresponding physical mixture

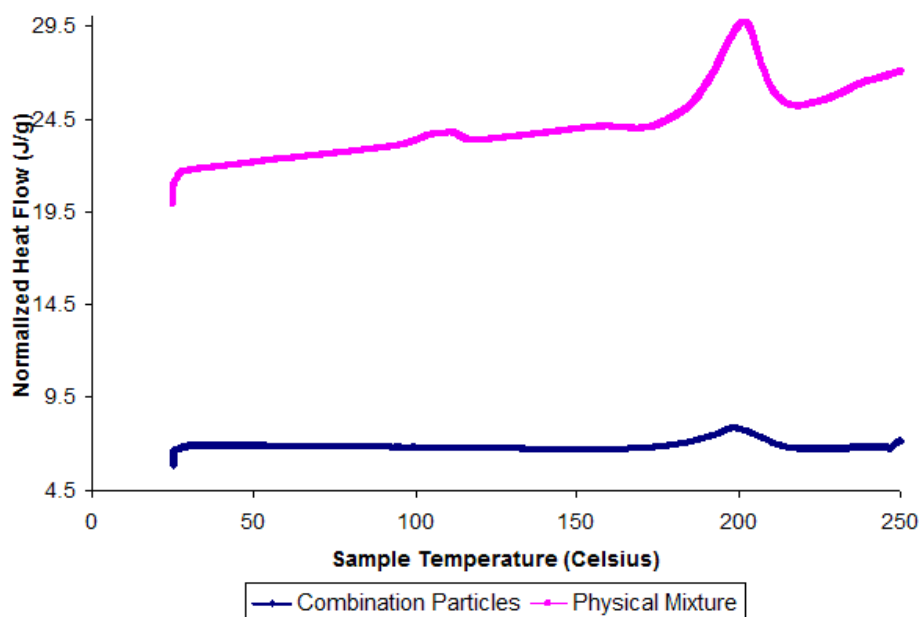


Figure IV.16 DSC thermograms of 6:1 (w/w) combination particles and the corresponding physical mixture

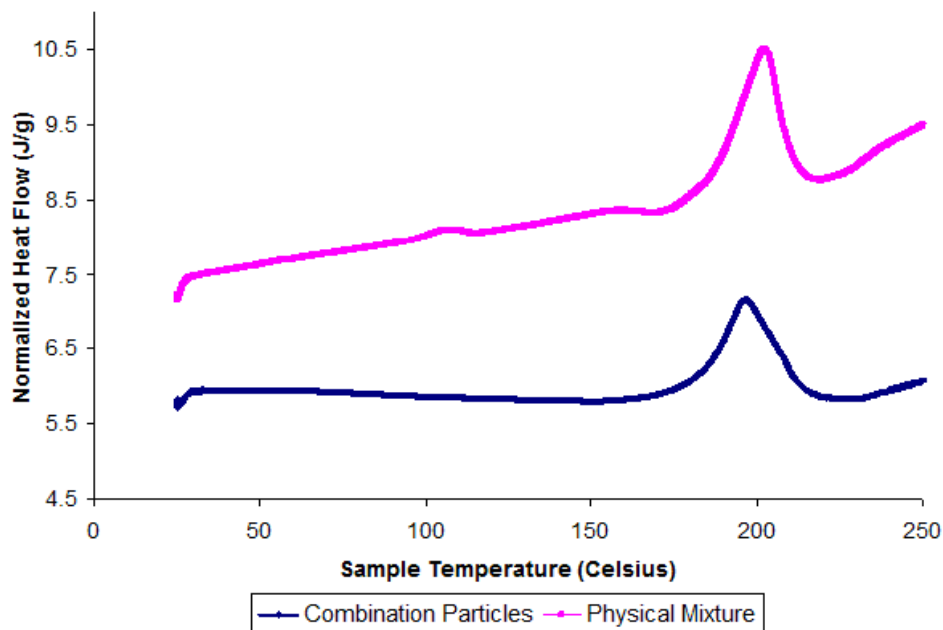


Figure IV.17 DSC thermograms of 10:1 (w/w) combination particles and the corresponding physical mixture

These studies therefore revealed a difference in the thermal characteristics of the combination particles relative to simple physical mixtures of AS and IB. It was of interest to see whether these combination particles resulted in the formation of co-crystals at these AS:IB ratios. Thermal characterization is a useful tool for this purpose. Stanton et al. (2008) have compared the melting points of 10 co-crystals to the API and their respective co-crystal formers (coformer). Each of the cocrystals displayed a melting point that fell between the melting point of the API and the respective coformer. Schultheiss et al. (2009) compiled a large survey based on reported cocrystal melting points, and these were compared with the melting points of the coformer and API. Within the survey, 50 cocrystalline samples were analyzed; 26/50 (51%) cocrystals had melting points between those of the API and coformer, while 19/50 (39%) were lower than either the API or coformer, only 3/50 (6%) were higher, and 2/50 (4%) had the same melting point as either the API or coformer. These statistics clearly show that the melting point of an API can be altered through forming cocrystals, and the outcome will usually be a product having a melting point that is in between that of the API and coformer or lower than the API or coformer. The melting points of the different combination particles produced from ethyl acetate were significantly lower than AS and IB which can be treated analogous to the API and coformer respectively. These results therefore agree with the reported melting point behavior for 39% of co-crystals reviewed by Schultheiss et al. (2009). However, in the absence of supporting crystal structure data, it is difficult to conclude unambiguously whether co-crystals are being formed or not. Within a homologous set of cocrystals (either the API or coformer is kept constant), where single crystal X-ray structures have been determined, comparisons could potentially be drawn between the intermolecular interactions and/or crystal packing existing within the lattice and the thermal behavior of the sample.

Therefore, analysis of the particles produced from ethyl acetate revealed some important findings. First and foremost, it was possible to precipitate out both AS and IB completely owing to their similar solubilities in ethyl acetate. This similarity made ethyl acetate an attractive anti-solvent for both drugs. The combination AS/IB particles showed different thermal characteristics from either AS, IB, or physical mixtures of the two. These results indicated that AS and IB did not precipitate separately as a physical mixture and were present together in combination particles which can be referred to as combination particles. This was a desirable phenomenon since one of the aims of this project was to produce such combination particles of AS and IB that would not segregate into individual components upon inhalation. Although, these results revealed possible interactions between AS and IB in these combination particles, it was not possible to conclude from the thermal analysis data whether co-crystals were being produced. Therefore, these particles were characterized by powder X-ray diffraction to further elucidate the nature of interaction between AS and IB.

IV.D.2.1.3 Powder X-ray diffraction

Powder X-ray diffraction is used to obtain information about crystal lattice changes owing to it being a relatively simple technique which can be used with pharmaceutical powders. The combination particles and the physical mixtures were analyzed by powder X-ray diffraction. Figures IV.18, and IV.19, show the diffractograms for the 1:1 (w/w) combination particles and the 1:1 (w/w) physical mixture. The diffractograms for the 2:1 and 6:1 (w/w) combination particles are shown in Figures IV.20 and IV.21 respectively. The 10:1 (w/w) combination particles were not characterized by powder X-ray diffraction since thermal analysis did not show a significant difference between the 6:1 and the 10:1 (w/w) combination particles in terms of

melting point and heat of fusion (p-value > 0.05, one-way ANOVA). The characteristic diffraction peaks for the 6:1 (w/w) combination particles are shown in Table IV.10.

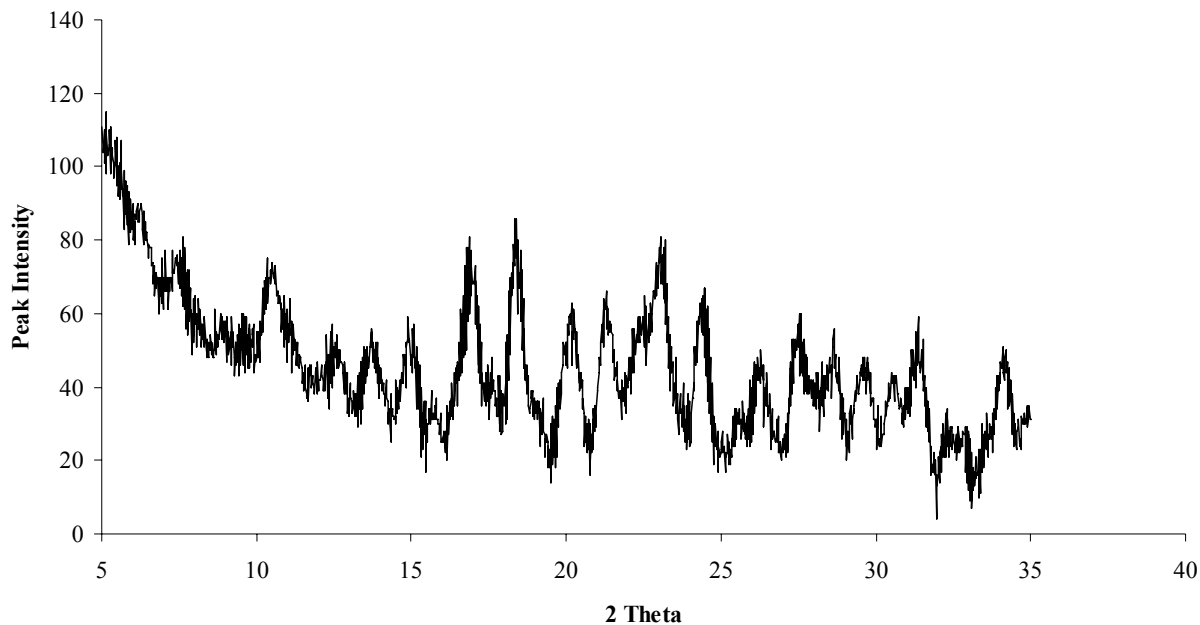


Figure IV.18 Powder X-ray diffractogram for 1:1 (w/w) AS/IB combination particles produced from ethyl acetate

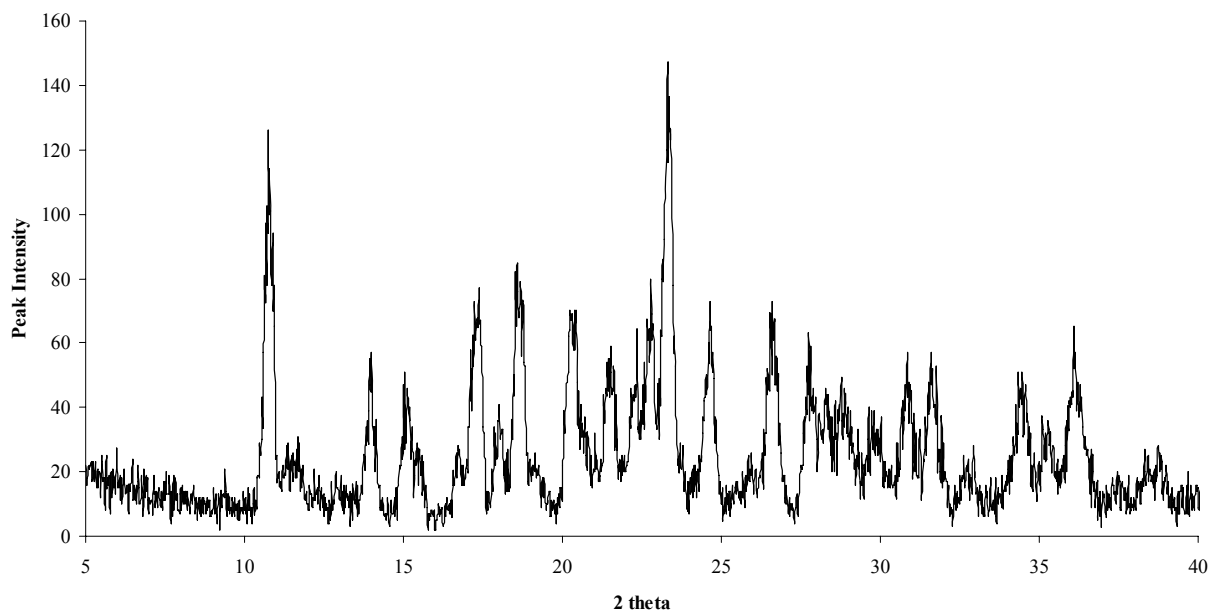


Figure IV.19 Powder X-ray diffractogram for 1:1 (w/w) AS/IB physical mixture

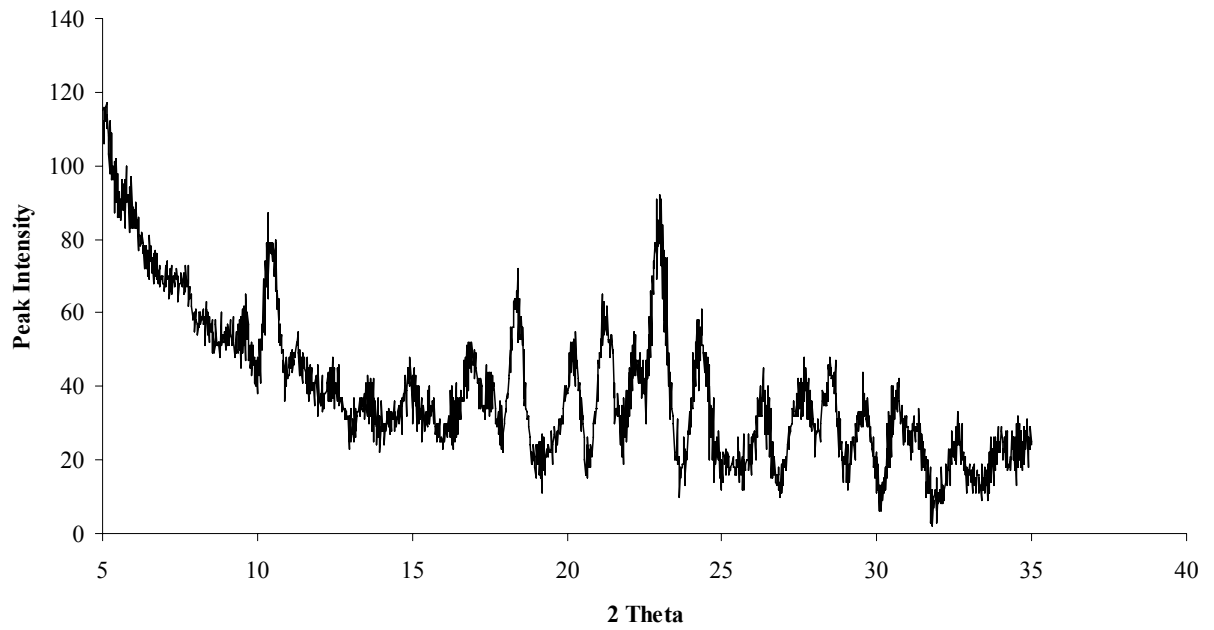


Figure IV.20 Powder X-ray diffractogram for 2:1 (w/w) AS/IB combination particles produced from ethyl acetate

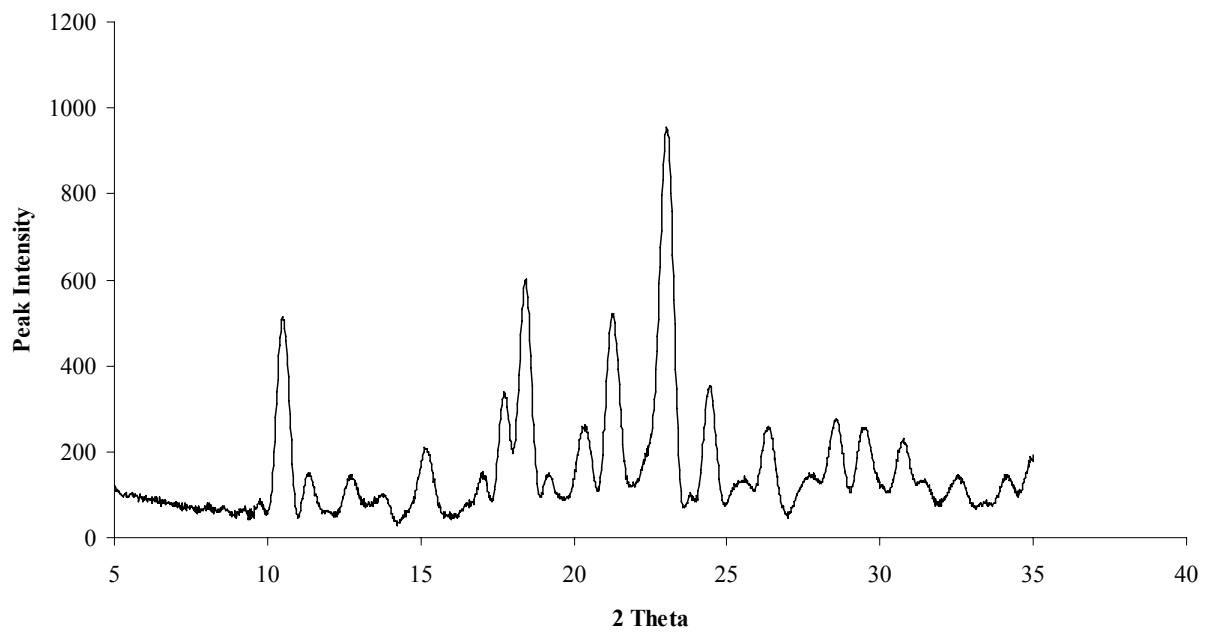


Figure IV.21 Powder X-ray diffractogram for 6:1 (w/w) AS/IB combination particles produced from ethyl acetate

Table IV.10 Characteristic diffraction peaks for the 6:1 (w/w) combination particles prepared using ethyl acetate as anti-solvent

Characteristic reference peaks for AS and IB		AS:IB 6:1 (w/w)	
2 theta	Intensity	2 theta	Intensity
10.45	2097	10.53	508
11.47	494		
		12.75^a	147^a
12.93	248		
13.93	65		
15.15	62		
15.27	508	15.19	207
17.33	101		
17.75	885	17.71	338
18.43	1177	18.43	602
19.35	228	19.17	152
20.29	113		
20.39	576	20.37	261
21.21	1325	21.29	523
22.35	60		
22.75	71		
23.03	4058	23.03	954
24.43	694	24.45	353
24.67	61		
25.67	280		
26.39	642	26.33	260
27.93	70		
28.63	652	28.63	260
29.51	434	29.55	253
30.85	448	30.83	221
31.59	71		
32.69	388	32.59	145

a Significantly shifted compared to the AS peak based on a % deviation of $\pm \geq 1\%$ calculated with reference to the AS peak

The % deviation of the 2θ value from the AS peaks was calculated. A % deviation value of $\geq 1.0\%$ was taken as a criterion for a significant peak shift. As shown in Table IV.10, the 6:1 (w/w) combination particles revealed only a single peak which satisfied this criterion. The diffractogram for the 1:1 (w/w) and 2:1 (w/w) combination particles revealed peaks that were significantly lower in intensity compared to AS. These XRPD results therefore corroborated the DSC results where these 1:1 and 2:1 (w/w) combination particles revealed significantly lower heats of fusion compared to reference standard AS (Table IV.7). These results were therefore indicative of lower crystallinity of these particles. This might attributed to the presence of a high proportion of IB which does not have long range crystalline order. Further, a number of characteristic AS peaks were absent. However, the particles were not completely amorphous since the characteristic halo associated with amorphous particles was absent. Such a characteristic halo has been reported by Corrigan et al. for the combination particles of AS and IB prepared by co-spray drying an aqueous solution of the two drugs as shown in Figure IV.22 (Corrigan et al., 2006).

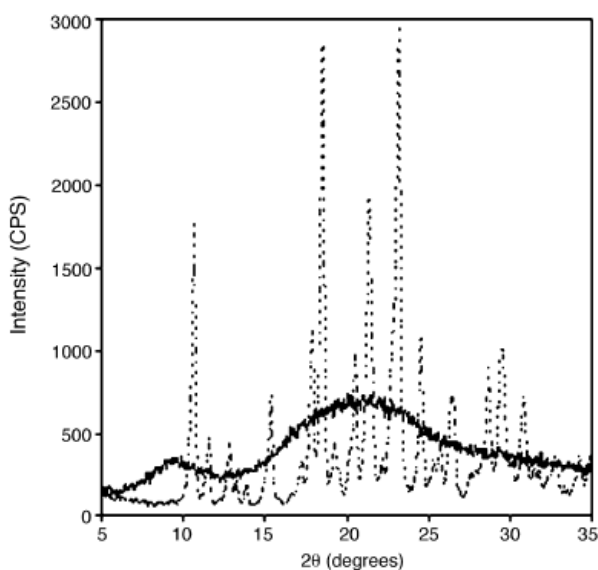


Figure IV.22 XRPD of AS:IB 10:1 co-spray dried (continuous line) and crystalline AS (dashed line) (Corrigan et al., 2006) (Reproduced with permission from Elsevier)

The diffractogram for the 6:1 (w/w) combination particles on the other hand, showed significantly higher peak intensities for the characteristic AS peaks compared to the 1:1 and 2:1 (w/w) combination particles. These results supported the DSC results where the heat of fusion increased as the proportion of AS in the combination particles increased indicating that the crystal lattice started to resemble AS as the IB percentage decreased.

A plausible scenario explaining the nature of formation of these co-precipitated particles may be the incorporation of IB in the interstitial spaces within the AS crystal lattice somewhat akin to the formation of an interstitial crystalline solid solution as shown in Figure IV.23.

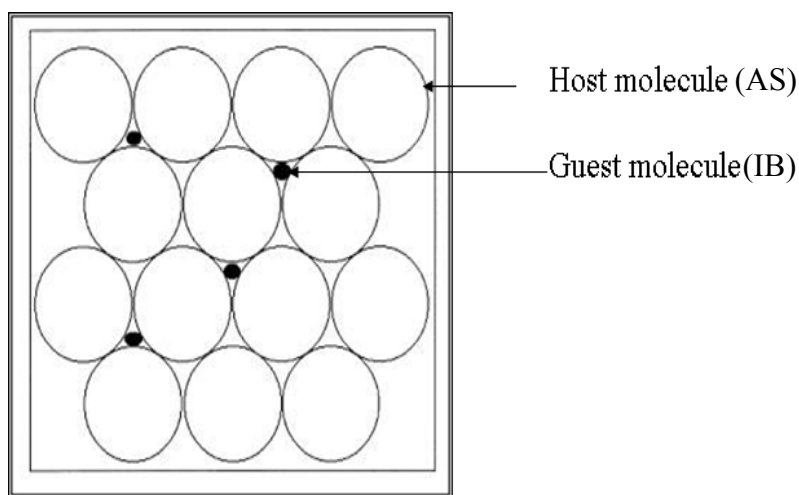


Figure IV.23 Representation of an interstitial crystalline solid solution (Adapted from Ghaste et al., 2009)

For the 1:1 and 2:1 (w/w) combination particles, the inclusion of a high proportion of IB may even have resulted in a breaking of the AS crystal lattice which would account for the reduced crystallinity of these particles. For the 6:1 (w/w) combination particles, this inclusion may stretch the unit cell of AS resulting in a decrease in crystal robustness which is then reflected in a decreased melting point and a lower heat of fusion implying that a lower heat / energy is required to melt the crystal compared to the more robust crystal of AS. This hypothesis was also supported by the fact that as the % IB in the particles decreased, there was an increase

in the heat of fusion. A lowered percentage of IB would lead to an increase in the purity of the crystal lattice which may start to resemble the lattice of AS as the IB percentage goes down. The increase in heat of fusion with an increase in the proportion of AS in the combination particles may be indicative of an increasing crystallinity brought about by an increasing purity of the crystal lattice which was also observed as an increase in the intensity of the X-ray peaks for the 6:1 (w/w) combination particles.

IV.D.2.1.4 Particle size distribution of combination particles produced from ethyl acetate

One of the primary aims of this project was to produce combination particles with suitable size characteristics for inhalation. Figure IV.24 shows the cumulative % undersize distributions of the four combination particles produced using ethyl acetate with their volume median diameters (VMDs) shown in Table IV.11.

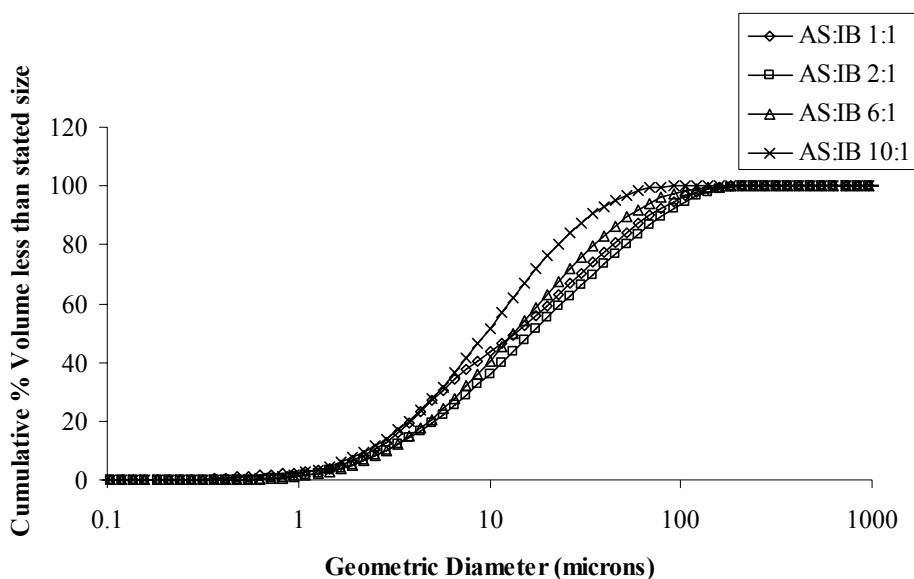


Figure IV.24 Cumulative % undersize volume distribution of different combination particles produced using ethyl acetate as the anti-solvent

Table IV.11 Mean \pm SD volume median diameters and cumulative % volumes $< 5.0 \mu\text{m}$ of combination particles produced using ethyl acetate as the anti-solvent

AS:IB (w/w)	VMD \pm SD (μm)	Volume % $< 5.0 \mu\text{m}$
1:1	19.5 \pm 4.0	19.4 \pm 2.4
2.1:1	15.6 \pm 5.0	20.7 \pm 3.2
6.2:1	15.3 \pm 0.9	26.9 \pm 1.8
10.7:1	11.1 \pm 1.1	27.5 \pm 1.2

Statistical analysis of the VMD data revealed that the 10:1 combination particles were significantly (p -value < 0.05 , Tukey's HSD) smaller with a VMD of $11.1 \pm 1.1 \mu\text{m}$ compared to the 1:1, 2:1, and 6:1 (w/w) combination particles. These particles had significantly higher and comparable VMDs (p -value > 0.05 , Tukey's HSD) of $19.5 \pm 4.0 \mu\text{m}$, $15.6 \pm 5.0 \mu\text{m}$, and $15.3 \pm 0.9 \mu\text{m}$ respectively. These results showed that the combination particles produced from ethyl acetate were too large for inhalation with VMDs above $10 \mu\text{m}$ for all particles. Further, The mean (SD) volumes % $< 5.0 \mu\text{m}$ for 1:1, 2:1, 6:1, and 10:1 (w/w) combination particles were 19.4 (2.4), 20.7 (3.2), 26.9 (1.8), and 27.5 (1.2) % respectively which is not suitable for inhalation. Therefore, ethyl acetate did not appear suitable for producing combination particles of AS and IB suitable for inhalation.

Particle morphology showed these particles to be predominantly tabular and plate-like in shape. Some elongated, rod-like particles were also observed. Figure IV.25 shows the representative optical microscopic images for a) 1:1 (w/w) combination particles, b) 2:1 (w/w) combination particles, c) 6:1 (w/w) combination particles, and d) 10:1 (w/w) combination particles produced from ethyl acetate as the anti-solvent.

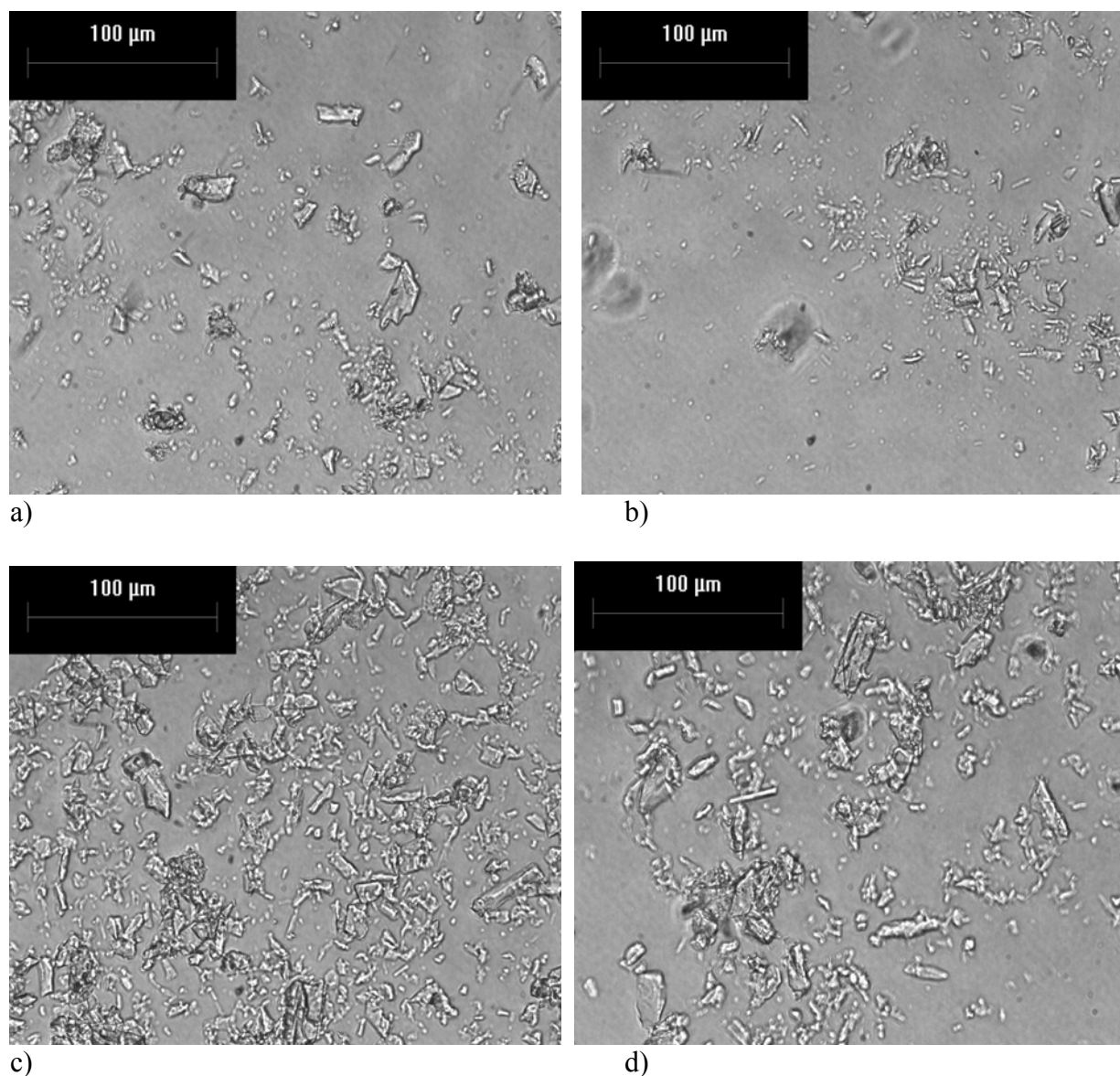


Figure IV.25 Optical microscopic images for a) 1:1 (w/w) combination particles, b) 2:1 (w/w) combination particles, c) 6:1 (w/w) combination particles, d) 10:1 (w/w) combination particles produced from ethyl acetate

In summary, ethyl acetate was a good anti-solvent for AS and IB leading to the co-precipitation of the two drugs and formation of combination particles. However, use of ethyl acetate as the anti-solvent did not lead to the formation of particles in a size suitable for inhalation and hence, further investigation and optimization of the crystallization process was necessary.

IV.D.2.2 Crystallization of combination particles produced using isopropyl alcohol as the anti-solvent

IV.D.2.2.1 HPLC content uniformity analysis

The primary aim of the studies carried out using isopropyl alcohol (IPA) as the anti-solvent was to produce 6:1 (w/w) combination particles of AS/IB in a size suitable for inhalation. Table IV.2 showed the different crystallization conditions used to produce these combination particles. The HPLC analysis results of the combination particles produced from isopropyl alcohol under the different conditions are shown in Table IV.12. In the first crystallization condition, the R_a ratio was 1:200 (w/w). The initial concentrations of AS and IB in the aqueous drug solution were 0.28 and 0.05 g/g resulting in an initial AS:IB ratio of 6:1 (w/w). However, the AS:IB ratio in the precipitated particles was measured as 97.1 :1 (w/w) suggesting negligible precipitation for IB.

Table IV.12 AS IB ratios in the combination particles produced using isopropyl alcohol as the anti-solvent

R_a ratio (w/w)	AS conc. (g/g)	IB conc. (g/g)	Crystal maturation time	Starting AS:IB ratio (w/w)	Measured AS:IB ratio (w/w)
1:200	0.28	0.05	24 hours	6:1	97.1:1
1:20	0.48	0.28	24 hours	1.7:1	6.6:1
1:20	0.48	0.28	5 minutes	1.7:1	2.8:1
1:20	0.48	0.08	30 seconds	6:1	5.7:1

Therefore, IPA did not act as a good anti-solvent for IB and it was not possible to obtain complete precipitation of IB under these crystallization conditions. These results may be explained by the high solubility of IB in IPA (i.e.; 4.9 mg/mL). At a R_a ratio of 1:200 (w/w), the final concentration of IB in IPA was 0.2 mg/mL which was below the solubility of IB in IPA. Therefore, no crystallization of IB was achieved under these conditions.

In order to get 6:1 (w/w) combination particles of AS and IB, the crystallization conditions were altered. The R_a ratio was decreased to 1:20 (w/w) in order to reduce IB dissolution. Further, the starting concentrations of both AS and IB were optimized in order to arrive at a final combination particle ratio of 6:1 (w/w). The starting drug concentrations were decided based on the solubility values of AS and IB in IPA which would yield a final AS:IB ratio of 6:1 (w/w) after a crystal maturation time of 24 hours. Using these crystallization conditions, combination particles with a nominal ratio of 6.6:1 (w/w) were obtained. Chemical analysis by HPLC revealed that these particles contained a reproducible percentage of AS (86.9%) and IB (13.1%) with corresponding % RSDs of 0.2 and 1.5 % respectively. However, *in vitro* aerosol performance testing of these combination particles carried out by the methods described in Chapter V revealed a variation in the AS:IB ratio as a function of particle size. Table IV.13 shows the AS:IB ratios (w/w) obtained from these particles on different stages of the next generation impactor (NGI) during *in vitro* aerosol performance testing.

Table IV.13 AS:IB ratio (w/w) in the impactor for the combination particles produced from IPA after 24 hours of crystallization

Stage	AS:IB (w/w)
Device	6.1:1
MA	5.9:1
Throat	6.0:1
PS	6.3:1
S1	5.9:1
S2	7.1:1
S3	8.0:1
S4	9.2:1
S5	10.8:1
S6	11.4:1

These results revealed the presence of distinct particle populations as a function of particle size with larger ($>5\mu\text{m}$) particles depositing on the top stages of the next generation impactor showing a nominal ratio of $\approx 6:1$ (w/w) and the smaller ($<5\mu\text{m}$) particles depositing on

the lower stages of the impactor showing varying ratios from 8:1 – 11:1 (w/w). These results were therefore contrary to the HPLC analysis and showed the formation of different particle populations as a function of particle size. HPLC, being a bulk analysis technique did not reveal this. Moreover, the issue of sampling also arises during HPLC analysis. Larger particles will have a greater tendency to be sampled. As mentioned, *in vitro* aerosol performance analysis showed these larger particles had a nominal 6:1 (w/w) AS:IB ratio which might account for the discrepant HPLC results.

In an attempt to explain the discrepancy between the chemical analysis results obtained by HPLC (showing the formation of combination particles with a nominal ratio of 6.6:1 (w/w) and the aerosol results (showing variability in the AS:IB ratio as a function of particle size), monitoring of the supernatant was carried out as a function of crystal maturation time. These results are shown in Figure IV.26.

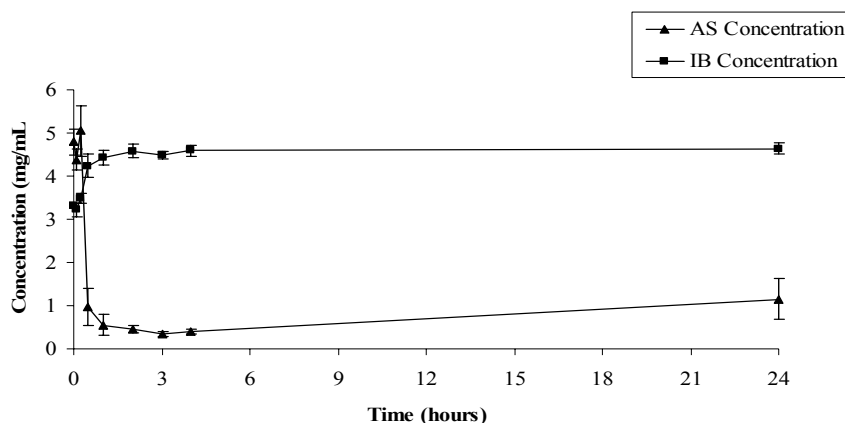


Figure IV.26 Concentrations of AS and IB in the supernatant over a crystallization period of 24 hours

It was observed that as soon as the aqueous drug solution was added to the anti-solvent, precipitation occurred with the drug concentrations in the supernatant remaining relatively stable for 15 minutes. However, between 15 – 30 minutes, a change occurred, wherein there was a massive crash out of AS with its concentration in the supernatant reaching approximately its

solubility limit in isopropyl alcohol. At the same time, there was re-dissolution of IB. This additional AS precipitation and corresponding IB re-dissolution led to the final concentrations in the supernatant reaching the solubility limits for the two components at the end of 24 hours which resulted in a final ratio of 6.6:1 (w/w) in the combination particles.

It is known that dissolution is higher from smaller particles due to larger surface areas. Therefore, it is expected that re-dissolution of IB from the precipitated particles would preferably take place from the smaller particles which might account for the lower proportion of IB in these particles as observed during *in vitro* analysis. These events occurring after the initial co-precipitation of the two drugs may have resulted in distinct particle populations being formed as a function of particle size. When the crystallization process was terminated after 5 minutes, the harvested particles were observed to contain AS and IB in a nominal 2.8:1 (w/w) ratio as shown in Table IV.12. Moreover, *in vitro* aerosol performance analysis did not reveal any significant variability in this ratio as a function of particle size (results presented in Chapter V).

These studies therefore demonstrated that the earlier non-homogeneity observed when the crystallization process was allowed to continue for 24 hours was due to the ongoing AS precipitation and IB dissolution processes occurring post the initial co-precipitation. Therefore, in order to produce combination particles containing AS and IB in a fixed nominal ratio of 6:1 (w/w), the initial concentration of the two drugs in the aqueous drug solution was changed to 0.48:0.08 g/g as shown in Table IV.12. Monitoring of the supernatant revealed that co-precipitation of AS and IB in a 6:1 (w/w) ratio occurred during the initial 30 second duration. Hence, crystallization was terminated 30 seconds after the infusion of drug solution into the anti-solvent. The harvested particles revealed a nominal AS:IB ratio of 5.7:1 (w/w). Chemical analysis by HPLC revealed that these particles contained a reproducible percentage of AS

(85.0%) and IB (15.0%) with corresponding % RSDs of 0.2 and 1.1 % respectively. *In vitro* analysis revealed uniform deposition in the impactor (results discussed in chapter V).

Therefore, in summary, solvent / anti-solvent crystallization using IPA as the anti-solvent yielded combination particles with two stoichiometric ratios; 2.8:1 (w/w), and 5.7:1 (w/w). These particles were further analyzed for their thermal and X-ray diffraction characteristics to investigate their crystallinity. Particle size distribution studies were also carried out.

IV.D.2.2.2 Thermal analysis of combination particles produced from isopropyl alcohol

Table IV.14 shows the results for thermal characterization of the combination particles produced from IPA. The numbers in parentheses indicate the calculated heat of dehydration for IB based on the nominal amount of IB in the particular stoichiometric proportion and the calculated heat of fusion for AS based on the nominal amount of AS in the particular proportion.

Table IV.14 Mean \pm SD thermal characteristics of AS / IB combination particles prepared using isopropyl alcohol as the anti-solvent

AS:IB (w/w)	Measured heat of dehydration (J/g) (Calculated)	Dehydration temperature (°C)		Heat of fusion (J/g) (Calculated)	Melting point (°C)
2.8:1	25.2 \pm 2.5 (26.1)	107.5 \pm 0.5	113.6 \pm 0.6	130.2 \pm 2.8 (140.6)	182.5 \pm 0.6
5.7:1	14.6 \pm 1.5 (14.8)	102.3 \pm 0.2	107.5 \pm 0.6	188.4 \pm 3.4 (162.9)	176.2 \pm 0.8

Figures IV.27 and IV.28 show the representative thermograms for the 2.8:1 and 5.7:1 (w/w) combination particles produced from isopropyl alcohol. The dehydration endotherm for the 2.8:1 (w/w) particles revealed a shoulder at 108.0°C similar to IB. This was different to the combination particles produced from ethyl acetate where the loss of water from IB was observed

to occur in a single phase. The heat of dehydration agreed with the calculated heat of dehydration for IB suggesting the presence of IB in a crystalline form in a manner similar to particles produced from ethyl acetate.

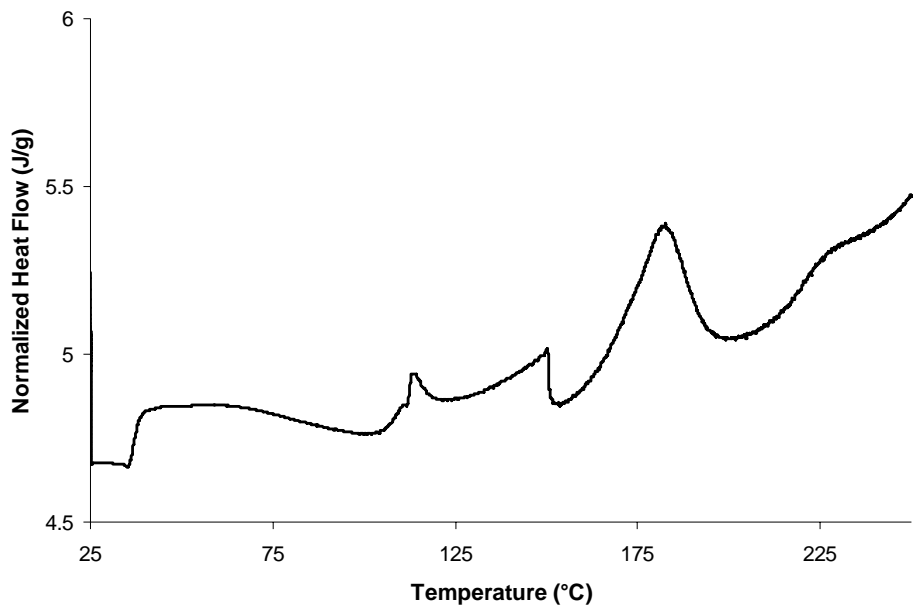


Figure IV.27 Representative DSC thermogram for 2.8:1 (w/w) combination particles produced from isopropyl alcohol

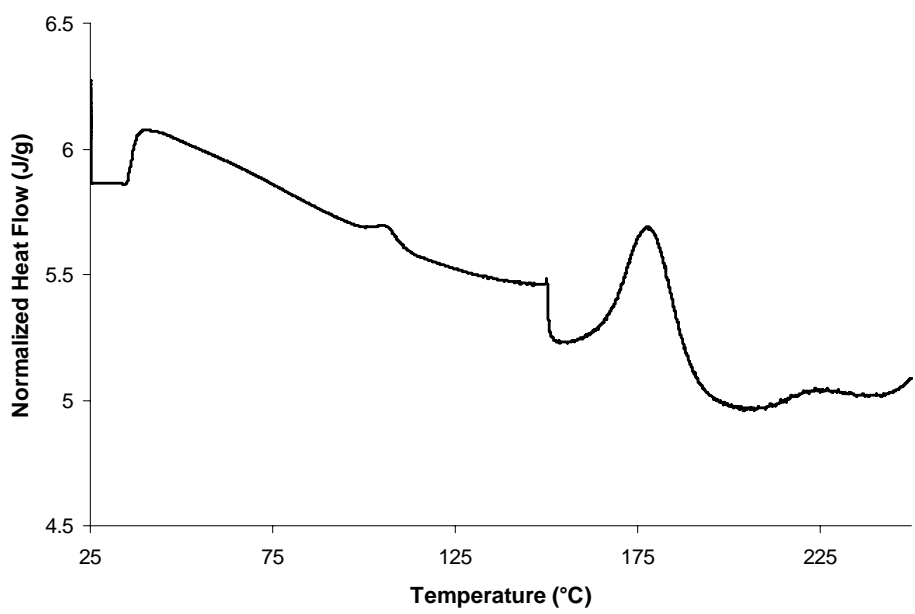


Figure IV.28 Representative DSC thermogram for 5.7:1 (w/w) combination particles produced from isopropyl alcohol

Further, the melting point, and heat of fusion of the 2.8:1 (w/w) combination particles were significantly lower compared to AS, and IB and the calculated heat of fusion for AS (p-value < 0.05, one-way ANOVA) suggesting interactions between the two APIs. The 5.7:1 (w/w) combination particles produced from IPA also revealed thermal characteristics different from AS, IB, and a 6:1 (w/w) physical mixture of AS and IB. The mean melting point for the 5.7:1 (w/w) combination particles produced from isopropyl alcohol was $176.2 \pm 0.8^{\circ}\text{C}$ which was significantly lower than the melting point for AS ($189.5 \pm 0.5^{\circ}\text{C}$) and IB ($232.6 \pm 0.7^{\circ}\text{C}$). The melting point was also significantly lower compared to a 6:1 (w/w) physical mixture of AS and IB ($188.8 \pm 0.1^{\circ}\text{C}$). The mean heat of fusion was $188.4 \pm 3.4 \text{ J/g}$ which was significantly higher than the calculated heat of fusion for AS in this proportion (162.9 J/g) and also significantly higher than the heat of fusion for the 6:1 (w/w) physical mixture ($166.0 \pm 2.8 \text{ J/g}$). These results were in contrast to the results for the 6:1 (w/w) combination particles produced from ethyl acetate that showed significantly lower heats of fusion compared to the expected heat of fusion for AS and physical mixtures. Therefore, the 5.7:1 (w/w) combination particles may have a different orientation of IB in the AS crystal lattice leading to a more robust crystal structure. However, it is difficult to come to a conclusion based on these results.

IV.D.2.2.3 Powder X-ray diffraction

To further understand the nature of interactions between AS and IB in the combination particles produced from IPA, powder X-ray diffraction studies were carried out. Figure IV.29 and IV.30 show the representative powder X-ray diffractograms for the 2.8:1 and 5.7:1 (w/w) combination particles respectively. The characteristic peak positions are shown in Table IV.15.

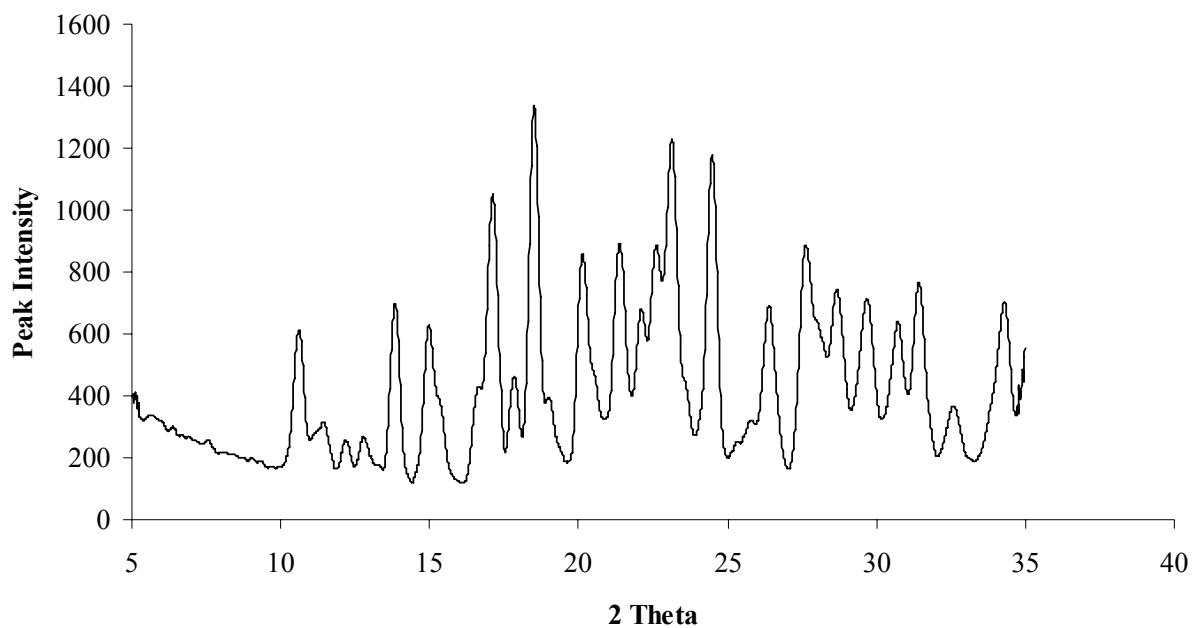


Figure IV.29 Powder X-ray diffractogram for 2.8:1 (w/w) combination particles

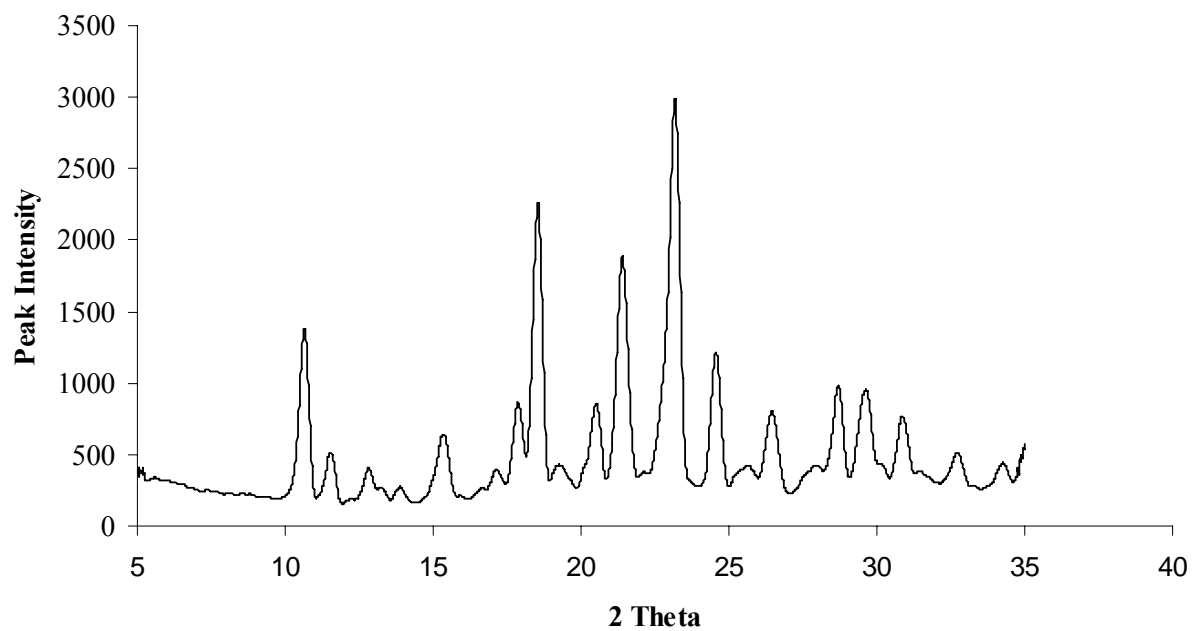


Figure IV.30 Powder X-ray diffractogram for 5.7:1 (w/w) combination particles

Table IV.15 Characteristic diffraction peaks for 2.8:1 (w/w) and 5.7:1 (w/w) combination particles produced from isopropyl alcohol

Characteristic reference peaks for AS and IB		AS:IB 2.8:1		AS:IB 5.7:1	
2 theta	Intensity	2 theta	Intensity	2 theta	Intensity
10.45	2097				
		10.65^a	604^a	10.71^a	1283^a
11.47	494	11.47	310	11.69	391
12.93	248	12.87	252	12.95	339
13.93	65				
				14.09^b	206^b
		15.07^a	577^a	15.47^a	559^a
15.15	62				
15.27	508				
17.33	101				
		17.15^b	1040^b		
17.75	885				
		17.91^a	435^a	17.95^a	813^a
18.43	1177	18.55	1301	18.61	2105
19.35	228				
		20.17^a	842^a	20.59^a	793^a
20.29	113				
20.39	576				
21.21	1325				
		21.43^a	876^a	21.47^a	1791^a
		22.17^b	657^b		
22.35	60				
22.75	71				
23.03	4058	23.17	1216		
				23.25^a	2746^a
24.43	694	24.51	1172	24.65	1096
24.67	61				
25.67	280				
26.39	642	26.47	652	26.55	750
		27.69^b	864^b		
27.93	70				
28.63	652	28.73	726	28.79	896
29.51	434	29.75	689	29.75	856
30.85	448	30.79	613	31.01	668
		31.57^b	653^b		
31.59	71				
32.69	388	32.67	356	32.89	436

a Significantly shifted compared to the AS peak based on a % deviation of $\pm \geq 1\%$ calculated with reference to the AS peak

b New peak not attributed to either AS or IB based on peak shift and peak intensity

The diffractogram for the 2.8:1 (w/w) combination particles showed sharp diffraction peaks indicating the crystalline nature of these particles. These peaks were also significantly higher in intensity than the peaks for the 2:1 (w/w) combination particles produced from ethyl acetate. The diffractogram also revealed changes in peak positions compared to AS and IB. As shown in Table IV.15, the characteristic AS peak at 2θ 10.45° was absent and a new peak at 10.65° was observed. The characteristic AS peak at 15.27° was absent and a new peak at 15.07° was observed, the characteristic AS peak at 17.75° was absent and a new peak at 17.91° was observed, and the characteristic AS peak at 21.21° was absent with a new peak appearing at 21.43° . Further, new peaks that could not be attributed to AS or IB were seen at 17.15° , 22.17° , 27.69° and 31.57° . Moreover, some of the characteristic AS peaks such as 18.55° , 24.51° , 28.73° , 29.75° , and 30.79° that did not shift significantly based on the $\geq 1.0\%$ standard deviation criterion showed higher peak intensities compared to reference AS peaks.

Peak changes were also observed in the diffractogram for the 5.7:1 (w/w) particles. As shown in Table IV.15, the characteristic AS peaks at 10.45° , 18.43° , 21.21° , and 23.03° were absent and new peaks were observed at 10.71° , 18.61° , 21.47° , 23.25° , and 24.65° . These characteristic AS peaks were different in position compared to the 6:1 (w/w) particles produced from ethyl acetate that revealed characteristic AS peaks close to reference AS (10.53° , 18.43° , 21.29° , and 23.03°). The peak intensities for the 5.7:1 (w/w) particles produced from IPA were also significantly higher compared to the peak intensities for the 6:1 (w/w) particles produced from EA. These results therefore supported the DSC results where the 5.7:1 (w/w) particles produced from IPA had significantly higher heat of fusion of 188.4 ± 3.4 J/g compared to 153.4 ± 1.3 J/g heat of fusion for the 6:1 (w/w) combination particles produced from EA. Therefore, it

appeared from these results that the combination particles produced from IPA were more crystalline compared to the corresponding particles produced from EA.

If these changes in peak positions for the 2.8:1 and 5.7:1 (w/w) combination particles produced from IPA are viewed as peak shifts then they may indicate a change in the crystal lattice of AS by the possible incorporation of IB. These changes can arise due to a variety of reasons. One of the main reasons is differences in sample preparation. However, given that the powdered sample is properly prepared i.e.; gently ground to avoid preferred orientation, remove any hard agglomerates, and be able to make a "monolayer" on the sample holder, any shifts should be considered as a result of a potentially new crystalline phase.

There are cases, however, where the changes could appear even though the same material exists. E.g. it could be due to systematic shifting (where all peaks are moved to the same direction), in result of a different sample prep or the instrument settings. In these studies, the changes in peak positions due to sample preparation or different instrument settings can be ruled out since all characterizations were performed on identically prepared samples under similar instrument settings. Moreover, replicate analysis did not change the peak positions indicating that the peaks were not a result of slight variations in sample preparation. Also isotropic shifting i.e.; shifting of all peaks in one direction was not observed. These anisotropic shifts can also originate from the unit cell expansion or shrinking due to different temperature during the measurement. However, shrinking or expansion of the unit cell due to a different temperature can also be ruled out since all runs were performed under controlled temperature conditions. Shrinking and expansion of a unit cell could be also due to the size of included guest molecule.

Therefore, analysis of the combination particles by powder X-ray diffraction revealed differences from AS and IB indicating interactions between the two APIs. These results also

supported the results from the thermal analysis. Moreover, the powder X-ray diffraction results with sharp peaks and the absence of a halo were indicative of the crystalline nature of these particles. Particle crystallinity was a desirable property for inhalation particles since crystalline particles are considered to be more stable compared to their amorphous counterparts. However, even with a combination of thermal and powder X-ray diffraction data, it was still not possible to come to an unequivocal conclusion about the formation of co-crystals. As, mentioned before, the thermal data revealed melting points lower than the two components which has been the case with 39% of the reported co-crystals in literature. However, although the PXRDs revealed peak changes, the diffractograms were not significantly different from those of AS and IB. The co-crystals reported in literature and analyzed by a number of analytical techniques such as DSC, PXRD, raman spectroscopy, near infrared and transmission spectroscopy have powder X-ray diffractograms with not only peak shifts but characteristic new peaks that are not present in either of the pure components. Elbagerma et al. (2010) have produced and characterized a number of different co-crystals by a variety of analytical techniques. Figure IV.31 shows a PXRD for salicylic acid, nicotinic acid and a 1:1 co-crystal of the two.

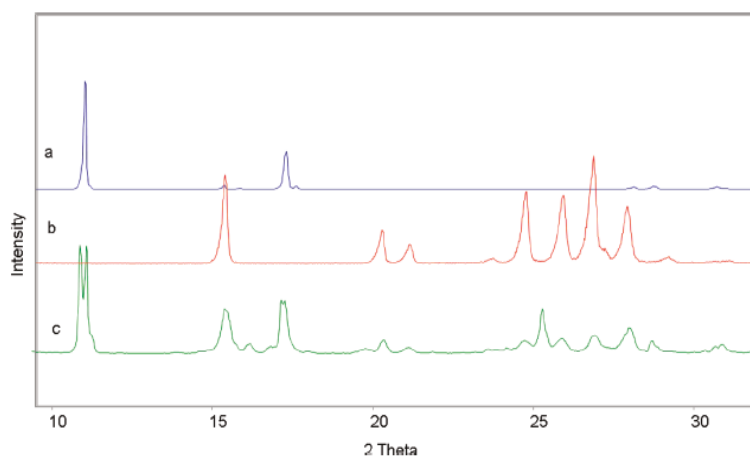


Figure IV.31 Powder X-ray diffraction spectra for a) Salicylic acid, b) Nicotinic acid, and c) 1:1 co-crystal of salicylic acid and nicotinic acid (Elbagerma et al., 2010) (Reproduced with permission from ACS)

Therefore, with the diffraction spectra for the particles with different proportions of AS and IB exhibiting only minor peak shifts relative to AS and IB, it was not possible to conclude the formation of a co-crystal. Co-crystallization is a thermodynamically unfavorable process and is strongly dictated by the functional groups present on the two components. Co-crystals are defined as structurally homogeneous crystalline materials that contain two or more neutral building blocks that are present in definite stoichiometric amounts (Aakeroy and Salmon, 2005). The two components interact by the formation of non-covalent bonds. Hydrogen bonding is the most common type of non-covalent bonding reported in literature for the formation of co-crystals (Vishweshwar et al., 2005; Almarsson et al., 2004; Shan et al., 2008; Rodriguez-Spong et al., 2004). Co-crystallization is viewed as a thermodynamically unfavorable process. The energy laws dictate the formation of separate crystals of two components because this process leads to a reduction of the total energy of the system and is hence favorable. On the other hand, two different molecules coming together is an energy unfavorable process and hence is difficult to conceive. Therefore, for co-crystallization to occur, the components should possess favorable functional groups capable of undergoing non-covalent interactions with each other. Etter and co-workers have proposed the following generalizations that support the formation of co-crystals between two or more components (Blagden et al., 2008):

1. All good proton donors and acceptors are used in hydrogen bonding.
2. Six-membered ring intramolecular hydrogen bonds form in preference to intermolecular hydrogen bonds.
3. The best proton donor and acceptor remaining after intramolecular hydrogen-bond formation will form intermolecular hydrogen bonds to one another (but not all acceptors will necessarily interact with donors).

In order to facilitate the formation of co-crystals between two components, a third component known as “co-crystal former” is generally added to the system. Co-crystal formers are small molecules that link the two co-crystal components by favorable non-covalent bonding between both co-crystal components and help in bringing the two disparate molecules together. In the absence of such co-crystal formers, spontaneous co-crystallization of two different compounds is difficult.

The chemical structure of AS and IB is shown in Figure IV.32. The two drugs have functional groups that might support the formation of a co-crystal. For example, the oxygen atom on the sulfate group of AS has a tendency to form a hydrogen bond with the hydrogen attached to the nitrogen atom of IB. Also, the carboxylic oxygen atom of IB has a tendency to form a hydrogen bond with the hydrogen attached to the tertiary nitrogen of AS. However, in the absence of any co-crystal formers, the spontaneous formation of a co-crystal between AS and IB is difficult.

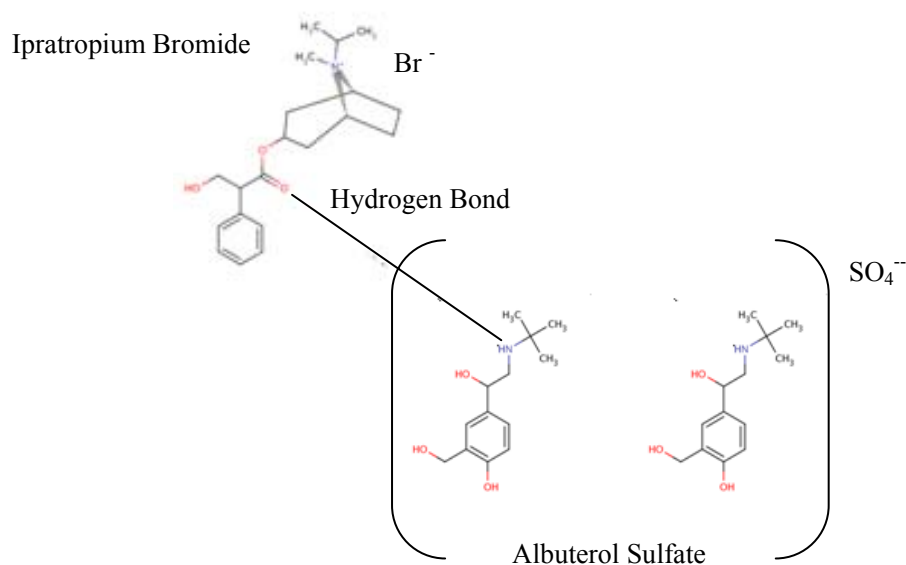


Figure IV.32 Chemical structures of albuterol sulfate and ipratropium bromide showing a possible site for H-bonding

IV.D.2.2.4 Particle size distribution of the combination particles produced from isopropyl alcohol

Table IV.16 shows the VMDs and volume % < 5.0 μm for the 2.8:1 and 5.7:1 (w/w) combination particles produced from isopropyl alcohol. The cumulative % undersize volume distributions and the volume frequency distributions for the 2.8:1 and 5.7:1 (w/w) particles are shown in Figures IV.33, IV.34, IV.35, and IV.36.

Table IV.16 Mean ± SD volume median diameters and cumulative % volume < 5.0 μm for the combination particles produced from isopropyl alcohol

AS:IB ratio (w/w)	VMD ± SD (μm)	Volume % < 5.0 μm
2.8:1	5.3 ± 1.0	48.4 ± 1.2
5.7:1	6.5 ± 0.3	46.7 ± 0.8

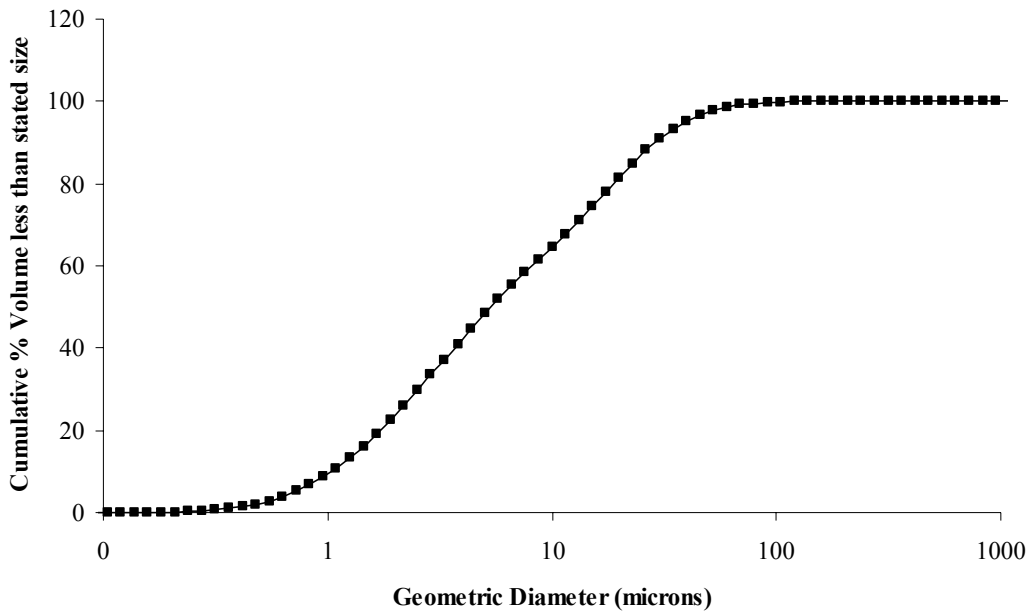


Figure IV.33 Cumulative % volume undersize distribution of 2.8:1 (w/w) combination particles produced from the anti-solvent isopropyl alcohol

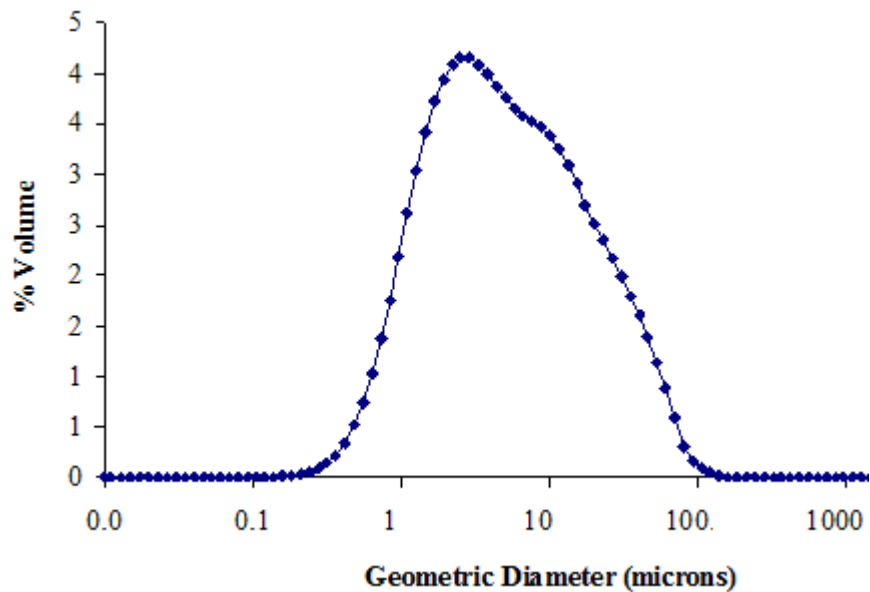


Figure IV.34 Volume frequency distribution of 2.8:1 (w/w) combination particles produced from the anti-solvent isopropyl alcohol

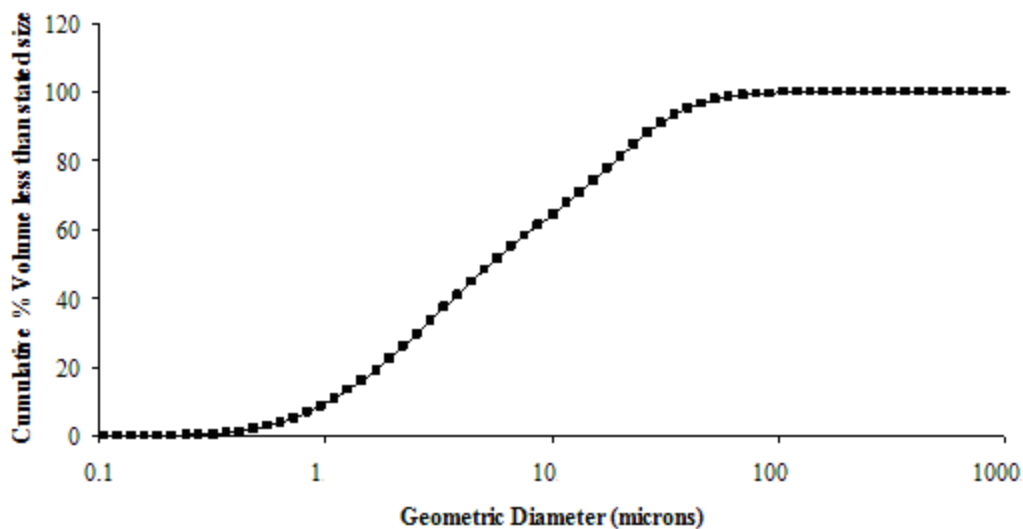


Figure IV.35 Cumulative % volume undersize distribution of 5.7:1 (w/w) combination particles produced from the anti-solvent isopropyl alcohol

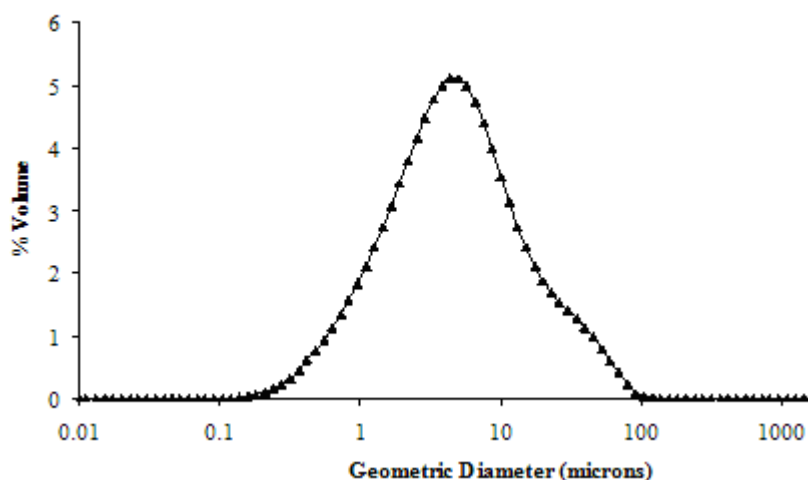


Figure IV.36 Volume frequency distribution of 5.7:1 (w/w) combination particles produced from the anti-solvent isopropyl alcohol

The 2.8:1 and 5.7:1 (w/w) combination particles produced from IPA were similar in their particle size distributions. Analysis of the VMD data did not reveal any significant differences (p -value > 0.05, one-way ANOVA). The particle size distributions appeared to be relatively unimodal. Particle morphology revealed these particles to be small in size and agglomerated together with a uniform morphology without two distinct particle populations as shown in Figure IV.37 and IV.38 for the 2.8:1 and 5.7:1 (w/w) combination particles respectively.

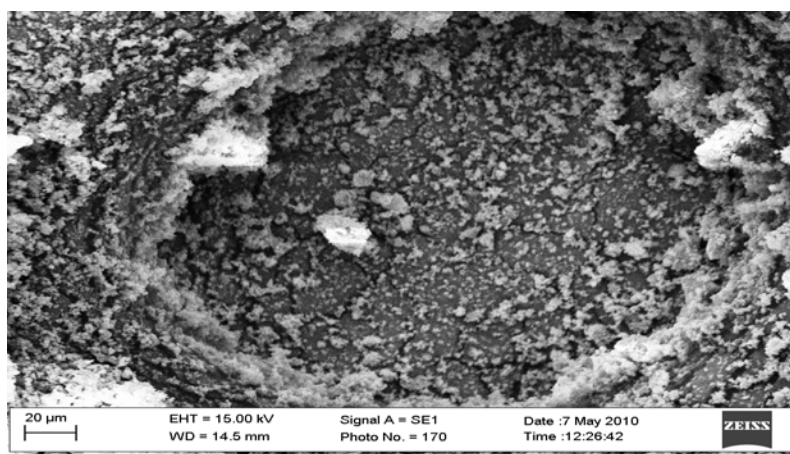


Figure IV.37 SEM image of combination particles containing AS and IB in a nominal ratio of 2.8:1 (w/w) produced using isopropyl alcohol as the anti-solvent

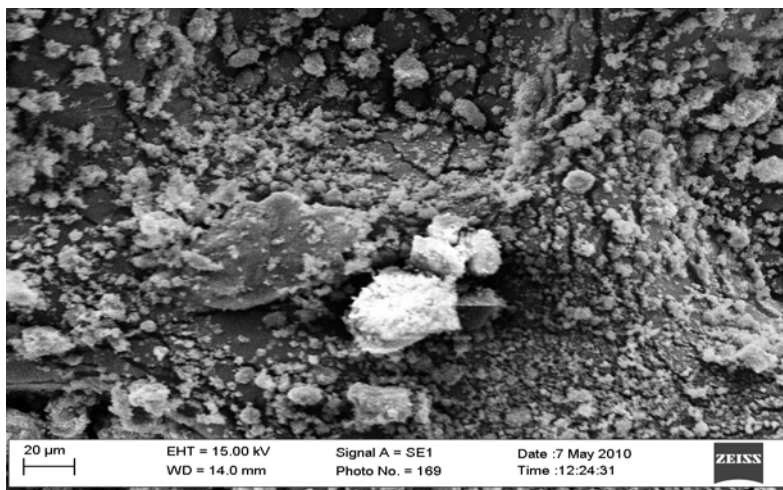


Figure IV.38 SEM image of combination particles containing AS and IB in a nominal ratio of 5.7:1 (w/w) produced using isopropyl alcohol as the anti-solvent

Compared to the combination particles produced from ethyl acetate, the particles produced from IPA therefore appeared to be more uniform. The VMDs and the cumulative % volume < 5.0 μm for 2.8:1 and 5.7:1 (w/w) combination particles suggested the suitability of these particles for inhalation. However, these particle size distributions were obtained with the Malvern Mastersizer which is calibrated for spherical particles. Therefore, the particle size data obtained from the Malvern should not be used as a criterion for judging the suitability of these irregular shaped particles for inhalation. The aerosol performance of the particles is determined by their aerodynamic diameter which can only be assessed by *in vitro* studies using impactors. Therefore, conclusions about the aerosol performance of the particles cannot be drawn from the particle size distribution data obtained from the Malvern. However, despite its limitations, the Malvern can still be used as an initial screen to make some judgments about the relative size of the particles produced under different crystallization conditions.

Therefore, in summary, use of isopropyl alcohol as the anti-solvent led to a significant reduction in particle size compared to combination particles produced from ethyl acetate. Further, by optimizing the crystallization conditions, it was possible to use IPA to produce

combination particles in two different stoichiometric ratios of 2.8:1 and 5.7:1 (w/w). The thermal and X-ray diffraction properties of these particles revealed differences from AS and IB. However, it was not possible to make conclusions about the formation of co-crystals. The PSD of these combination particles revealed them to be small in size. However, conclusions about their aerosol performance could not be drawn. These particles were therefore tested for their *in vitro* aerosol performance and the results will be discussed in Chapter V.

IV.D.2.3 Crystallization of combination particles produced using mixtures of isopropyl alcohol and ethyl acetate as the anti-solvent

It has been discussed that using ethyl acetate as the anti-solvent did not yield particles in a size small enough for inhalation. In an attempt to reduce the particle size IPA was tried as the anti-solvent. However, due to the solubility differences between AS and IB in IPA, the crystallization conditions such as the R_a ratio, crystal maturation time and the initial AS and IB concentration had to be varied and optimized in order to produce combination particles in a size small enough for inhalation. Therefore, using IPA as the anti-solvent, it was not possible to predict the final AS:IB ratio in the combination particles from the initial ratio.

The size reduction properties of IPA can also be utilized by combining it with ethyl acetate and using the mixture as the anti-solvent. Addition of ethyl acetate will lead to a reduction in the IB solubility and therefore, complete precipitation of both drugs can be achieved. This will make it possible to predict the final AS:IB ratio from the initial ratio. Further, it is easier to produce combination particles from an anti-solvent in which both drugs have similar solubilities (Chiarella et al., 2007). Therefore, IPA in combination with ethyl acetate was investigated as the anti-solvent.

IV.D.2.3.1 Content uniformity analysis by HPLC

Table IV.17 shows the results for the HPLC analysis of the combination particles produced from mixtures of IPA and ethyl acetate in different proportions of 1:1, 1:2, 1:5, and 1:10 (w/w). The expected percentages of AS and IB in the combination particles were calculated based on the starting ratio of AS and IB assuming complete precipitation of both drugs which would result in the final AS:IB ratio being same as the starting AS:IB ratio. The values in parentheses indicate the % deviation from the expected percentage of AS and IB respectively. A % deviation of < 5% was taken as an acceptable criterion for the formation of combination particles of AS and IB in the expected ratio.

Table IV.17 HPLC analysis results for combination particles produced from mixtures of isopropyl alcohol and ethyl acetate in different proportions

IPA:EA 1:1 (w/w)			
Starting AS:IB (w/w)	Measured AS:IB (w/w)	% AS (% deviation from expected)	%IB (% deviation from expected)
1:1	No precipitation
2:1	28.9:1	96.7 (48.3)	3.3 (-909.1)
6:1	69.5:1	98.6 (32.4)	1.4 (-921.4)
10:1	89.1:1	98.8 (13.3)	1.1 (-727.3)
IPA:EA 1:2 (w/w)			
Starting AS:IB (w/w)	Measured AS:IB (w/w)	% AS (% deviation from expected)	%IB (% deviation from expected)
1:1	6.8:1	87.2 (42.7)	12.8 (-290.6)
2:1	13.1:1	92.9 (28.2)	7.1 (-369.0)
6:1	36.8:1	97.1 (12.0)	2.6 (-450.0)
10:1	57.4:1	98.3 (7.5)	1.7 (-435.3)
IPA:EA 1:5 (w/w)			
Starting AS:IB (w/w)	Measured AS:IB (w/w)	% AS (% deviation from expected)	%IB (% deviation from expected)
1:1	1.2:1	54.5 (8.3)	45.5 (-9.8)
2:1	3.3:1	76.7 (13.0)	23.3 (-42.9)
6:1	7.8:1	88.6 (3.3)	11.4 (-25.4)
10:1	15.4:1	93.9 (3.2)	6.1 (-49.2)
IPA:EA 1:10 (w/w)			
Starting AS:IB (w/w)	Measured AS:IB (w/w)	% AS (% deviation from expected)	%IB (% deviation from expected)
1:1	1.1:1	52.4 (4.6)	47.6 (-5.0)
2:1	2.1:1	67.7 (1.5)	32.3 (-3.1)
6:1	5.6:1	84.8 (-1.1)	15.2 (5.9)
10:1	11.8:1	92.2 (1.4)	7.8 (-16.7)

These results showed that in anti-solvents containing a high proportion of IPA (IPA:EA 1:1, 1:2 (w/w)), IB did not precipitate out to a significant extent resulting in large % deviations from the expected percentage. For example, for the 1:1 (w/w) combination particles, the AS:IB ratio in the particles precipitated from isopropyl alcohol:ethyl acetate = 1:2 (w/w) was 6.8:1 (w/w) even though the starting drug solution contained the two APIs in a 1:1 (w/w) ratio. Increasing the proportion of ethyl acetate resulted in an increase in IB precipitation for the combination particles. The solvent / anti-solvent composed of isopropyl alcohol:ethyl acetate = 1:10 (w/w) was found to be suitable for the production of AS/IB combination particles with acceptable ratios. In these particles, the AS and IB percentages were not found to show large deviations from the expected and hence the final AS:IB ratio in the combination particles could be predicted reasonably well from the initial AS:IB ratio in the drug solution.

The influence of temperature difference between the solvent and anti-solvent on particle characteristics was also investigated for the anti-solvent composed of isopropyl alcohol:ethyl acetate = 1:10 (w/w). The HPLC analysis results are shown in Table IV.18.

Table IV.18 HPLC analysis results for combination particles produced from isopropyl alcohol:ethyl acetate = 1:10 (w/w) at a temperature difference of 65°C between the solvent and anti-solvent

Starting AS:IB ratio (w/w)	Measured AS:IB ratio (w/w)	% AS (% deviation from expected)	% IB (% deviation from expected)
1:1	1:1	50.0 (0.0)	50.0 (0.0)
2:1	1.9:1	65.5 (-1.8)	34.5 (3.5)
6:1	6.6:1	86.8 (1.3)	13.2 (8.3)
10:1	8.6:1	89.6 (-1.5)	10.4 (12.5)

These results demonstrated that a temperature difference of 65°C between the solvent and anti-solvent did not lead to any significant differences in AS and IB precipitation compared to the studies performed at a temperature difference of 0°C. The percentages of AS and IB in the combination particles were within the $\pm 5\%$ acceptable deviation from expected (except for IB in 10:1 (w/w) combination particles) and therefore the final ratio in the combination particles could be predicted reasonably well from the initial ratio in the drug solution.

IV.D.2.3.2 Thermal analysis of combination particles produced from isopropyl alcohol:ethyl acetate = 1:10 (w/w)

Table IV.19 shows the thermal characteristics for the combination particles produced from isopropyl alcohol:ethyl acetate = 1:10 (w/w). The representative thermograms are shown in Figures IV.39, IV.40, IV.41, and IV.42 for the 1:1, 2:1, 6:1, and 10:1 (w/w) combination particles.

Table IV.19 Mean \pm SD thermal characteristics for the combination particles produced from isopropyl alcohol : ethyl acetate = 1:10 (w/w)

Measured AS:IB Ratio (w/w)	Measured heat of dehydration (calculated)	Dehydration temperature (°C)	Melting point (°C)	Heat of fusion (J/g)
1.1:1	52.8 \pm 3.2 (54.9)	113.8 \pm 0.2	172.5 \pm 2.1	37.7 \pm 6.9
2.1:1	31.1 \pm 2.8 (34.8)	111.2 \pm 0.1	185.2 \pm 2.3	44.0 \pm 10.5
5.6:1	15.8 \pm 1.9 (14.8)	108.9 \pm 0.1	182.9 \pm 0.5	145.2 \pm 10.4
11.8:1		184.2 \pm 0.4	161.9 \pm 8.3

There was no difference in the dehydration endotherms compared with the results for the combination particles produced from ethyl acetate described in section IV.D.2.1.2 for similar drug ratios. The heats of fusion for the 1:1 and 2:1 (w/w) combination particles produced from isopropyl alcohol:ethyl acetate = 1:10 (w/w) were significantly lower compared to the

corresponding values for the particles produced from ethyl acetate (p-value < 0.05, one-way ANOVA) described in section IV.D.2.1.2 indicating lower crystallinity for these particles.

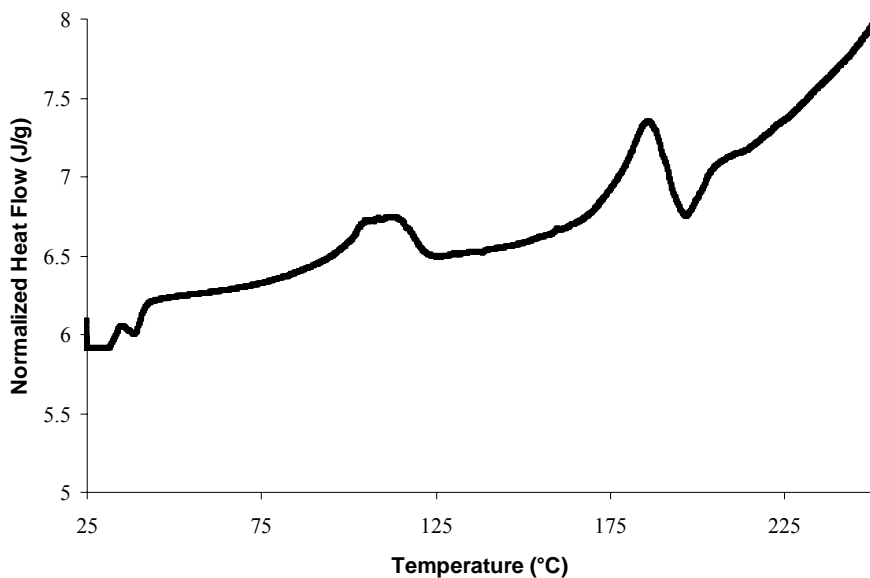


Figure IV.39 Representative differential scanning thermogram for 1:1 (w/w) combination particles produced from isopropyl alcohol : ethyl acetate = 1:10 (w/w)

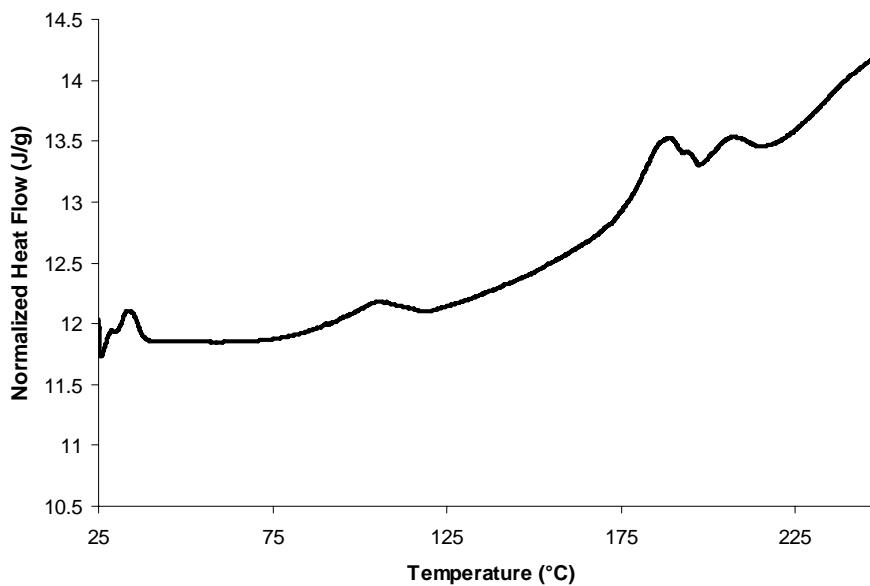


Figure IV.40 Representative differential scanning thermogram for 2:1 (w/w) combination particles produced from isopropyl alcohol : ethyl acetate = 1:10 (w/w)

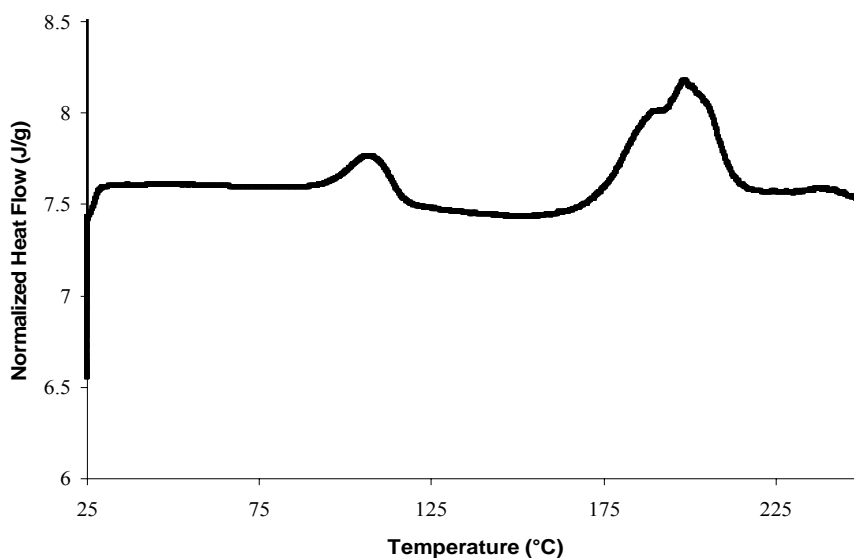


Figure IV.41 Representative differential scanning thermogram for 6:1 (w/w) combination particles produced from isopropyl alcohol : ethyl acetate = 1:10 (w/w)

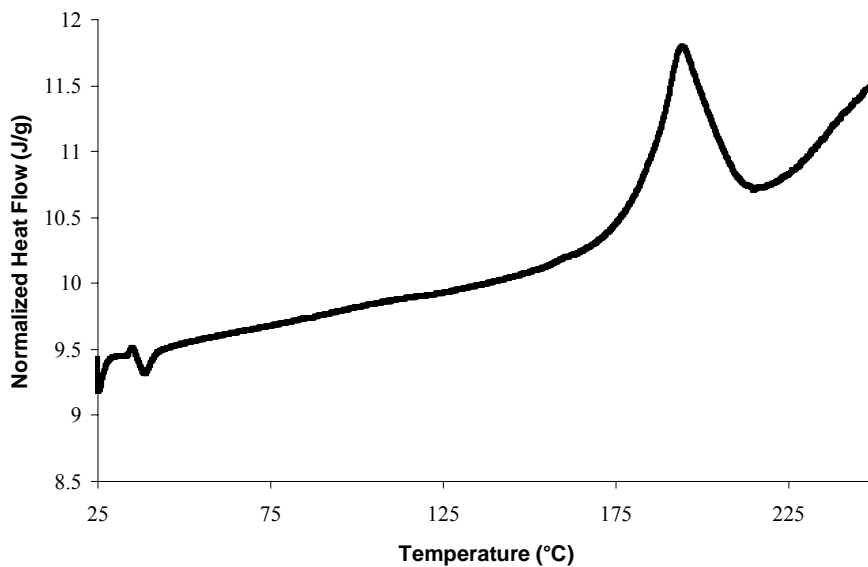


Figure IV.42 Representative differential scanning thermogram for 10:1 (w/w) combination particles produced from isopropyl alcohol : ethyl acetate = 1:10 (w/w)

However, for the 6:1 and 10:1 (w/w) combination particles, there was no difference in the heats of fusion compared to the combination particles with similar drug ratios produced from

ethyl acetate. In a manner similar to the particles produced from ethyl acetate, the thermal properties of the combination particles produced from isopropyl alcohol:ethyl acetate = 1:10 (w/w) were significantly different from AS, IB, and their physical mixtures indicating interactions between AS and IB. However, it was not possible to conclude the formation of co-crystals. The PXRD of the 6.6:1 (w/w) combination particles is shown in Figure IV.43. The peak intensities were comparable to the 6:1 (w/w) combination particles produced from EA thereby supporting the DSC results showing similar heats of fusion.

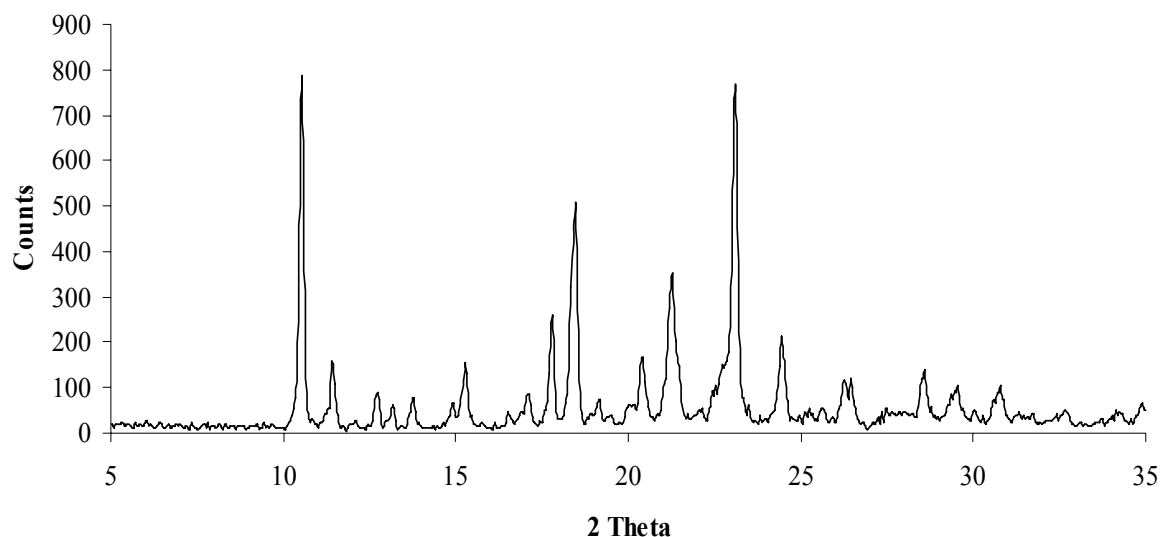


Figure IV.43 Powder X-ray diffractogram for 6.6:1 (w/w) combination particles produced from IPA:EA 1:10 (w/w)

Table IV.20 shows the results for the thermal analysis of the combination particles produced at a temperature difference of 65°C between the solvent and anti-solvent. These results were similar to the results for the combination particles produced at a temperature difference of 0°C.

Table IV.20 Mean \pm SD thermal characteristics of AS / IB combination particles prepared using isopropyl alcohol:ethyl acetate = 1:10 (w/w) as the anti-solvent at a temperature difference of 65°C between the solvent and anti-solvent

Measured AS:IB ratio (w/w)	Heat of dehydration (J/g)	Dehydration temperature (°C)	Melting point (°C)	Heat of fusion (J/g)
1.1:1	50.2 \pm 3.7	113.7 \pm 0.5	173.8 \pm 1.8	39.8 \pm 4.5
1.9:1	33.6 \pm 1.5	110.2 \pm 0.2	184.2 \pm 0.9	46.8 \pm 6.8
6.6:1	13.8 \pm 2.6	108.3 \pm 0.1	183.6 \pm 0.2	145.6 \pm 8.3
8.6:1	184.2 \pm 0.3	164.3 \pm 4.2

IV.D.2.3.3 Particle size distribution of combination particles produced from isopropyl alcohol:ethyl acetate = 1:10 (w/w)

Figures IV.44, IV.45, IV.46, and IV.47 show the cumulative % undersize volume distributions of 1:1, 2:1, 6:1, and 10:1 (w/w) combination particles produced from isopropyl alcohol:ethyl acetate = 1:10 (w/w), isopropyl alcohol:ethyl acetate = 1:10 at a temperature difference of 65°C, and ethyl acetate. The volume median diameters are shown in Table IV.21 and the cumulative % volumes < 5.0 μm in Table IV.22.

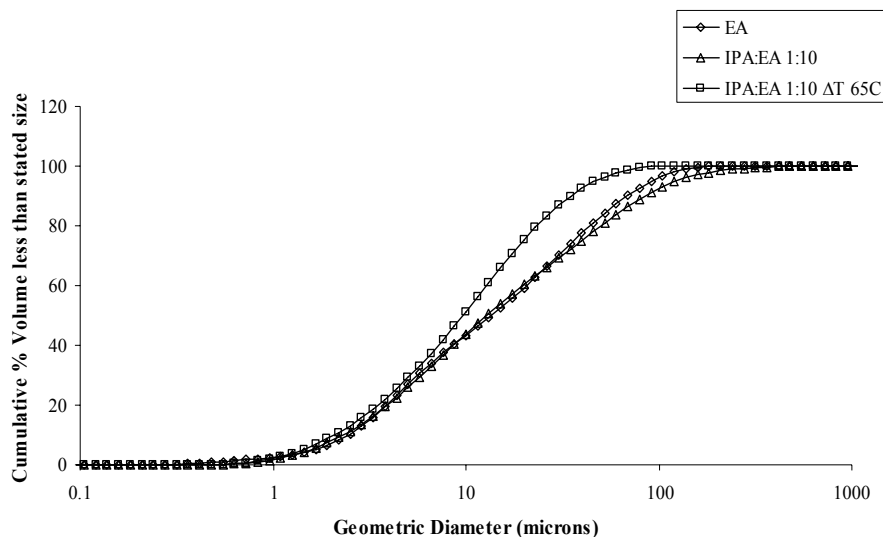


Figure IV.44 Cumulative % volume undersize distribution for 1:1 (w/w) combination particles produced from different anti-solvents

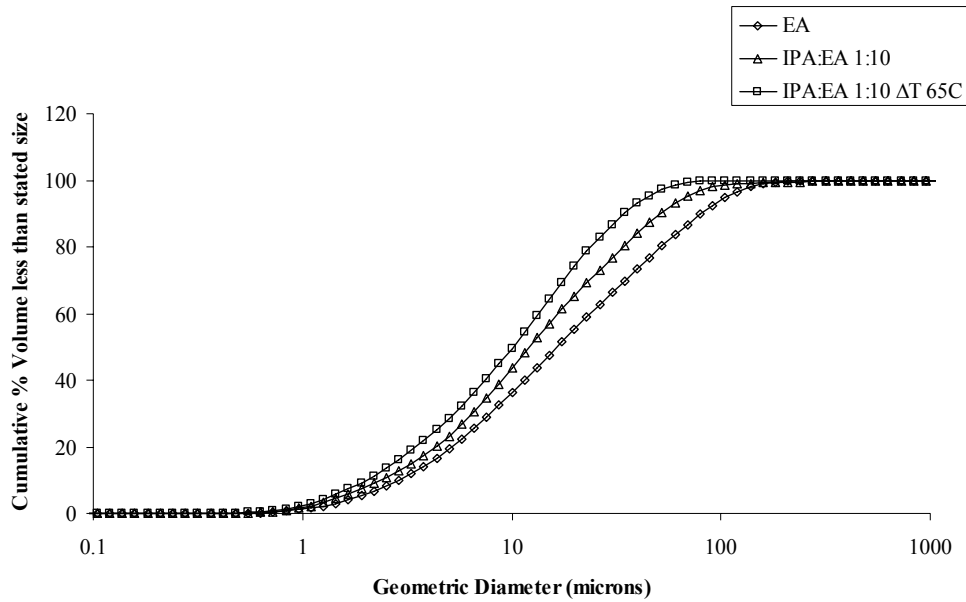


Figure IV.45 Cumulative % volume undersize distribution for 2:1 (w/w) combination particles produced from different anti-solvents

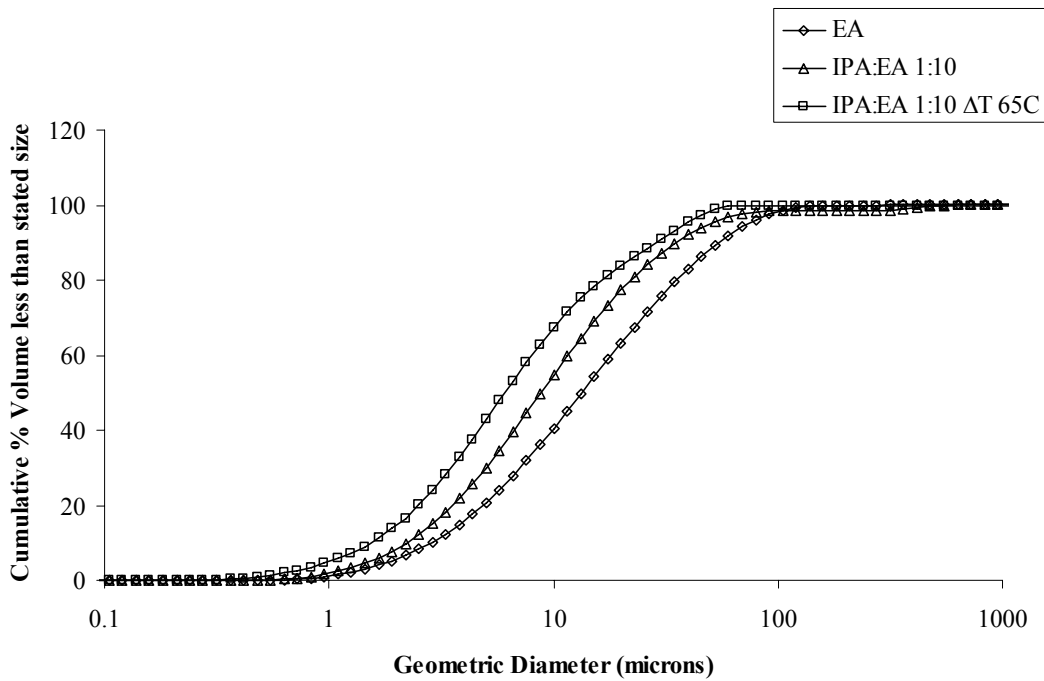


Figure IV.46 Cumulative % volume undersize distribution for 6:1 (w/w) combination particles produced from different anti-solvents

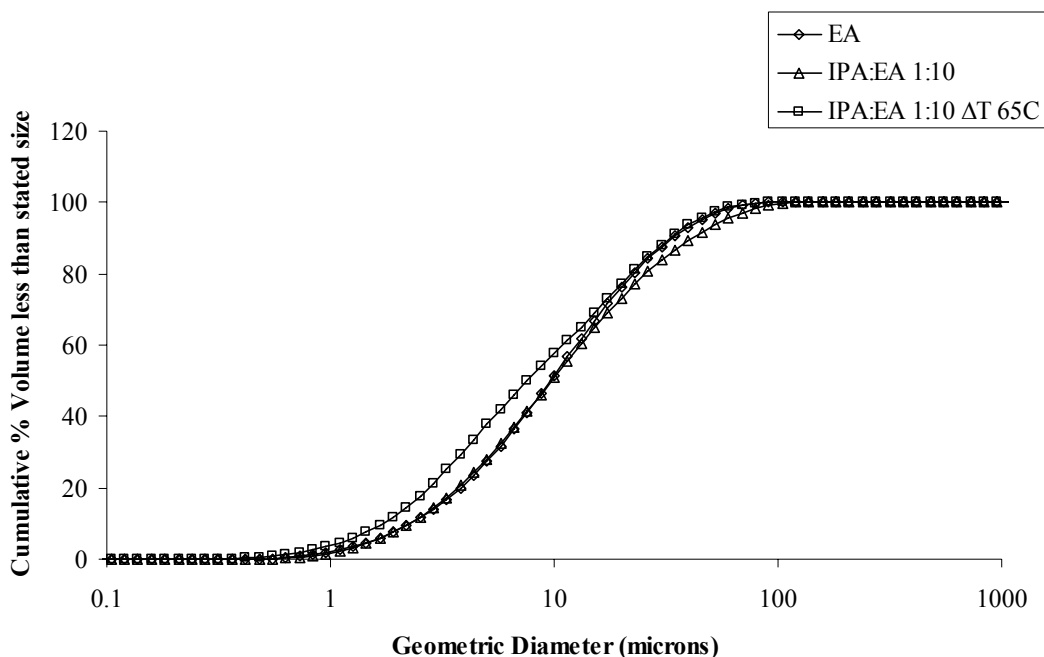


Figure IV.47 Cumulative % volume undersize distribution for 10:1 (w/w) combination particles produced from different anti-solvents

Table IV.21 Mean \pm SD volume median diameters (μm) of combination particles produced from different anti-solvents

Nominal AS:IB ratio (w/w)	Ethyl acetate	IPA:EA 1:10 (w/w)	IPA:EA 1:10 Δ T 65°C
1:1	19.5 \pm 4.0	16.7 \pm 3.0	11.2 \pm 0.7
2:1	15.6 \pm 4.0	14.0 \pm 1.4	11.7 \pm 1.0
6:1	15.3 \pm 0.9	9.5 \pm 1.1	6.9 \pm 1.1
10:1	11.1 \pm 1.1	11.3 \pm 0.7	7.1 \pm 0.8

Table IV.22 Mean \pm SD cumulative % volumes $<$ 5.0 μm for combination particles produced from different anti-solvents

Nominal AS:IB ratio (w/w)	Ethyl acetate	IPA:EA 1:10 (w/w)	IPA:EA 1:10 Δ T 65°C
1:1	19.4 \pm 1.7	23.3 \pm 2.5	28.5 \pm 1.5
2:1	20.7 \pm 2.6	25.9 \pm 1.7	28.7 \pm 2.2
6:1	21.2 \pm 2.3	30.1 \pm 1.2	42.8 \pm 2.3
10:1	27.5 \pm 1.6	28.2 \pm 1.9	39.8 \pm 2.7

Compared to ethyl acetate, no significant reduction in particle size was observed for the 1:1, 2:1, and 10:1 (w/w) combination particles produced from isopropyl alcohol:ethyl acetate 1:10 (w/w) (p-value > 0.05, one-way ANOVA). However, significantly smaller 6:1 (w/w) combination particles with mean \pm SD VMD of $9.5 \pm 1.1 \mu\text{m}$ were produced from isopropyl alcohol : ethyl acetate 1:10 (w/w) compared to the larger 6:1 (w/w) combination particles with a mean \pm SD VMD of $15.3 \pm 0.9 \mu\text{m}$ produced from ethyl acetate (p-value > 0.05, Tukey's HSD). These differences were also observed in the cumulative % volumes < 5.0 μm . It was also seen that a temperature difference between the drug solution and anti-solvent did lead to a significant reduction in particle size for all combination particles (p-value < 0.05, one-way ANOVA) compared to the particles produced at a temperature difference = 0°C and the particles produced from ethyl acetate. For example, the mean VMD \pm SD for the 6:1 (w/w) combination particles decreased significantly to $6.9 \pm 1.1 \mu\text{m}$ when produced from isopropyl alcohol:ethyl acetate 1:10 (w/w) at a temperature difference of 65°C compared to the particles produced from ethyl acetate and isopropyl alcohol:ethyl acetate 1:10 (w/w) at a temperature difference of 0°C. These 6:1 (w/w) particles were of particular interest since this is the ratio in the commercial formulation of AS and IB (i.e.; Combivent® pMDI). The PSD results indicated that these particles were in a size suitable for inhalation. However, since aerodynamic characteristics are a correct measure of inhalation performance, therefore, the 6.6:1 (w/w) particles produced from isopropyl alcohol:ethyl acetate 1:10 (w/w) were tested for their *in vitro* aerosol performance efficiency as discussed in Chapter V.

IV.D.3 A summary of the combination particles produced from different solvent / anti-solvent systems

One of the primary aims of this project was to use solvent / anti-solvent crystallization as a particle engineering technique to produce combination particles of AS and IB in defined stoichiometric ratios in a size suitable for inhalation. The stoichiometric ratio of primary interest was AS:IB :: 6:1 (w/w) since this was the ratio employed in the commercial combination formulation i.e.; the Combivent® pMDI which is a physical mixture of individually micronized AS and IB. However, since the two drugs are present as a physical mixture, they tend to behave individually during inhalation and hence show differences in their aerosol performance. This leads to the loss of the fixed drug ratio of 6:1 (w/w) which is desired from these combination products. Hence, formulating the two APIs in single combination particles wherein each particle contains a fixed 6:1 (w/w) ratio of AS:IB is expected to overcome these problems. Furthermore, if these combination particles can be produced directly in a size suitable for inhalation, the disadvantages of micronization can also be overcome.

This chapter therefore looked at investigation and optimization of solvent / anti-solvent crystallization to produce combination particles for inhalation. Furthermore, by preparing these particles in different stoichiometric ratios, the interactions between AS and IB and the possibility of formation of co-crystals was also investigated. The first solvent / anti-solvent system of water / ethyl acetate revealed the co-precipitation of AS and IB which resulted in the formation of combination particles in stoichiometric ratios of 1:1, 2:1, 6:1, and 10:1 (w/w). However, these combination particles were too large for inhalation as revealed by the PSD results which were used as an initial screen to estimate the suitability of the particles for inhalation based on their physical size.

Therefore, in an attempt to reduce the size of these particles, isopropyl alcohol was investigated as the anti-solvent. Due to the solubility differences between AS and IB in isopropyl

alcohol, the crystallization process required further optimization. Using the optimized conditions, it was possible to produce combination particles with AS:IB ratios of 2.8:1 (w/w) and 5.7:1 (w/w) in a size suitable for inhalation as demonstrated by the PSD results. However, due to the inappropriateness of the Malvern to provide a true measure of the aerosol performance of these particles, *in vitro* aerosol performance was tested using cascade impactor studies. These results will be discussed in Chapter V. Thermal and PXRD analysis revealed that the combination particles produced from IPA were more crystalline compared to the particles produced from EA.

Although isopropyl alcohol resulted in 6:1 AS:IB particles, it was desirable to use an anti-solvent with similar solubilities of AS and IB in order to simplify the process and aid the prediction of the final AS:IB ratio from the initial ratio in the drug solution. Therefore, mixtures of isopropyl alcohol and ethyl acetate were investigated as alternate anti-solvents. Due to solubility differences between AS and IB in isopropyl alcohol, only isopropyl alcohol:ethyl acetate 1:10 (w/w) could be used as an effective anti-solvent for complete precipitation of IB. The 6:1 (w/w) combination particles produced from these anti-solvents revealed a significantly smaller size compared to ethyl acetate produced particles, however, they were still not small enough for inhalation. Further optimization of the process looked at reduction in the anti-solvent temperature wherein isopropyl alcohol : ethyl acetate :: 1:10 (w/w) was used as the anti-solvent. These experiments resulted in the formation of 6.6:1 (w/w) combination particles in a size range small enough for inhalation as revealed by the PSD. Therefore, it was of interest to test the aerosol performance of these combination particles and compare it with the aerosol performance of the 2.8:1 and 5.7: 1 (w/w) combination particles produced from isopropyl alcohol. The *in vitro* aerosol performance studies and the results obtained will be discussed in Chapter V.

IV.D.4 Molecular modeling of the combination particles

Molecular modeling tools were used in order to study the possible interactions between AS and IB within a combination particle matrix. These molecular modeling methods function on the principle of molecular mechanics, often referred to as the Force Field method. Molecular mechanics is the application of classical mechanics to molecules. Classical mechanics is used to describe the motion of macroscopic objects. In molecular mechanics, atoms are treated as spheres whose mass depends on the element. Chemical bonds are treated as springs whose stiffness depends on which elements are bound together and whether the bond is single, double or triple. Other types of springs are used to model changes in bond angles, dihedral angles, etc. Each of these springs will have spring constants associated with them. Experimental and theoretical methods are used to determine these parameters. Additional equations from classical physics, such as Coulomb's law are used to handle any electrostatic interactions present within a molecule. The sum of all energy terms that apply to a particular molecule are added together to give the potential energy of the molecule. All the equations and associated parameters used to calculate each energy term are collectively called the force field.

In real molecules, there are other forces present than those between bonded atoms. There may be charges present that can repel or attract. Repulsions between non-bonded atoms that are close together in space might also occur. These forces may act to change bond angles or cause twisting around single bonds. To describe the energy of the system, all of the different types of applicable interactions need to be accounted for. The sum of the energy of all of these various components is the basis of a force field. A force field allows for calculation of all the forces on the system which in turn gives the energy of the system. There is an intimate connection between structure and energy and hence, molecular mechanics calculations always involve both. In order

to find the structure or predict geometry, it is necessary to examine the energy to find where energy minima and hence the stable geometries exist.

Figures IV.48 and IV.49 show the crystal structures for AS and IB downloaded from the Cambridge crystallographic database. The interactions between the two molecules could be studied in vacuum. However, since in practice all interactions occur in the presence of solvent, solvation using water was carried out. This solvation process where the two manually oriented molecules were surrounded by water molecules in a water box is shown in Figure IV.50. Post solvation, energy minimization was carried out. As described before, energy minimization is an important part of molecular mechanics calculations.

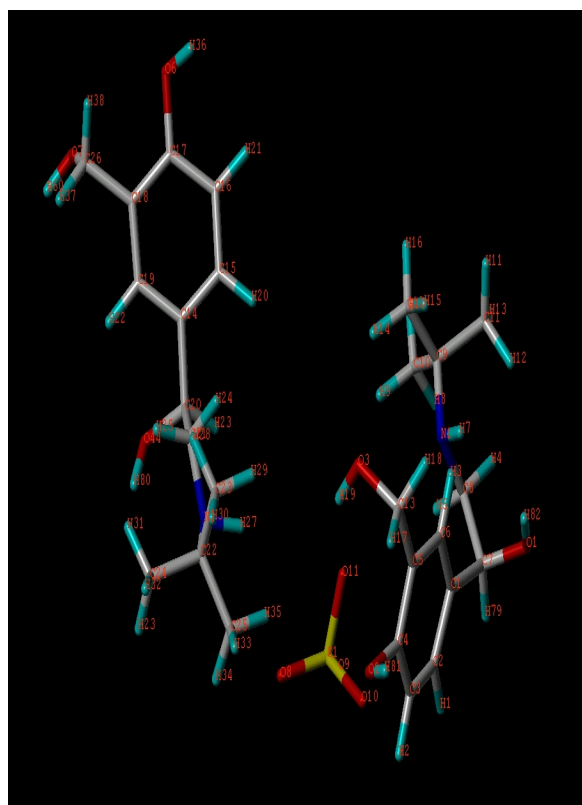


Figure IV.48 AS Crystal

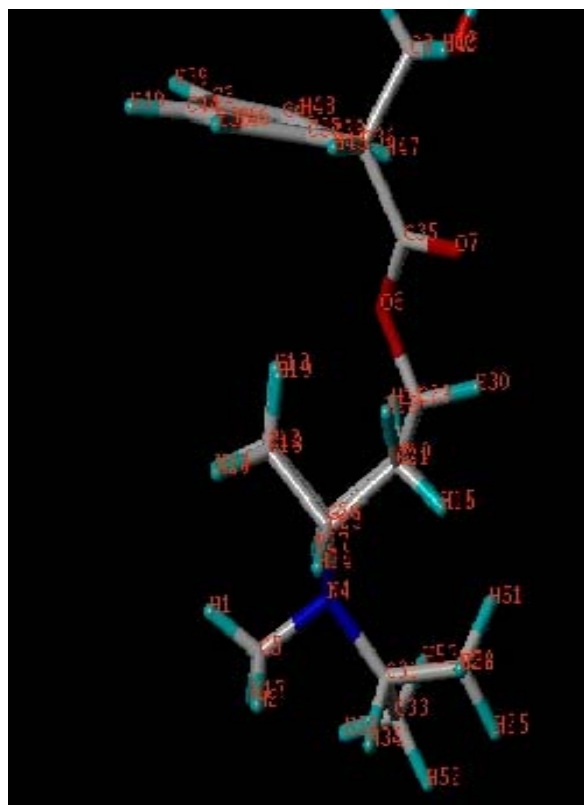


Figure IV.49 IB Crystal

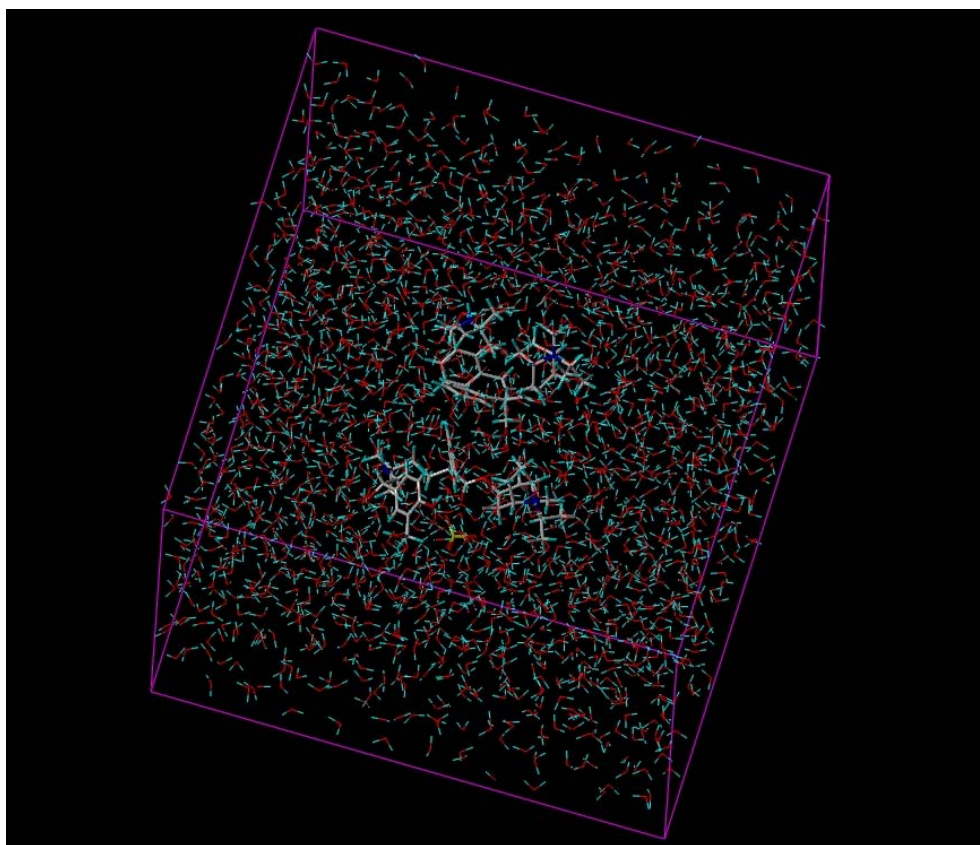


Figure IV.50 Water box for solvation of AS and IB molecules

Energy is a function of the atomic coordinates and the program attempts to generate the coordinates which correspond to a minimum energy during the minimization procedure. This is an iterative process where the atomic coordinates are modified from one iteration to the next in order to decrease the energy. During the process, force field constraints are used to force particular atoms or groups into spatial relationships. These constraints are defined and stored within the molecule. However, it should be understood that these energy minimizations are very rarely able to find the global energy minimum. Only a local minimum, the one closest to the starting set of coordinates is reached.

Once the energy minimization process was over, molecular partitioning was carried out using the eslc platform in HINT. This partitioning performs the basis for all HINT score

calculations. HINT uses the experimental data from solvent partitioning experiments between water and 1-octanol (LogPo/w) for interaction classification and quantitative scoring. HINT was created to specifically include all non-covalent interactions. Hydrophobic and polar interactions, which are collectively referred to as hydrophathy, between molecules in biologically important systems are empirically quantified. In this scheme, hydrophathic attractions between species include hydrogen-bonding, acid–base interactions, Coulombic attractions as well as hydrophobic interactions. All of these are related to solvent partitioning phenomena because the dissolution of a ligand in a mixed solvent system (such as water/1-octanol) involves the same fundamental processes and atom–atom interactions as biomolecular interactions within or between proteins and ligands. HINT scores each atom-atom interaction, within or between the molecules with the following equation (Kellogg et al., 2000):

$$b_{ij} = a_i S_i a_j S_j T_{ij} R_{ij} + r_{ij} \quad \text{Equation IV.2}$$

where b_{ij} is the interaction score between atoms i and j , a is the hydrophobic atom constant, S is the solvent accessible area, T_{ij} is a logic function which returns a value of 1 or -1 depending on the character of the interacting polar atoms ($a < 0$ for polar atoms), there are three possibilities: acid-acid, base-base and acid-base of which only the acid-base interactions are scored positively/favorably. R_{ij} is the exponential e^{-r} (r is the distance between the atoms i and j) and r_{ij} is an implementation of the Lennard-Jones potential function. The total HINT interaction score is given by the sum of the individual interaction scores ($\sum \sum b_{ij}$). The HINT convention is that favourable interactions are scored with $\mathbf{bij} > 0$ and unfavourable interactions are scored with $\mathbf{bij} < 0$. The logic function \mathbf{Tij} returns a value of 1 or -1 depending on the character of the interacting polar atoms (i.e. $\mathbf{a} < 0$): there are three possibilities: acid–acid, acid–base, or base–

base; only acid–base is scored favourably. **Tij** also flags hydrogen bonds which are in the HINT model a special case of acid–base interactions.

Out of the 25 manual orientations between AS and IB, 3 orientations gave positive HINT scores. The favorable orientation of AS and IB with the highest positive HINT score is shown in Figure IV.51. The positive interactions were mainly between hydrophobic carbon atoms and hydrogen bond formation while majority of the negative interactions were contributed by those between hydrophobic carbon atoms and polar atoms such as nitrogen and oxygen. The breakup of the different interactions that contribute to this highest total positive HINT score is shown in Table IV.23. These results imply that in a combination particle matrix, AS and IB will preferably arrange in a way such that the hydrophobic carbon atoms of one molecule are oriented away from the polar atoms such as the nitrogen and oxygen on the other molecule. For e.g., the tertiary nitrogen of AS will try and orient away from carbon atoms of IB.

As mentioned before, manual orientation lends itself to the possibility of bias. Moreover, an interaction study involving a single molecule of AS and IB is not realistic since in the combination particle matrix, the likelihood is that the IB molecules will orient themselves in the interstitial spaces in the AS crystal lattice. In this situation, each IB molecule will be surrounded by a number of AS molecules. In order to simulate this situation, a unit cell of AS was constructed using the AS crystal structure. 8 of these unit cells were then used to build a 2×2×2 cube. This is shown in Figure IV.52.

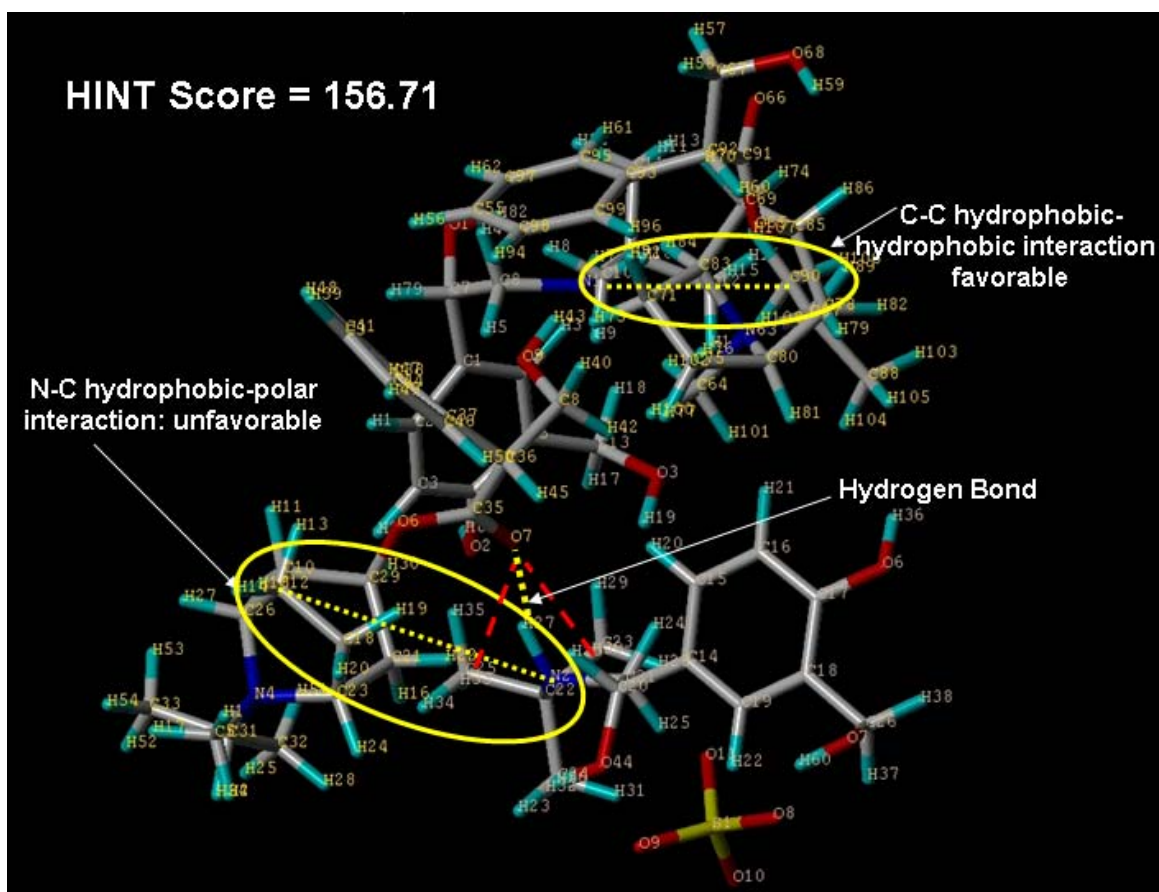


Figure IV.51 Manual orientation between AS and IB with the highest HINT score

Table IV.23 Favorable and unfavorable interactions between AS and IB

Interaction type	Contribution to HINT score
Hydrogen Bond	405.92
Acid/Base	219.44
Hydrophobic	458.13
Acid/Acid	-6.46
Hydrophobic/Polar	-616.89
Base/Base	-303.44

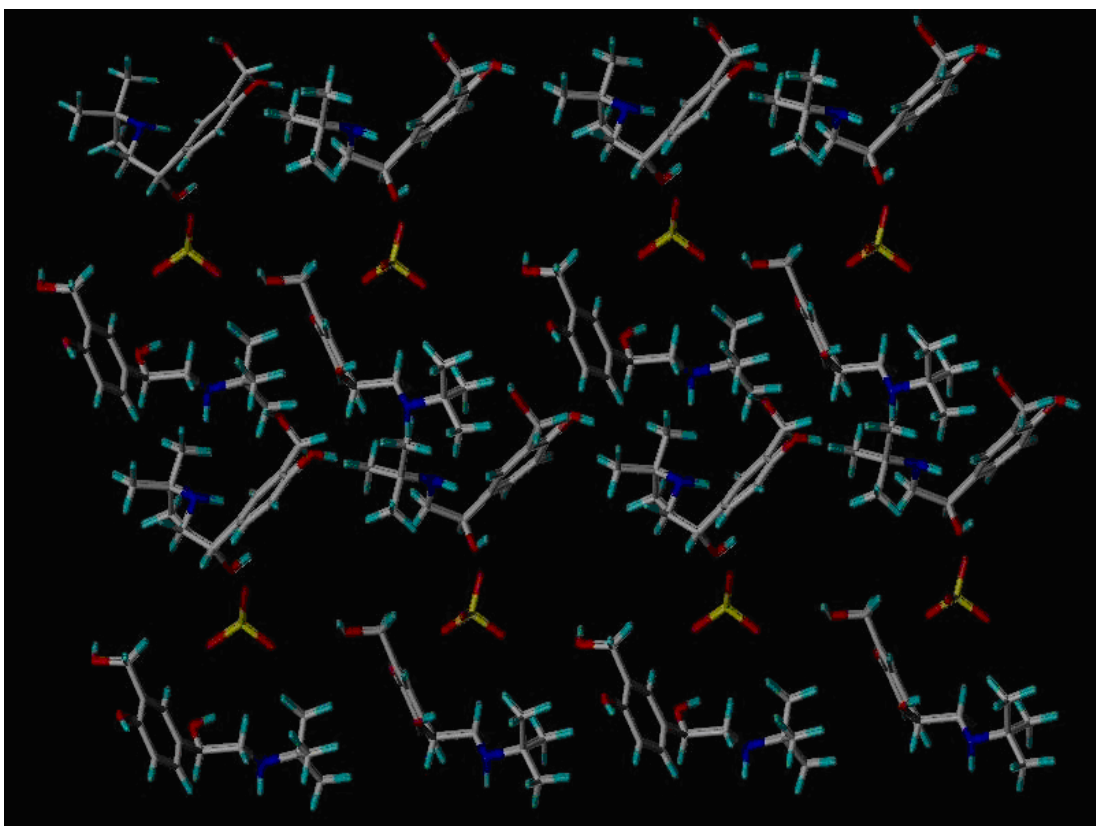


Figure IV.52 Albuterol Sulfate cube constructed of unit cells

At a time, one molecule of albuterol was removed from each corner of the cube and IB was docked into this cavity using GOLD program as shown in Fig. IV.53. This resulted in a total of 8 dockings. These dockings resulted in one IB molecule being in close proximity to 9 albuterol molecules, a situation simulating a combination particle with a nominal 6:1 (w/w) ratio of albuterol sulfate to ipratropium bromide. GOLD is a program for calculating the docking modes of small molecules in protein binding sites. However, in this case, the large cube consisting of the AS unit cells was used as the protein with IB functioning as the ligand. 10 genetic algorithm (GA) runs were performed for each docking run. Post docking, each of the GA run was cored with HINT. This scoring process once again involved molecular partitioning and Log P calculation.

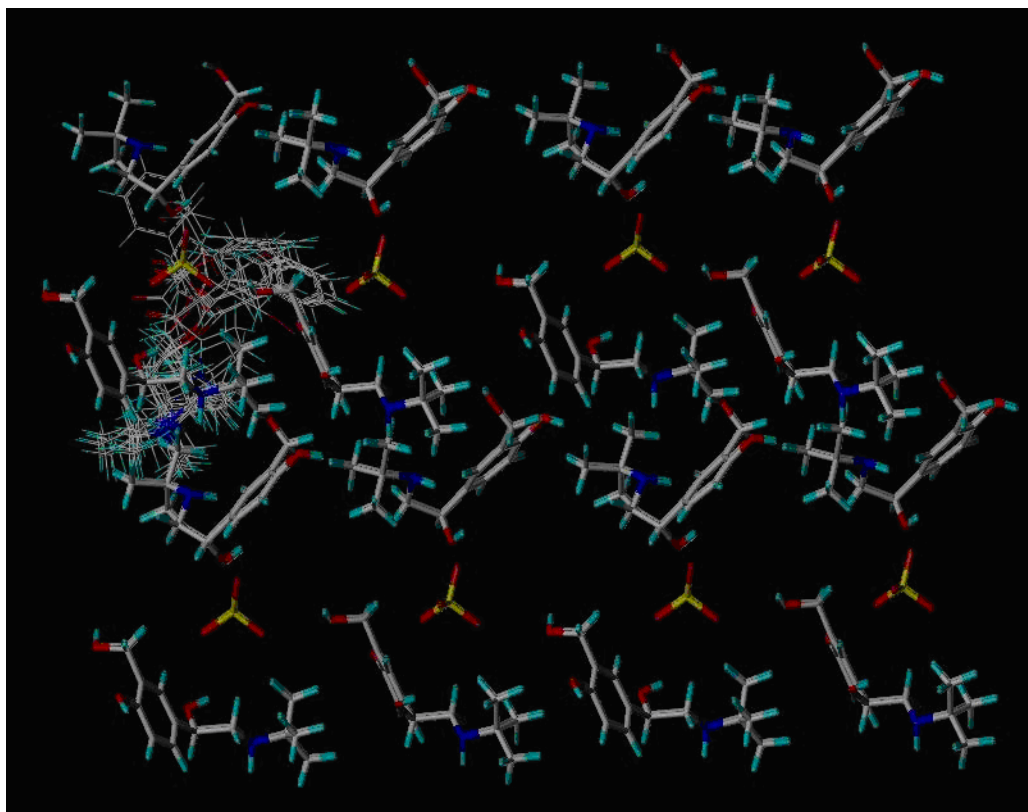


Figure IV.53 A representative docking of IB in the AS crystal lattice

The total HINT scores obtained for each of the dockings were negative except for one run which will be discussed shortly. At first glance, these negative total HINT scores implied an overall unfavorable interaction between AS and IB. However, upon looking into the breakup of the total HINT scores (Appendix), it was observed that there were positive components as well that were contributed mainly by hydrogen bonding and hydrophobic interactions. However, since the IB molecule was surrounded by tightly packed AS molecules, the close proximity led to unfavorable acid-acid and base-base interactions which resulted in a total negative HINT score. These studies however showed that there were a number of positive interactive sites present on both molecules. The one docking that resulted in a positive total HINT score is shown in Figure IV.54.

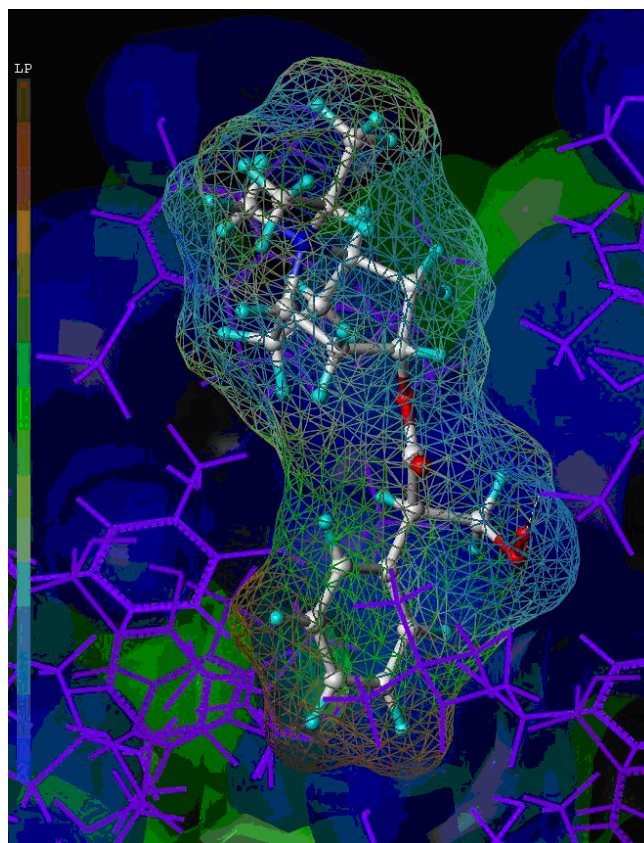


Figure IV.54 IB orientation with the highest HINT score

This HINT score was 248.2 and incorporated favorable hydrophobic interactions and favorable hydrogen bonding interactions. Figure IV.54 shows IB in a net. The bar designates the lipophilic potential. Higher the lipophilic potential, more hydrophobic is the particular site. It can be observed that IB has oriented itself in a way that its hydrophobic bonding sites (predominantly the benzene ring) are close to the hydrophobic binding sites of albuterol sulfate while the polar sites are close to the polar AS sites such as the one resulting the formation of a H-bond between the IB hydrogen atom and the oxygen atom of the $(\text{SO}_4)^{2-}$ group of AS. These studies therefore show us some of the plausible interactions between AS and IB in a combination particle matrix.

IV.E CONCLUSIONS

Combination particles containing AS and IB in reproducible stoichiometric proportions were produced by the optimized solvent / anti-solvent crystallization process using ethyl acetate as the anti-solvent. However, the process required further optimization in order to bring the size of these combination particles in a range suitable for inhalation. Combination particles containing AS and IB in a stoichiometric 6:1 (w/w) ratio were produced from two different solvent / anti-solvent systems of isopropyl alcohol and isopropyl alcohol:ethyl acetate 1:10 (w/w). These particles had VMDs $\approx 6.5 \mu\text{m}$ and revealed $\approx 45\%$ of the particle mass $< 5 \mu\text{m}$. Hence, they were deemed suitable for inhalation. Characterization of the combination particles indicated a difference in characteristics between these particles and physical mixtures. However, it was not possible to conclude unequivocally about the formation of co-crystals. The plausible scenario explaining the different results was the formation of an interstitial crystalline solid solution with IB molecules incorporated within the interstitial spaces of the AS crystal lattice.

These studies therefore led to the development of a single step particle engineering technique to produce combination particles of AS and IB. These particles were crystalline and in a size suitable for inhalation thereby presenting two major advantages. They did not have to be micronized which therefore offered a solution over the well known disadvantages of particle charging, cohesiveness and generation of partially amorphous domains associated with micronization. These particles, by virtue of containing AS and IB in single combination particles, were also expected to show uniform co-deposition during *in vitro* testing which will be discussed in the next chapter.

CHAPTER V

***IN VITRO* AEROSOL PERFORMANCE TESTING OF ALBUTEROL SULFATE PARTICLES AND COMBINATION PARTICLES OF ALBUTEROL SULFATE AND IPRATROPIUM BROMIDE MONOHYDRATE**

V.A INTRODUCTION

In this chapter the *in vitro* aerosol performance testing of the engineered albuterol sulfate particles and combination particles of albuterol sulfate and ipratropium bromide monohydrate will be discussed. Since one of the primary specific aims of this project is to develop a particle engineering technique capable of directly producing albuterol sulfate particles and combination particles of AS and IB suitable for inhalation, it is hypothesized that the engineered particles will have equivalent or superior aerosol performance compared to the commercial products which are comprised of either micronized drug (as in the case of albuterol sulfate commercial formulations) or a physical mixture of two individually micronized drugs (as in the case of combination products of albuterol sulfate and ipratropium bromide monohydrate).

V.B MATERIALS

Albuterol sulfate ((RS)-1- (4-hydroxy-3-hydroxymethylphenyl)-2-(tert-butylamino) ethanol sulfate): Spectrum Chemical Mfg. Corp., New Brunswick, NJ)

Ipratropium bromide monohydrate ([8-methyl-8-(1-methylethyl)- 8-azoniabicyclo[3.2.1] oct-3-yl] 3-hydroxy-2-phenyl-propanoate): Spectrum Chemical Mfg. Corp., New Brunswick, NJ)

Micronized albuterol sulfate: In-house Lot Number 970118

Lactose monohydrate (Pharmatose® 90M): DMV Fonterra Excipients, Princeton, NJ

Novolizer® Dry Powder Inhaler: Meda Pharmaceuticals, Somerset, NJ

Rotahaler® Dry Powder Inhaler: Allen and Hanburys

Nektar PDS® Dry Powder Inhaler: Nektar Pharmaceuticals, San Carlos, CA

Next Generation Impactor: MSP Corporation, Shoreview, MN

Vacuum Pump: Copley Scientific, MSP Corporation, Shoreview, MN

Flow Controller: Copley Scientific, MSP Corporation, Shoreview, MN

V.C METHODS

V.C.1 Aerosol performance testing of albuterol sulfate particles

AS particle production from the solvent / anti-solvent crystallization process was discussed in chapter III. Section III.D.2.2.2 described the production of AS particles from two optimized solvent / anti-solvent systems of water / ethyl acetate and water / isopropyl alcohol. These optimized processes resulted in AS particles with 100% crystallinity and smallest size among the crystallization conditions investigated. These particles will henceforth be designated as EA-AS and IPA-AS respectively. Table V.1 shows the crystallization conditions used to produce these particles. The average volume median diameters of these particles as measured by laser diffraction described in section III.C.1.8 are also shown. The EA-AS and IPA-AS particles were tested for their *in vitro* aerosol performance as drug only formulations and as drug / lactose blends. These studies are described in the subsequent sections.

Table V.1 Description of optimized crystallization conditions used to produce albuterol sulfate particles

Particles	Initial AS concentration (g/g)	Anti-solvent	R_a ratio (w/w)	ΔT between drug solution and anti-solvent (°C)	Crystal maturation time (hours)	Average VMD ± SD (μm)
EA-AS	0.22	Ethyl Acetate	1:200	65	24	8.8 ± 0.6
IPA-AS	0.22	Isopropyl Alcohol	1:200	0	24	4.9 ± 0.3
MIC-AS						3.9 ± 0.3

V.C.1.1 Drug only studies

The prototype dry powder inhalers used for these studies were the Novolizer®, Rotahaler® and the Nektar PDS®. The nominal dose of albuterol sulfate in each of these studies was 200 μg which was weighed and filled into either the Novolizer® cartridge, the Rotahaler® capsule or the Nektar PDS® blister. The aerosol performance was tested by firing a single dose into the NGI operating at 60L/min for 4 seconds. This flow rate was achieved by means of a vacuum pump connected to a flow controller. It is recognized that 60L/min is not the optimum flow rate that achieves a pressure drop of 4KPa for all three devices. For the Novolizer®, Nektar PDS®, and Rotahaler®, the optimum flow rates are 72L/min, 28.3L/min, and 90L/min. However, in order to compare the powder performance across devices, a single flow rate of 60L/min was chosen. Impactor stages were coated with silicone to prevent particle bounce and a glass fiber filter (Type A/E, Gilman, Ann Arbor, MI) was employed in the NGI internal filter holder. The device, mouth-piece adapter, throat, pre-separator and the NGI stages were washed with water and the samples were tested by the previously described HPLC method (Section III.C.1.9). The aerosol performance of the engineered albuterol sulfate particles was compared to

that of micronized albuterol sulfate (designated henceforth as MIC-AS). The characteristics for the MIC-AS particles were discussed in section III.D.2.3. The *in vitro* aerosol performance testing of MIC-AS particles was carried out in the same way as those for the IPA-AS and EA-AS particles.

The *in vitro* aerosol performance was characterized by a number of parameters. These included the emitted fraction, fine particle fraction, mass median aerodynamic diameter (MMAD), and geometric standard deviation (GSD). These parameters were calculated using the following equations:

$$\text{Emitted Fraction} = \left(\frac{\text{Mass of drug emitted from the inhaler}}{\text{Nominal drug dose}} \right) \times 100 \quad \text{Equation V.1}$$

$$\% \text{ Fine Particle Fraction} = \left(\frac{\text{Mass of drug} < 5\mu\text{m in size}}{\text{Emitted drug dose}} \right) \times 100 \quad \text{Equation V.2}$$

$$\text{Geometric Standard Deviation} = (X/Y)^{0.5} \quad \text{Equation V.3}$$

In Equation V.3, X and Y are the sizes associated with a cumulative count of 84% and 16%, respectively based on the mass percentages calculated relative to the impactor dose. The MMAD was directly calculated as the size associated with a cumulative count of 50% based on the mass percentages calculated relative to the impactor dose.

V.C.1.2 Drug / lactose blend studies

Because of the limitations associated with metering a 200 µg dose, a more practical approach was to blend albuterol sulfate particles with lactose monohydrate as a carrier. These studies were only performed for IPA-AS particles since these particles showed a significantly improved aerosol performance compared to the EA-AS particles in the drug only studies as will be discussed in section V.D.1.1. For these studies, the Novolizer® was used as the test DPI. Lactose monohydrate (Grade: Pharmatose® 90M) was chosen as the carrier. The VMD of this lactose was measured as $67.5 \pm 0.2 \mu\text{m}$ and the volume % of particles $< 10 \mu\text{m}$ was $9.7 \pm 0.4\%$. The drug / lactose blend studies employed a nominal dose of 120 µg and a nominal metered mass of 11.5 mg. The drug : lactose ratio was 1:95 (w/w) which was the same as that employed in the commercial Novolizer® dry powder formulation for albuterol sulfate. A homogeneous blend of the AS particles in lactose monohydrate (Pharmatose® 90M) was produced by geometric addition and manual mixing using a mortar and pestle. The blend homogeneity was tested by accurately sampling a mass of powder equivalent to the nominal dose of 11.5 mg. The sample was dissolved in an appropriate volume of water and the amount of AS was determined using the previously described HPLC method (Section III.C.1.9). A % RSD of less than 5.0% calculated from the analysis of 10 samples was taken as an indication of acceptable blend homogeneity. The *in vitro* aerosol performance of the drug / lactose blend was measured using the method described in section V.C.1.1 and compared to the commercial Novolizer® dry powder formulation for albuterol sulfate. *In vitro* aerosol performance parameters as mentioned in section V.C.1.1 were similarly calculated.

V.C.2 Aerosol performance testing of combination particles

Combination particle formation from the solvent / anti-solvent crystallization process was discussed in chapter IV. Sections IV.D.2.3 and IV.D.2.2 described the production of combination particles with a nominal 6:1 (w/w) ratio of AS:IB from two different optimized solvent / anti-solvent crystallization processes. These particles will henceforth be referred to as Combination 1 and Combination 2. In addition to the 6:1 (w/w) combination particles, a further set of particles with a nominal AS:IB ratio of 2.8:1 (w/w) were also produced as described in section IV.D.2.2. These particles will henceforth be referred to as Combination 3. Table V.2 shows the crystallization parameters used to produce these particles. In addition, the average VMDs of these particles measured by laser diffraction as described in section IV.C.3.6 are also shown. The PSDs of these particles were shown in Section IV.D.2.3 for Combination 1 and IV.D.2.2 for Combination 2 and 3. The *in vitro* aerosol performance testing of these particles was carried out as drug only formulations and drug/lactose blends as described in the subsequent sections.

Table V.2 Description of crystallization conditions used to produce combination particles of AS/IB

Particles	Initial AS:IB concentration (g/g)	Anti-solvent	Ra ratio (w/w)	ΔT between the drug solution and anti-solvent	Crystallization time	Final AS:IB ratio (w/w)	Average VMD \pm SD (μm)
Combination 1	0.28:0.04	1:10 IPA:EA (w/w)	1:200	65	24 hours	6.6:1	6.9 \pm 1.1
Combination 2	0.38:0.06	IPA	1:20	0	30 seconds	5.7:1	6.5 \pm 0.3
Combination 3	0.38:0.22	IPA	1:20	0	5 minutes	2.8:1	5.3 \pm 1.0

V.C.2.1 *In vitro* aerosol performance testing of combination particles

V.C.2.1.1 Drug only studies

Combination 1, 2, and 3 were tested for their *in vitro* aerosol performance as drug only formulations using the Novolizer® as the test inhaler. The nominal powder mass of 5.0 mg was weighed and filled into the Novolizer® cartridge. The aerosol performance was tested by firing a single dose of 5.0 mg into the NGI operating at 60L/min for 4 seconds. This flow rate was achieved by means of a vacuum pump connected to a flow controller. Impactor stages were coated with silicone to prevent particle bounce and a glass fiber filter (Type A/E, Gilman, Ann Arbor, MI) was employed in the NGI internal filter holder. The device, mouth-piece adapter, throat, pre-separator and the NGI stages were washed with water and the samples were tested by the previously described HPLC method (Section IV.C.2.2). *In vitro* aerosol performance parameters were calculated as mentioned in section V.C.1.1. The aerosol performance of the engineered combination particles was compared to that of the commercial formulation (Combivent® pMDI) which is a physical mixture of individually milled AS and IB in a nominal 6:1 (w/w) ratio suspended in CFC propellant.

V.C.2.1.2 Drug / lactose blend studies

Combination particles 1, 2, and 3 were tested as drug / lactose blends. For these studies, the Novolizer® was used as the test DPI. Lactose monohydrate (Grade: Pharmatose® 90M) was chosen as the carrier. The drug / lactose blend studies employed a nominal dose of 120 µg for the combination particles and a nominal blend mass of 11.5 mg. The combination particle:lactose ratio was 1:95 (w/w). A homogeneous blend of the combination particles in lactose monohydrate (Pharmatose® 90M) was produced by geometric addition and manual mixing using a mortar and pestle. The blend homogeneity was tested by accurately sampling a mass of powder equivalent to the blend mass during aerosolization. The sample was dissolved in an appropriate volume of

water and the amount of AS and IB were determined using the previously described HPLC method (Section IV.C.2.2). A % RSD of less than 5.0% for both AS and IB calculated from the analysis of 10 samples was taken as an indication of acceptable blend homogeneity. The nominal blend mass of 11.5 mg was loaded into the Novolizer® cartridge. The *in vitro* aerosol performance of the drug / lactose blend was measured by firing a single dose of 11.5 mg into the NGI operating at 60L/min for 4 seconds. This flow rate was achieved by means of a vacuum pump connected to a flow controller. Impactor stages were coated with silicone to prevent particle bounce and a glass fiber filter (Type A/E, Gilman, Ann Arbor, MI) was employed in the NGI internal filter holder. The device, mouth-piece adapter, throat, pre-separator and the NGI stages were washed with water and the samples were tested by the previously described HPLC method (Section IV.C.2.2). *In vitro* aerosol performance parameters were calculated as mentioned in section V.C.1.1.

V.D RESULTS AND DISCUSSIONS

V.D.1 Aerosol performance testing of albuterol sulfate particles

V.D.1.1 Drug only studies

The particles shown in Table V.1 were selected for *in vitro* aerosol performance characterization. These particles were produced from the optimized solvent / anti-solvent crystallization process using isopropyl alcohol and ethyl acetate as anti-solvents and had the smallest size (VMDs shown in Table V.1). Since one of the primary aims of this project was to produce AS particles with suitable inhalation characteristics from a single-step solvent / anti-solvent crystallization process, the *in vitro* aerosol performance of these particles was compared with conventionally used micronized albuterol sulfate (MIC-AS). The results for drug only

studies for the three different types of AS particles are shown in Table V.3. The performance of the different types of AS particles will be discussed under emitted fraction dealing with device emptying and powder flow, fine particle fraction dealing with device deagglomeration principles and powder dispersivity, and fine particle dose indicating the overall performance of the particles.

Table V.3 Mean \pm SD *in vitro* aerosol performance characteristics of AS particles tested from different DPIs as drug only formulations (n=3)

Novolizer®					
AS Particles	% Emitted Fraction	Fine Particle Dose (μg)	% FPF	MMAD (μm)	GSD
MIC-AS	40.8 \pm 0.7	51.4 \pm 0.1	59.4 \pm 0.1	2.7 \pm 0.0	2.0 \pm 0.0
EA-AS	61.0 \pm 9.9	28.3 \pm 4.8	23.6 \pm 7.1	3.2 \pm 0.4	2.2 \pm 0.2
IPA-AS	68.8 \pm 1.8	70.2 \pm 6.4	46.6 \pm 1.3	2.8 \pm 0.1	2.2 \pm 0.0
Rotahaler®					
MIC-AS	21.9 \pm 0.7	24.6 \pm 0.3	53.3 \pm 0.7	2.6 \pm 0.0	2.6 \pm 0.0
EA-AS	66.5 \pm 5.6	9.6 \pm 4.7	5.6 \pm 1.0	5.7 \pm 0.6	2.1 \pm 0.2
IPA-AS	61.4 \pm 1.2	21.8 \pm 0.2	16.1 \pm 0.1	3.3 \pm 0.0	2.9 \pm 0.0
Exubera®					
MIC-AS	36.4 \pm 0.2	56.6 \pm 0.6	68.5 \pm 0.4	3.3 \pm 0.0	1.9 \pm 0.0
EA-AS	33.6 \pm 4.8	29.6 \pm 7.8	38.7 \pm 1.4	3.7 \pm 0.0	2.5 \pm 0.0
IPA-AS	53.2 \pm 0.4	39.8 \pm 4.3	34.8 \pm 2.1	3.3 \pm 0.1	2.3 \pm 0.0

The emitted fraction of a dry powder formulation is used to estimate the amount of drug coming out from the device since it is only this amount that is available for deposition. This emitted fraction is dependent on both powder and device characteristics. The emitted fractions for the AS particles will therefore be discussed based on these two parameters. Table V.3 shows that MIC-AS resulted in emitted fractions < 40% when aerosolized from all three devices. MIC-AS when aerosolized in the Rotahaler® produced a significantly smaller emitted fraction of 21.9 \pm 0.7% compared to both the Novolizer® and the Nektar PDS® (p-value < 0.05, Tukey’s HSD). The emitted fraction for MIC-AS was comparable between Novolizer® and Nektar PDS® (p-

value > 0.05, Tukey's HSD). When tested using the Novolizer® and the Rotahaler®, EA-AS drug only formulation produced similar (p-value > 0.05, one-way ANOVA) emitted fractions of 61.0 ± 9.9 and $66.5 \pm 5.6\%$ respectively. IPA-AS particles also showed similar (p-value > 0.05, one-way ANOVA) emitted fractions of 68.8 ± 1.8 and $61.4 \pm 1.2\%$ when tested from the Novolizer® and the Rotahaler® respectively. This performance was significantly improved compared to the % emitted fraction observed for the MIC-AS. However, aerosolization using the Nektar PDS® resulted in significantly smaller emitted fractions for both EA-AS ($33.6 \pm 4.8\%$) and IPA-AS ($53.2 \pm 0.4\%$) particles when compared to the emitted fractions obtained from the Novolizer® and the Rotahaler® (p-values < 0.05, Tukey's HSD).

For a dry powder formulation, the dose emission efficiency is determined by a complex interplay between the particle characteristics and device properties (de Boer et al., 2003; Dunbar et al., 1998). Inhaler devices contain special design features to empty and deagglomerate the powder (Crowder et al., 2001). The Novolizer® is a multi-dose, passive, breath-actuated, moderate airflow resistance inhaler which utilizes the air-classifier technology to achieve particle deaggregation (de Boer et al., 2006; de Boer et al., 2006; Fenton et al., 2003). Figure V.1 shows a schematic diagram of the Novolizer®. The powder is contained in a reservoir cartridge from which it empties into a powder channel and is then inhaled through the mouthpiece. The drug emptying from this inhaler is improved by a hammer which shakes the powder reservoir during the device actuation. The hammer also helps to remove the powder on the powder channel walls and therefore aids emptying (Fenton et al., 2003).

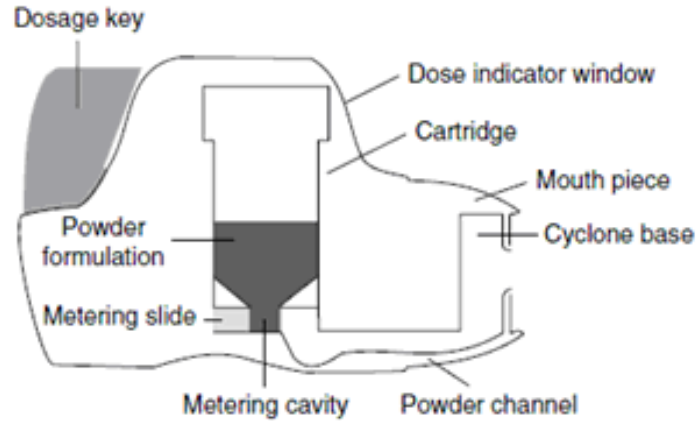


Figure V.1 Schematic diagram of a Novolizer® (Fenton et al., 2003) (Reproduced with permission from Wolters Kluwer)

Nektar PDS® is an active inhaler with the drug packaged into a unit-dose blister. The actuation process requires lifting the handle above the base once and squeezing it until it snaps shut (Davis et al., 2008). This pulls in compressed air into the air pump shown in Figure V.2.

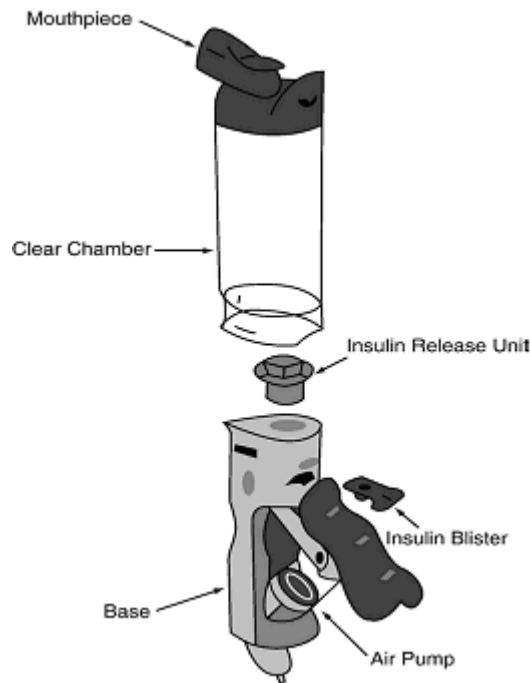


Figure V.2 Schematic diagram for the Nektar PDS® dry powder inhaler (Davis et al., 2008) (Reproduced with permission from Elsevier)

Upon actuation, the blister is pierced and the stored compressed air rushes into the blister and fluidizes the powder which is then expelled into the release unit and then into the spacer chamber. The active fluidization process aids both blister emptying and powder deaggregation. In contrast to the Novolizer® and Nektar PDS® devices which have inbuilt design features to promote device emptying, Rotahaler® which is a first generation dry powder inhaler does not incorporate any special features to aid device emptying (Hallworth, 1977). As shown in Figure V.3, a small capsule containing the drug is loaded into a small hole at the end of the barrel. The barrel is then twisted to allow the plastic blade inside to separate the capsule body from the cap, thus exposing the powder for dispersion. Upon patient inhalation, the powder is emptied by the rattling motion of the capsule body and dispersed through the grid in the mouthpiece by the entraining air (Chew et al., 2002).

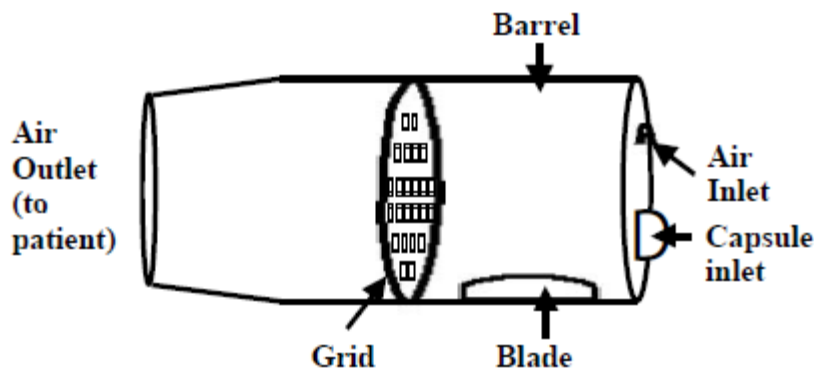


Figure V.3 Schematic diagram of a Rotahaler® (Chew et al., 2002) (Reproduced with permission from Elsevier)

The absence of any special design features in the Rotahaler® in contrast to the Novolizer® and Nektar PDS® may have accounted for the lowest emitted fraction for MIC-AS observed from this device compared to the other two DPIs. However, IPA-AS and EA-AS particles when

aerosolized from the Novolizer and Rotahaler resulted in comparable emitted fractions which were significantly higher compared to MIC-AS particles from both the Novolizer® and the Rotahaler®. These observations may be explained by an interplay between the device and formulation. The emitted fraction of a powder is a function of its flow properties with better flowing powders exhibiting improved device emptying (Terzano and Colombo, 1999; Chow et al., 2007; Iida et al., 2001). Micronized powders are generally cohesive due to two characteristics: small size and electrostatically charged surfaces produced during the milling process, filling and device manipulation (Terzano and Colombo, 1999; Chow et al., 2007, Louey et al., 2006; Danniher and Zhu, 2008; Iida et al., 2001). The small size brings about particle cohesion by reducing the interparticulate distances. This results in an increase in Van der Waals forces of interaction thereby making the powders stick together as clumps and adversely affecting their flowability (Terzano and Colombo, 1999). Electrostatically charged surfaces are subject to Coulombic forces of interaction and it has been suggested in literature that such interactions are comparable in strength to the Van der Waals forces (Chan, 2006; Keil et al., 2006). The emitted fraction is strongly and negatively influenced by the electrostatic deposition in the inhalers and on the mouthpieces (Chan, 2006). The lower emitted fraction for the micronized albuterol sulfate from both the Novolizer® and Rotahaler® compared to EA-AS and IPA-AS particles may be attributed to the high cohesive properties of these particles which lead to significant device retention by the particles adhering to the device. The EA-AS and IPA-AS particles produced from a controlled crystallization process were not subjected to micronization. This might have led to a reduction in particle cohesion, and hence improved flow properties. Furthermore, the EA-AS and IPA-AS particles had a higher percentage of larger particles > 10 µm compared to the MIC-AS particles (% Volume < 10 µm = MIC-AS: 92.7 ± 1.2%; IPA-AS:

82.6 ± 0.6%; EA-AS: 57.1 ± 0.8%). These larger particles may act as an in built binary mixture akin to the presence of larger carrier particles to improve flow properties and hence help device emptying. Figures V.4 and V.5 showing the individual site deposition expressed as % mass relative to the nominal drug dose for the AS particles aerosolized from the Rotahaler® and Novolizer® also reveal the poor device emptying for the MIC-AS particles relative to the IPA-AS and EA-AS particles.

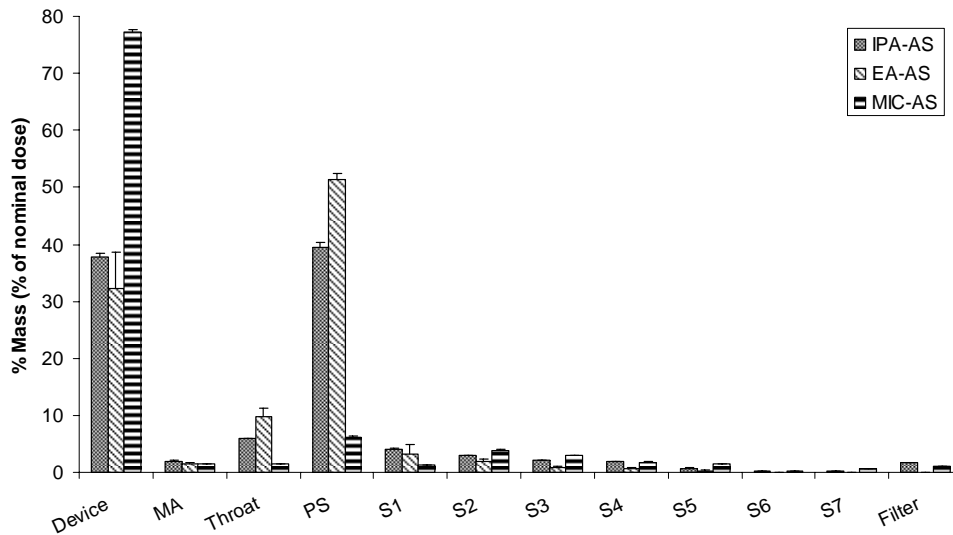


Figure V.4 Individual site deposition of different types of AS particles aerosolized from the Rotahaler® as drug only formulations (n=3)

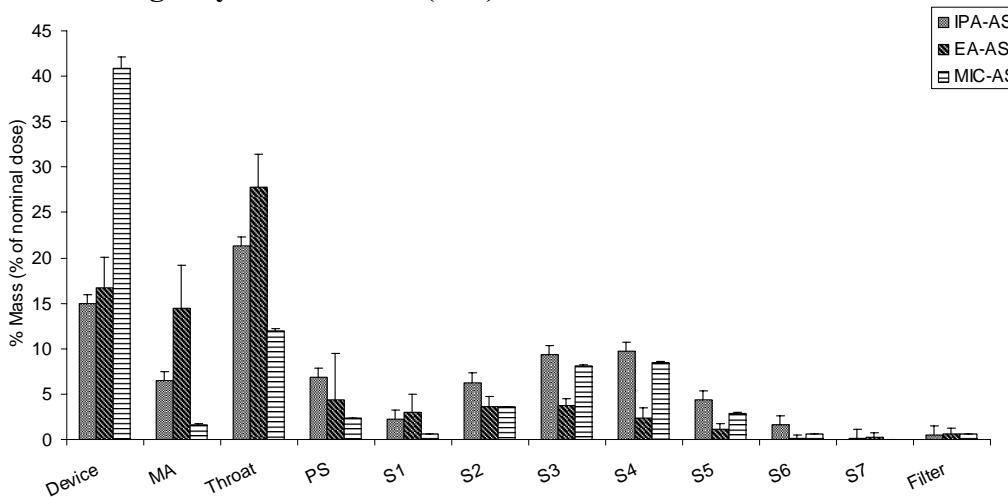


Figure V.5 Individual site deposition of different types of AS particles aerosolized from the Novolizer® as drug only formulations (n=3)

The comparable emitted fractions for EA-AS and IPA-AS particles between the Novolizer® and the Rotahaler® may be a result of a decreased device dependency for these particles relative to MIC-AS particles. The emitted fraction of the EA-AS and IPA-AS particles from the Nektar PDS® was significantly lower (p-value < 0.05, Tukey’s HSD) compared to that obtained from the Novolizer® and the Rotahaler®. These results may be attributed to the fact that the Nektar PDS® device was designed to work most efficiently with a formulation consisting of a flow aid such as mannitol as an excipient. Therefore, the device emptying might be adversely affected when testing drug only formulations. Further, the large spacer incorporated in the Nektar PDS® design presents a possible site for particle adherence. It was observed that IPA-AS particles produced a significantly higher emitted fractions (p-value > 0.05, Tukey’s HSD) compared to MIC-AS and EA-AS particles when aerosolized from the Nektar PDS® as shown in Figure V.6.

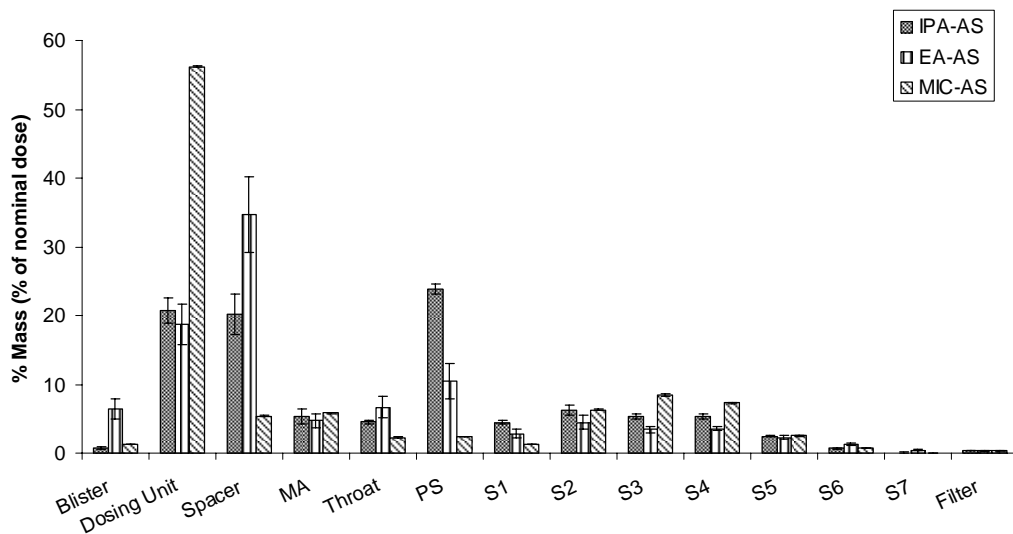


Figure V.6 Stage-wise deposition of different types of AS particles aerosolized from the Nektar PDS® as drug only formulations (n=3)

These differences might be attributed to the particle characteristics. The IPA-AS particles shown in Figure III.52 were elongated, rod-like in shape. Therefore, they are likely to have lower cohesive and adhesive forces compared to the tabular particles of EA-AS shown in Figure III.49 and the tabular, possibly electrostatically charged MIC-AS particles (Fig. III.56). The poor device emptying of Nektar PDS® when aerosolizing drug only formulations may be more significant for the cohesive MIC-AS and EA-AS particles compared to the less cohesive IPA-AS particles resulting in the differences in emitted fractions. Therefore, in summary, the emitted fraction was found to be significantly influenced by both powder and device characteristics. The IPA-AS and EA-AS particles produced a significantly improved emitted fraction from the Novolizer® compared to MIC-AS particles.

The % FPF results also revealed differences in the aerosol performance of the three types of AS particles together with the device. The % FPF represents the mass fraction of the aerosol less than 5.0 µm and is considered to be respirable. The % FPF is calculated as the percentage of drug mass < 5.0 µm (mass of drug depositing on stage 2 and below in the NGI operating at 60 L/min) relative to the emitted drug dose and is representative of powder dispersivity. This is the ability of the particle agglomerates to disperse into discrete individual particles during aerosolization.

Table V.3 shows that MIC-AS particles resulted in similar % FPFs (p-value > 0.05, Tukey's HSD) of 59.4 ± 0.1 % and 68.5 ± 0.4 % when aerosolized from the Novolizer® and the Nektar PDS® respectively. Rotahaler® resulted in the smallest % FPF (p-value < 0.05, Tukey's HSD) of 53.3 ± 0.7 % for MIC-AS particles compared to the Novolizer® and the Nektar PDS®. The EA-AS particles also showed a similar trend with similar % FPFs of 23.6 ± 7.1 % and 38.7 ± 1.4 % (p-value > 0.05, Tukey's HSD) being produced from the Novolizer® and the Nektar

PDS® respectively. Rotahaler® once again produced a significantly smaller (p-value < 0.05, Tukey’s HSD) % FPF of 5.6 ± 0.9 % for the EA-AS particles when compared to the Novolizer® and the Nektar PDS®. With the IPA-AS particles also, Rotahaler® resulted in the lowest % FPF of 16.1 ± 0.1 % compared to the Novolizer® and the Nektar PDS® which resulted in significantly higher % FPFs (p-values > 0.05, Tukey’s HSD) of 46.6 ± 1.3 % and 34.8 ± 2.1 % respectively. Dry powder inhaler dispersion efficiency is influenced once again by an interplay between the device and formulation.

MIC-AS particles resulted in the highest % FPFs regardless of the employed device. This might be attributed to their smallest size which results in higher deposition on stages < 5.0 µm. However, the % FPFs obtained were significantly lower than the volume % of particles < 5.0 µm obtained from laser diffraction sizing. These results are shown in Table V.4.

Table V.4 Volume / mass fraction of AS particles < 5.0 µm obtained during laser diffraction and aerosolization (n=3)

Particles	Volume / Mass % < 5.0 µm			
	Laser Diffraction	Aerosolization		
		Novolizer	Rotahaler	Exubera
MIC-AS	71.8 ± 3.4	59.4 ± 0.1	24.6 ± 0.3	68.5 ± 0.4
IPA-AS	55.6 ± 0.8	46.6 ± 1.3	16.1 ± 0.1	34.8 ± 2.1
EA-AS	34.4 ± 1.2	23.6 ± 7.1	5.6 ± 1.0	38.7 ± 1.4

The volume fractions < 5.0 µm obtained from laser diffraction are indicative of completely dispersed particles since the laser diffraction method was developed to achieve complete deagglomeration without particle attrition. The lower volume / mass fractions obtained during aerosolization are therefore indicative of incomplete dispersion of the AS particles from

all devices. However, Novolizer® and Nektar PDS® resulted in significantly higher % FPFs compared to the Rotahaler indicating more efficient dispersivity.

Novolizer® employs the principle of air classifier technology to bring about particle dispersion. This air classifier technology is depicted in Figure V.7.

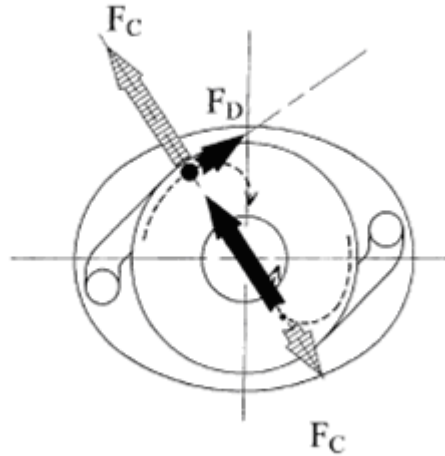


Figure V.7 Air classifier technology in a Novolizer® dry powder inhaler (de Boer et al., 2003) (Reproduced with permission from Elsevier)

The air classifier technology classifies particles based on particle size. The basic design of such a classifier has a cylindrical chamber with a tangential air supply channel and a discharge channel starting from the centre of one of its circular ends. The larger particles in such a classifier can be retained and only detached / deagglomerated drug particles are discharged with the inspiratory airstream. The classification is the result of the counter acting of two forces; the drag force (F_D) and the centrifugal force (F_C). This air classifier technology in the Novolizer® therefore brings about efficient particle deagglomeration and increased dispersivity (de Boer et al., 2003).

Nektar PDS® also employs specific design principles to bring about particle deagglomeration. This is active powder fluidization by compressed air. Discharge of compressed

air through the powder blister upon actuation releases the powder which is then dispersed into primary particles by the energy of compressed air discharged through the release unit. The particles are inhaled as a standing cloud from the holding chamber (Davis et al., 2008). In contrast to the Novolizer® and the Nektar PDS®, the deagglomeration principles employed in the Rotahaler® are relatively less efficient (Chew et al., 2002). The powder released from the capsule upon actuation passes through the grid shown in Figure V.3 which disperses it into primary particles together with the rattling of the capsule produced during inhalation. These device differences in terms of the mechanisms for deagglomeration may explain the lowest % FPF for all types of AS particles when aerosolized from the Rotahaler® compared to Novolizer® and Nektar PDS®.

The % FPF was also observed to be a function of the AS particles themselves with differences being seen in the same device. Rotahaler®, with its weakest dispersivity principles can be used to assess the inherent powder dispersivity. In this device, the MIC-AS particles resulted in a significantly higher (p -value > 0.05 , one-way ANOVA) % FPF of $53.3 \pm 0.7\%$ compared to the IPA-AS particles (% FPF = $16.1 \pm 0.1\%$). Thus once emitted, the small mass of the MIC-AS particles was more efficiently dispersed compared to IPA-AS particles. This might be attributed to the smaller size of MIC-AS particles relative to IPA-AS particles. EA-AS particles, once again produced the smallest % FPF of $5.6 \pm 1.0\%$ among the three types of particles. In this case the maximum loss in % FPF occurred due to deposition of the EA-AS particles in the pre-separator as shown in Figure V.4. The pre-separator collects the large particles in the powder and hence, the highest drug loss in the pre-separator for the EA-AS particles may be due to their largest particle size compared to MIC-AS and IPA-AS particles. In the Novolizer® also, MIC-AS resulted in a significantly higher % FPF of $59.4 \pm 0.1\%$ compared

to the % FPFs of 46.6 ± 1.3 % and 23.6 ± 7.1 % produced by IPA-AS and EA –AS respectively. Therefore, once emitted, MIC-AS showed significantly higher dispersivity compared to the IPA-AS and EA-AS particles. This may once again be attributed to the smallest size of the MIC-AS particles. The Nektar PDS® showed a similar trend to the Rotahaler® and Novolizer® wherein the MIC-AS particles resulted in a significantly higher % FPF (p-value < 0.05, one-way ANOVA) of 68.5 ± 0.4 % compared to IPA-AS particles (% FPF = 34.8 ± 2.1 %) and EA-AS particles (% FPF = 38.7 ± 1.4 %). This higher dispersivity of MIC-AS particles may once again be related to their small size compared to IPA-AS and EA-AS particles.

Therefore, the results for % FPF revealed that MIC-AS particles had the highest dispersivity compared to the particles engineered from the solvent / anti-solvent crystallization process. This was attributed to their smaller size. However, it was also observed that MIC-AS particles had significantly lower emitted fractions compared to the engineered particles particularly in the Novolizer® and Rotahaler®. Both emitted fraction and % FPF are important aerosol performance features and it is necessary to arrive at an optimum balance between the two. Therefore, IPA-AS particles with higher emitted fractions compared to MIC-AS and reasonably high % FPFs for a dry powder formulation may have more benefits.

The overall efficiency of a dry powder formulation can be assessed in terms of its fine particle dose (FPD) which represents the total mass of drug < 5.0 μm and indicates the respirable amount. Since it takes into account both powder emission and powder dispersivity, it is a useful parameter to classify the formulation efficiency. The FPD for the different types of AS particles were shown in Table V.3. It was observed that in the Novolizer®, IPA-AS particles had a significantly higher FPD of 70.2 ± 6.2 μg compared to MIC-AS (FPD = 51.4 ± 0.1 μg) and EA-AS (FPD = 28.3 ± 4.8 μg) (p-value < 0.05, Tukey's HSD). Therefore, even though MIC-AS had

higher dispersivity from the Novolizer®, IPA-AS particles showed improved overall performance by virtue of their higher emitted fractions. In the Rotahaler®, comparable FPDs of $24.6 \pm 0.3 \mu\text{g}$ and $21.8 \pm 0.2 \mu\text{g}$ were produced by MIC-AS and IPA-AS particles respectively ($p\text{-value} > 0.05$, Tukey's HSD) with EA-AS particles producing the smallest FPD of $9.6 \pm 4.7 \mu\text{g}$. Therefore, in spite of their significantly higher dispersivity, MIC-AS particles did not show any significant improvement in the overall performance. When aerosolized from the Nektar PDS®, MIC-AS particles produced the highest FPD of $56.6 \pm 0.6 \mu\text{g}$ compared to IPA-AS (FPD = $39.8 \pm 4.3 \mu\text{g}$) and EA-AS (FPD = $29.6 \pm 7.8 \mu\text{g}$). These differences were attributed to the very high dispersivity of MIC-AS particles compared to the IPA-AS and EA-AS particles.

These results therefore demonstrated that the performance was dependent on both particle properties as well as device characteristics. The significantly improved aerosol performance of IPA-AS particles from the Novolizer® was therefore indicative of the highest efficiency for this particle / device combination.

Figures V.8, V.9, and V.10 show the cumulative % undersize mass distributions based on the mass percentage as a function of the impactor dose for the Novolizer®, Rotahaler®, and Nektar PDS® respectively. The differences in the *in vitro* aerosol performance for the three types of AS particles and the interdependency of the device and formulation were also reflected in the MMADs wherein EA-AS particles resulted in the highest MMAD of $5.6 \pm 1.0 \mu\text{m}$ when aerosolized from the Rotahaler®. The MMADs of the AS particles when aerosolized from the other devices were comparable. No differences were observed in the GSD values for the different types of AS particles aerosolized from different devices indicating similarity in the width of the particle size distribution within the impactor.

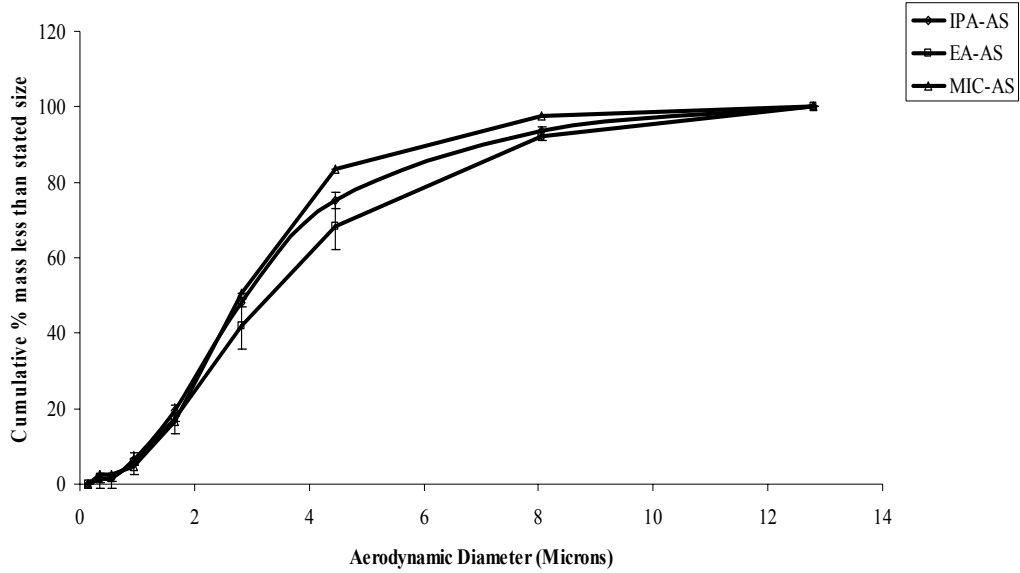


Figure V.8 Cumulative % undersize mass distribution for the three types of AS particles tested from the Novolizer® as drug only formulations (n=3)

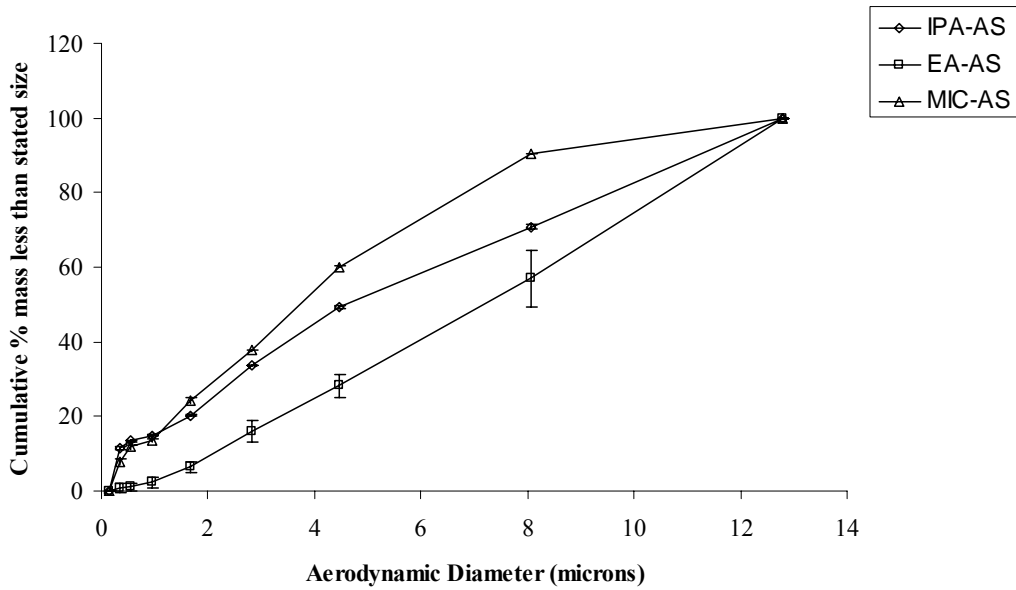


Figure V.9 Cumulative % undersize mass distribution for the three types of AS particles tested from the Rotahaler® as drug only formulations (n=3)

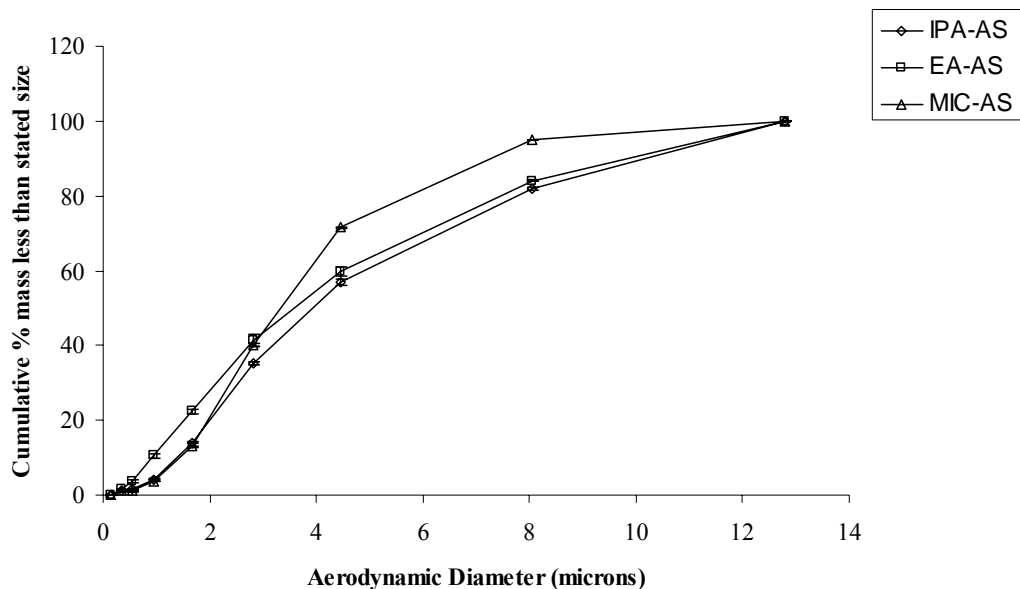


Figure V.10 Cumulative % undersize mass distribution for the three types of AS particles (n=3)

Therefore, in summary, drug only studies of the AS particles revealed that the performance of the formulation was an interplay between particle and device characteristics. AS particles engineered from the solvent / anti-solvent crystallization process using isopropyl alcohol and ethyl acetate resulted in significantly higher emitted fractions compared to the conventionally used micronized particles when aerosolized from the Novolizer® and Rotahaler®. These higher emitted fractions were indicative of better flow properties of these particles and were attributed to decreased cohesive forces. The reasons for these decreased cohesion was attributed to the presence of larger particles acting as inbuilt binary mixtures as well as reduced surface energy for these engineered particles relative to micronized particles. Powder dispersivity represented as the fine particle fraction was found to be highest for micronized AS. However, this increased powder dispersivity did not translate into improved overall performance of these particles represented by the fine particle dose. AS particles produced from the solvent / anti-solvent crystallization process using isopropyl alcohol as the

anti-solvent resulted in a superior aerosol performance compared to micronized albuterol sulfate when aerosolized from the Novolizer®. These results once again reiterated the complex interaction between the device and formulation affecting the overall dry powder performance.

V.D.1.2 Drug / lactose blend studies

In the previous section, it was found that IPA-AS particles in drug only DPI formulations, produced the highest emitted fraction and fine particle dose when tested in the Novolizer® DPI. These particles were selected for further investigation in drug / lactose blend formulations using the Novolizer®. The drug / lactose blend studies were carried out to overcome the practical limitations of metering out a small mass of 200 µg of the drug alone. A homogeneous blend of these particles was prepared with lactose monohydrate as described in section V.C.1.2. The blend homogeneity was measured as described in section V.C.1.2. The % RSD obtained during the blend homogeneity studies was 2.9% which was therefore acceptable. In order to test the aerosol performance of micronized AS when present as a homogeneous binary mixture with carrier lactose, the commercial Novolizer® dry powder formulation for AS was chosen since it contained a physical mixture of micronized AS blended with lactose monohydrate. The results for drug / lactose blend studies are shown in Table V.5.

Table V.5 *In vitro* aerosol performance of IPA-AS particles tested from the Novolizer® as drug / lactose formulations (n=3)

Formulation	Emitted Fraction (%)	Fine Particle dose (µg)	% FPF	MMAD (µm)	GSD
Novolizer® Blend	88.0 ± 7.9	25.1 ± 2.1	23.7 ± 2.6	3.2 ± 0.1	2.1 ± 0.2
IPA-AS Blend	90.3 ± 3.9	33.4 ± 0.8	32.6 ± 0.6	2.5 ± 0.5	2.6 ± 0.6

These results will once again be discussed in terms of the emitted fraction, fine particle fraction and fine particle dose. The emitted fractions for the commercial formulation and IPA-AS blend were comparable (p-value > 0.05, One-way ANOVA) at 88.0 ± 7.9 % and 90.3 ± 3.9 % respectively. These emitted fractions were also significantly higher (p-value < 0.05, One-way ANOVA) compared to the values obtained in the drug only studies for MIC-AS (40.8 ± 0.7 %) and IPA-AS (68.8 ± 1.8 %) particles. Furthermore, the emitted fractions for the commercial Novolizer® formulation were similar to the emitted fraction of 90.0% reported in literature (de Boer et al., 2006). These results can be explained by the presence of the larger size lactose particles. The drug only formulations consist of small drug molecules which exhibit strong interparticulate forces. These interparticulate forces were discussed in detail in section V.D.1 and include the Van der Waal's forces and possibly electrostatic forces in micronized particles (Visser, 1981). The Van der Waal's forces become particularly noticeable when the interparticulate distance is small. These Van der Waal's forces lead to interparticulate cohesion which adversely effects powder flow and therefore produces a low emitted dose fraction (Daniher and Zhu, 2008; Louey et al., 2004). Addition of large (50-100 μm) carrier particles in the form of lactose results in an increase in the interparticulate distances which therefore reduces the Van der Waal's forces making the particles less cohesive (Daniher and Zhu, 2008; Chow et al., 2007; Iida et al., 2001). The drug particles adhere to the surfaces of the carrier lactose particles. This adherence further reduces the cohesive forces between the drug-drug particles and promotes powder flow. The improvement in powder flow for dry powder formulations of fluticasone propionate in the presence of lactose as a carrier has been studied by Louey et al. (2004). They employed measures of flowability such as the Carr's compressibility index calculated from tapped and bulk powder density and the vibrating spatula method to generate

powder mass flow vs. time profiles. They showed an increase in powder flow with an increase in the lactose proportion in the dry powder formulation. Therefore, it is believed that the increase in emitted fraction in drug / lactose blend formulations is attributed to the role of lactose in promoting powder flow.

Comparison between the % FPFs of IPA-AS particles tested as a drug / lactose formulation and commercial Novolizer® formulation revealed that the IPA-AS particles produced a significantly higher % FPF (p-value < 0.05, one-way ANOVA) of 33.4 ± 0.8 % compared to a % FPF of 23.7 ± 2.6 % produced by the commercial Novolizer® formulation. The higher % FPFs for the IPA-AS blend are also evident from Figure V.11 which shows higher AS deposition on stages 4, 5, 6, and 7 of the NGI from the IPA-AS blend compared to the commercial Novolizer® formulation.

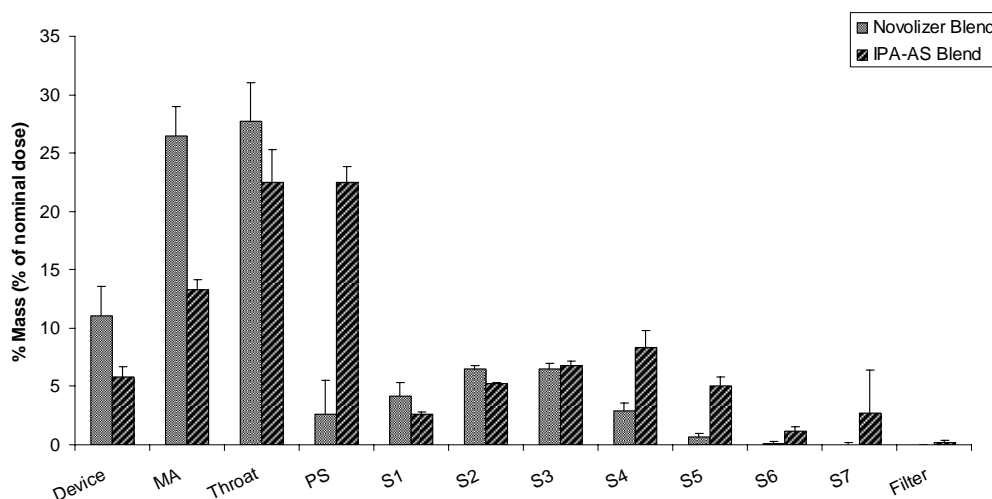


Figure V.11 Stage-wise deposition of commercial Novolizer® formulation and IPA-AS particles tested as drug / lactose formulations (n=3)

Dhumal et al. (2009) have produced AS particles by a sonocrystallization technique and tested their *in vitro* aerosol performance from the Rotahaler® as drug / lactose formulations (drug : lactose = 1:67.5 (w/w)) at 28.3 L/min. They have reported a high % FPF of 44.2 ± 1.3 %

as a function of nominal dose. However, due to the differences in the device and the drug : lactose ratio between the IPA-AS blend and the sonocrystallized AS particles, no direct comparisons are possible.

The significantly higher % FPF of the IPA-AS particles when tested as a drug / lactose formulation compared to the commercial Novolizer® formulation may be explained by the relative strength of adherence of the drug particles to the lactose particles. Commercial Novolizer® formulation contains micronized AS. These micronized particles have surfaces with higher energy as a function of the micronization process and therefore might adhere more strongly to the lactose particles compared to the particles engineered from isopropyl alcohol and not subjected to micronization (Islam et al., 2003; Louey et al., 2004; Zeng et al., 1996; Sriracha et al., 1998). The stronger adherence will lead to reduced deaggregation and hence account for the smaller % FPF for the commercial Novolizer® formulation compared to the IPA-AS blend.

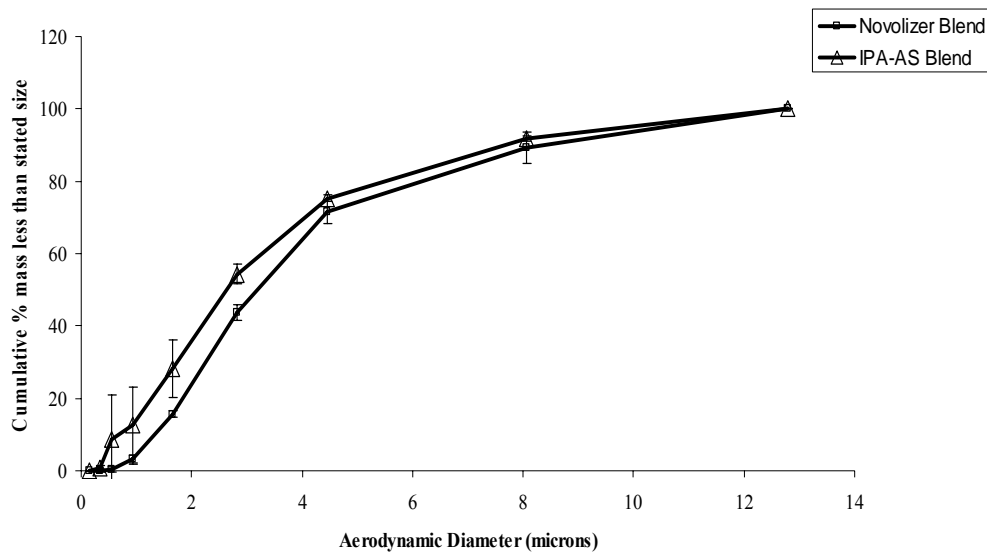


Figure V.12 Cumulative % undersize mass distribution for IPA-AS blend and the commercial Novolizer® formulation aerosolized from the Novolizer® (n=3)

The improved aerosol performance of the IPA-AS / lactose blend compared to the commercial Novolizer formulation was also represented by their MMADs wherein IPA-AS / lactose blend had an MMAD of $2.5 \pm 0.5 \mu\text{m}$ which was significantly lower (p-value < 0.05, one-way ANOVA) compared to the MMAD of $3.2 \pm 0.1 \mu\text{m}$ for the commercial Novolizer® formulation. This difference in MMAD is illustrated in Figure V.12.

The improved aerosol performance of the IPA-AS blend compared to the commercial Novolizer® formulation can also be seen from the fine particle dose with IPA-AS blend producing a significantly higher amount of FPD ($33.4 \pm 0.8 \mu\text{g}$) compared to the commercial Novolizer® formulation (FPD = $25.1 \pm 2.1 \mu\text{g}$). In order to compare the IPA-AS blend performance with the IPA-AS drug only formulation, the fine particle dose had to be normalized with respect to the nominal dose because of the different nominal doses in the two formulations. The IPA-AS drug only formulations employed a nominal dose of 200 μg whereas the IPA-AS / lactose blend used a nominal dose of 120 μg . Table V.6 shows the comparison between the fine particle dose normalized with respect to nominal dose and expressed as a percentage for the two formulations.

Table V.6 Comparison between aerosol performance of IPA-AS drug only formulation and IPA-AS / lactose blend (n=3)

Formulation	(Fine Particle Dose / Nominal Dose) × 100 (μg)
IPA-AS drug only	32.0 ± 0.6
IPA-AS / lactose blend	29.4 ± 0.7

The fine particle dose normalized with respect to the nominal dose was comparable between IPA-AS drug only formulation and IPA-AS / lactose blend (p-value >0.05, one-way

ANOVA). These results demonstrated that the performance of IPA-AS particles was not significantly different when tested either as drug only formulations or as drug / lactose blends.

To summarize the drug / lactose blend studies, significantly higher emitted fractions were obtained compared to the drug / only studies for both IPA-AS blend and the commercial Novolizer® formulation due to the effect of lactose on the cohesive interactions between the drug particles. However, this increase in emitted fraction was accompanied by a decrease in the % FPF (when calculated with respect to emitted dose) for both these formulations relative to the drug only formulations. This was attributed to adherence of drug particles to lactose carrier particles resulting in decreased deaggregation compared to drug only formulations. Furthermore, IPA-AS blend produced a significantly higher % FPF relative to the commercial Novolizer® formulation indicating improved aerosol performance characteristics.

V.D.2 Aerosol performance testing of combination particles

Combination particles 1, 2, and 3 produced from the three separately optimized solvent / anti-solvent crystallization processes were selected for testing their *in vitro* aerosol performance. These particles were comparable in terms of their physical diameter as shown in Table V.2. Combination 1 and 2 were revealed to contain a nominal AS:IB ratio of $\approx 6:1$ (w/w) as described in sections IVD.2.3 and IV.D.2.2. These particles were produced from different solvent / anti-solvent systems as shown in Table V.2. It was discussed in section IV.D.2.3.1 that the relative solubilities of the two drugs in the anti-solvent influence the co-precipitation as combination particles. Since, it was a primary research aim of this project to produce combination particles with a nominal AS:IB ratio of 6:1 (w/w) that show uniform co-deposition, it was of interest to characterize the *in vitro* aerosol performance of combination 1 and 2 to verify whether the

produced particles contained AS and IB in a uniform proportion or not. Furthermore, combination 3 contained AS:IB in a nominal ratio of 2.8:1 (w/w). Therefore, *in vitro* aerosol performance of these particles was characterized to see whether the solvent / anti-solvent crystallization process is capable of producing combination particles in different stoichiometric ratios and also whether the ratio of AS and IB in the combination particles influences their aerosol performance or not.

V.D.2.1 Drug only studies

One of the primary aims of this project is to produce homogeneous combination particles to obtain uniform co-deposition of AS and IB in a fixed nominal ratio of 6:1 (w/w). This is because the conventional combination product containing AS and IB is Combivent® pMDI which is a physical mixture of individually micronized AS and IB in a nominal ratio of 6:1 (w/w) suspended in CFC propellants and soya lecithin (Combivent® package insert). However, such a physical mixture undergoes segregation into individual components resulting in a loss of the fixed drug ratio (Jin et al., 2006). The *in vitro* aerosol performance of the commercial Combivent® pMDI was carried out by Jin et al. (2006) using a NGI at a flow rate of 28.3 L/min. The AS:IB ratios (w/w) across the impactor are shown in Table V.7.

Table V.7 Variation in the AS:IB ratio during aerosolization of the Combivent® pMDI

Stage	AS:IB (w/w)
Throat	5.4:1
S1	5.2:1
S2	4.4:1
S3	4.0:1
S4	5.2:1
S5	10.7:1
S6	20.1:1

Co-deposition of AS and IB in ratios close to the claimed 6:1 (w/w) nominal ratio was observed in the throat and upper impactor stages, However, on the lower stages of the impactor, there were wide variations in the AS:IB ratio with higher AS deposition compared to IB indicating a difference in the aerosolization performance of the two drugs in a physical mixture. Such segregation is undesirable if a uniform co-deposition of the two drugs is needed. Therefore, formulation of combination particles with a fixed proportion of AS and IB that show uniform co-deposition is advantageous and hence constituted a primary aim of this project. Figures V.13 and V.14 show the % AS and % IB expressed as a percentage of the nominal AS and IB dose respectively for combination 1 and 2.

It was seen that the percentage of AS was similar to the percentage of IB on each stage indicating uniform co-deposition for both combination 1 and 2. The AS:IB ratios on the different impactor stages are shown in Tables V.8 and V.9 for combination particles 1 and 2 respectively. The ratios remained consistent at $\approx 6:1$ (w/w) thereby proving that AS and IB deposited uniformly throughout the impactor. These results were therefore superior in terms of co-deposition of AS and IB compared to the commercial Combivent® pMDI.

These results demonstrated that using two different solvent / anti-solvent crystallization systems operating under optimized crystallization conditions, it was possible to produce combination particles which resulted in a uniform *in vitro* co-deposition for the two drugs in a 6:1 (w/w) ratio. Apart from particles containing a 6:1 (w/w) AS:IB ratio, combination particles with a nominal AS:IB ratio of 2.8:1 (w/w) were also produced (combination 3). Figure V.15 shows the % AS and % IB expressed as a percentage of the nominal AS and IB dose respectively for combination particles 3. It was seen that the percentage of AS was similar to the percentage of IB on each stage indicating uniform co-deposition. The AS:IB ratios on the different impactor

stages are shown in Table V.10. The ratios remained consistent at $\approx 2.8:1$ (w/w) thereby proving that AS and IB deposited uniformly throughout the impactor.

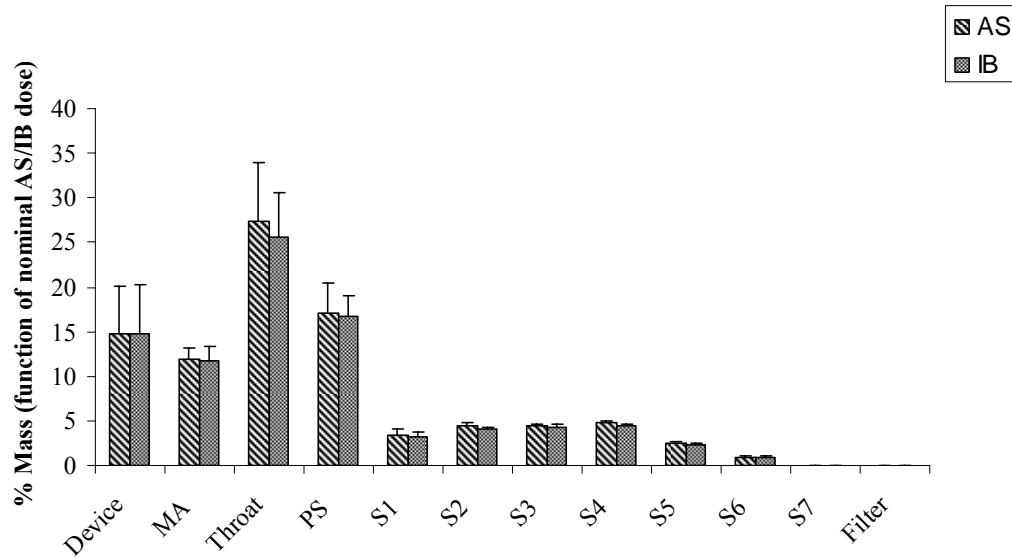


Figure V.13 % mass depositions of AS and IB from combination 1 aerosolized through the Novolizer® as drug only formulations (n=3)

Table V.8 AS and IB ratio for combination particles 1 aerosolized through the Novolizer® as drug only formulations

Stage	AS:IB (w/w)
Device	6.2:1
MA	6.2:1
Throat	6.5:1
PS	6.2:1
S1	6.5:1
S2	6.6:1
S3	6.5:1
S4	6.6:1
S5	6.5:1
S6	5.9:1

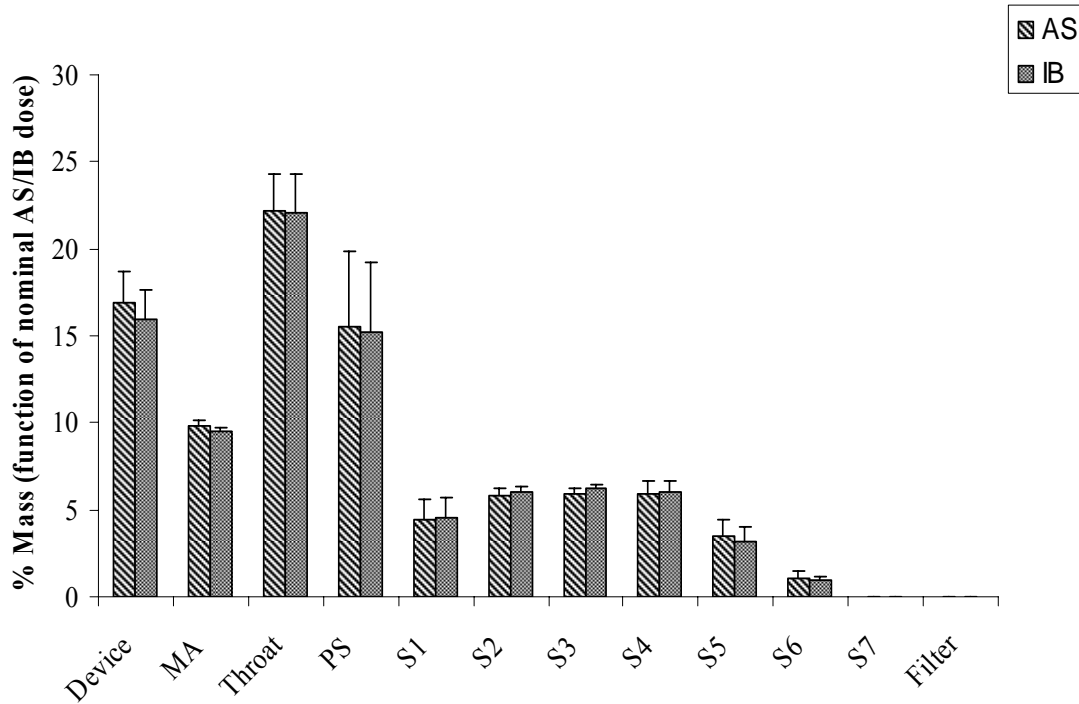


Figure V.14 % mass depositions of AS and IB from combination 2 aerosolized through the Novolizer® as drug only formulations (n=3)

Table V.9 AS and IB ratio for combination particles 2 aerosolized through the Novolizer® as drug only formulations

Stage	AS:IB (w/w)
Device	6.0:1
MA	5.9:1
Throat	5.7:1
PS	5.8:1
S1	5.6:1
S2	5.5:1
S3	5.5:1
S4	5.7:1
S5	6.1:1
S6	6.7:1

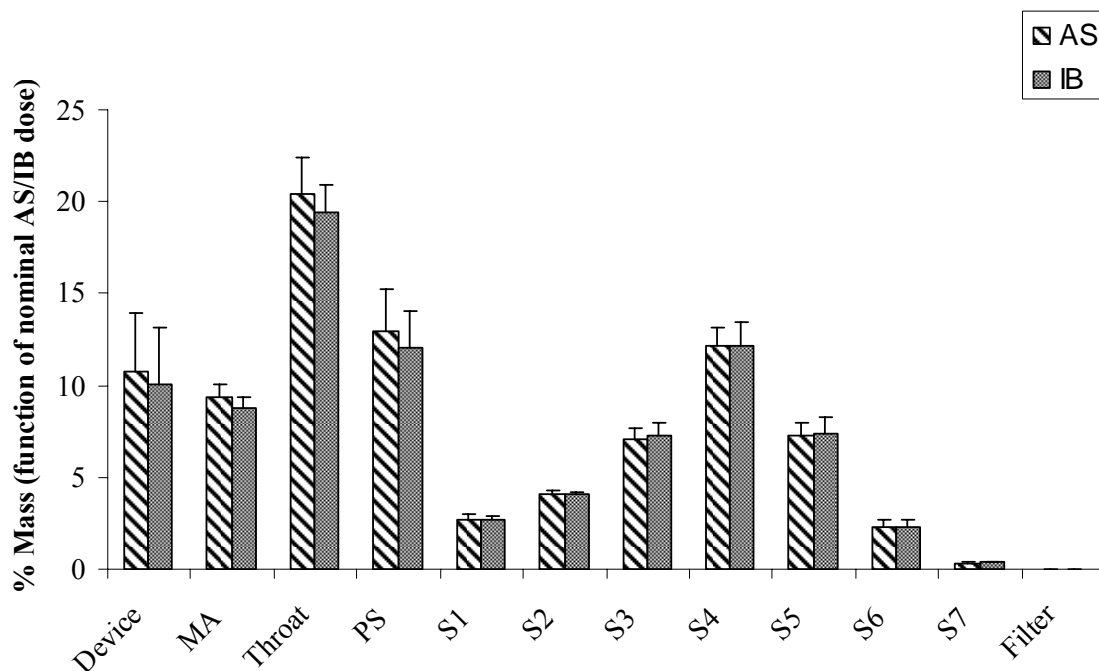


Figure V.15 % mass depositions of AS and IB from combination particles 3 aerosolized through the Novolizer® as drug only formulations (n=3)

Table V.10 AS and IB ratio for combination particles 3 aerosolized through the Novolizer® as drug only formulations

Stage	AS:IB (w/w)
Device	3.1:1
MA	3.1:1
Throat	3.1:1
PS	3.1:1
S1	2.9:1
S2	3.0:1
S3	2.9:1
S4	2.9:1
S5	2.9:1
S6	2.9:1
S7	2.6:1

These results therefore revealed that it was possible to produce combination particles in different proportions using optimized solvent / anti-solvent crystallization processes. These combination particles showed uniform co-deposition on different stages of the impactor during *in*

vitro aerosol performance characterization thereby indicating that the produced particles contained AS and IB in fixed proportions in single particles which resulted in similar aerosol performance for both drugs.

Table V.11 shows the aerosol performance characteristics for combination 1, 2, and 3.

Table V.11 *In vitro* aerosol performance characteristics of combination 1, 2, and 3 tested as drug only formulations (n=3)

Albuterol Sulfate						
Formulation	% Emitted Fraction	Fine Particle Dose (µg)	% FPF	MMAD (µm)	GSD	
Combination 1	75.4 ± 5.5	729.5 ± 24.9	22.3 ± 1.4	3.5 ± 0.1	2.3 ± 0.2	
Combination 2	74.0 ± 1.5	898.6 ± 92.9	28.6 ± 2.6	3.6 ± 0.5	2.3 ± 0.0	
Combination 3	78.4 ± 2.9	1118.3 ± 117.3	39.0 ± 4.0	2.5 ± 0.1	2.2 ± 0.0	
Ipratropium Bromide						
Formulation	% Emitted Fraction	Fine Particle Dose (µg)	% FPF	MMAD (µm)	GSD	
Combination 1	72.9 ± 2.2	112.2 ± 4.7	21.9 ± 1.7	3.4 ± 0.1	2.4 ± 0.0	
Combination 2	73.5 ± 1.2	165.9 ± 17.0	30.3 ± 2.7	3.7 ± 0.5	2.3 ± 0.1	
Combination 3	76.4 ± 1.4	416.7 ± 48.4	43.8 ± 4.5	2.5 ± 0.1	2.2 ± 0.0	

The total emitted fractions for combination 1, 2, and 3 calculated as a function of the total nominal dose of AS+IB were 75.3 ± 5.3 %, 73.9 ± 1.6 %, and 77.4 ± 2.2 % respectively. These emitted fractions were comparable to each other (p-value > 0.05, Tukey’s HSD). However, the % FPFs for combination 3 were significantly higher compared to combination 1 and 2 (p-value < 0.05, Tukey’s HSD) indicating improved dispersivity. The improved aerosol performance for combination 3 was also reflected in the higher fine particle dose for these particles compared to combination 1 and 2 (p-value < 0.05, Tukey’s HSD). This improved aerosol performance for combination 3 may be attributed to their smaller particle size compared to combination 1 and 2 as shown in Table V.2. Furthermore, combination 3 also had a higher volume fraction < 5.0 µm of 48.4 ± 2.2 % compared to combination 1 (42.8 ± 1.6 %) and combination 2 (46.7 ± 1.5 %) which may have contributed to their higher dispersivity and hence a higher fine particle fraction.

Table V.10 also demonstrates that AS and IB exhibited similar emitted fractions, fine particle fractions, MMADs and GSDs in combination 1, 2, and 3. These similarities indicated that AS and IB behaved in a similar manner during aerosolization and there were no particle size differences for the two drugs which indicated the formation of combination particles.

These studies therefore revealed that it was possible to produce homogeneous combination particles with a 6:1 (w/w) nominal ratio from two different solvent / anti-solvent systems different. The nature of these combination particles was confirmed by uniform co-deposition and similar aerodynamic characteristics of emitted fraction, % FPF, MMAD and GSD for AS and IB during *in vitro* aerosolization. Furthermore, it was also possible to produce homogeneous AS/IB particles with different stoichiometric ratios that showed uniform co-deposition during *in vitro* characterization from the solvent / anti-solvent crystallization process.

V.D.2.2 Drug / lactose blend studies

Combination 1, 2, and 3 were tested as drug / lactose blends as described in section V.C.2.1.2. The % RSDs for AS and IB for combination 1, 2, and 3 lactose blends are shown in Table V.12. % RSDs < 5% for all combination particles were indicative of acceptable blend homogeneity.

Table V.12 Blend homogeneity for combination 1, 2, and 3

Formulation	% RSD	
	AS	IB
Combination 1 / lactose blend	2.2	4.9
Combination 2 / lactose blend	2.0	3.8
Combination 3/ lactose blend	2.1	3.0

The AS:IB (w/w) ratios on the different stages of the impactor for combination 1, 2, and 3 are shown in Table V.13.

Table V.13 AS:IB (w/w) ratios deposited on different stages of the impactor after aerosolization of combination 1, 2, and 3 as drug / lactose blends

Stage	Combination 1	Combination 2	Combination 3
Device	6.2:1	6.1:1	2.9:1
MA	6.2:1	5.7:1	2.8:1
Throat	6.5:1	5.7:1	3.0:1
PS	6.2:1	6.1:1	3.1:1
S1	6.5:1	6.0:1	2.9:1
S2	6.6:1	5.8:1	3.0:1
S3	6.5:1	5.7:1	2.8:1
S4	6.6:1	5.9:1	2.9:1
S5	6.5:1	5.8:1	3.0:1
S6	5.9:1	6.5:1	3.0:1

These results demonstrated that AS and IB co-deposited during aerosolization of combination 1, 2, and 3 as drug / lactose blends. Table V.14 shows the *in vitro* aerosol performance characterization results for combination 1, 2, and 3.

Table V.14 *In vitro* aerosol performance characteristics of combination 1, 2, and 3 tested as drug / lactose blends (n=3)

Albuterol Sulfate					
Formulation	% Emitted Fraction	Fine Particle Dose	% FPF	MMAD (µm)	GSD
Combination 1	77.3 ± 0.6	15.2 ± 0.4	20.3 ± 0.3	3.3 ± 0.0	2.7 ± 0.0
Combination 2	81.8 ± 1.9	16.8 ± 1.3	21.2 ± 1.1	3.3 ± 0.1	2.6 ± 0.0
Combination 3	96.4 ± 0.9	13.0 ± 1.2	14.6 ± 1.3	2.8 ± 0.1	3.5 ± 0.0
Ipratropium Bromide					
Formulation	% Emitted Fraction	Fine Particle Dose	% FPF	MMAD (µm)	GSD
Combination 1	77.4 ± 0.6	2.3 ± 0.1	20.1 ± 0.3	3.3 ± 0.0	2.7 ± 0.0
Combination 2	80.7 ± 2.0	2.9 ± 0.2	21.3 ± 1.2	3.4 ± 0.1	2.6 ± 0.0
Combination 3	94.7 ± 0.8	4.6 ± 0.4	15.6 ± 1.4	2.7 ± 0.1	3.6 ± 0.0

Comparisons between the aerosol characteristics such as emitted fraction, % FPF, MMAD, and GSD of AS and IB for all three types of combination particles did not reveal any significant differences (p -values > 0.05 , one-way ANOVA) between the aerodynamic performances of the two drugs. For example, combination particles 1 produced an emitted fraction of $77.3 \pm 0.6 \%$ for AS and $77.4 \pm 0.6 \%$ for IB. The corresponding % FPFs were 20.3 ± 0.3 and $20.1 \pm 0.3 \%$ respectively. Similarly, combination particles 2 produced an emitted fraction of $81.8 \pm 1.9 \%$ for AS and $80.7 \pm 2.0 \%$ for IB. The corresponding % FPFs were 21.2 ± 1.1 and $21.3 \pm 1.2 \%$ respectively. Combination particles 3 produced an emitted fraction of $96.4 \pm 0.9 \%$ for AS and $94.7 \pm 0.8 \%$ for IB. The corresponding % FPFs were 14.06 ± 1.3 and $15.6 \pm 1.4 \%$ respectively. These results indicated that AS and IB interacted in a similar fashion with lactose carrier particles by virtue of being present as combination particles.

Combination particles prepared by other particle engineering techniques have been reported in literature. Using the SAXS technique, Dhillon et al have produced 1:1 (w/w) combination particles of theophylline and fluticasone propionate with a reported VMD of $1.6 \mu\text{m}$. They tested the *in vitro* aerosol performance of these particles as dry powder formulations by preparing a 1.6% w/w blend with lactose monohydrate and testing it via a Cyclohaler and NGI at 90 L/min . Their results indicated that upon aerosolization more theophylline was delivered compared to fluticasone propionate (% FPF of $33.4 (7.7) \%$ vs. $15.5 (1.1) \%$). The authors have attributed this difference to mechanical disruption of particles upon blending with lactose. These results were therefore in contrast to the similar fine particle fractions for AS and IB in our studies and therefore suggested the formation of combination particles.

The drug / lactose blend studies therefore provided further proof for the formation of combination particles in which both AS and IB interacted in a similar fashion with lactose by

virtue of being present in fixed proportions in single combination particles. These combination particles showed uniform co-deposition of AS and IB during *in vitro* aerosolization and were therefore superior to the commercial Combivent® pMDI formulation containing a physical mixture of individually micronized AS and IB.

V.E CONCLUSIONS

The *in vitro* aerosol performance testing of the engineered AS particles and combination particles of AS and IB revealed several important points. For AS particles, the single most overriding conclusion was that using an optimized solvent / anti-solvent crystallization process with hydrodynamic control alone led to the formation of particles with suitable characteristics for inhalation. The aerodynamic characteristics of these engineered AS particles were found to be superior to the conventionally used micronized AS in terms of higher emitted fractions and % fine particle fraction. However, the aerosol performance was a strong function of the device used to aerosolize these formulations with the best performance being achieved from the Novolizer® DPI. This was attributed to the design features incorporated in the Novolizer® for device emptying and powder dispersion.

The *in vitro* aerosol performance characterization of combination particles of AS and IB revealed similar aerodynamic characteristics of AS and IB due to the incorporation of the two drugs into single combination particles. These combination particles resulted in uniform co-deposition of the two drugs in a fixed nominal ratio throughout the impactor. This was contrary to the undesirable segregation behavior of a physical mixture of individually micronized AS and IB employed in the commercial combination formulation, Combivent® pMDI.

CHAPTER VI

OVERALL DISCUSSION AND SUMMARY

Dry powder inhalers (DPIs) are becoming increasingly popular for pulmonary drug delivery. A critical component of the DPI system is the drug particle used in the formulation. The drug particles should possess a number of key properties for successful formulation and lung delivery. They should be of a suitable aerodynamic diameter for inhalation; the particles should be crystalline for long term shelf life formulation stability and have a reproducible morphology. Presently, the most commonly used technique to produce inhalation drug particles is micronization which is an energy intensive milling process to reduce the size of large particles to a suitable size for inhalation. However, this technique offers limited opportunities to optimize and control the physical and chemical particle properties described above. Micronization is also known to induce crystalline disorder in the particles leading to formulation instability. Therefore, it would be advantageous to develop single step particle engineering processes capable of directly yielding particles suitable for inhalation without the need for further size reduction.

Several particle engineering processes have been studied in literature. These include spray drying, supercritical fluids and controlled precipitation. Among controlled precipitation, sonocrystallization (Dennehy et al., 2003; Dhumal et al., 2009; Kaerger et al., 2003), *in situ* micronization (Rasenack et al., 2002), and high gravity controlled precipitation (Chiou et al., 2007) have been investigated. These controlled precipitation techniques employ solvent / anti-solvent crystallization coupled with an external energy source (sonocrystallization, high gravity

controlled precipitation) or crystal growth modifiers (*in situ* micronization) to control the particle size. However, most of these techniques are either complex with special equipment needs or difficult to scale up. The solvent / anti-solvent crystallization process has a number of parameters that lend themselves to optimization and control in order to manipulate the final product characteristics. It would therefore be desirable to develop a simple solvent / anti-solvent crystallization process that controls particle size through optimization of the hydrodynamic factors alone. However, to do so, it is important to understand the mechanism of solvent / anti-solvent crystallization and the influence of critical processing variables on particle characteristics.

In this project, a design of experiment (DoE) approach was used to investigate the influence of critical crystallization variables associated with solvent / anti-solvent crystallization of albuterol sulfate on two response variables: particle crystallinity and particle size. The aim was to produce completely crystalline particles of albuterol sulfate in a single step in a size suitable for inhalation, using hydrodynamic control alone without any crystal growth modifiers or an external energy source. Water and ethyl acetate have been used as solvent and anti-solvent for albuterol sulfate (Nocent et al., 2001). Complete crystallization of albuterol sulfate after a crystal maturation time of 30 minutes is reported. Using this solvent / anti-solvent system, the crystallization variables investigated included the solvent / anti-solvent ratio (R_a ratio; w/w) at three levels of 1:200, 1:500, and 1:1000 (w/w), stirring speed at four levels of 100, 200, 500, and 800 r.p.m., and crystal maturation time varying from 0-24 hours. Particle formation was observed to be complete after 30 minutes of stirring designated as crystal maturation time = 0. In contrast to the results reported in literature by Nocent et al., the particles were found to be partially crystalline under all crystallization conditions at crystal maturation time = 0. However,

complete crystallization of these particles was observed when they were harvested and dried under ambient conditions indicating that the particle crystallinity reported in literature is a function of harvesting and drying the particles. The particle size of these particles was found to be too large for inhalation (i.e. $> 20 \mu\text{m}$ for all crystallization conditions). It was hypothesized that the large particle size was contributed in part by solid-state crystallization of these partially crystalline particles upon harvesting which led to the formation of crystal bridges between adjacent particles and particle fusion. This was an undesirable phenomenon particularly for aerosol formulations where size is a primary concern.

Therefore, to bring about complete crystallization prior to harvesting, the effect of longer crystal maturation times was investigated. As a function of longer crystal maturation time, differences in crystallization behavior of the particles were observed. Particles produced from R_a ratio 1:200 and 1:500 (w/w) at all stirring speeds were observed to increase in crystallinity as a function of increasing crystal maturation time and were observed to be completely crystalline at the end of 24 hours. A similar increase in crystallinity was demonstrated by the particles produced from R_a ratio 1:1000 (w/w) produced under low stirring speeds of 100 and 200 r.p.m. when they were allowed to remain in the solvent / anti-solvent mixture. In contrast, particles produced at higher stirring speeds of 500 and 800 r.p.m. did not undergo an increase in crystallinity as a function of longer crystal maturation times and remained incompletely crystalline at the end of 24 hours. These studies therefore revealed a significant influence of crystallization conditions on particle crystallinity. A statistical analysis of the effect of different crystallization variables on particle crystallinity revealed that R_a ratio, stirring speed, and crystal maturation time demonstrated significant interaction with each other and the effect of any one crystallization variable could not be discussed in isolation with the rest. This was a potentially

important finding since there are currently no studies in literature that characterize the effects of different crystallization variables on solution crystallinity of albuterol sulfate particles.

The differences in crystallization behavior of the particles were explained by the role of supersaturation and the % water content of the particles. The plasticizing effect of water has been extensively studied in literature and it has been shown that water uptake into the partially crystalline regions results in re-crystallization (Crowley and Zografí, 2002; Marsac et al., 2008; Wu and Yu, 2006; Ward and Schultz, 1995). However, any studies characterizing the role of water in solution crystallization are currently absent. The studies with albuterol sulfate revealed a significant role of water in solution crystallization, wherein particles undergoing complete solution crystallization (R_a ratio 1:200, 1:500 at all stirring speeds and R_a ratio 1:1000 at 100 and 200 r.p.m.) contained water at higher levels (> 20%) at crystal maturation time = 0 compared to particles that did not show complete solution crystallization within 24 hours (R_a ratio 1:1000 at 500 and 800 r.p.m.). These latter particles contained significantly lower % water contents (9-10%). Further, TGA analysis revealed that the higher % water content was lost at lower temperatures (25°C) compared to the lower % water contents which were lost at higher temperatures (60°C). This indicated that the lower % water was bound more tightly to the particles compared to the higher % water. Zografí et al. have reported lower plasticizing efficiency of water when it is present in a tightly bound form (Zografí et al., 1988). This lower plasticizing efficiency may have contributed towards the incomplete solution crystallization for the particles produced from R_a ratio 1:1000 (w/w) at higher stirring speeds of 500 and 800 r.p.m.

Measurement of particle size distribution of the particles at crystal maturation time = 24 hours revealed the formation of significantly smaller particles compared to crystal maturation time = 0 for all particles except those produced from R_a ratio 1:1000 (w/w) under 500 and 800

r.p.m. This finding lent support to the hypothesis that the large particle sizes observed at crystal maturation time = 0 were a function of incomplete solution crystallization, subsequent solid-state crystallization and formation of crystal bridges between particles. Therefore, these results emphasized the importance of harvesting completely crystalline particles. The particle size was found to be significantly influenced by an interaction between R_a ratio, stirring speed and crystal maturation time in a manner similar to that observed for particle crystallinity. The smallest particles among all crystallization conditions were produced from R_a ratio 1:200 (w/w) at 200 r.p.m. after a crystal maturation time of 24 hours and had a VMD of $9.7 \pm 0.7 \mu\text{m}$. These results were explained by the supersaturation levels for the three R_a ratios. R_a ratio 1:200 (w/w) with the highest supersaturation ratios of 5.2 compared to R_a ratio 1:500 and 1:1000 (w/w) with lower supersaturation ratios of 4.5 and 3.4 would exhibit a higher driving force for nucleation, cause a narrower MSZW and result in increased formation of smaller particles as described in section III.D.2.1.2.

These studies cast insight into the mechanisms of solvent / anti-solvent crystallization and the influence of crystallization variables on particle crystallinity and particle size. Further, the effects of the crystallization variables were not treated in isolation from each other which has been the case with similar studies reported in literature (O'Grady et al., 2001; Abdel-Al et al., 2004; Genoveva et al., 2007). Crystallization is a dynamic process with a complex interplay between the different crystallization conditions influencing the particle characteristics. Therefore, it is necessary to understand these interactions in order to control and optimize the crystallization variables and produce particles with the desirable characteristics.

The investigational studies with solvent / anti-solvent crystallization yielded a set of crystallization conditions resulting in the smallest AS particles with a VMD of $9.7 \pm 0.7 \mu\text{m}$.

However, these particles were not in a size suitable for inhalation. Therefore, in order to reduce the particle size, the role of temperature difference between the solvent and anti-solvent was investigated. These studies were carried out for the optimized set of crystallization conditions i.e.; a R_a ratio of 1:200, a stirring speed of 200 r.p.m. and a crystal maturation time of 24 hours. A temperature difference of 65°C between the drug solution and anti-solvent resulted in the formation of AS particles with a smaller VMD of $8.8 \pm 0.6 \mu\text{m}$. Though the particles obtained were small, they were not in the particle size range suitable for inhalation. Further, this diameter was obtained using Malvern Mastersizer which is calibrated with spherical particles. Therefore, accuracy in the particle size for non-spherical particles such as the ones in these studies cannot be ascertained. But, it still serves as a useful estimate to get a preliminary idea about the size of the produced particles. However, it is the aerodynamic diameter of the particles that is important for their aerosol performance and not the geometric diameter obtained from the Malvern Mastersizer. Therefore, it is necessary to carry out *in vitro* aerosol performance tests using impaction studies in order to estimate the inhalation efficiency of these particles.

Based on the PSD results, ethyl acetate did not result in particles small enough for inhalation. Therefore, isopropyl alcohol was investigated as an alternate anti-solvent. Dhumal et al. have reported the formation of inhalation sized particles with IPA when used in conjunction with ultrasonication (Dhumal et al., 2009). Using the previously optimized set of crystallization conditions (R_a ratio 1:200, stirring speed 200 r.p.m., crystal maturation time 24 hours) and isopropyl alcohol as the new anti-solvent, significantly smaller AS particles with a VMD of $4.9 \pm 0.3 \mu\text{m}$ were produced. These particles were in a size range of 1-5 μm and were therefore deemed to be suitable for inhalation. These particles were smaller compared to the $\approx 20 \mu\text{m}$ particles reported by Dhumal et al. from the solvent / anti-solvent system of water / IPA using

mechanical stirring alone in the absence of ultrasonication. These results therefore, reiterated the importance of optimization of crystallization conditions and demonstrated that it was possible to utilize hydrodynamic control alone without the use of an external energy source or crystal growth modifiers to produce particles with suitable size characteristics for inhalation. However, as was the case with the ethyl acetate particles, *in vitro* aerosol performance testing of these particles was necessary in order to make judgments about their inhalation efficiency.

Proceeding forward from the development of an optimized single step solvent / anti-solvent crystallization process for the production of inhalation particles of albuterol sulfate, this project also aimed at extending this process to produce combination particles of albuterol sulfate and ipratropium bromide monohydrate in different ratios in a size suitable for inhalation. It was hypothesized that these combination particles would result in uniform co-deposition of AS and IB and hence overcome the disadvantages of segregation and loss of fixed drug ratio associated with physical mixtures of individually micronized AS and IB. Such segregation has been reported by Jin et al. (2006) for Combivent® pMDI which is a physical mixture of AS and IB in a nominal 6:1 (w/w) ratio.

The initial solvent / anti-solvent system chosen for these studies was water / ethyl acetate with a R_a ratio of 1:200, a stirring speed of 200 r.p.m. and a crystal maturation time of 24 hours. This process resulted in the formation of combination particles containing AS and IB in a nominal ratio of 1:1, 2.1:1, 6.2:1, and 10.7:1 (w/w). These ratios were achieved from starting drug solutions containing similar AS:IB ratios of 1:1, 2:1, 6:1, and 10:1 (w/w). These results indicated complete precipitation of AS and IB and demonstrated that ethyl acetate acted as a good anti-solvent for both drugs. Further, it was possible to predict the final AS:IB ratio based on the known initial ratio of the drug solution which is a useful characteristic.

Thermal analysis of these particles revealed them to have a single melting peak and the heat of fusion of this melt was observed to increase with the proportion of AS. Furthermore, IB was found to be in a completely hydrated form in these particles containing one mole of water of crystallization. Since this water is incorporated in the IB crystal lattice, this observation indicated the crystalline nature of IB in these particles. Thermal analysis coupled with powder X-ray diffraction analysis revealed these particles to have different properties compared to pure AS, pure IB, or a physical mixture of AS and IB. These results indicated interactions between AS and IB which were not present when these drugs were blended together. However, the exact nature of these interactions could not be elucidated and the presence or absence of co-crystals could not be concluded. Therefore, these particles were designated as combination particles. All of these particles were revealed to be in a size range too large for inhalation (VMD = 11 - 20 μm) with the smallest size obtained for the 10:1 (w/w) combination particles.

Further optimization of the process to reduce the particle size investigated IPA as anti-solvent since it had earlier resulted in smaller AS particles. Due to the solubility differences between AS and IB in IPA, the initial drug concentrations, solvent anti-solvent ratio, and crystal maturation time had to be optimized in order to achieve co-precipitation and form combination particles from this anti-solvent. The optimized R_a ratio was 1:20 (w/w). Starting with an initial AS:IB ratio of 0.48:0.28 g/g (AS:IB = 1.7:1 w/w), combination particles with a final AS:IB ratio of 2.8:1 (w/w) were produced after a crystal maturation time of 5 minutes. Changing the initial AS:IB ratio to 0.48:0.08 g/g (AS:IB = 6:1 w/w), resulted in combination particles with a final AS:IB ratio of 5.7:1 (w/w). Therefore, it was not possible to predict the final ratio in the combination particles from the initial ratio in all cases. The VMDs for the 2.8:1 (w/w), and 5.7:1 (w/w) combination particles were $5.3 \pm 1.0 \mu\text{m}$ and $6.5 \pm 0.3 \mu\text{m}$ respectively. These particles

were therefore deemed to be in a size range suitable for inhalation. However, as was the case with AS particles, it was important to test the *in vitro* aerosol performance of these particles to make conclusions about their inhalation efficiency. Thermal analysis and PXRD revealed differences from AS, IB and physical mixtures. However, no conclusions about the formation of co-crystals could be drawn.

Although IPA yielded combination particles in a stoichiometric ratio in a size suitable for inhalation, the solubility differences between AS and IB make it a difficult anti-solvent for the production of combination particles (Chiarella et al., 2007). Further, it is not possible to predict the final AS:IB ratio from the initial ratio in the drug solution. Therefore, in an attempt to utilize the size reduction efforts of IPA and achieve co-precipitation of AS and IB, IPA was mixed with ethyl acetate in different proportions of 1:1, 1:2, 1:5, and 1:10 (w/w) and used as the anti-solvent at a R_a ratio of 1:200 (w/w), a stirring speed of 200 r.p.m. and a crystal maturation time of 24 hours. Co-precipitation of AS and IB was only achieved from IPA:EA 1:10 (w/w). However, this anti-solvent did not produce particles in an optimum size for inhalation. Therefore, in an attempt to reduce the particle size, the anti-solvent comprised of IPA:EA 1:10 (w/w) was cooled in dry ice to achieve a temperature difference of 65°C between the solvent and anti-solvent. These studies led to the formation of significantly smaller combination particles with AS:IB ratios of 1.:1, 1.9:1, 6.6:1, and 8.6:1 (w/w) when starting with an initial AS:IB ratio of 1:1, 2:1, 6:1, and 10:1 (w/w) respectively. These results demonstrated that AS and IB precipitated out completely from this anti-solvent and it was possible to predict the final ratio in the combination particles based on the starting drug concentrations of AS and IB. The thermal properties of these combination particles were similar to the combination particles with the corresponding drug

proportions produced from ethyl acetate. However, the formation of co-crystals could not be concluded.

The particles of particular interest were the 6.6:1 (w/w) particles since they contained AS and IB in a similar stoichiometric ratio as the commercial formulation; Combivent® pMDI. Using IPA:EA 1:10 (w/w) as the anti-solvent at a temperature difference of 65°C resulted in the formation of combination particles with a nominal AS:IB ratio of 6.6:1 (w/w) and a VMD of $6.9 \pm 1.1 \mu\text{m}$. These particles were therefore in a size suitable for inhalation. However, it is necessary to test the *in vitro* aerosol performance of these particles to further assess their inhalation efficiency.

These studies therefore demonstrated that it was possible to optimize the solvent / anti-solvent crystallization process developed for AS to produce combination particles of AS and IB in a size suitable for inhalation. These combination particles also revealed differences from AS, IB, and their physical mixtures indicating that AS and IB interacted with each other within a combination particle matrix. A plausible scenario explaining the thermal and powder X-ray diffraction results for the combination particles was the formation of interstitial crystalline solid solution with IB molecules occupying the interstitial spaces within the AS crystal lattice. Pilot molecular modeling studies were carried out to investigate the nature of interaction between AS and IB. Using computational methods employing HINT to classify and score the interactions between AS and IB molecules revealed sites on both molecules with the capability to participate in non covalent interactions. Manual orientation studies revealed three orientations between AS and IB that resulted in an overall positive HINT score indicating favorable interactions. The highest HINT score obtained was 156.71. The positive interactions contributing to this overall score were H-bonding, acid-base interactions and hydrophobic interactions while the negative

interactions were acid-acid, hydrophobic-polar and acid-base interactions. These studies therefore revealed that within a combination particle matrix, AS and IB will orient in a way to maximize the positive interactions.

Due to the possibility of bias associated with manual orientation studies, docking studies using GOLD were carried out where a single ipratropium molecule was docked in a 2×2×2 cube constructed of AS unit cells with a cavity created in it by the removal of a single AS molecule. The total HINT scores obtained for each of the dockings were negative except for one GA run in docking position # 5 which resulted in a positive HINT score of 248.2. At first glance, these negative total HINT scores implied an overall unfavorable interaction between AS and IB. However, upon looking into the breakup of the total HINT scores, it was observed that there were positive components as well that were contributed mainly by hydrogen bonding and hydrophobic interactions. However, since the IB molecule was surrounded by tightly packed AS molecules, the close proximity led to unfavorable acid-acid and base-base interactions which resulted in a total negative HINT score. These studies however showed that there were a number of positive interactive sites present on both molecules. These computational studies therefore revealed that within a combination particle matrix, IB will orient itself to present its hydrophobic bonding sites close to the hydrophobic binding sites of albuterol sulfate and its polar binding sites close to the polar AS sites which will favor the formation of H-bonds and other non-covalent positive interactions.

Since this project hypothesized that the engineered AS particles and combination particles of AS and IB would have a superior aerosol performance compared to conventionally used micronized drug and individually micronized physical mixtures respectively, the *in vitro* aerosol performance testing of AS particles and combination particles of AS and IB was carried

out. AS particles produced from the optimized crystallization conditions using ethyl acetate (EA-AS) and IPA (IPA-AS) were tested as drug only formulations from three DPIs; Novolizer®, Rotahaler®, and Nektar PDS®. The aerosol performance was compared with micronized AS (MIC-AS). A significant powder-device interaction was observed. IPA-AS and EA-AS particles resulted in significantly higher emitted fractions compared to the conventionally used micronized particles when aerosolized from the Novolizer® and Rotahaler®. These higher emitted fractions were indicative of better flow properties of these particles and were attributed to decreased cohesive forces. The reasons for these decreased cohesion was attributed to the presence of larger particles acting as inbuilt binary mixtures as well as reduced surface energy for these engineered particles relative to micronized particles. Powder dispersivity represented as the fine particle fraction was found to be highest for micronized AS. However, this increased powder dispersivity did not translate into improved overall performance of these particles represented by the fine particle dose. AS particles produced from the solvent / anti-solvent crystallization process using isopropyl alcohol as the anti-solvent resulted in a superior aerosol performance compared to micronized albuterol sulfate when aerosolized from the Novolizer®. Drug / lactose blend studies also revealed a significantly improved aerosol performance for IPA-AS blend compared to the commercial Novolizer® dry powder formulation for AS. These results therefore demonstrated that the optimized solvent / anti-solvent crystallization process yielded AS particles with superior aerosol performance characteristics compared to conventionally used micronized particles. This was an important observation since it signified the applicability of a well understood and controlled solvent / anti-solvent crystallization process as a simple single-step particle engineering technique to produce inhalation particles.

In vitro aerosol performance testing of the combination particles as drug only formulations from the Novolizer® revealed uniform co-deposition of AS and IB in a fixed nominal ratio throughout the impactor from 2.8:1 and 5.7:1 (w/w) combination particles produced from IPA and 6.6:1 (w/w) combination particles produced from IPA:EA 1:10 (w/w). These studies were in contrast to the results reported by Jin et al. for the commercial Combivent® pMDI (Jin et al., 2006). This commercial formulation is a physical mixture of individually micronized AS and IB which shows segregation and loss of the fixed drug ratio during aerosolization. Testing of these combination particles as lactose blends from the Novolizer® also revealed uniform co-deposition of AS and IB in a fixed nominal ratio. Combination particles prepared by other particle engineering techniques have been reported in literature. Corrigan et al. have used spray drying to prepare combination particles of AS and IB. These particles were however amorphous in nature (Corrigan et al., 2006). Using sonocrystallization, Pitchayajittipong et al. have reported combination particles of formoterol and budesonide. However, *in vitro* aerosol performance testing of these particles has revealed a loss of the fixed drug ratio (Pitchayajittipong et al., 2009).

Therefore, in these studies, it was possible to produce combination particles demonstrating co-deposition of AS and IB from two separate solvent / anti-solvent systems. These combination particles demonstrated advantages over conventionally used physical mixtures and signified that it was possible to develop a simple solvent / anti-solvent crystallization process that could be used as a particle engineering technique to produce combination particles of AS and IB.

In summary, crystallization conditions were found to significantly influence particle characteristics of AS. Investigation and optimization of these conditions resulted in the

development of a solvent / anti-solvent crystallization process capable of producing albuterol sulfate particles and combination particles of albuterol sulfate and ipratropium bromide with suitable characteristics for inhalation. These particles engineered from the optimized solvent / anti-solvent crystallization process showed superior aerosol performance characteristics compared to the conventionally used micronized powders for inhalation therapy by dry powder formulations. It was also possible to extend the solvent / anti-solvent crystallization process to produce combination particles of AS and IB in different ratios in a size suitable for inhalation. These combination particles resulted in co-deposition of AS and IB in a fixed ratio during *in vitro* studies and hence provided a significant advantage over the physical mixtures used for combination therapy. Further, as it was possible to produce these combination particles from a simple single-step particle engineering technique, they also offered advantages over the conventionally used micronized particles. Therefore, these studies revealed that if investigated and optimized, it was possible to use only hydrodynamic conditions associated with solvent / anti-solvent crystallization to produce particles for inhalation.

LIST OF REFERENCES

- Aakeroy, C.B.; Salmon, D.J. (2005). Building Cocrystals with molecular sense and supramolecular sensibility. *Crys. Eng. Comm.*, **7**, 439-448.
- Abdel-Al, E.A.; Rashad, M.M.; El-Shall, H. (2004). Crystallization of calcium sulfate dihydrate at different supersaturation ratios and different free sulfate concentrations. *Cryst. Res. Technol.*, **39**, 313-321.
- Almarsson, O.; Zaworotko, M.J. (2004). Crystal engineering of the composition of pharmaceutical phases. Do pharmaceutical co-crystals represent a new path to improved medicines? *Chem. Commun.*, 1889-1896.
- Balashazy, I.; Martonen, T.B.; Hoffman, W. (1990). Fiber deposition in airway bifurcations. *J. Aerosol Med*, **3**, 243-260.
- Barrett, P.; Smith, B.; Worlitschek, J.; Bracken, V.; O'Sullivan, B.; O'Grady, D. (2005). A Review of the use of Process Analytical Technology for the understanding and Optimization of Production Batch Crystallization Processes. *Org Process Res and Dev.*, **9**, 348-355.
- Bassett, D.C.; Olley, R.H.; Al Raheil, A.M. (1988). On crystallization phenomenon in PEEK. *Polymer*, **29**, 1745-1754.
- Beckmann, W. (2000). Seeding the desired polymorph: background, possibilities, limitations, and case studies. *Org Process Res Dev*, **4**, 372-383.
- Begat, P.; Young, P.M.; Edge, S.; Kaerger, J.S.; Price, R. (2002). The effect of mechanical processing on surface stability of pharmaceutical powders: visualization by atomic force microscopy. *J. Pharm. Sci.*, **92**, 611-620.
- Berard, V.; Lesniewska, E.; Andres, C.; Pertuy, D.; Laroche, C.; Pourcelot, Y. (2002). Affinity scale between a carrier and a drug in DPI studied by atomic force microscopy. *Int. J. Pharm.*, **247**, 127-137.
- Blagden, N.; Berry, D.J.; parkin, A.; Javed, H.; Ibrahim, A.; Gavan, P.T.; De Matos, L.L.; Seaton, C.C. (2008). Current directions in co-crystal growth. *New J. Chem.*, **32**, 1659-1672.

Bodemeier, R.A.; Wang, H.; Dixon, D.J.; Mawson, S.; Johnston, K.P. (1995). Polymeric microspheres prepared by spraying into compressed carbon dioxide. *Pharm. Res.*, **12**, 1211-1217.

Bryant, D.H. (1985). Nebulized Ipratropium Bromide in the Treatment of Acute Asthma. *Chest*. **88**, 24-29.

Burton, W.K.; Cabrera, N.; Frank, F.C. (1951). The growth of crystals and the equilibrium structure of their surfaces. *Phil Trans. R. Soc.*, **A243**, 299–358.

Calderdale and Huddersfield. Discontinuation of Combivent Metered Dose Inhaler (MDI). NHS Foundation Trust.

Cegla U.H.U. (2004). Pressure and inspiratory flow characteristics of dry powder inhalers. *Respir. Med.*, **98**, S22-S28.

Chan, H.K.; Gonda I. (1995). Physicochemical characterization of a new respirable form of nedocromil. *J. Pharm. Sci.*, **84**, 692-696.

Chan, H.K.; Chew, N.Y.K. (2003). Novel alternative methods for the delivery of drugs for the treatment of asthma. *Adv. Drug Deliv. Rev.*, **55**, 793-805.

Chan, H.K. (2006). Dry powder aerosol drug delivery opportunities for colloid and surface scientists. *Colloids Surf.*, **A284-285**, 50-55.

Chattopadhyay, S.; Erdemir, D.; Evans, J.M.B.; Ilavsky, J.; Amenitsch, H.; Segre, C.U.; Myerson, A.S. (2005). SAXS study of the nucleation of glycine crystals from a supersaturated solution. *Cryst. Growth Des.*, **5**, 523 – 527.

Chew, N.Y.K.; Tang, P.; Chan, H.K.; Raper, J.A. (2005). How much particle surface corrugation is sufficient to improve aerosol performance of powders? *Pharm. Res.*, **22**, 148-152.

Chew, N.Y.K.; Chan, H.K.; Bagster, D.F.; Mukhraya, J. (2002). Characterization of pharmaceutical powder inhalers: estimation of energy input for powder dispersion and effect of capsule device configuration. *J. Aerosol Sc.*, **33**, 999-1008.

Chiarella, R.A.; Davey, R.J.; Peterson, M.A. (2007). Making Cocrystals- The utility of Ternary Phase Diagrams. *Crys. Growth Des.*, **7**, 1223-1226.

Chiou, H.; Li, L.; Hu, T.; Chan, H.K.; Chen, J.F.; Yun, J. (2007). Production of Salbutamol Sulfate for inhalation by high-gravity controlled antisolvent precipitation. *Int J Pharm.*, **331**, 93-98.

Chow, A.H.; Tong, H.H.; Chattopadhyay, P.; Shekunov, B.Y. (2007). Particle engineering for pulmonary drug delivery. *Pharm Res*, **24**, 411–437.

Combivent Package Insert, Boehringer Ingelheim.

Corrigan, D.O.; Corrigan, O.I.; Healy, A.M. (2006). Physicochemical and In Vitro Deposition Properties of Salbutamol Sulfate / Ipratropium Bromide and Salbutamol Sulfate / Excipient Spray Dried Mixtures for Use in Dry Powder Inhalers. *Int. J. Pharm.*, **322**, 22-30.

Crowder, T.M.; Rosati, J.A.; Schroeter, J.D.; Hickey, A.J.; Martonen, T.B. (2002). Fundamental effects of particle morphology on lung delivery: predictions of Stokes' law and the particular relevance to dry powder inhaler formulation and development. *Pharm. Res*, **19**, 239-245.

Crowder, T.; Hickey, A. (2006). Powder specific active dispersion for generation of pharmaceutical aerosols. *Int. J. Pharm.*, **327**, 65-72.

Davey, R.; Garside, J. (2000). From molecules to crystallizers: an introduction to crystallization. Oxford: Oxford University Press.

Davey, R.J.; Allen, K.; Blagden, N.; Cross, W.I.; Lieberman, H.F.; Quayle, M.J.; Righini, S.; Seton, L.; Tiddy, G.J.T. (2002). Crystal engineering – nucleation the key step. *CrystEngComm*, **4**, 257–264.

Davis, S.N. (2008). The role of inhaled insulin in the treatment of type II diabetes. *J. Diabetes and its complications*, **22**, 420-429.

De Boer, A.H.; Hagedoorn, P.; Gjaltema, D.; Goede, J.; Frijlink, H.W. (2003). Air classifier technology (ACT) in dry powder inhalation. Part 1. Introduction of a novel force distribution concept (FDC) explaining the performance of a basic air classifier on adhesive mixtures. *Int J Pharm.*, **260**, 187-200.

De Boer, A.H.; Hagedoorn, P.; Gjaltema, D.; Goede, J.; Frijlink, H.W. (2003). Air classifier technology (ACT) in dry powder inhalation. Part 2. The effect of lactose surface carrier properties on the drug-to-carrier interactions in adhesive mixtures for inhalation. *Int J Pharm.*, **260**, 201-216.

De Boer, A.H.; Hagedoorn, P.; Gjaltema, D.; Goede, J.; Frijlink, H.W. (2006). Air classifier technology (ACT) in dry powder inhalation. Part 3. Design and development of an air classifier family for the Novolizer multi-dose dry powder inhaler. *Int J Pharm.*, **310**, 72-80.

De Boer, A.H.; Hagedoorn, P.; Gjaltema, D.; Goede, J.; Frijlink, H.W. (2006). Air classifier technology (ACT) in dry powder inhalation. Part 4. Performance of air classifier technology in the Novolizer multi-dose dry powder inhaler. *Int J Pharm.*, **310**, 81-90.

Dennehy, R.D. (2003). Particle engineering using power ultrasound. *Org. Process Res. Dev.*, **7**, 1002-1006.

Dhillon, A.S.; Pitchayajittipong, C.; Shur, J.; Price, R. (2006). Combination particles containing fluticasone propionate and theophylline for lung delivery.

- Dhumal, R.S.; Biradar, S.V.; Paradkar, A.R.; York, P. (2009). Particle engineering using sonocrystallization: Salbutamol sulfate for pulmonary delivery. *Int.J.Pharm.*, **368**, 129-137.
- Dixon, D.J.; Johnston, K.P.; Bodmeier, R.A. (1993). Polymeric material formed by precipitation with a compressed fluid antisolvent. *AIChE. J.*, **39**, 127-139.
- Dunbar, C.A.; Concessio, N.M.; Hickey, A.J. (1998). Evaluation of atomizer performance in production of respirable spray dried particles. *Pharm. Dev. Technol.*, **3**, 433-441.
- Edwards, D.A.; Langer, R.S.; Vanbever, R.; Mintzes, J.; Wang, J.; Chen, D.H. (2003). Preparation of novel particles for inhalation. United States Patent. 6,652,837.
- Elbagerma, M.A.; Edwards, H.G.M.; Munshi, T.; Hargreaves, M.D.; Matousek, P.; Scowen, I.J. (2010). Characterization of New Cocrystals by Raman Spectroscopy, Powder X-Ray Diffraction, Differential Scanning Calorimetry, and Transmission Raman Spectroscopy. *Crys. Growth Des.*, **10**, 2360-2371.
- Falcon, J.A.; Berglund, K.A. (2004). In Situ Monitoring of Antisolvent Addition Crystallization with Principal Component Analysis of Raman Spectra. *Crystal Growth and Design.*, **4**, 457-463.
- Fenton, C.; Keating, G.M.; Plosker, G.L. (2003). Novolizer® A multidose dry powder inhaler. *Drugs*, **63**, 2437-2445.
- Galkin, O.; Vekilov, P.G. (2000). Are nucleation kinetics of protein crystals similar to those of liquid droplets? *J Am. Chem. Soc.*, **122**, 156–163.
- Gallagher, P.M.; M.P., Krukonis; Klasutis, N. (1989). Gas antisolvent recrystallization: New process to recrystallize compounds insoluble in supercritical fluids. *Supercritical Fluid Science and Technology*, **406**, 334-354.
- Genoveva, G.R.; Enrique, O.R.; Teresita, R.G.E.; Eduardo, O.R. (2007). The influence of agitation speed on the morphology and size particle synthesis of $Zr(HPO_4)_2 \cdot H_2O$ from Mexican sand. *J. Minerals and Materials Characterization Engg.*, **6**, 39-51.
- Ghaste, R. (2009). Solid dispersions: an overview. *Latest Rev.*, **7**.
- Gibbs, J.W. (1948). Collected works, Vol. I: Thermodynamics. New Haven: Yale University Press.
- Gilani, K.; Najafabadi, A.R.; Barghi, M.; Tehrani, M.R. (2005). The effect of water to ethanol feed ratio on physical properties and aerosolization behaviour of spray dried cromolyn sodium particles. *J. Pharm. Sci.*, **94**, 1048-1059.
- Gunton, J.D. (1999). Homogeneous nucleation. *J Stat Phys*, **95**, 903–923.

Hartman, P.; Perdock, W.G. (1955). On the relations between structure and morphology of crystals. I. *Acta Cryst*, **8**, 49–52.

Hipp, A.K.; Walker, B.; Mazzotti, M.; Mobidelli, M. (2000). In-Situ Monitoring of Batch Crystallization by Ultrasound Spectroscopy. *Ind. Eng. Chem. Res.*, **39**, 783-789.

Huang, J.M.; Chu, P.P.; Chang, F.C. (2000). Conformational changes and molecular motion of (ethylene terephthalate) annealed above glass transition temperature. *Polymer*, **41**, 1741-1748.

Islam, N.; Stewart, P.; Larson, I.; Hartley, P. (2003). Effect of carrier size on the dispersion of Salmeterol Xinafoate from interactive mixtures. *J. Pharm. Sci.*, **93**, 1030-1038.

Jaarmo, S.; Rantakyla, M.; Aaltonen, O. (1997). Particle tailoring with supercritical fluid production of amorphous pharmaceutical particles. Proceedings of the 4th International Symposium on Supercritical Fluids, Sendai, Japan, 263-266.

Jin, F.; Hindle, M.; Byron, P.R. (2007). Co-deposition of Albuterol Sulfate and Ipratropium Bromide co-crystal aerosols. Dalby, R.N., Byron, P.R., Peart, J., Suman, J.D. and Farr, S.J. (eds), Respiratory Drug Delivery X, DHI Publishing, River Grove, IL., 373-376.

Kaerger, J.S.; Price, R. (2003). Processing of spherical crystalline particles via a novel solution atomization and crystallization by sonication (SAXS) technique. *Pharm. Res.*, **21**, 372-381.

Keil, J.C.; Kotian, R.; Peart, J. (2006). Using and interpreting aerosol electrostatic data from electrical low pressure impactor. Proceedings of the Conference on Respiratory Drug Delivery, Boca Raton, Florida, 605-608.

Kellogg, G.E.; Abraham, D.J. (2000). Hydrophobicity: Is Log P more than the Sum of its Parts? *Eur.J.Med.Chem.*, **35**, 651-661.

Leger, J.M.; Goursolle, M.; Gadret, M. (1978). Structure Cristalline du Sulfate de Salbutamol [tert butylamino-2 (Hydroxy-4hydroxymethyl- 3 phenyl)-1 Ethanol. 1/2 H₂SO₄. *Acta Crystallogr.*, **B34**, 1203-1208.

Listiohadi, Y.; Hourigan, J.A.; Sleigh, R.W.; Steele, R.J. (2008). Thermal analysis of amorphous lactose and α -lactose monohydrate. *Dairy Sci. Technol.*, **89**, 43-67.

Louey, M.D.; Oort, M.V.; Hickey, A.J. (2004). Aerosol dispersion of respirable particles in narrow size distributions produced by jet-milling and spray-drying techniques. *Pharm. Res.*, **21**, 1200-1206.

Louey, M.D.; Oort, M.V.; Hickey, A.J. (2006). Standardized entrainment tubes for the evaluation of pharmaceutical dry powder dispersion. *Aerosol Science*, **37**, 1520-1531.

- Maa, Y.F.; Constantino, H.R.; Nguyen, P.A.; Hsu, C.C. (1997). The effect of operating and formulation variables on the morphology of spray-dried protein particles. *Pharm. Dev. Technol.*, **2**, 213-223.
- Martino, P.D.; Censi, R.; Malaj, L.; Capsoni, D.; Massarotti, V.; Martelli, S. (2007). Influence of solvent and crystallization method on the crystal habit of metronidazole. *Cryst. Res. Technol.*, **42**, 800-806.
- Master, L. (1991). *Spray Drying Handbook*. 5th ed. Longman, New York.
- Markande, A.; Aerts, L.; Nezzal, A. (2007). In-Line Monitoring of Dextrose Crystallization in Batch Crystallizer using Focused Beam Reflectance Measurement (FBRM). *Partec*.
- McCausland, L.J.; Cains, P.W. Sonocrystallization – ultrasonically promoted crystallization for the optimal isolation of drug actives. 1-11.
- Meenan, P.A.; Anderson, S.R.; Klug, D.L. (2002). The influence of impurities and solvents on crystallization. *Handbook of industrial crystallization*. Boston: Butter-Worth-Heinemann, 67–97.
- Mersmann, A. (2001). *Crystallization technology handbook*. *Marcel Dekker*, 2nd Ed. 45-127.
- Myerson, A.S. (1999). *Crystallization basics. Molecular modeling applications in crystallization*. New York: Cambridge University Press. 55–105.
- Mullin, J.W. (2001). *Crystallization*. *Elsevier Ltd.*, 4th Ed. 181-284.
- Murnane, D.; Marriott, C.; Martin, G.P. (2008). Polymorphic control of inhalation microparticles prepared by crystallization. *Int. J Pharm.*, **36**, 141-149.
- Najafabadi, A.R.; Gilani, K.; Hozan, A. (2001). Design and evaluation of a new dry powder inhaler. *DARU*, **9**, 46-49.
- Najafabadi, A.R.; Vantanara, A.; Gilani, K.; Tehrani, M.R. (2005). Formation of Salbutamol Sulfate microparticles using solution enhanced dispersion by supercritical carbon dioxide. *DARU*, **13**, 1-5.
- Nelson, H.S.; Chapman, K.R.; Pyke, S.D.; Johnson, M.; Pritchard, J.N. (2003). Enhanced synergy between fluticasone propionate and salmeterol inhaled from a single inhaler versus separate inhalers. *J. Allergy Clin. Immunol.*, **112**, 29-36.
- Newman, S.P.; Busse, W.W. (2002). Evolution of dry powder inhaler design, formulation, and performance. *Respir. Med.*, **96**, 293-304.
- Nielsen, A.E. (1964). *Kinetics of precipitation*. New York: Macmillan. 153.

- Nocent, M.; Bertocchi, L.; Espitalier, F.; Baron, M.; Couarraze, G. (2001). Definition of a solvent system for spherical crystallization of salbutamol sulfate by Quasi-Emulsion Solvent Diffusion (QESD) method. *J. Pharm. Sci.*, **90**, 1620-1627.
- O'Grady, D.; Barrett, M.; Casey, E.; Glennon, B. (2001). The effect of mixing on the metastable zone width and nucleation kinetics in the anti-solvent crystallization of benzoic acid. *IChemE*, **85**, 945-952.
- Oxtoby, D.W. (1998). Nucleation of first-order phase transitions. *Acc Chem Res*, **31**, 91.
- Parveen, S.; Davey, R.J.; Dent, G.; Pritchard, R.G. (2005). Linking solution chemistry to crystal nucleation: the case of tetrolic acid. *Chem Commun*, **12**, 1531–1533.
- Pauwels, R.; Newman, S.; Borgstrom, L. (1997). Airway deposition and airway effects of antiasthma drugs delivered from metered dose inhalers. *Eur. Respir. J.*, **10**, 2127-2138.
- Penttila, M.U.; Berglund, K.A. (1996). Spectroscopic monitoring of environmentally benign anti-solvent crystallization. *J. Crystal Growth*, **166**, 967-970.
- Perepezko, J.H. (1994). Nucleation reactions in undercooled liquids. *Mater Sci Eng A*, **178**, 105–111.
- Pfeiffer, B.K.; Hausler, H.; Grab, P.; Langguth, P. (2003). Conditioning following powder micronization: Influence on particle growth of Salbutamol Sulfate. *Drug Dev. Ind. Pharm*, **29**, 1077-1084.
- Pitchayajittipong, C.; Shur, J.; Price, R. (2009). Engineering of crystalline combination inhalation particles of a long acting β -2 agonist and a corticosteroid. *Pharm. Res.*, **26**, 2657-2666.
- Pitchayajittipong, C.; Shur, J.; Price, R. *De Novo* engineering of crystalline low dose combination inhalation particles of a long acting β -2 agonist and a corticosteroid.
- Platz, R.M.; Patton, J.S.; Foster, L.; Eljamal, M. (2003). Spray drying of macromolecules to produce inhalable dry powders. United States Patent. 6,582,728.
- Price, D.; Thomas, M.; Mitchell, G.; Niziol, C.; Featherstone, R. (2003). Improvement of asthma control with a breath actuated pressurized metered dose inhaler (BAI): a prescribing claims study of 5556 patients using a traditional pressurized metered dose inhaler (MDI) or a breath actuated device. *Respir. Med.*, **97**, 12-19.
- Pritchard, J.N. (2001). The influence of lung deposition on clinical response. *J. Aerosol. Med.*, **14**, S19-S26.
- Ragab, D.M.; Rohani, S. (2009). Particle engineering strategies via crystallization for pulmonary drug delivery. *Org. Process Res. Dev.*, **13**, 1215-1223.

Rasenack, N.; Steckel, H.; Muller, B.W. (2002). Micronization of anti-inflammatory drugs for pulmonary delivery by a controlled crystallization process. *J. Pharm. Sci.*, **92**, 35-44.

Raseneack, M.; Muller, B.W. (2004). Micron-size drug particles: common and novel micronization techniques. *Pharm. Dev. Technol.*, **9**, 1-13.

Rehman, M.; Shekunov, B.Y.; York, P.; Lechuga-Ballesteros, D.; Miller, D.P.; Tan, T.; Colthorpe, P. (2004). Optimization of powders for pulmonary delivery using supercritical fluid technology. *Eur. J. Pharm. Sci.*, **22**, 1-17.

Rodríguez-Hornedo, N.; Murphy, D. (1999). Significance of controlling crystallization mechanisms and kinetics in pharmaceutical systems. *J. Pharm. Sci.*, **88**, 651–660.

Rodríguez-Hornedo, N.; Kelly, R.C.; Sinclair, B.D.; Miller, J.M. (2006a). Crystallization: general principles and significance on product development. Encyclopedia of pharmaceutical technology, 3rd ed. New York: Informa Healthcare USA, Inc., 834–857.

Rodriguez-Spong, B.; Price, C.P.; Jayasankar, A.; Matzger, A.J.; Hornedo, N.R. (2004). General principles of pharmaceutical solid polymorphism: a supramolecular perspective. *Adv. Drug Del. Rev.*, **56**, 241-274.

Saska, M.; Myerson, A.S. (1987). Crystal aging and crystal habit of terephthalic acid. *AIChE Journal*, **33**, 848.

Schmitt, W.J.; Salada, M.C.; Shook, G.G.; Speaker, S.M. (1995). Finely divided powders by carrier solution injection into a near or supercritical fluid. *AIChE J.*, **41**, 2746-2486.

Schreck, D.M. (2006). Asthma Pathophysiology and Evidence Based Treatment of Severe Exacerbations. *Am J Health-Syst Pharm.*, **63**, S5-S13.

Schultheiss, N.; Newman, A. (2009). Pharmaceutical cocrystals and their physicochemical properties. *Crys Growth Des.*, **9**, 2950-2967.

Shan, N.; Zaworotko, M.J. (2008). The role of cocrystals in pharmaceutical science. *Drug Discovery Today*, **13**, 440-446.

Sheikhzadeh, M.; Rohani, M.T.S. (2008). Real time optimal control of an anti-solvent isothermal semi-batch crystallization process. *Chem. Engg. Science*, **63**, 829-839.

Shekunov, B.Y.; Feeley, J.C.; Chow, A.H.L.; Tong, H.H.Y.; York, P. (2003). Aerosolisation behaviour of micronised and supercritically-processed powders. *J. Aerosol Sci*, **34**, 553-568.

Shekunov, B.Y.; Chattopadhyay, B.; Seitzinger, J. (2004). Production of respirable particles using spray-freeze-drying with compressed CO₂. Proceedings of the Conference on Respiratory Drug Delivery, Palm Springs, California, 489-492.

Shekunov, B.V. (2004). Production of powders for respiratory drug delivery. *Supercritical Fluid Technology for Drug Product Development*, Marcel Dekker, New York, 247-282.

Shekunov, B.Y. (2005). Nanoparticle technology for drug delivery from nanoparticles to cutting-edge delivery strategies. Part I. *Drugs*, **8**, 399-401.

Shekunov, B.Y.; Chattopadhyay, B.; Tong, H.H.Y.; Chow, A.H.L. (2006). Particle size analysis in pharmaceuticals: principles, methods and applications. *Pharm. Res.*

Shekunov, B.Y.; Chattopadhyay, P.; Gibson, A.; Lekhmukhl, C. (2006). Influence of spray-freezing parameters on particle size and morphology of insulin. *Proceedings of the Conference on Respiratory Drug Delivery*, Boca Raton, Florida, 605-608.

Smyth, H.D.C. (2003). The influence of formulation variables on the performance of alternative propellant driven metered dose inhalers. *Adv. Drug Deliv. Rev.*, **55**, 807-828.

Tobyn, M.; Staniforth, J.N.; Morton, D.; Harmer, Q.; Newton M.E. (2004). Active and intelligent inhaler device development. *Int. J. Pharm.*, **277**, 31-37.

Stanton, M.K.; Bak, A. (2008). Physicochemical Properties of Pharmaceutical Cocrystals- A Case Study of Ten AMG 517 Cocrystals. *Crys. Growth Des.*, **8**, 3856-3862.

Stranski, I.N.; Honigmann, B. (1950). The spontaneous appearance of equilibrium forms in crystals of hexamethylenetetramine. *Z. Phys. Chem.*, **194**, 180-198.

Subramaniam, B.; Rajewski, R.A.; Snavely, K. (1997). Pharmaceutical processing with supercritical carbon dioxide. *J. Pharm. Sci.*, **86**, 885-890.

Taki, M.; Zeng, X.M.; Marriott, C.; Martin, G. (2006). An assessment of the in vitro deposition of aerosolized drugs from a combination dry powder inhaler using the Andersen cascade impactor (ACI). Dalby, R.N., Byron, P.R., Peart, J., Suman, J.D. and Farr, S.J. (eds), *Respiratory Drug Delivery X*, DHI Publishing, River Grove, IL. 655-658.

Thompson, L.H.; Doraiswamy, L.K. (1999). Sonochemistry: Science and engineering. *Ind. Eng. Chem. Res.* **38**, 1215-1249.

Ticehurst, M.D.; Rowe, R.C.; York, P. (1994). Determination of the surface properties of two batches of salbutamol sulfate by inverse gas chromatography. *Int. J. Pharm.*, **111**, 241-249.

Toda, T.; Yoshida, H. (1995). Structure and molecular motion changes in poly (ethylene terephthalate) induced by annealing under dry and wet conditions. *Polymer*, **36**, 699-706.

Tong, H.H.Y.; Chow, A.H.L. (2006). Control of physical forms of drug particles for pulmonary delivery by spray drying and supercritical fluid processing. *KONA*, **24**, 27-40.

Tripos Force Field Manual. Sybyl 7.3, **2006**.

Truong-Lee, V.; Pham, B.V.; Carpeneter, J.F.; Seid, R.; Randolph, T.W. (2004). Spray freeze drying of compositions for pulmonary administration. United States Patent Application. 0042971 A1.

Vekilov, P.G. (2004). Dense liquid precursor for the nucleation of ordered solid phases from solution. *Cryst Growth Des*, **4**, 671–685.

Vishweshwar, P.; McMahon, J.A.; Peterson, M.L.; Hickey, M.B.; Shattock, T.R.; Zaworotko, M.J. (2005). Crystal engineering of pharmaceutical cocrystals from polymorphic active pharmaceutical ingredients. *Chem. Commun.*, 4601-4603.

Volmer, M. (1939). Die chemische reaktion. Bd. IV. Kinetik der phasenbildung. Leipzig: Steinkopf. 220.

Ward, M.J.; Macfarlane, J.T.; Davies, D. (1985). A Place for Ipratropium Bromide in the Treatment of Severe Acute Asthma. *Br J Dis Chest*. **79**, 374-378.

Ward, G.H.; Schultz, R.K. (1995). Process induced crystallinity changes in albuterol sulfate and its effect on powder physical stability. *Pharm. Res.*, **12**, 773-779.

Wierik, H.T; Diepenmatt, P. (2002). Formulation of lactose for inhaled delivery systems. *Pharmaceutical Technology Europe*, 1-5.

Wolde, P.R.; Frenkel, D. (1997). Enhancement of protein crystal nucleation by critical density fluctuations. *Science*, **277**, 1975–1978.

York, P. (1999). Strategies for particle design using supercritical fluid technologies. *Pharmaceutical Science and Technology Today*, **2**, 430-440.

Yu, Z.Q.; Chow, P.S.; Tan, R.B.H. (2006). Seeding and constant supersaturation control by ATR-FTIR in anti-solvent crystallization. *Org. Process Res. Dev.*, **10**, 717-722.

Zeng, X.M.; Lahrib, H.; Martin, G.P.; Marriott, C.; Pritchard, J. (1999). The use of different grades of lactose as a carrier for aerosolized salbutamol sulfate. *Int. J. Pharm.*, **191**, 1-14.

Zettlemoyer, A.C. (1969). Nucleation. New York: Marcel Dekker.

Zografi, G. (1988). States of water associated with solids. *Drug Dev. Ind. Pharm.*, **14**, 1905-1926.

APPENDIX

Table A.1 Summary of HINT interaction scores for the 10 GA runs performed in Docking # 1

GA Run #	LOGP	Total HINT Score	Hydrogen Bonding	Hydrophobic-Hydrophobic Interactions	Hydrophobic-Polar Interactions
1	-0.63	-659.47	0	914.9	-2447.73
2	-0.63	-1135.24	677.5	726.37	-2543.56
3	-0.63	-662.6	0	921.84	-2297.51
4	-0.63	-544.11	419.05	432.82	-1446.75
5	-0.63	-734.18	0	858.33	-2247.49
6	-0.63	-559.15	480.83	876.67	-2198.16
7	-0.63	-688.96	0	894.14	-2243
8	-0.63	-523.27	0	346.59	-1608.19
9	-0.63	-978.3	0	639.8	-2313.64
10	-0.63	-601.37	666.64	784.05	-2474.69

Table A.2 Summary of HINT interaction scores for the 10 GA runs performed in Docking # 2

GA Run #	LOGP	Total HINT Score	Hydrogen Bonding	Hydrophobic-Hydrophobic Interactions	Hydrophobic-Polar Interactions
1	-0.63	-901.83	728.66	520.17	-2030.23
2	-0.63	-1116.85	944.18	777.76	-2259.99
3	-0.63	-1103.05	760.99	684.36	-2531.83
4	-0.63	-262.7	0	479.01	-1550.62
5	-0.63	-1503.08	0	687.17	-2509.35
6	-0.63	-737.16	1746.32	698.05	-1947.96
7	-0.63	-835.09	1649.46	648.15	-2108.98
8	-0.63	-1223.42	930.7	666.63	-2497.84
9	-0.63	-934.74	347.49	502.77	-2207.75
10	-0.63	-723.06	0	604.05	-2013.59

Table A.3 Summary of HINT interaction scores for the 10 GA runs performed in Docking # 3

GA Run #	LOGP	Total HINT Score	Hydrogen Bonding	Hydrophobic-Hydrophobic Interactions	Hydrophobic-Polar Interactions
1	-0.63	-287.94	363.9	668.36	-1694.57
2	-0.63	-453.7	0	558.06	-1828.95
3	-0.63	-232.71	420.77	679.35	-1707.69
4	-0.63	-343.69	366.04	689.37	-1716.42
5	-0.63	-506.35	296.37	651.21	-1809.39
6	-0.63	-824.53	0	660.31	-1619.99
7	-0.63	-364.35	468.22	660.89	-1790.87
8	-0.63	-595.2	0	628.3	-1723.89
9	-0.63	-396.54	415.18	676.65	-1753.61
10	-0.63	-201.96	0	701.48	-1637.18

Table A.4 Summary of HINT interaction scores for the 10 GA runs performed in Docking # 4

GA Run #	LOGP	Total HINT Score	Hydrogen Bonding	Hydrophobic-Hydrophobic Interactions	Hydrophobic-Polar Interactions
1	-0.63	-1138.43	0	878.35	-2976.05
2	-0.63	-2321.9	399.93	340.09	-2330.86
3	-0.63	-1245.18	0	543.31	-2234.72
4	-0.63	-1439.12	0	247.25	-2232.02
5	-0.63	-1345.87	0	666.46	-2787.31
6	-0.63	-703.29	237.79	263.69	-1779.13
7	-0.63	248.23	506.49	443.32	-1343.2
8	-0.63	-868.76	272.32	304.28	-1871.62
9	-0.63	-687.56	107.33	101.66	-1431.53
10	-0.63	-1440.82	349.07	336.46	-2169.64

Table A.5 Summary of HINT interaction scores for the 10 GA runs performed in Docking # 5

GA Run #	LOGP	Total HINT Score	Hydrogen Bonding	Hydrophobic-Hydrophobic Interactions	Hydrophobic-Polar Interactions
1	-0.63	-1537.5	0	502.08	-2346.56
2	-0.63	-776.43	0	595.05	-2276.32
3	-0.63	-1427.99	0	488.88	-2343.99
4	-0.63	-1146.87	211.76	590.43	-2599.49
5	-0.63	-1374.51	591.26	492.23	-2283.36
6	-0.63	-1414.49	0	461.02	-2302.5
7	-0.63	-850.31	295.81	579.89	-2297.27
8	-0.63	-1065.54	317.44	538.13	-2383.92
9	-0.63	-3015.7	1255.91	614.72	-2193.77
10	-0.63	-1342.53	0	499.8	-2403.15

Table A.6 Summary of HINT interaction scores for the 10 GA runs performed in Docking # 6

GA Run #	LOGP	Total HINT Score	Hydrogen Bonding	Hydrophobic-Hydrophobic Interactions	Hydrophobic-Polar Interactions
1	-0.63	-685.55	521.31	831.9	-2197.52
2	-0.63	-829.1	398.79	671.95	-2280.88
3	-0.63	-1104.3	101.7	656.99	-2548.71
4	-0.63	-2064.46	0	632.3	-2720.23
5	-0.63	-886.8	500.84	800.93	-2132.84
6	-0.63	-2445.42	348.59	660.68	-3015.63
7	-0.63	-823.42	97.88	697.85	-2001.78
8	-0.63	-747.98	514.18	859.68	-2173.38
9	-0.63	-2457.78	677.19	821.96	-3317.01
10	-0.63	-600.74	627.59	807.44	-2123.21

Table A.7 Summary of HINT interaction scores for the 10 GA runs performed in Docking # 7

GA Run #	LOGP	Total HINT Score	Hydrogen Bonding	Hydrophobic-Hydrophobic Interactions	Hydrophobic-Polar Interactions
1	-0.63	-541.88	96.16	667.5	-1934.32
2	-0.63	-3651.08	1023.65	613.41	-2821.45
3	-0.63	-834.42	0	574.44	-2224.53
4	-0.63	-1555.39	0	667.38	-2417.18
5	-0.63	-540.49	0	680.93	-1947.66
6	-0.63	-627.71	0	475.91	-1673.77
7	-0.63	-730.17	0	586.52	-1985.24
8	-0.63	-1358.18	0	540.49	-2104.87
9	-0.63	-2902.78	569.99	620.19	-3509.82
10	-0.63	-2701.99	0	663.57	-3579.83

Table A.8 Summary of HINT interaction scores for the 10 GA runs performed in Docking # 8

GA Run #	LOGP	Total HINT Score	Hydrogen Bonding	Hydrophobic-Hydrophobic Interactions	Hydrophobic-Polar Interactions
1	-0.63	-1058.21	400.96	577.72	-1952.62
2	-0.63	-1097.05	0	658.46	-2075.8
3	-0.63	-1231.66	0	726.52	-2146.54
4	-0.63	-1492.2	418.87	937.04	-2341.4
5	-0.63	-962.9	348.76	986.5	-2186.2
6	-0.63	-1121.36	0	768.76	-2026.21
7	-0.63	-1682.57	0	802.6	-2831.23
8	-0.63	-1114.71	0	840.63	-2338.83
9	-0.63	-569.41	0	882.47	-1997.01
10	-0.63	-1079.49	0	805.33	-2031.73

VITA

Swati Agrawal was born on August 7, 1981 in Lucknow, India and is an Indian citizen. She graduated from Uttar Pradesh Technical University, Lucknow, India with a Bachelor of Pharmacy in 2004 and from Birla Institute of Technology and Science, Rajasthan, India with a Master of Pharmacy in 2006. She worked as a research intern at Ipca Laboratories Ltd., Mumbai, India before joining the Department of Pharmaceutics, Virginia Commonwealth University (VCU) in 2006.

During the course of her Ph.D. studies, Swati has published four abstracts. She has presented her research at the Annual Meeting of the American Association of Pharmaceutical Scientists (AAPS, 2009) and the Respiratory Drug Delivery Conference (RDD, 2010) in addition to poster presentations within VCU. She received the 2009 American Association of Indian Pharmaceutical Scientists (AAiPS) outstanding graduate student research award for her work. In 2009, she received the VCU graduate school dissertation assistantship for the 2009-2010 academic year.

Swati is a member of the AAPS and served as the Secretary-Treasurer and Vice-Chair of the Graduate Student Association (GSA) in the Department of Pharmaceutics and the AAPS-VCU student chapter in 2007 and 2008, respectively.

Abstracts:

1. Agrawal S., Hindle, M. *In vitro* aerosol performance of albuterol sulfate particles produced using a solvent / anti-solvent crystallization technique. (Abstract accepted for AAPS 2010)
2. Agrawal, S., Hindle, M. Formulation and analysis of inhalation sized combination particles containing albuterol sulfate and ipratropium bromide. (Abstract accepted for AAPS 2010)
3. Agrawal, S., Hindle, M. *In vitro* aerosol performance of albuterol sulfate particles produced using a solvent / anti-solvent crystallization technique. Respiratory Drug Delivery Conference, Orlando, Florida (Poster and Respiratory Drug Delivery 2010, In: Dalby, R.N., Byron, P.R., Peart, J., Suman, J.D., and Farr, S.J., editors, Davis Healthcare International Publishing, LLC, River Grove, IL, 3, 903-906).
4. Agrawal, S., Hindle, M. Investigation of a solvent/anti-solvent crystallization process for Albuterol Sulfate. Annual Meeting of the AAPS, Los Angeles, California (The AAPS Journal 11 (S2): W1275; Nov. 2009).